Geochemistry and Paragenesis of Magnetite Bearing Gabbros from the Mine Block Intrusion at Lac des Iles Mine, Northern Ontario

Sergio Y. Bautista G.

A thesis submitted in partial fulfillment of the requirements for

the Degree of Master of Science (Geology)

Lakehead University, Thunder Bay, Ontario

April 2024

Abstract

The Mine Block Intrusion (MBI) is a 3 km by 1.5 km tear-shaped mafic complex that was emplaced along with other mafic-ultramafic plutonic rocks of the South Lac des Iles Complex (LDIC) between 2,699 and 2,686 Ma in the Marmion terrane of the Superior Province. The MBI consists of gabbronorite and magnetite-rich gabbronorite, and a later series of noritic rocks and their metamorphosed altered equivalents.

Major element data of the MBI indicate that the rocks have a broadly gabbroic composition with protoliths dominated by plagioclase, a predominance of orthopyroxenes over clinopyroxene, and titano-magnetite, which is consistent with the petrographic observations. Magnetite gabbronorite rocks in the MBI were derived from a metasomatized mantle, consistent with the arc setting proposed for the Lac des Iles Complex as a whole.

Plagioclase compositions decrease up the analyzed section, with no sharp change, suggesting a normal fractionation process with no magma injection events. Plagioclase identified within the magnetite gabbronorite of the MBI is labradorite-bytownite (An-number ranging from 0.58 to 0.75), which is less evolved than observed in layered intrusions globally suggesting that saturation of Fe-Ti oxides occurred at an early stage of differentiation compared with other mafic intrusions.

Coarse primary ilmenite grains with hematite lamellae in the MBI indicate early ilmenite crystallization, which could suggest a high TiO_2 concentration in the magma. However, comparison with rocks of deposits dominated by hemo-ilmenite (high Ti content) and titanomagnetite (low Ti content) suggest that the primary ilmenite crystallized from a low-Ti magma.

When comparing the analyzed samples of magnetite gabbronorite from the MBI with Fe-oxides of well-characterized rocks from the lowermost layers of Fe-Ti-V deposits (primitive signature) and the uppermost layers of Fe-Ti-P deposits (evolved signature), the pattern of compatible elements such as V, Ni, and Cr in magnetite show a distribution from primitive to evolved magnetite. This suggests that magnetite at the MBI crystallized from a magma of primitive composition associated with Fe-Ti-V deposits rather than from a more evolved magma typically linked to Fe-Ti-P mineralisation. This is consistent with the absence of apatite and the low P contents observed in whole rock geochemistry in the MBI. The upward decrease of elements compatible

with magnetite, such as Mg, Ni, V, and Cr, and the upward increase of magnetite from elements incompatible with magnetite, such as Mo, Zn, and Ti in the magnetite from the MBI, indicate fractionation of the silicate melt from a less evolved melt to a more evolved one. It is likely that during fractionation plagioclase would have accumulated at the top of the magma chamber whereas the denser iron oxides would sink, resulting in the cumulate textures observed in the magnetite gabbronorite in the MBI.

The magnetite in the MBI gabbronorite at Lac des Iles can be considered to belong to the Fe-Ti-V deposit group hosted in the lower parts of a layered intrusion, characterized by titanomagnetite as the dominant oxide mineral occurring in layers and oxide mineralization associated with gabbronoritic cumulates. Magnetite chemistry also suggests a magmatic Fe-Ti-V deposit with a potential for V mineralization at Lac des Iles since several samples have concentrations (up to 1.3 wt. % V_2O_5) above those of the Panzhihua V mine (0.3 wt. % V_2O_5) or the Rhovan (Bushveld Complex) mine (0.5 wt. % V_2O_5).

Acknowledgments

My greatest thanks to my supervisor, Dr. Peter Hollings, for his guidance and patience throughout the process of completion of this project. I appreciate him taking the risk of giving me this opportunity and all his advice and help during this journey. I would also like to thank Dr. Sarah Dare at the Université du Québec à Chicoutimi for her assistance with LA-ICP-MS analyses and guidance with data interpretation. Thank you, Dr. Lionnel Djon at Impala Canada, for the conception of this research project and his assistance in collecting samples and data analysis. I want to express my gratitude to the revisors of the manuscript Dr. Diochon and Dr. Sappin.

Thanks to all who supported this project, Lakehead University, a National Sciences and Engineering Research Council (NSERC) Collaborative Research and Development Grant, and the Society of Economic Geologists Canada Foundation.

Thanks to my fellow MSc. students. In particular Spencer Killins, Justin Jonsson, and Daniel Thomson for their support and valued opinions throughout this project.

Lastly, thank you to my family for non-stop support and to my beloved Carolina; your strength, determination, and encouragement keep me going.

Table of Contents

List of Figures

List of Tables

List of Abbreviations

Ab - Albite

An – Anorthite

Aug - Augite

Byt – Bytownite

Di – Diopside

En – Enstatite

Hyp – Hypersthene

Ilm - Ilmenite

MBI – Mine Block Intrusion

Ple – Pleonaste

Lbd - Labradorite

Mt – Magnetite

ss – Solid solution

Usp – Ulvospinel

LDIC – Lac des Iles Intrusive Complex

North LDI – North Lac des Iles

ppl - Plane polarized light

xpl – Cross polarized light

PGE – Platinum Group Elements

PGM – Platinum Group Metals

SEM - scanning electron microscopy

LA-ICP-MS - Laser Ablation Inductively Coupled Mass Spectrometry

LDI – Lac des Iles

Mag - Magnetite

EDS/EDX – Energy-dispersive X-ray spectroscopy

LREE – Light Rare Earth Elements

HREE – Heavy Rare Earth Elements

LUIL - Lakehead University Instrumentation Laboratory

μXRF - Micro X-Ray Fluorescence

Chapter 1. Introduction

Large mafic-ultramafic intrusions can be subdivided into layered intrusions, unlayered intrusions, zoned ultramafic complexes (Ural-Alaskan-type complexes), and ophiolites (Cawthorn et al., 2005). Large, layered intrusions usually show significant lateral layering; where vertical mineralogical changes in the layers may follow a predictable, repeated sequence of cyclic layering, as well as systematic changes in mineral compositions, called cryptic layering (Cawthorn et al., 2005).

Magnetite can form in a wide variety of different environments, from high-temperature magmatic (upper zones of layered intrusions, or within massif-type anorthosite complexes and volcanic rocks) to lower-temperature hydrothermal and sedimentary deposits (Dare et al., 2012). Magnetite can be concentrated to form ore deposits such as banded iron formations, magmatic Fe-Ti-V oxide, iron skarns, iron oxide-copper–gold (IOCG), and Kiruna-type iron oxide-apatite (IOA) deposits (Dare et al., 2014).

Ore deposits associated with mafic-ultramafic intrusions can generally be divided into 1) those where the metals of interest are hosted in stratiform, podiform, and breccia-related chromite; magnetite-rich layers (often Ti and V-bearing), and ilmenite-rich layers or discordant bodies, and 2) those where the metals of interest are held as sulfides or are strongly associated with sulfides (Ripley and Li, 2018).

There are three series within the spinel group according to the trivalent cation (Table 1.1): the spinel series (Al^{3+}), the magnetite series (Fe^{3+}), and the chromite series (Cr^{3+}). In magnetite ($Fe^{2+}Fe_2^{3+}O_4$), Mg, Mn, Co, Zn, and Ni may substitute for Fe^{2+}, whereas Fe^{3+} can be replaced by Al, Mn, Ga, V, and Cr. Vanadium, which has a range of possible oxidation states depending on prevailing oxygen fugacity conditions, is mainly present as V^{3+} in titanomagnetites but commonly shows variable minor amounts of V^{4+}. Titanium, with a 4+ charge, can also occupy the Fe_2^{3+} site when substitution is coupled with a divalent cation (Nadoll et al., 2014; Brzozowski et al., 2021). In the "magnetite series", magnetite forms a complete solid solution with magnesioferrite

($MgFe_2O_4$) and ulvöspinel (Fe_2TiO_4), also known as titanomagnetite. Magnetite displays partial solid solutions with franklinite ($ZnFe_2O_4$), jacobsite ($MnFe_2O_4$), and trevorite ($NiFe_2O_4$) and contains both ferrous (Fe^{2+}) and ferric (Fe^{3+}) ions, implying synthesis, growth, and stability within an environment where oxidized and reduced states of iron are present and maintained (Nesse, 2012; Skinner & Ehrlich, 2014). Octahedral sites in the magnetite structure can be randomly occupied by subequal amounts of ferric (Fe^{3+}) and ferrous (Fe^{2+}) iron atoms, whereas tetrahedral sites are exclusively occupied by the smaller ferric iron atoms $Fe^{3+}[Fe^{2+}Fe^{3+}]O_4$ (Klein & Dutrow, 2007; Nadoll et al., 2014).

Table 1.1 Spinel group minerals (From Nesse, 2012)

Mineral	Composition	Mineral	Composition
Spinel Series		Magnetite Series	
Spinel	$MgAl_2O_4$	Magnetite	$FeFe_2O_4$
Hercynite	$FeAl_2O_4$	Magnesioferrite	$MgFe_2O_4$
Gahnite	$ZnAl_2O_4$	Ulvospinel	$FeFeTi_2O_4$
Galaxite	$MnAl_2O_4$	Franklinite	$ZnFe_2O_4$
Chromite Series		Jacobsite	$MnFe_2O_4$
Chromite	$FeCr_2O_4$	Trevorite	$NiFe_2O_4$
Magnesiochromite	$MgCr_2O_4$	Hausmanite	$MnMn_2O_4$

The ability of magnetite to incorporate trace elements into its crystalline structure is controlled by physical and geochemical controls such as temperature, oxygen fugacity, sulfur fugacity, silica activity, and matrix/melt composition (Dare et al., 2014; Duran et al., 2020). This makes it a potential tracer for geochemical processes, as variations in trace elements reflect the geochemical conditions and geological environment in which it crystallized. Consequently, the texture and trace element variations can be used to evaluate the geological environment at the time of its crystallization (Nadoll & Koenig, 2011; Dupuis & Beaudoin, 2011).

Different exsolutions in Ti-rich magnetite ($spinel_{ss}$) can be caused by sub-solidus re-equilibration on slow cooling in mafic to ultramafic rocks (Tan & Liu, 2016). The exsolved phases are mainly composed of ulvospinel and pleonaste and are considered to form because of the miscibility gap of the solid-solution series (Tan et al., 2016). The solvus of the pleonaste–magnetite solid solution (Ple–Mt_{ss}) lies below ~900 C, and that of the ulvospinel–magnetite solid solution (Usp–Mt_{ss}) lies below ~600 C (Tan et al., 2016).

The FeO-Fe_2O_3-TiO_2 system can be divided into a spinel series characterized by a solid solution between magnetite and ulvöspinel, and a rhombohedral series characterized by a solid solution between hematite and ilmenite (Fig. 1.1).

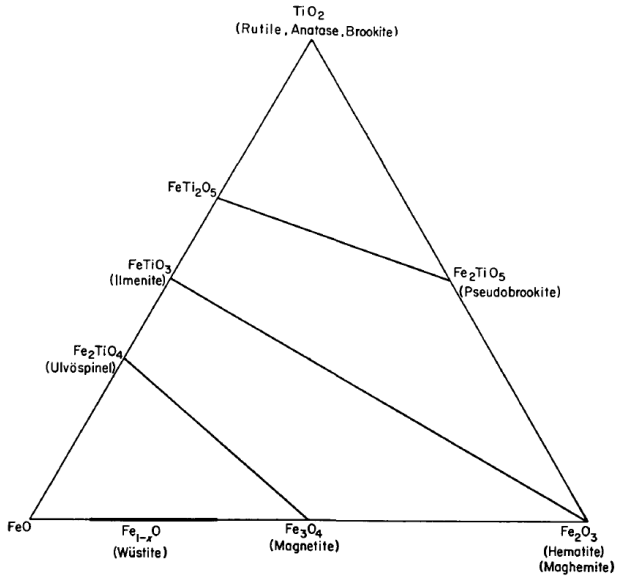

Figure 1.1. The FeO-Fe_2O_3-TiO_2 system (from Buddington and Lindsley, 1964).

Titanomagnetite is a term used for magnetite containing titaniferous exsolutions that result from the decomposition of the magnetite- ulvöspinel (solid solution) series. Ilmenite ($FeTiO_3$) inclusions in magnetite were believed to have originated by exsolution from a solid solution of the two components. However, in the early 1960s, various authors determined that the ulvöspinel (Fe_2TiO_4) component is more likely to accommodate most of the Ti (Arguin et al., 2018).

In response to a decrease in the solubility of its solid solution state at lower temperatures, ulvöspinel exsolves (Arguin et al., 2018). The solid solution between magnetite and ulvöspinel is the result of Fe^{3+} replacement by Ti^{4+} accompanied by a proportional increase in Fe^{2+} to maintain charge neutrality. Magnetite-ulvöspinel intergrowths have the appearance of a closely woven piece of cloth known as "cloth-textured" intergrowths recognizable by a network of very fine ulvöspinel lamellae (Arguin et al., 2018).

To establish the primary and secondary conditions which affected ulvöspinel-magnetite, and hematite-ilmenite preserved exsolution textures, Buddington and Lindsley (1964) suggested that either the magnetite and/or ilmenite grains were the result of secondary processes, rather than a primary intergrowth of minerals. They proposed that the solid solutions of magnetite-ulvöspinel and hematite-ilmenite coexist in equilibrium to form titanomagnetite. They also proposed that, upon cooling of the solid solution series, exsolution at submagmatic temperatures (as low as 500 °C) can occur to produce primarily magnetite-ilmenite pairs with variable titanium concentrations within magnetite and Fe_2O_3 in ilmenite.

Intergrowths of titaniferous spinel (ulvöspinel, titanomagnetite, or magnetite) with ilmenite are widespread in igneous and metamorphic rocks (Lattard, 1995). From the microtextures of natural oxide minerals. Buddington and Lindsley (1964) concluded that increasing degrees of oxidation and diffusion result in a systematic series of fabrics from (1) a single-phase homogeneous spinel; through (2) trellis intergrowths of thin ilmenite lamellae in all sets of (111) planes of the host; (3) sandwich intergrowths of thick ilmenite lamellae predominantly in one set of (111) planes; (4) granules of ilmenite within the magnetite; to (5) granules or occasional lamellae of ilmenite on the external borders of the magnetite, or recrystallized granular aggregates of ilmenite and titaniferous magnetite. Although each type may occur alone; types 2 and 3, 3 and 4, or 2, 3, and 4 may occur together in the same grain or in different grains in the same rock. Haggerty (1991) recognized the textural types described by Buddington and Lindsley (1964) and summarized them as: Trellis intergrowths involving thin ilmenite lamellae in all directions of (111) planes of the host magnetite; sandwich intergrowths with thick

ilmenite lamellae generally restricted to one direction of the (111) planes of magnetite; and composite types consist of ilmenite granules in magnetite which are generally not oriented.

In general, magnetite hosts most of the V in coarse-grained mafic igneous rocks where it is present in solid solution, with no discrete V-rich phases (Cawthorn et al., 2005). The V content of magnetite varies greatly, and the proportion of magnetite in layered mafic rocks is also highly variable (Cawthorn et al., 2005). Vanadiferous magnetite typically occurs as layers within the magmatic stratigraphy usually associated with differentiated gabbroic rocks with the grades of V in orebodies rarely exceeding 1 wt. % (Cawthorn et al., 2005).

Vanadium (V) is a minor element in the crust, averaging ~138 ppm in crustal abundance, with upper crustal abundances of ~97 ppm and lower crustal abundances of ~196 ppm (Rudnick and Gao 2003). In rocks, V concentrations range from ~40 ppm in ultramafic rocks, and ~60 ppm in granitic rocks, to ~250 ppm in basaltic rocks (Liu et al., 2018). In sedimentary rocks, the average V content of quartzitic sandstone and pure carbonate sediments is <15 ppm, with higher values in greywackes (40 to 150 ppm) and shales (90 to 260 ppm; Huang et al., 2015; Lui et al., 2018).

Vanadium is a little-known but increasingly important economic commodity. Around 85% of the V produced globally is used as an additive to steel in the form of ferrovanadium, often in combination with Cr, Ni, Mn, B, and W (Kerr et al., 2013). Alloys of V, Cr, and Ti also have suitable properties for the construction of nuclear reactors. (Kerr et al., 2013; Gilligan and Nikoloski, 2020). Vanadium typically occurs as an accessory component of minerals and is incorporated into rock-forming minerals as a trace element, since V^{3+}, V^{4+}, and V^{5+} readily substitute Fe^{3+}/Al^{3+}, Ti^{4+}, and P^{5+} in many common minerals (Huang et al., 2015; Gustafsson, 2019). Titaniferous magnetite is the principal source of mined V, it is produced primarily as a byproduct of Fe and Ti mining, associated with layered intrusions or large anorthosite complexes (Liu et al., 2008; Kerr et al., 2013; Huang et al., 2015; Gustafsson, 2019).

Vanadium deposits in mafic igneous intrusions generally occur as stratiform, Fe-Ti oxide-rich layers, in which V is primarily concentrated in titaniferous magnetite (Polivchuk, 2017). It is unclear whether the V-rich magnetite forms from immiscible Fe-Ti oxide liquid at the late-stage of tholeiitic magma differentiation or whether the titano-magnetite accumulation is the result of crystallization of a liquidus phase (Huang et al., 2015).

Host rocks of vanadium deposits are derived from the mantle by partial melting to produce mafic to ultramafic magmas (Cawthorn et al., 2005). Magmatic processes, such as fractional crystallization with crystal settling and sorting, liquid immiscibility, magma addition, and mixing, and variations in oxygen fugacity and pressure, have been linked to the development of Fe-Ti (-V) oxide deposits (Lee et al., 2022). These ore-forming processes are not mutually exclusive, and deposits may be the product of numerous processes working together in a cooling magma (Lee et al., 2022).

Major deposits of vanadium are restricted to large mafic-ultramafic igneous bodies such as the Bushveld Complex in South Africa and the Panzhihua intrusion in China (Kerr et al., 2013). For example, the Main Magnetitite Layer, which ranges in thickness from 1 to 2 m in the Upper Zone of the Bushveld Complex, comprises nearly massive magnetite layers. Magnetitite, gabbronorite, and anorthosite make up the cyclic strata in subzones A and B of the Upper Zone. Ilmenite can be found in the oxide layers that are covered by ferrodiorites in the C subzone (Ripley and Li, 2018). In gabbros from the Emeishan Large Igneous Province in China, which host Panzhihua, Hongge, Baima, and Taihe Fe-Ti oxide deposits, magnetite, titanomagnetite, and ilmenite can be found as disseminated grains. With a few lesser deposits located in the upper layers of the intrusive strata, the largest deposits are found in the lower regions of the gabbroic-layered intrusions (Ripley and Li, 2018). They are also associated with Proterozoic anorthositic rocks (Lee et al., 2022). The Kachkanar intrusion produces the bulk of V in Russia. It consists principally of clinopyroxenites and is considered an ultramafic Ural-Alaskan type intrusion. Both massive titanomagnetitite and titanomagnetite disseminated in clinopyroxenite are present (Ripley and Li, 2018).

Several authors have previously studied the geochemistry and petrogenesis of the Lac des Iles Complex, but with a focus on Pd mineralization. This study characterized the petrography and geochemical of the Magnetite Gabbro within the Mine Block Intrusion at the Lac des Iles mine with a focus on the Fe-V-Ti oxide mineralization.

The objectives of this thesis were.

1. To characterize the magnetite gabbronorite within the Mine Block Intrusion and discuss its paragenesis and magmatic history
2. To compare the magnetite gabbro with similar vanadium occurrences and deposits

Chapter 2. Regional Geology

2.1. The Superior Province

The Superior Province, one of the world's largest Archean cratons, records the formation and modification of the continental and oceanic crust in different tectonic environments over the 1.73-billion-year interval between 4.3 and 2.57 Ga (Percival et al., 2012). It is exposed in the central part of North America, covering an area of ~1,572,000 km2, and, together with other Archean cratons and Proterozoic orogens, makes up the Canadian Shield. It extends from eastern Manitoba and northern Minnesota, through Northern Ontario, and into Quebec (Fig. 2.1; Card and Ciesielski, 1985; Stott, 1997; Percival et al., 2006).

Card and Ciesielski (1985) proposed that the Superior Province consisted of four types of litho-tectonic domains (Fig. 2.1): (1) volcano-plutonic; (2) metasedimentary; (3) plutonic; and (4) high-grade gneiss. They placed the subprovince boundaries along faults (mainly along major east-west dextral transcurrent systems), zones of structural and metamorphic transition of appreciable width (in which faulting and igneous activity may have masked any primary lithological transition) or zones of lithological, metamorphic, or structural transition. Volcano-plutonic subprovinces such as the Abitibi, Uchi, and Wabigoon are characterized by dominantly metavolcanic supracrustal sequences, greenstone belts, and are bordered and intruded by voluminous felsic plutonic rocks, including early synvolcanic plutons (e.g., the Lac des Iles complex in the Wabigoon Subprovince) and tonalitic gneiss, as well as younger foliated to massive plutons ranging from quartz diorite to granite and syenite (Card & Ciesielski, 1985). The Quetico and Pontiac are metasedimentary subprovinces characterized by dominantly sedimentary supracrustal rocks, mainly turbiditic wacke, and pelite metamorphosed to schist, paragneiss, and migmatite (Card & Ciesielski, 1985).

Plutonic subprovinces such as the Winnipeg River and Winisk plutonic domains are distinguished by the near absence of supracrustal rocks (Card & Ciesielski, 1985). Plutonic rocks include tonalitic gneiss, commonly with mafic enclaves of both extrusive (metavolcanic) and intrusive (dike) origin (Card and Ciesielski, 1985). High-

grade domains contain intermediate to high-pressure upper amphibolite facies of plutonic and supracrustal origin, commonly with layered gabbro-anorthosite bodies and tonalitic, granodioritic, and syenitic intrusions, many of which are foliated and pyroxene-bearing (Card and Ciesielski, 1985).

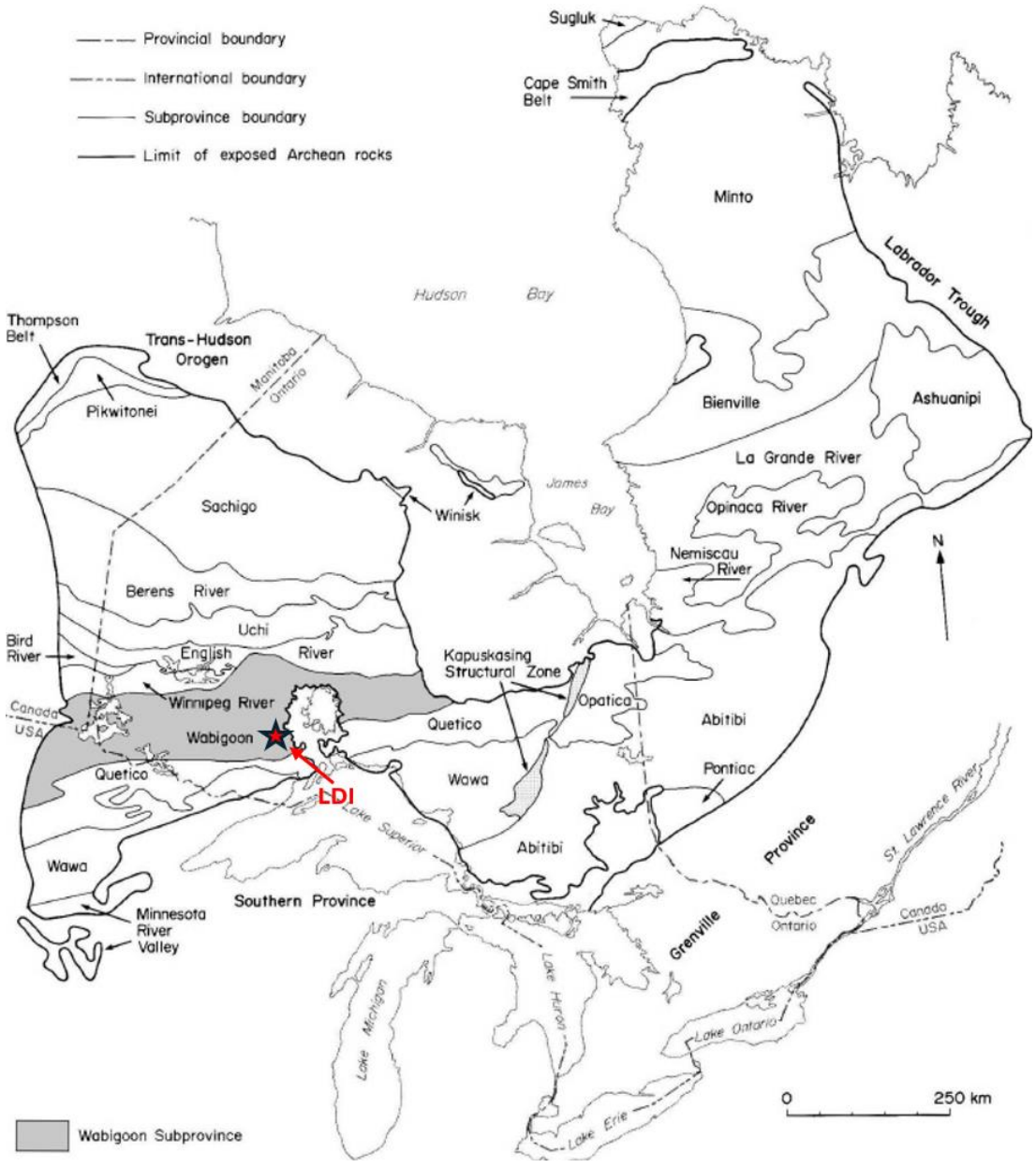

Figure 2.1. Subprovince subdivisions of the Superior Province, highlighting the Wabigoon Subprovince (From Blackburn et al., 1991).

Stott (1997) proposed that although the traditional subdivision of the Superior Province provides a basic descriptive framework and categorization based on lithology, its value is limited when tectonic analyses have been attempted. Consequently, he proposed subdividing the Superior Province into three general regions of contrasting lithotypes, ages and geophysical characteristics: 1) the Uchi-Sachigo-Goudalie (USG) superterrane of volcanic and granitoid plutonic rocks, 2) the Central Belts Domain, an aggregate of alternating, linear, volcano-plutonic, plutonic and metasedimentary terranes and superterranes, and 3) the Minnesota River Valley (MRV) gneiss terrane.

Stott et al. (2010) proposed a new subdivision of terrane and domain boundaries across the Superior Province. These subdivisions, while based in part on subprovince terminology, incorporated developments in regional bedrock geology mapping coupled with geophysical surveys and interpretations, geochronology, and geochemical and isotopic syntheses. In this scheme, a superterrane is defined as an amalgamation of two or more terranes before Neoarchean assembly of the Superior Province. Whereas a tectonically bounded region with internal characteristics distinct from those in adjacent regions prior to Neoarchean assembly of the Superior Province is a terrane. A domain is typically a younger, lithologically distinct part of a terrane, either with juvenile crust or sharing a common basement, and a tectonic or tectonostratigraphic assemblage is composed of one or more stratigraphic groups or formations distinct in lithology, time, and tectonic setting (Stott et al., 2010).

Percival et al. (2006) used geophysical interpretations and isotopic and zircon studies to propose that the western Superior Province was created by the collision of accretionary orogens where distinct protocontinental and oceanic terranes were juxtaposed during five distinct Mesoarchean orogenies to form a coherent craton by ~2.60 Ga. Although recent interpretations incorporate new mapping and modern geochronology and geophysical techniques, the boundaries used in both Stott's terrane classification system and Card and Ciesielski's subprovince system are slightly different, and the terrane classification system uses most of the names used in the subprovinces system. However, this is not the case in the study area, which lies in a zone

where both systems disagree. In this study, the terrane classification system was used, although some terms from the subprovinces system were used when necessary.

2.2. The Wabigoon Superterrane

Card and Ciesielski (1985) described the Wabigoon subprovince as a middle to late Archean volcanic-plutonic subprovince, averaging 100 km wide, that is exposed for some 900 km eastward from Manitoba and Minnesota. It is bounded to the north by plutonic and metasedimentary rocks of the Winnipeg River and English River subprovinces, and on the south by the Quetico metasedimentary subprovince (Fig. 2.1.). Plutonic rocks form large batholithic complexes both within and around the greenstone belts and can be subdivided into early, synvolcanic ultramafic, mafic and granitoid intrusions, and later, syn- to post-tectonic granitoid intrusions (Card, 1990).

Stott (1997) proposed that the Wabigoon superterrane could be subdivided into three regions; in the western portion, tholeiitic to calc-alkaline volcanic units dominate; in the central part, tonalitic gneisses, felsic plutons, and narrow greenstone belts dominate; whereas the eastern region, in part overlain by the Nipigon Embayment comprises tholeiitic subaqueous basaltic flows and associated gabbroic intrusions and three felsic volcanic centers (Fig. 2.2).

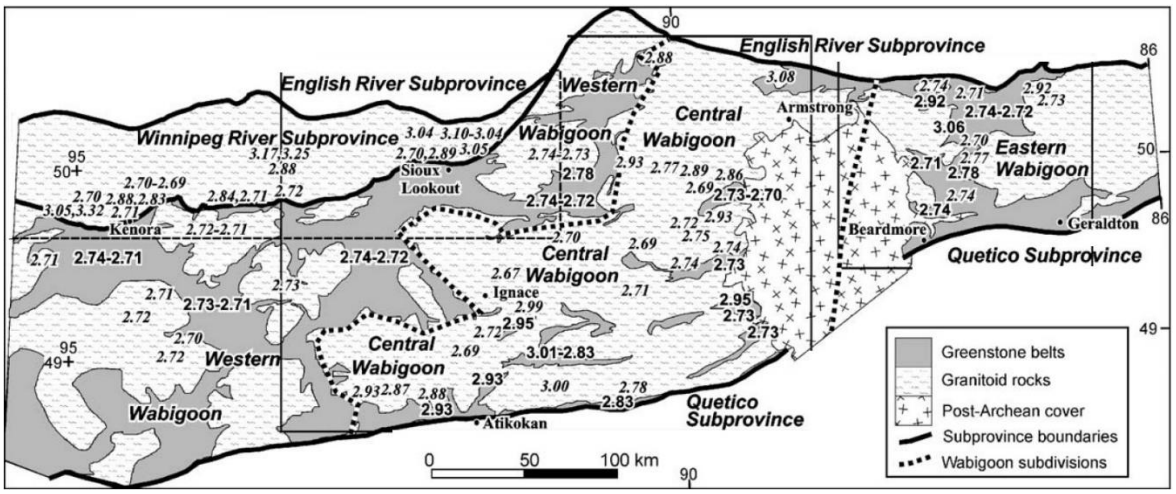

Figure 2.2 The Wabigoon subprovince. The dotted lines show the subdivisions of the Wabigoon subprovince into western, central, and eastern portions. Numbers show the age (in Ga) of selected volcanic and plutonic units (From Tomlinson et al., 2003).

Tomlinson et al. (2003) subsequently divided the Wabigoon subprovince into: 1) the western Wabigoon subprovince, which is a metavolcanic-dominated terrane with a purely Neoarchean history; 2) the eastern Wabigoon subprovince that shows a much more protracted history with crystallization ages from 3,056 Ma to about 2,680 Ma; and 3) the central Wabigoon subprovince that is dominated by several generations of tonalite and tonalite gneiss, some of which act as basement, whereas some intrude several small greenstone belts. As the southern part of the central Wabigoon subprovince shows distinct age and isotopic characteristics compared to surrounding areas it was proposed that the south-central Wabigoon subprovince, south of the Garden Lake greenstone belt, be designated the Marmion terrane (Tomlinson et al., 2003).

Percival et al. (2006) argued that the Wabigoon subprovince is a composite terrane comprising volcanic-dominated domains with a central axis of variable-age plutonic rocks. They argued that the subprovince comprises distinct western and eastern domains separated by the Marmion terrane, formerly included as part of the south-central Wabigoon subprovince. In this subdivision, the western Wabigoon domain is dominated by mafic volcanic rocks with large tonalite-granodiorite plutons. Whereas the eastern Wabigoon domain is a composite terrane with greenstone belts and intervening granitoids plutons that show variable Mesoarchean and Neoarchean ancestry. The Marmion terrane consists of 3.01-2.999 Ga Marmion tonalite basement, upon

which several greenstone belts formed between 2.99 and 2.78 Ga (Percival et al., 2006). The Marmion terrane underwent little, if any, Neoarchean (i.e., 2.745–2.72 Ga) magmatic activity in contrast to the Winnipeg River terrane to the north and the Wabigoon terranes to the west and east (Percival et al., 2006).

The Marmion Terrane may have been accreted to the Winnipeg River terrane by 2920 Ma, thereby formed part of the Winnipeg River "superterrane". At least two Neoarchean deformation events affected the Marmion terrane: east-striking D1 structures (<2706 Ma) and east-striking, dextral transpressive D2 shear zones (>2694 Ma; Percival et al., 2012).

2.3. The Lac des Iles area

The Lac des Iles area, located in the Marmion Terrane, is underlain by parts of three east-trending Archean greenstone belts consisting of felsic to intermediate and mafic to ultramafic plutonic rocks (Fig. 2.3). From south to north, the greenstone belts are the Lac des Iles, Heaven Lake, and Garden Lake belts (Stone et al., 2003). Situated approximately 100 km north-northwest of Thunder Bay, Ontario, the Lac des Iles area (Fig. 2.3) encompasses several mafic to ultramafic intrusions with associated Pd, Pt, Au, Cu, and Ni mineralization (Lavigne et al., 2005). Archean mafic to ultramafic intrusions include Buck Lake, Dog River, Taman Lake, Tib Lake, and the Lac des Iles Complex, which make up the Lac des Iles suite. These intrusions range in size from 1 to 10 km and vary compositionally from leucogabbro and gabbronorite with rare anorthosite to peridotite and pyroxenite (Stone et al., 2003; Bain et al., 2024). Uranium-lead age determinations for zircons contained in the mafic rocks showed that the Lac des Iles suite intrusions were likely emplaced between 2,699 Ma and 2,686 Ma (Decharte et al., 2018). The Lac des Iles suite has been interpreted to represent a continuum of the Quetico suite of mafic to ultramafic intrusions that are scattered over 200 km west-southwest from Lac des Iles through the southern Wabigoon and northern Quetico subprovinces (MacTavish 1999; Stone et al., 2003).

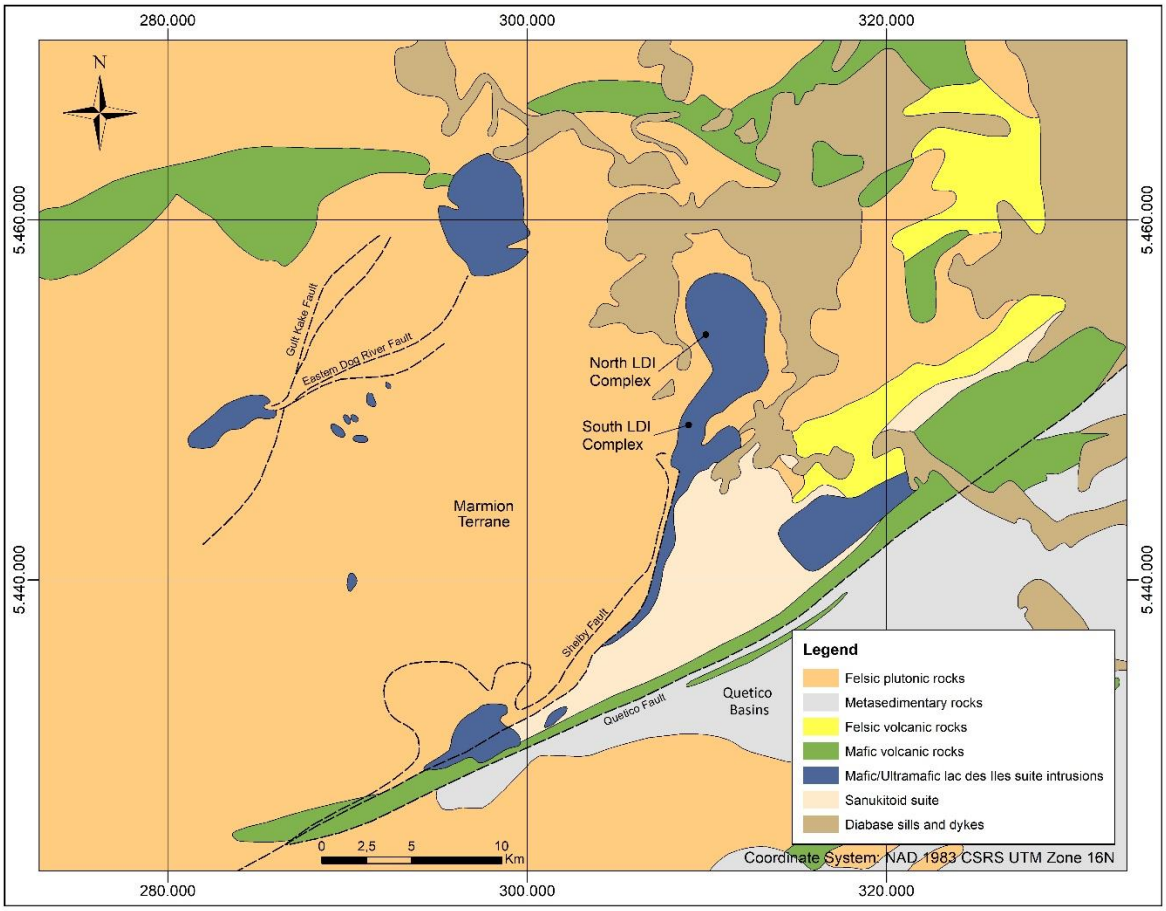

Figure 2.3 Simplified geological map of the Lac des Iles area showing mafic to ultramafic intrusions (From Djon et al., 2017). Archean mafic to ultramafic intrusions that comprise the Lac des Iles suite include Buck Lake, Dog River, Taman Lake, Tib Lake, and the Lac des Iles Complex.

The mafic components of the Lac des Iles suite intrusions are mainly norite units with gabbronorite and diorite forming the most evolved units that typically occupy the interior or upper portions of the intrusions (Decharte et al., 2018). Ultramafic components occurring in some of the Lac des Iles suite intrusions include dunite, peridotite, and pyroxenite, with orthopyroxene or clinopyroxene as the dominant ferromagnesium silicate mineral (Stone et al., 2003; Decharte et al., 2018).

2.4. The Lac des Iles Intrusive Complex (LDI-IC)

The Lac des Iles Intrusive Complex (LDI-IC) is an irregularly shaped mafic-ultramafic intrusive body extending approximately 9 km north-south and 4 km east-west (Buss et al., 2017). It is the largest of a series of mafic to

ultramafic intrusions that exhibits inward dipping igneous layering typically composed of mafic rocks including leucogabbro, hornblende gabbro, norite, and gabbronorite, with minor anorthosite and magnetite gabbro. The LDI-IC can be divided into a dominantly mafic suite of intrusions occurring to the south, the South LDI, and a suite of complexly nested layered intrusions composed predominantly of ultramafic cumulates called the North LDI (Fig. 2.4; Lavigne et al., 2005; Djon, 2017). The Neoarchean LDI-IC intrudes tonalitic gneisses of the Marmion Terrane (Tomlinson et al., 2003), immediately north of the Wabigoon-Quetico subprovince boundary (Fig. 2.3). The LDI-IC and related intrusions were emplaced synchronously with sanukitoid magmatism, along pre-existing northeast-trending fault splays at the collisional structural boundary zone between the Quetico and Wabigoon subprovinces (Djon, 2017).

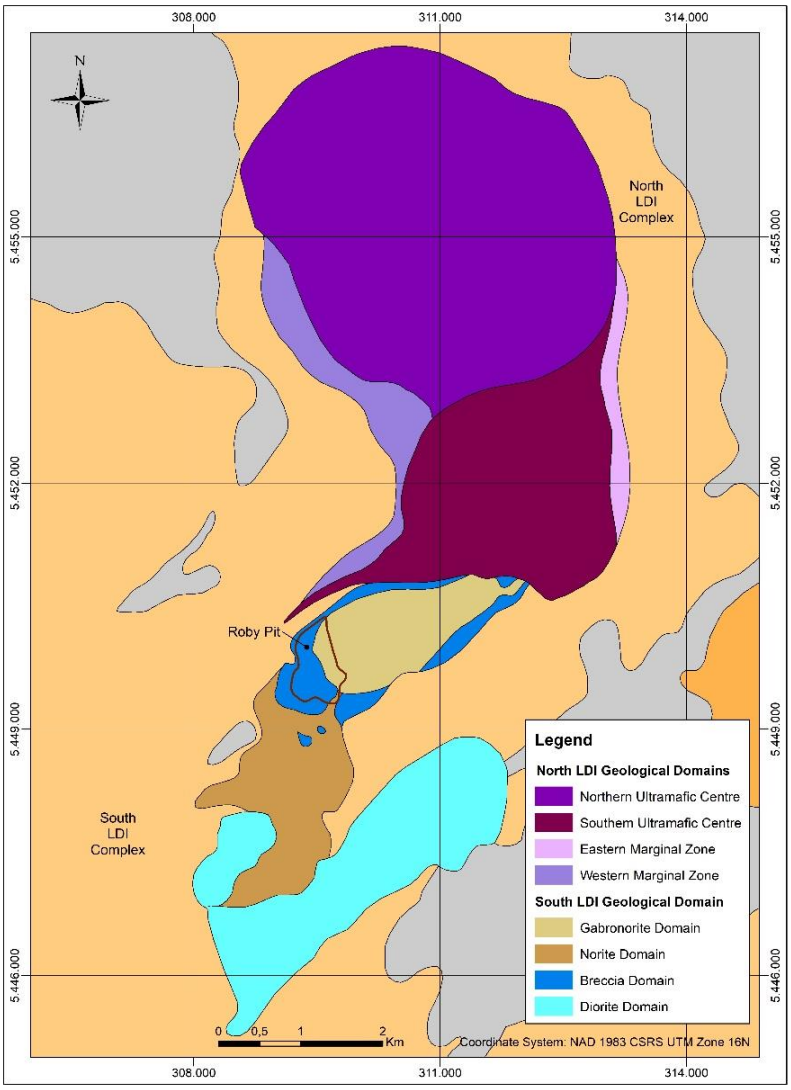

Figure 2.4. Simplified geological map of the Lac des Iles complex and location of the open pit of the Lac des Iles mine (From Djon et al., 2017).

The North LDI is a composite, tadpole-shaped (6 by 4.5 km) and predominantly ultramafic intrusive body with minor occurrences of mafic rocks (Fig. 2.4). It comprises a stacked series of relatively flat-lying, saucer-shaped bodies emplaced into intermediate orthogneiss basement rocks. Based on the distribution of rock types, orientation of layering, and trends of regional aeromagnetic anomalies, two major intrusive centers have been identified – the Northern Ultramafic Centre (NUC) and the Southern Ultramafic Centre (SUC; Djon et al., 2017).

The western flank of the Northern Ultramafic Centre comprises a marginal hornblende gabbro and associated hornblendite units (Djon et al., 2017). In contrast, the eastern flank can be divided into two major zones. The Eastern Marginal Zone and the Layered Series, which consists of at least fourteen cyclic units of ultramafic cumulates with minor gabbroic (plagioclase-bearing) intervals (Djon et al., 2017). Cyclic variations in cumulate rock types similar to those observed in the NUC are locally recognized in the SUC. Field observations indicate that the SUC is a concentrically zoned body with a largely wehrlite core surrounded by websterite and locally cut by gabbronorite (Djon et al., 2017). Historical surface prospecting, mapping, limited trenching, and diamond drilling have identified several areas in the North LDI that host platinum group elements (PGE) occurrences exceeding 1.0g/t of combined Pd+Pt+Au. These PGM occurrences are interpreted to represent stratiform or reef-type magmatic PGM mineralization (Implats, 2022).

The South LDI is a horseshoe-shaped area 6 km long by 1.5–2.5 km wide that is composed from North to South of three discrete intrusions, namely the Mine Block, South Lac des Iles, and Camp Lake (Fig. 2.5). The Mine Block Intrusion is a small, teardrop-shaped mafic complex with maximum dimensions of 3 km by 1.5 km elongated east-northeast that was emplaced into predominantly intermediate orthogneiss basement rocks (Lavigne & Michaud, 2001). The geology of the Mine Block Intrusion (Fig. 2.5) is dominated by a structurally and texturally complex suite of gabbronorite and magnetite-rich gabbronorite, and a later series of noritic rocks and their metamorphosed and/or hydrothermally altered equivalents with highly variable plagioclase-pyroxene proportions, textures and structures (Lavigne and Michaud, 2001). Accessory igneous minerals include magnetite and titanium-rich magnetite, ilmenite, and quartz-feldspar granophyre (Buss et al., 2017). The Mine Block Intrusion is the best known of the individual intrusions within the LDI-IC due to the presence of significant Pd-rich PGE mineralization that has been mined since 1993 (McCracken et al., 2013).

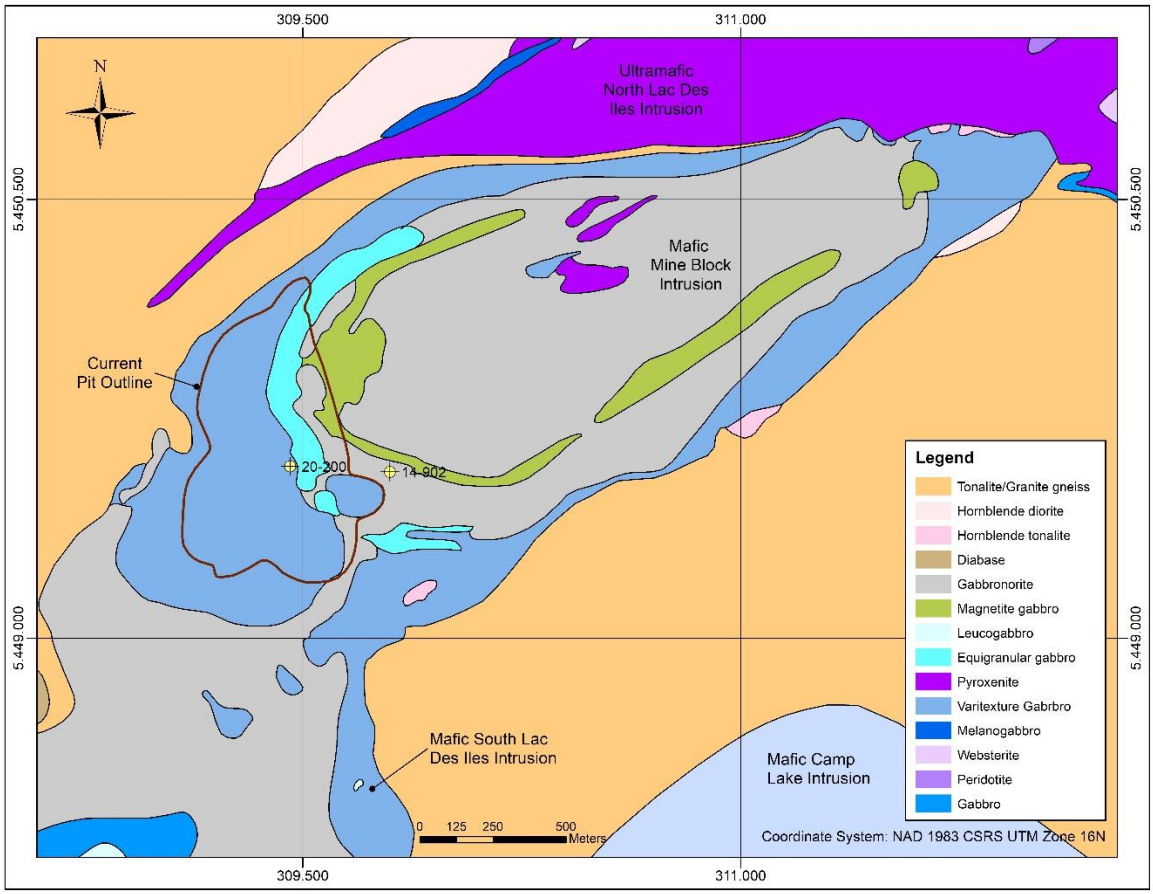

Figure 2.5. Simplified geological map of Mine Block Intrusion Complex and location of the open pit of the Lac des Iles mine (From North American Palladium, 2020).

The South LDI and Camp Lake intrusions are poorly exposed and poorly characterized. The South LDI comprises noritic rocks with many similarities to the western part of the Mine Block Intrusion in terms of petrology and textures (Djon et al., 2017). Anomalous PGE abundances in excess of 1 g/t Pd + Au have been recognized from historical surface sampling and limited drilling in the South LDI intrusion (Djon et al., 2017). In contrast, limited exploration of the Camp Lake Intrusion suggests that it is a relatively homogeneous body of hornblende gabbro that lacks significant PGE enrichment (Djon et al., 2017).

Based on a review of the mineralogical, petrological, geochemical, and geophysical characteristics of the major rock units within the South LDI, Decharte et al. (2018) presented a revision to the general Lac des Iles deposit

model that defined four major intrusive sequences or series (Fig. 2.6) in three discrete magmatic episodes in the southern area. The oldest series is the gabbronorite series and consists of a plagioclase-rich, equigranular gabbronorite unit, and a magnetite-rich gabbronorite unit. Subsequently, a major period of noritic magmatism produced the norite and breccia series. Finally, the youngest magmatism produced the diorite series, which is dominant in the southwestern part of the complex.

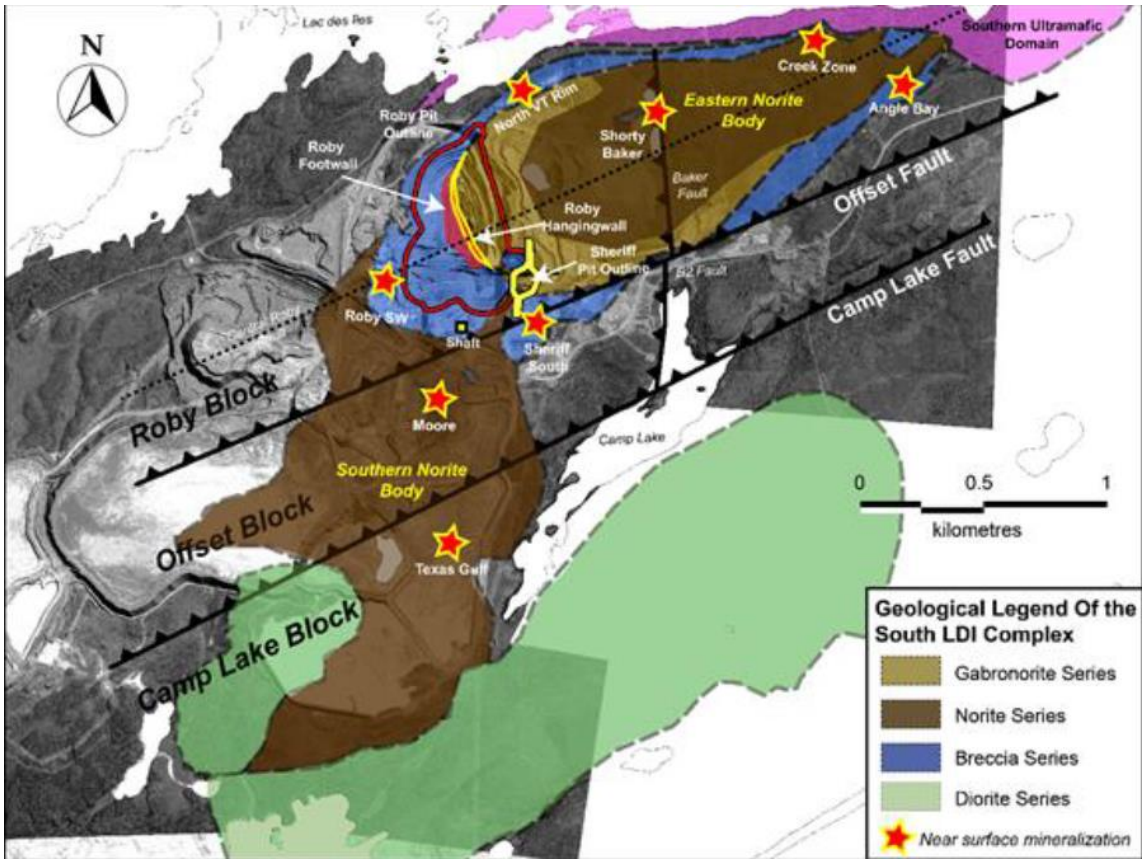

Figure 2.6. Simplified revised geological interpretation map of the South LDI Complex (From Decharte et al., 2018).

2.5. The Lac des Iles Palladium Deposit

Geological mapping began in the early 1930s and continued in the 1960s after aeromagnetic anomalies were recognized in the late 1950s (Implats, 2022). Different companies undertook various exploration programs. Open-pit production started after the land changed ownership to North American Palladium Limited in 1993 (Implats, 2022). Open-pit mining initially centered on the Roby Zone. Underground mining with ramp access began in 2006. A large mine expansion that included the development of the ramp system and the excavation of a shaft to access the Offset Zone for underground mining started in 2010 (Implats, 2022). In the primary Offset Zone, the switch from longhole stopping to sub-level shrinkage (SLS) mining began in 2016. In 2019, Impala Platinum Holdings Limited acquired North American Palladium Limited to form Impala Canada Limited (Implats, 2022). Platinum group element mineralization occurs in a variety of structural and geological settings but is predominantly associated with the presence of small amounts (<1–3%) of fine- to coarse-grained disseminated Fe-Cu-Ni sulfides (Lavigne et al., 2005). The sulfides occur within broadly stratabound zones of PGE and Au enrichment commonly associated with varitextured gabbroic rocks, coarse-grained noritic rocks, and areas of intense alteration (amphibole and, chlorite) and shearing (Lavigne et al., 2005). As of 2022 the Mineral Reserves are 40.4 Mt @ 1.90 g/t Pd, 0.18 g/t Pt, 0.14 g/t Au, 0.06% Ni, 0.06% Cu (Impala Platinum Holdings Limited, 2022).

Chapter 3. Methods

3.1. Sampling

Sampling was conducted from two drill holes that cut approximately 300 m of the magnetite gabbro body of the Lac Des Iles mine. The company provided core logs, drill collar locations, and downhole surveys from drill holes 14-902 and 20-200. The location of the drill hole collars is listed in Table 3.1.

Table 3.1. Location of drill collars and orientation of drill core.

Drill hole	Projection UTM	North	East	Elevation	Collar dip	Collar Az
14-902	NAD83 Zone 16	5449569.18	309799.35	507	-49.13	267.40
20-200	NAD83 Zone 16	5449588.11	309457.97	511	0.10	74.13

With a KT10 magnetic susceptibility meter, spot measurements were acquired every 25 centimeters to define areas with high and low magnetic susceptibility across different lithologies (Fig. 3.1). Seventy-five representative mineralized samples from the magnetite gabbronorite observed in the two drill holes were collected (Fig. 3.1).

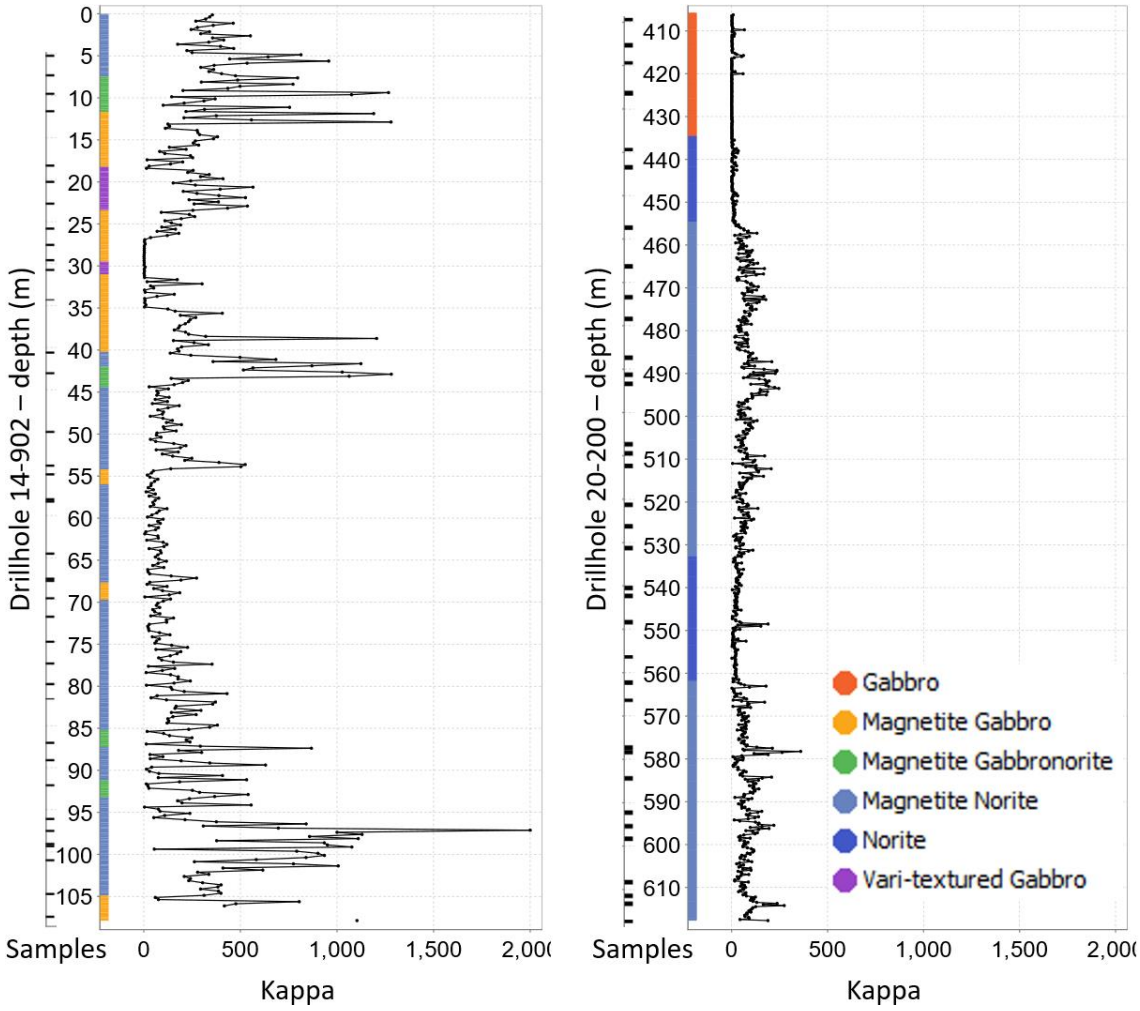

Figure 3.1. Magnetic susceptibility and sample location in drill holes 14-902 and 20-200.

Based on lithology and oxide contents, 58 samples were sent to the lapidary laboratory at Lakehead University to be made into polished thin sections. The thin sections were prepared to examine mineral compositions across layers. The polished thin sections were taken from the same samples used for geochemical analysis. Polished thin sections were made for petrographic studies using transmitted and reflected light microscopy, scanning electron microscopy (SEM), and Laser Ablation Inductively Coupled Mass Spectrometry (LA-ICP-MS).

3.2. Whole Rock Geochemistry

Seventy-four samples from representative mineralized samples from both drill holes were sent to ALS Geochemistry laboratory in Thunder Bay. Samples were prepared using the preparation package (PREP-31) in which at least 70% of the sample was crushed to less than 2 mm, then 250 representative grams are pulverized until 85% can pass through 75 μm. Then, for whole-rock major, minor, and trace element geochemical analysis, the complete characterization package (CCP-PKG01) was run. This package combines whole rock analysis, trace elements by fusion, aqua regia digestion for the volatile trace elements, carbon, and sulphur by combustion analysis (ALS, 2021).

Table 3.2. CCP-PKG01 ALS Package.

Package	Method	Analyte(s)	Description
CCP-PKG01	ME-ICP06	SiO_2; Al_2O_3; Fe_2O_3; CaO; MgO; Na_2O; K_2O; Cr_2O_3; TiO_2; MnO; P_2O_5; SrO, and BaO	Fusion decomposition followed by ICP-AES measurement
	OA-GRA05	LOI	Loss on Ignition at 500ºC after the sample is pre-dried at 105ºC.
	C-IR07	C (Total)	Total carbon by induction furnace/IR.
	S-IR08	S (Total)	Total sulfur by induction furnace/IR.
	ME-MS81	Ba, Ce, Cr, Cs, Dy, Er, Eu, Ga, Gd, Ge, Hf, Ho, La, Lu, Nb, Nd, Pr, Rb, Sm, Sn, Sr, Ta, Tb, Th, Tm, U, V, W, Y, Yb, Yb, and Zr	Four acid digestion followed by ICP-AES measurement
	ME-MS42	As, Bi, Hg, In, Re, Sb, Se, Te, and Tl	Aqua regia digestion followed by ICP-MS measurement
	ME-4ACD81	Ag, Cd, Co, Cu, Li, Mo, Ni, Pb, Sc, and Zn	Four acid digestion followed by ICP-AES measurement

3.3. Petrography

Petrographic studies were carried out using the Olympus BX2M microscope at Lakehead University to determine modal mineralogy, alteration, magnetite texture, and mineral assemblages. Photomicrographs were taken using an Olympus SC180 camera. Optical analysis was used to identify representative grains and microtextures of magnetite and ilmenite, which were subsequently analyzed using SEM and LA-ICP-MS. Microscope Images of entire thin sections were obtained using a Metasystems automated digital microscope

where individual images were automatically captured in combination with a motorized microscope, motorized stage, and a high-resolution camera. Complete petrographic descriptions are provided in Appendix A.

3.4. Scanning Electron Microscopy (SEM)

A representative subset of fourteen thin sections was selected based on magnetite content and iron oxide exsolution textures. The SEM was then used to characterize the nature of magnetite. This includes determining the V_2O_5 content of the magnetite and identifying and quantifying the amount of ilmenite exsolution lamellae, inclusions, and intergrowths within the magnetite.

Polished thin sections were carbon coated using an Edwards Auto 306 Carbon Coater. Measurements of major-elements chemistry of magnetite, its textures, mineral inclusions, and exsolutions were conducted at the Lakehead University Instrumentation Laboratory (LUIL) using a Hitachi SU-70 Schottky Field Emission Scanning Electron Microscope (SEM) outfitted with an Oxford Aztec 80mm/124eV Energy-dispersive X-ray spectrometer (EDS). The beam was calibrated to a standard nickel block. At the start of each session and periodically, EDS was tested on a "GI-Ilmenite" standard to ensure an accuracy of within 1% of the true value total for the ilmenite.

3.5. Laser Ablation Inductively Coupled Mass Spectrometry (LA-ICP-MS)

The in-situ concentrations of trace elements in coarse-grained (i.e. primary) magnetite were analyzed using single-line rasters with LA-ICP-MS on polished thin sections from Fe-Ti oxides from the mine block intrusion. Trace element concentrations in magnetite and secondary ilmenite were determined by LA-ICP-MS at the Laboratoire des Matériaux Terrestres (LabMaTer), Université du Québec à Chicoutimi following the methods of Dare et al. (2014) using an Agilent 7700x ICPMS interfaced to a Laurin technic S155 RESolution (193 nm-ArF excimer laser ablation system). Line analyses were performed on the identified textural types of magnetite and ilmenite, where coarse enough to do so, to determine the composition of the mixture mostly consisting of

magnetite and ilmenite, which better represents the original composition before the exsolution process started. Three certified reference materials were used for external calibration of the LA–ICP-MS data: a) GSE, which is a synthetic glass supplied by the United States Geological Survey (USGS), was used to calibrate all elements. b) GP6, and c) BC28 which is a natural magnetite from the Main Magnet Seam of the Bushveld Complex, were both used as in-house reference materials to monitor the calibration of GSE.

Data gathered by LA-ICP-MS were reduced using the Iolite software version 4.8.3 (Iolite, Carlton, Australia) by subtracting the gas blank from each of the analyzed isotopes, which allowed for manual selection within the spectra for regions of interest to be integrated. The comparison of elements such as Fe, Ti, and Si allowed the selection and integration of areas of interest in the spectrum where magnetite was cleaner, thus avoiding contaminated sections, including silicates (Fig. 3.2).

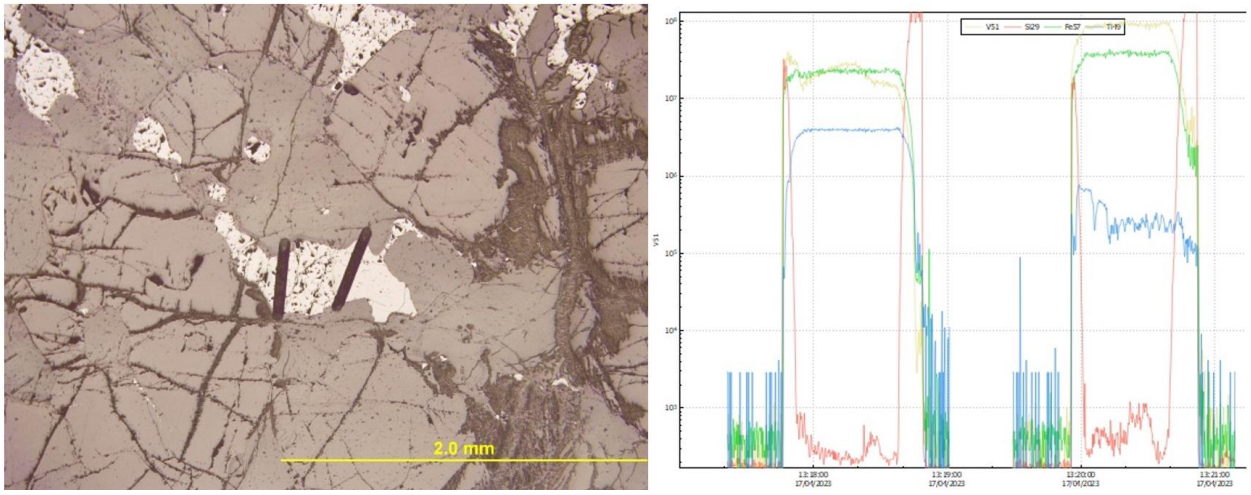

Figure 3.2. Laser ablation lines in SB021 grain 024 and laser ablation spectra illustrating clean magnetite and clean ilmenite.

3.6. Micro X-Ray Fluorescence (μXRF)

Micro x-ray fluorescence (μXRF) is a non-destructive elemental analysis technique used here to generate maps for individual elements to incorporate ilmenite granules back into titanomagnetite. Micro-X-ray fluorescence spectroscopy was completed at the Laboratoire de Microanalyse of the Universite Laval. The operation

conditions of the Tornado M4 (Bruker) with two detectors and a rhodium tub were: model 1, voltage: 50 kV, current: 600 μA, step: 20 μm, time: 5 ms.

Chapter 4. Results

4.1. Field Observations

Core logging was completed on core collected from two drill holes that cut a magnetite-enriched mafic unit of the Mine Block Intrusion. A total of 335 m of core was logged. When the rock was weakly altered, it was possible to identify bronzite by its characteristic high reflectivity and semi-translucent appearance; however, it was generally not possible to distinguish between orthopyroxene and clinopyroxene. In this case, the rock was classified as a gabbronorite and magnetite gabbronorite. The field terms "magnetite-gabbro", "magnetite-norite", and "magnetite-gabbronorite" used by the Impala Canada exploration team are referred to here as lithological domains (Fig. 4.1).

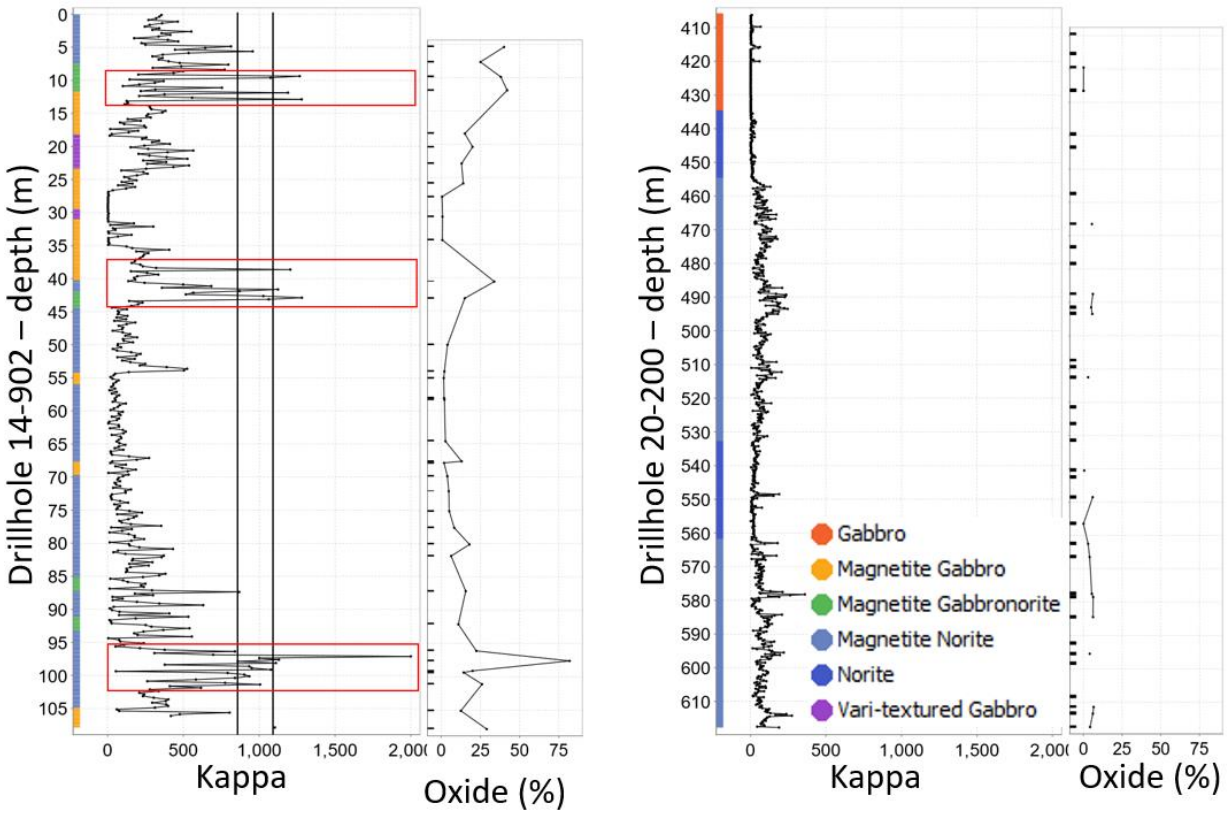

Figure 4.1. Magnetic susceptibility compared with Fe-Ti oxide content. Red squares showing massive magnetite layers.

Drill hole 14-902 intercepts the magnetite gabbro from 0.00 to 110.91 m. The unit is a brown to green and grey, layered, medium-grained gabbronorite rock. It comprises subhedral laths of plagioclase (7 to 63 %) and anhedral to subhedral pyroxene (11 to 80 %), and hosts disseminated and net-texture magnetite and magnetite layers (up to 81 %) with a massive layer at 97 m (Fig. 4.2). Traces of disseminated pyrite are visible, especially towards altered sections and filling fractures. Pyroxene is altered by chlorite and amphibole. The unit is cut by felsic and mafic veins and dykes.

Figure 4.2. Layered, medium-grained mafic intrusive rock showing magnetite layers. Drill hole 14-902.

Drill hole 20-200 intercepts the magnetite gabbro from 403.23 to 618.70 m. The rock unit consists of a dark green to purple and grey, granular groundmass with subhedral fine- to coarse-grained plagioclase (30 to 69 %), and fine subhedral pyroxene (30 to 70 %) with moderate to strong chlorite and amphibole alteration. Magnetite (up to 6.6 %) occurs interstitially and as veins. Trace disseminated pyrite is also present. The unit is cut by felsic and mafic veins and dykes.

Magnetic susceptibility measurements were classified as low (0.57-700), medium (701-1100), and high (1101-2000). Compared to drill hole 14-902 where the magnetic susceptibility reaches values between 1000 and 2000, drill hole 20-200 shows a lower magnetic susceptibility likely due to a lower Fe oxide content (Fig. 4.1). Magnetic susceptibility measurements are presented in Appendix B.

4.2. Petrography

A total of 58 thin sections were prepared from drill holes 14-902 and 20-200 from the magnetite gabbro of the Mine Block Intrusion. Due to the difficulty in distinguishing orthopyroxene and clinopyroxene caused by their alteration and the abundance of Fe oxides, a modification of the IUGS classification proposed by Kuzmich (2014) was utilized. This modification specifically considered the Fe oxide content present, and the identification process followed the classification system established by the International Union of Geological Sciences (IUGS). During the petrographic and mineral analysis, the rock units were classified based on the dominant silicate minerals, and a prefix modifier was applied to these classifications, using the relative proportions of Fe oxides, as depicted in Figure 4.3.

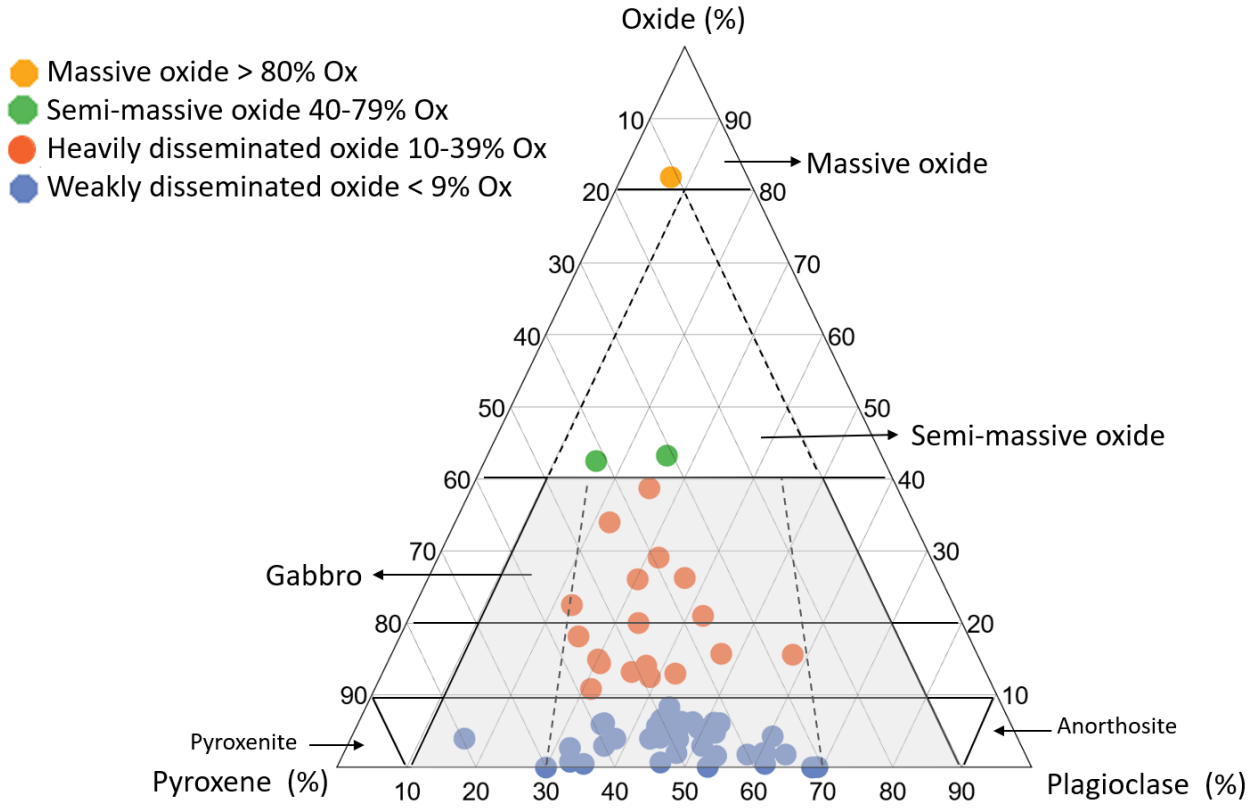

Figure 4.3. Rock classification chart (oxides = magnetite + ilmenite) from magnetite gabbronorite at Lac des Iles. Modification of the IUGS classification used by Kuzmich (2014).

The degree of alteration was classified as weak in rocks where it was possible to identify plagioclase and pyroxene crystals, moderate when it was not possible to distinguish pyroxene crystals, and strong when, in

addition to pyroxene, plagioclase was difficult to distinguish (Fig. 4.4). Alteration assemblages were common within the magnetite gabbronorite unit, ranging from weakly to strongly altered. The main alteration assemblages were tremolite, actinolite, and epidote that altered pyroxenes and sericite, talc, and chlorite that altered plagioclase. Alteration minerals range from weak, occurring as replacement rims around silicates or along fractures, to pervasive as masses or fibrous to tabular replacements. Tremolite and actinolite form discrete tabular and bladed very fine- to medium-grained crystals. Epidote occurs as very fine granular crystals along with talc and chlorite. Masses of very fine fibrous crystals of talc and chlorite are often found as interstitial alteration products of the main silicates.

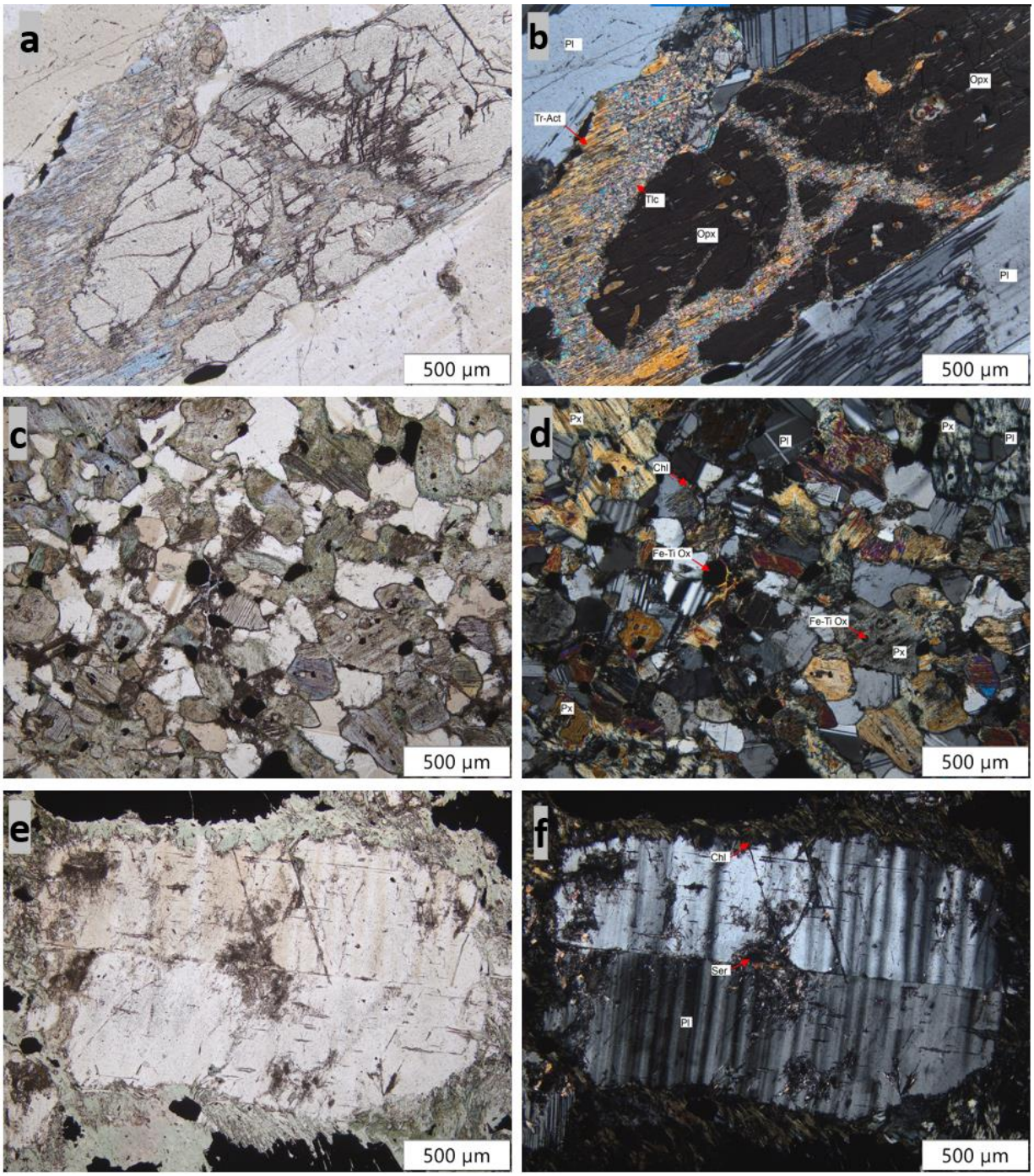

Figure 4.4. Degree of alteration. Weak with orthopyroxene slightly altered to talc and tremolite-actinolite, a) ppl – b), xpl), moderate with pyroxene complete altered to tremolite-actinolite and chlorite, c) ppl – d), xpl), and strong with plagioclase altered to sericite and chlorite and pyroxene complete altered to tremolite-actinolite, e) ppl – f) xpl).

Using this classification, host rocks in this study are predominantly weakly disseminated Fe-Ti oxide gabbros (n=37), heavily disseminated Fe-Ti oxides gabbros (n=18), semi-massive Fe-Ti oxides (n=2), and massive Fe-Ti oxide (n=1).

Massive oxide and semi-massive oxide are the main Fe-oxide lithology. The oxide is composed of 40-82 % magnetite, 7 – 25 % plagioclase, 11 – 39 % pyroxene, 0.2 – 6 % sulfide, and they are moderate to strongly altered. Heavily and weakly oxide-disseminated gabbronorite comprise the main silicate lithology. The gabbronorite is composed of 25-75 % plagioclase, 25-65 % pyroxenes, 1-5% sulfides, and 1-39 % oxides, and they are weakly to strongly altered.

Plagioclase is the predominant feldspar in the heavily and weakly disseminated oxides. The grains are euhedral to subhedral and range from 1 to 4 millimeters. Plagioclase shows bending of the twin planes (Fig. 4.5a and b). Alteration of plagioclase (Fig. 4.5 c and d) ranges from weak, consisting of sericitization along fractures to moderate, with replacement of the plagioclase by sericite and chlorite.

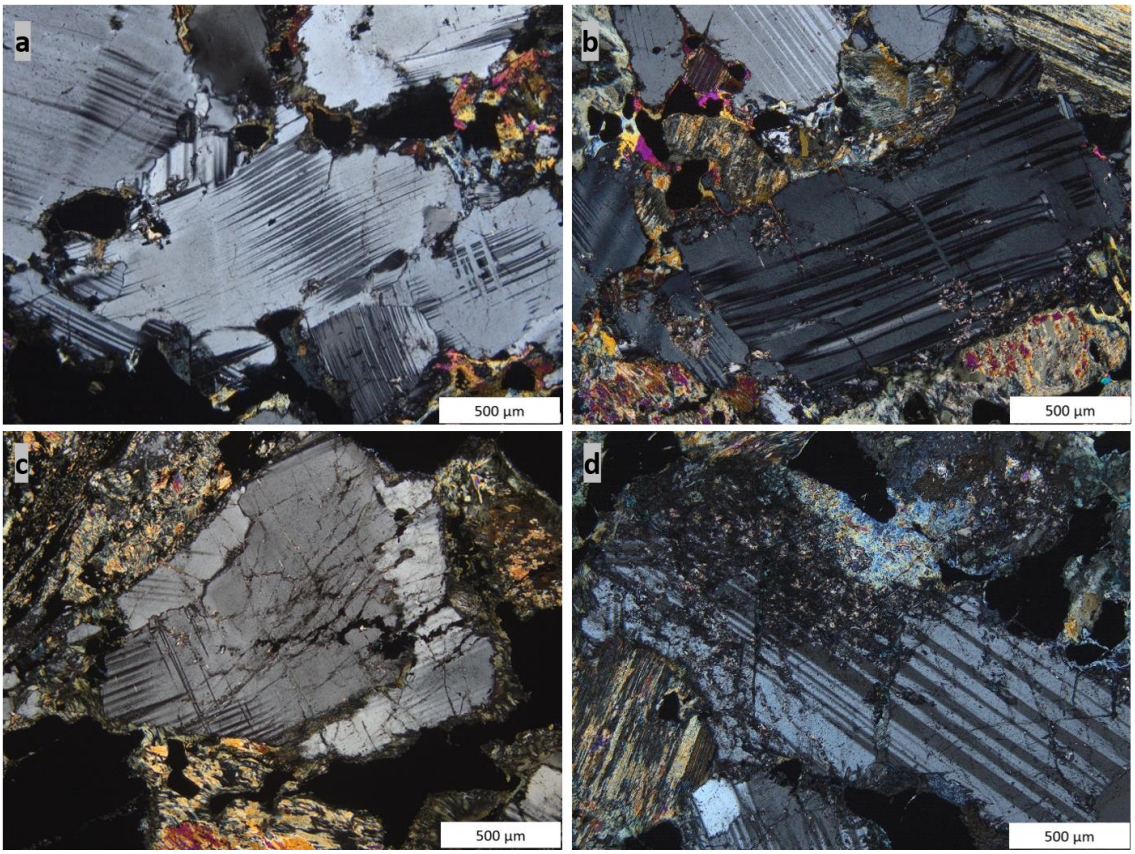

Figure 4.5. Bending of the twin planes in plagioclase. a) Sample SB003 (transmitted light — xpl). b) Sample SB008 (transmitted light — xpl). c) Subhedral plagioclase crystal weakly sericite altered. Sample SB013 (transmitted light — xpl). d) Euhedral to subhedral plagioclase crystals intensely sericite altered. Sample SB017 (transmitted light-xpl).

Compositional data for plagioclase from the magnetite gabbronorite at LDI was obtained from 17 EDS analyses and is presented in full in Appendix C. Representative compositions are presented in Table 4.1 with structural formulae calculated on the basis of eight atoms of O. The major oxides range from 28.5 to 31.2 wt. % (Al_2O_3), 45.2 to 52.1 wt. % (SiO_2), and 2.8 to 4.4 wt. % (Na_2O). The plagioclase composition plot along the labradorite-bytownite join between 24-40 (apfu) Ab (Ca-Plagioclase; Fig. 4.6).

Table 4.1. Representative compositions of plagioclase from magnetite gabbronorite at LDI. Below detection limit (bdl).

Sample	SB027	SB029	SB036
Grain	pl3	pl5	pl5-2
Na_2O	3.5	4.09	4.4
MgO	bdl	bdl	bdl
Al_2O_3	30.92	29.92	30.09
SiO_2	50.5	52.12	51.84
K_2O	0	0	0
CaO	14.88	13.4	13.23
FeO	bdl	bdl	0.32
Total	99.8	99.52	99.89
Structural formulae calculated on the basis of 8 oxygens			
Ca (apfu)	0.72	0.64	0.63
Na (apfu)	0.30	0.35	0.38
K (apfu)	0	0	0

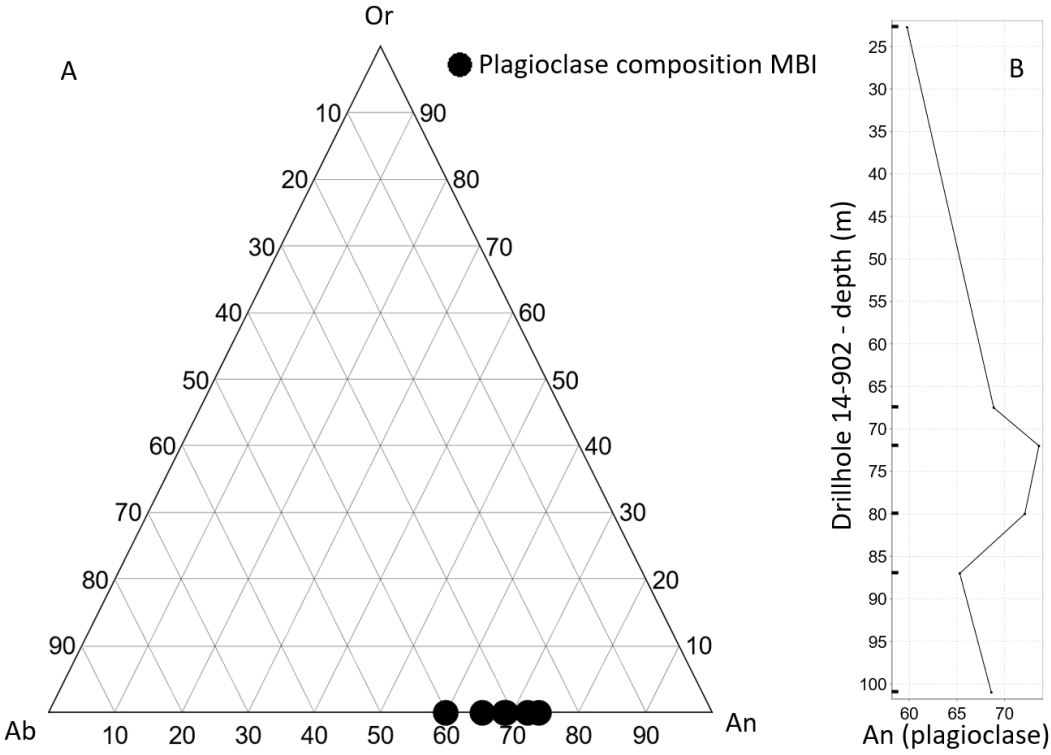

Figure 4.6. Magnetite gabbronorite plagioclase composition. A) ternary diagram. B) 14-902 drill hole

Pyroxenes grains range from 1 to 3 mm. They are generally subhedral to rounded and make up between 25 and 65 modal percent of the rock. Alteration of pyroxene to actinolite-tremolite and talc occurs along fractures and at the edges of the pyroxene grains. In most of the samples, the pyroxene has been completely replaced by fine-grained acicular actinolite-tremolite mats, talc, and chlorite (Fig. 4.7).

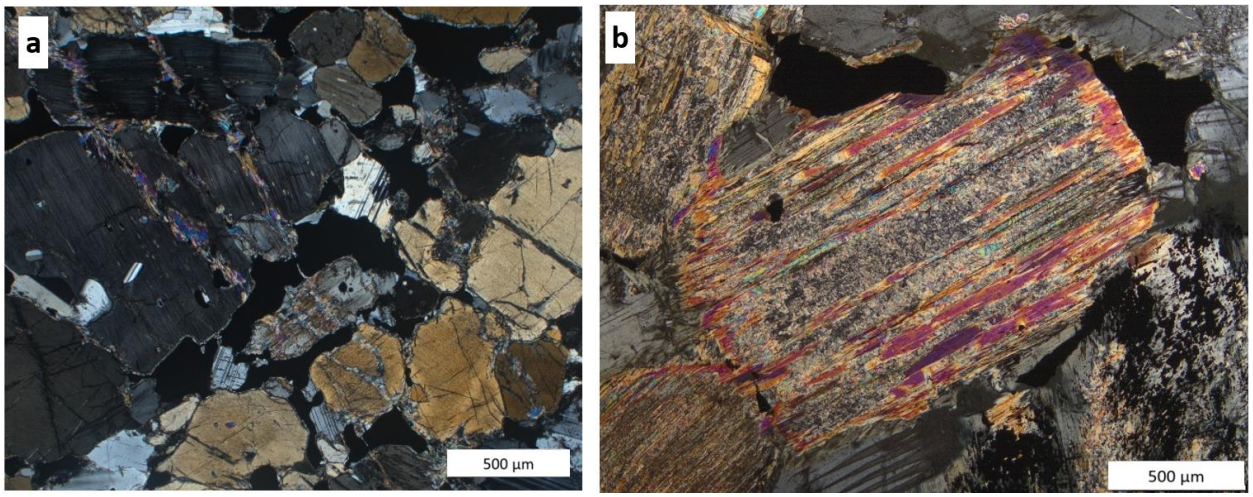

Figure 4.7. Orthopyroxene alteration. a) Euhedral to subhedral medium- to coarse-grained orthopyroxene grains occurring with weakly sericite-altered plagioclase and Fe-oxide grains. Sample SB020 (transmitted light — xpl). b) Subhedral coarse-grained pyroxene grain intensely tremolite-altered. Sample SB030 (transmitted light-xpl).

Compositional data for pyroxene from the magnetite gabbronorite at LDI was obtained from 10 EDS analyses and is presented in full in Appendix C. Representative compositions are presented in Table 4.2 with structural formulae calculated on the basis of six atoms of O. Major oxide content ranges from 8.4 to 19.1 wt. % (FeO), 13.3 to 24.7 wt. % (MgO), and 0.8 to 12.7 wt. % (CaO). The pyroxene plot in the clinopyroxene field (augite) and the orthopyroxene field (enstatite; Fig. 4.8).

Table 4.2. Representative compositions of pyroxene from magnetite gabbronorite at LDI. Below detection limit (bdl).

Sample	SB027	SB029	SB029
Grain	px2	px-1	px5-1
Na_2O	bdl	0.41	0.48
MgO	24.19	16.61	16.47
Al_2O_3	2.43	2.74	3.19
SiO_2	51.93	53.41	53.39
TiO_2	0.37	bdl	bdl
CaO	1.21	12.31	12.16
MnO	0.39	bdl	bdl
FeO	19.07	11.95	12.38
Total	99.59	97.43	98.07
Structural formulae calculated on the basis of 6 oxygens			
Ca (apfu)	0.0	0.5	0.5
Mg (apfu)	1.3	0.9	0.9
Fe (apfu)	0.6	0.4	0.4

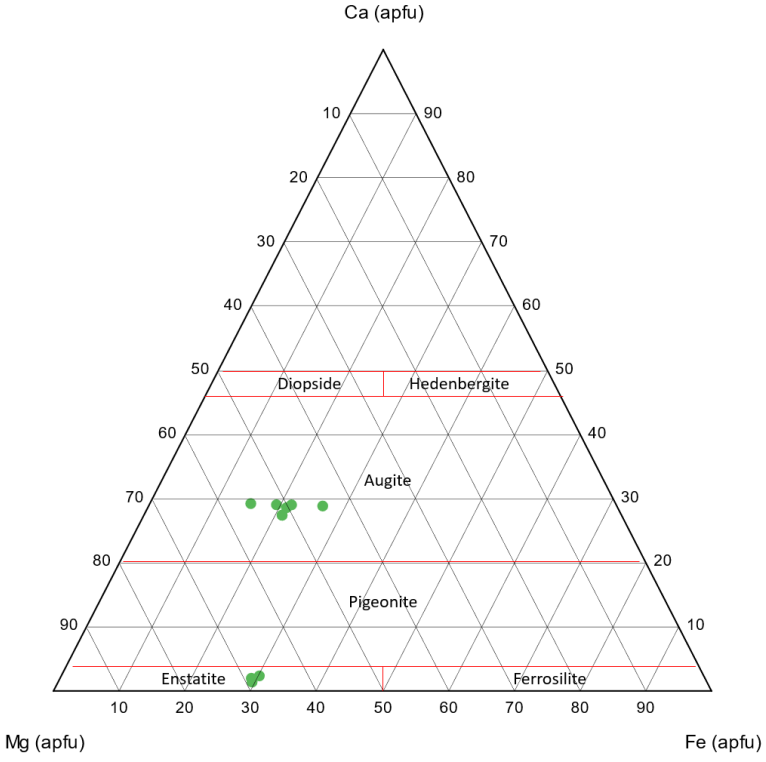

Figure 4.8. MBI magnetite gabbronorite pyroxene compositions plotted on a ternary diagram.

Sulfides are ubiquitous throughout the heavily and weakly disseminated oxides and are generally disseminated, forming interstitial patches to the silicates (Fig. 4.9). The percentage of sulfides varies from 1 to 5 modal percent, with sizes between 1 to 5 millimeters. Pyrite is the most common sulfide and occurs as blebs of anhedral to subhedral fine- to medium-grained grains, occasionally filling veins. Chalcopyrite, the second most prevalent sulfide, is commonly found in two forms: embedded as small inclusions within pyrite crystals or as separate anhedral fine-grained particles closely linked to pyrite. Pyrrhotite and pentlandite are quite rare but when present, they occur as fine-grained anhedral grains associated with pyrite and magnetite.

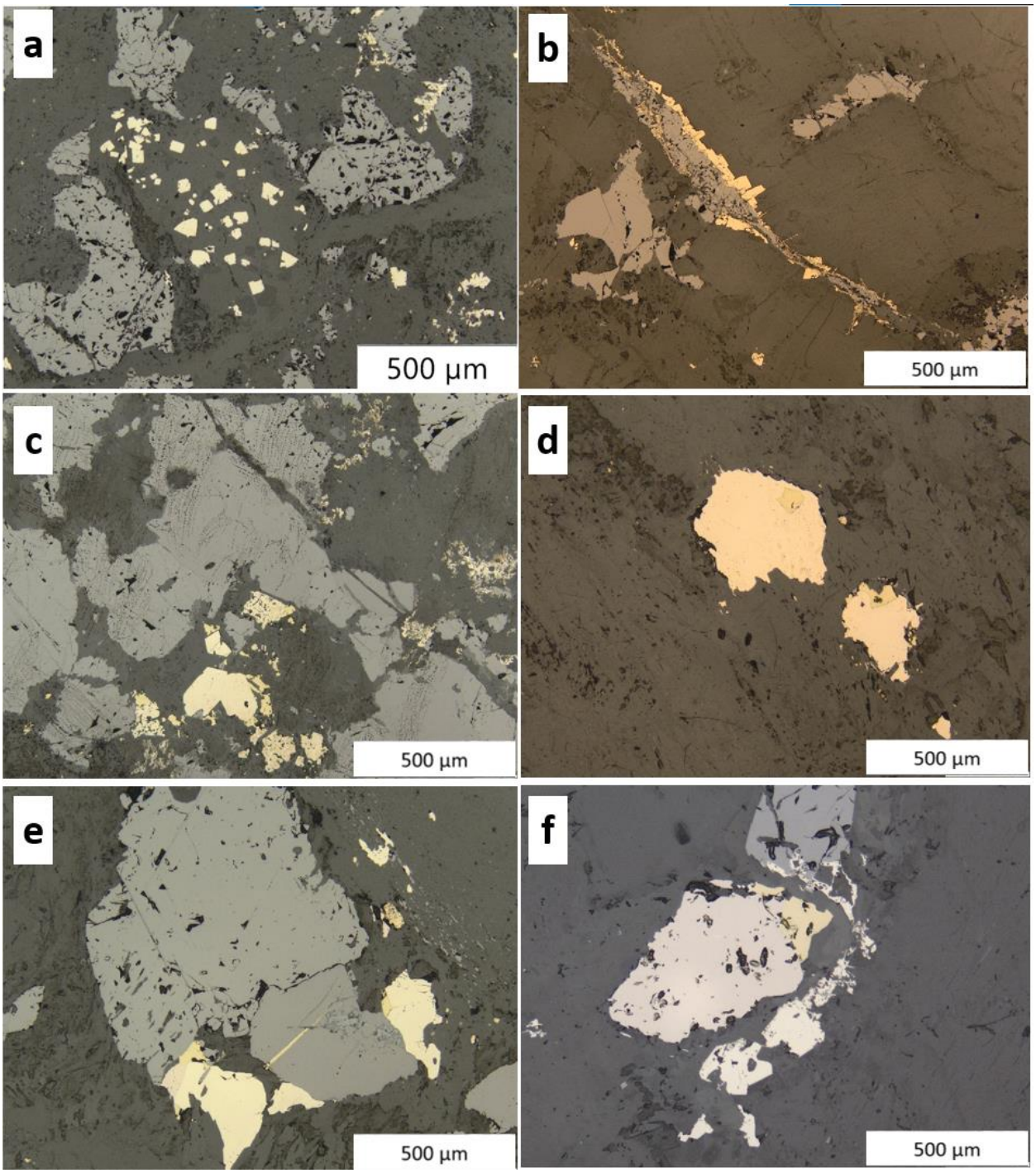

Figure 4.9. a-b) Anhedral to subhedral fine- to medium-grained pyrite grains, occasionally filling veins. c-d) Chalcopyrite embedded small inclusions within pyrite crystals and as fine-grained particles linked to pyrite. e-f) Fine-grained pyrrhotite associated with pyrite and magnetite.

Magnetite is more common than ilmenite in both the gabbronorite and the massive and semi-massive oxides. They occur disseminated and as interstitial fillings between the silicate minerals in the gabbronorite or as an interconnected matrix of aggregated oxide grains surrounding the silicate minerals in the massive and semi-massive oxide rocks (Fig. 4.10). Semi-massive and massive oxides are characterized by a massive granular texture consisting of medium to coarse sub-rounded grains of magnetite and rounded grains of ilmenite. Grains of polygonal magnetite occasionally display boundaries that meet at ~120-degree triple junctions in massive and semi-massive oxide rocks (Fig. 4.10 c and d).

Primary coarse-grained ilmenite grains commonly display hematite exsolution textures (Fig. 4.11). Secondary ilmenite includes three types of ilmenite exsolution textures identified in the magnetite: trellis-type texture, sandwich-type texture, and granular texture. Granular and sandwich-type are the most common exsolutions and correspond to medium to thick lamellae along all sets of lattice planes of the magnetite. The granular texture corresponds to irregularly shaped or elongated external granules at magnetite boundaries (Fig. 4.12). Fine discrete grains and lamellae of spinel exsolution are sporadically present in the titanomagnetite (Fig. 4.13).

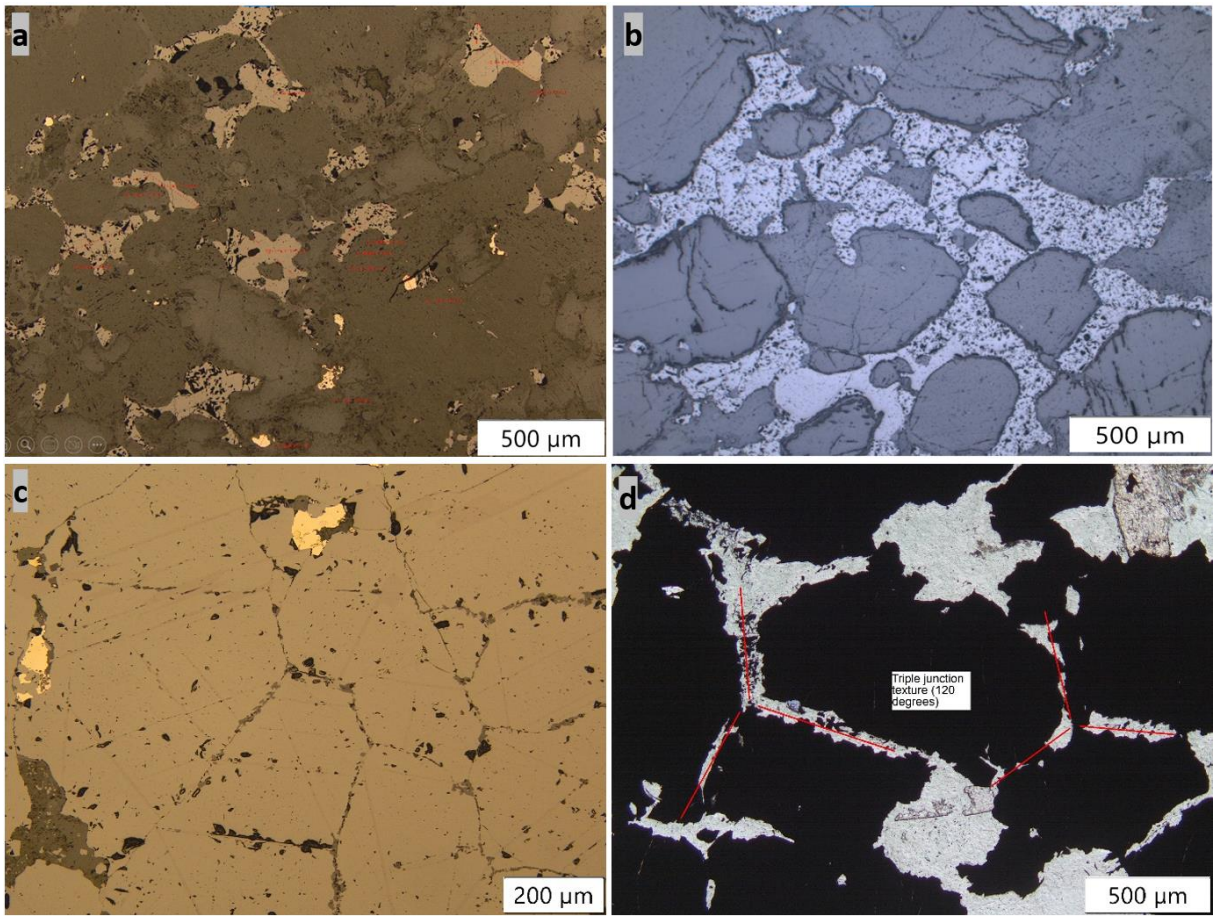

Figure 4.10. a) Sample SB008. Interstitial disseminated magnetite and ilmenite fillings between silicates (reflected light — ppl). b) Aggregated interconnected magnetite surrounding silicates (reflected light — ppl). c, d) Samples SB034 (reflected light — ppl) and SB038 (reflected light – ppl). Grains of polygonal magnetite display boundaries that meet at ~120 degrees triple junction.

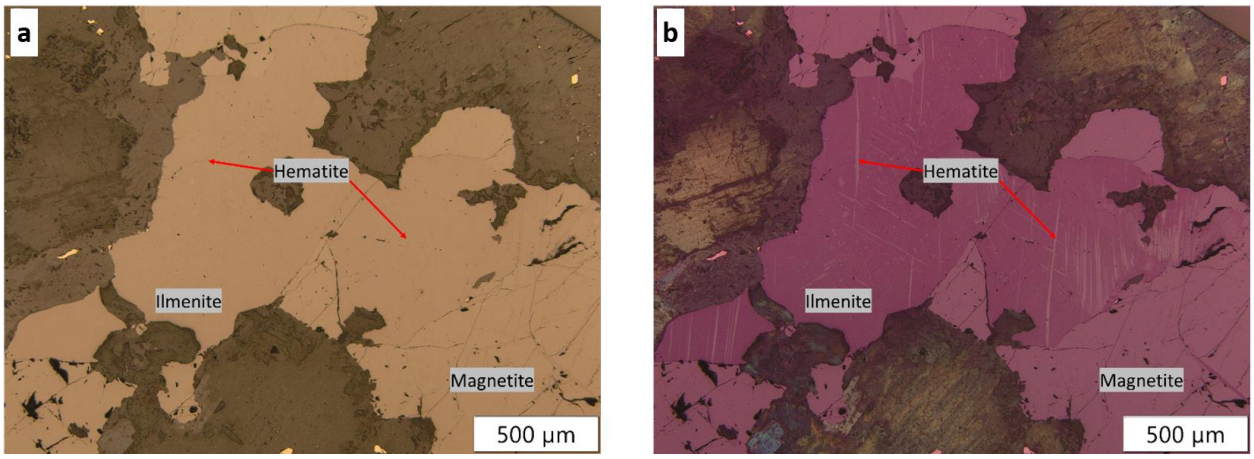

Figure 4.11. Hematite exsolutions in ilmenite (reflected light). Sample SB038. a) ppl. b) xpl.

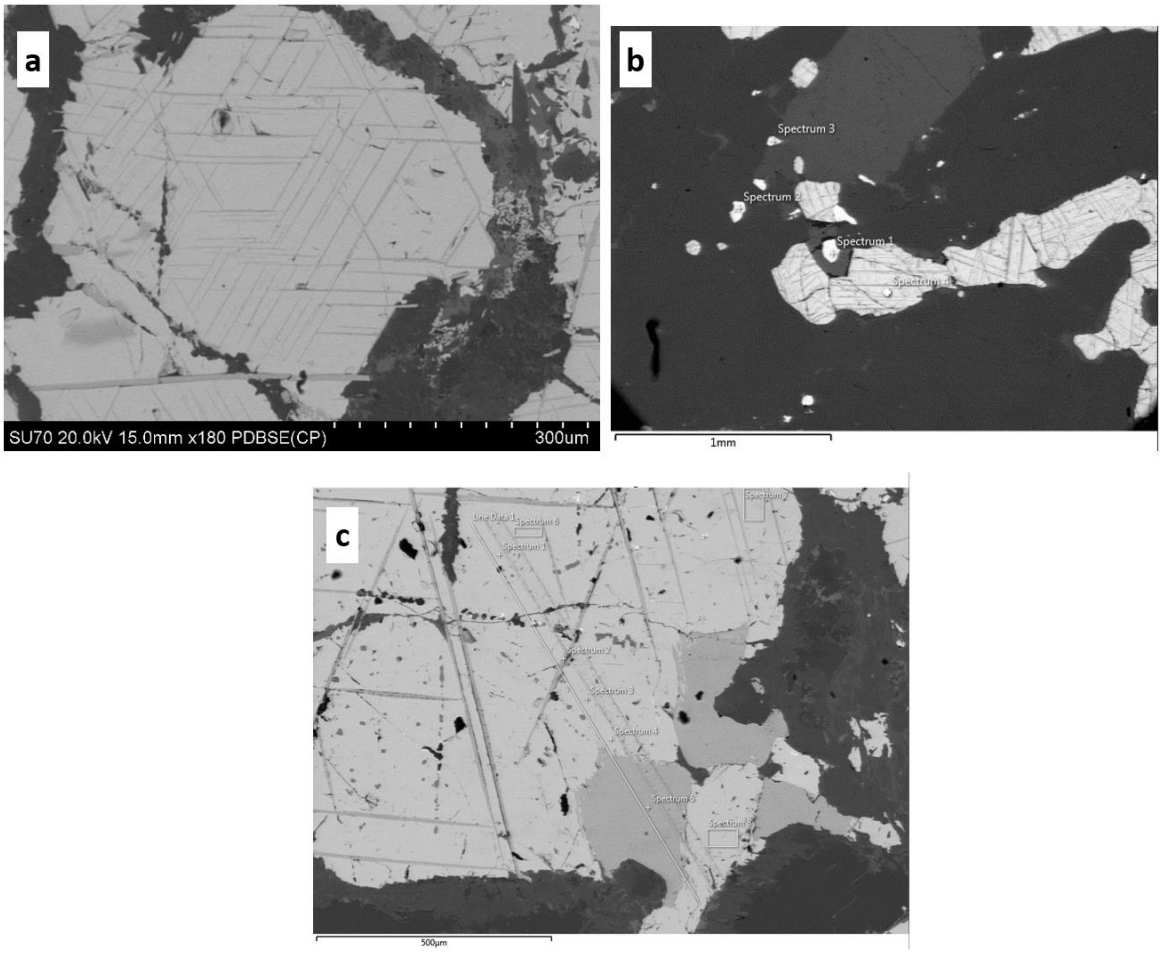

Figure 4.12. Backscattered electron images of the Fe oxides a) Trellis-type texture (massive and interstitial magnetite). b) Sandwich-type texture. c) Granular-type texture. The scale in the image b represent 10 mm and the scale in the image c represent 500 µm.

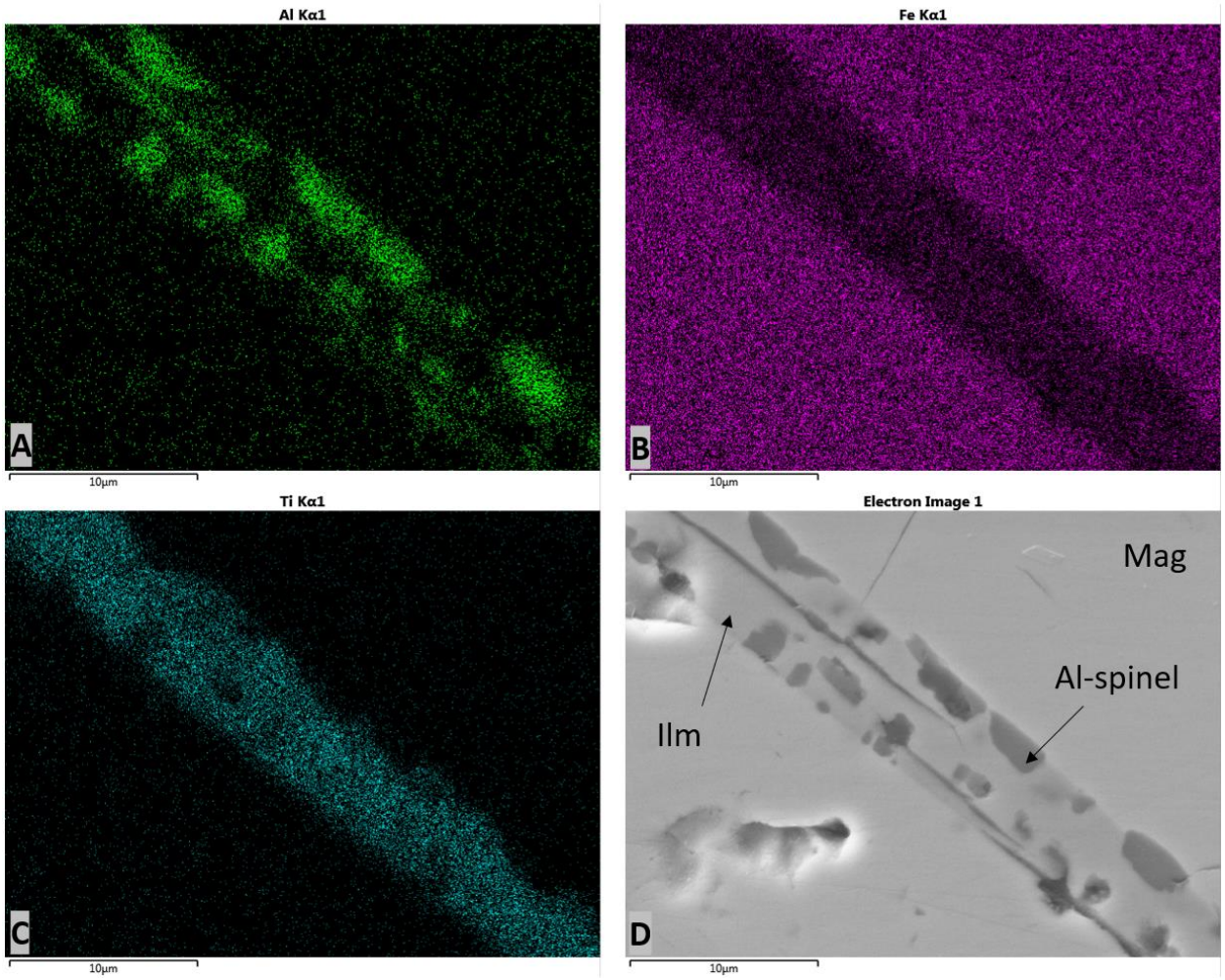

Figure 4.13. SEM image and EDS elementary mapping (Sample SB013). A) Al EDS image. b) Fe EDS image. C) Ti EDS image. D) SEM image. The scale in the images represents 10 µm.

4.3. Whole-Rock Geochemistry

The samples were grouped into the following categories based on petrography: 1) Massive oxides (> 80% magnetite and ilmenite); 2) semi-massive oxides (40 — 79% magnetite and ilmenite); 3) heavily disseminated oxides (10 — 39% magnetite and ilmenite); and, weakly disseminated oxides (< 9% magnetite and ilmenite).

Samples from the magnetite gabbro (i.e., heavily and weakly disseminated oxides) contain between 36 to 58 wt% SiO_2, 5,2 to 78.5 wt% Fe_2O_3, and 0.01 to 1.3 wt% V_2O_5. Representative analyses from major elements are

provided in Table 4.3. Full whole-rock geochemical results, including mineralization styles, are presented in Appendix D.

Table 4.3. Average whole-rock analysis performed on LDI.

Element	*Massive oxide*	*Semi-massive oxide**	*Heavily disseminated oxide**	*Weakly disseminated oxide**
SiO_2 (wt. %)	4.26	30.26	34.68+/-1.43	47.77+/-0.44
Al_2O_3	6.91	10.70	13.40+/-0.25	18.41+/-0.34
Fe_2O_3	78.56	40.76	30.95+/-0.27	12.60+/-0.63
CaO	0.74	7.14	8.05+/-0.27	8.91+/-0.17
MgO	2.98	6.25	6.51+/-0.25	8.12+/-0.27
Na_2O	0.06	0.98	1.26+/-0.27	1.79+/-0.06
K_2O	0.02	0.09	0.10+/-0.28	0.22+/-0.02
TiO_2	6.25	3.57	2.31+/-0.28	0.38+/-0.05
MnO	0.18	0.21	0.16+/-0.25	0.12+/-0.01
P_2O_5	0.01	0.01	0.01+/-0.28	0.01+/-0.00
SrO	0.01	0.01	0.02+/-0.27	0.02+/-0.00
BaO	0.01	0.01	0.01+/-0.25	0.01+/-0.00
LOI	0.02	0.89	0.75+/-0.45	1.17+/-0.11
Total	99.98	100.87	101.18	101.48
Mg#	0.08	0.25	0.31+/-0.26	0.58+/-0.01
V (ppm)	7321	2578	2004.77+/-0.28	431.80+/-52.03
Cr	210	100	127.57+/-0.43	248.35+/-25.63
Ni	951	193	203.87+/-0.37	244.66+/-12.63
Sr	18.80	114.03	139.96+/-0.27	211.33+/-9.33
Cu	340.07	286.57	206.71+/-0.34	21.11+/-9.42
Zn	234.05	170.03	122.36+/-0.26	62.34+/-2.16
Co	264.05	177.08	134.66+/-0.26	71.46+/-2.71
Ga	45.21	28.05	24.00+/-0.25	17.36+/-0.28
Sc	13.00	33.80	29.05+/-0.30	18.36+/-0.81
Li	10.00	10.09	10.52+/-0.28	9.51+/-0.44
Ge	2.50	2.52	2.53+/-0.24	2.54+/-0.00
Zr	5.00	4.54	4.10+/-0.29	4.63+/-1.61
Pb	6.00	2.02	1.99+/-0.28	1.69+/-0.12
Ce	0.60	1.16	1.16+/-0.29	1.76+/-0.62
W	2.00	0.50	0.59+/-0.29	0.64+/-0.10
Y	0.10	1.97	1.47+/-0.32	1.20+/-0.19
Nd	0.30	0.66	0.71+/-0.30	0.74+/-0.33
Mo	0.50	0.50	0.53+/-0.25	0.57+/-0.03
	** Geometric mean plus-minus standard error*			

According to their major element content, the studied rocks have protoliths dominated by plagioclase, pyroxene, and titano-magnetite. The data cluster in the central-left part of Figure 4.14 suggesting there is no dominance between ortho- or clinopyroxene. Vanadium enrichment is observed in all rocks, although it is less in weakly disseminated oxide samples since they have less titanomagnetite (Fig. 4.14).

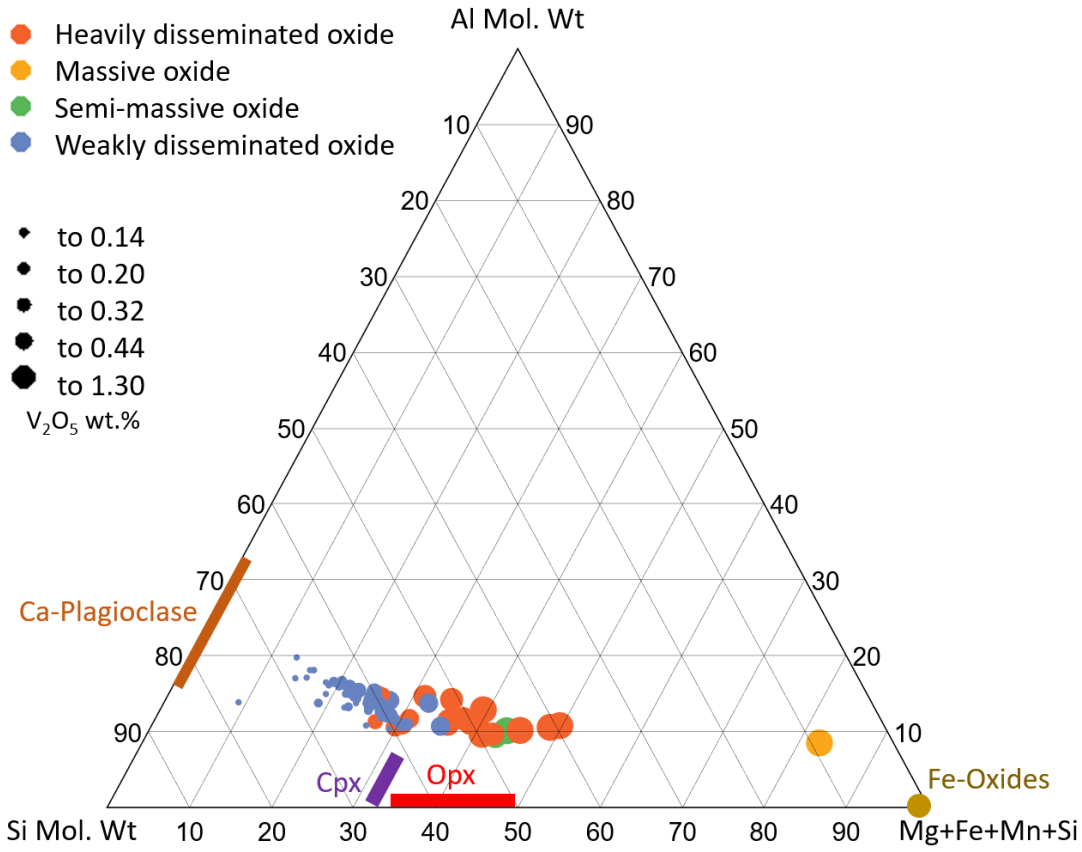

Figure 4.14. Ternary diagram displaying whole-rock analyses (n=74) performed for this study. The size of circles represents vanadium content (Adapted from Mokchah and Mathieu 2022).

Primitive mantle normalized multi-element diagrams were plotted for the magnetite gabbro (Fig. 4.15). Heavily disseminated and weakly disseminated gabbro show a slight enrichment in LREE compared to massive and semi-massive oxide gabbro, which do not show an enrichment. In the massive oxide, the normalized La/Sm_N is 1.93. The value of Gd/Yb_N is 1.38. The Nb/Nb* value is 0.75 and corresponds to the negative anomaly observed. The Ti/Ti* value is 160.38 and corresponds to the positive anomaly observed.

For the heavily disseminated oxide gabbro La/Sm_N ranges from 0.74 to 8.61, with a mean of 2.49. The values of Gd/Yb_N range from 0.55 to 1.62, with a mean of 0.98. The Nb/Nb* values range from 0.12 to 0.67 and correspond to the negative anomaly observed with a mean of 0.29. The Ti/Ti* values range from 5.58 to 128.43 and correspond to the positive anomaly observed with a mean of 29.64 (Fig. 4.15c).

For the weakly disseminated oxide gabbro, normalized La/Sm_N ranges from 1.31 to 43.08, with a mean of 5.28. The values of Gd/Yb_N range from 0.37 to 3.02, with a mean of 0.93. The Nb/Nb* values range from 0.03 to 0.41 and correspond to the negative anomaly observed with a mean of 0.15. The Ti/Ti* values range from 0.32 to 34.86 and correspond to the positive anomaly observed with a mean of 7.08 (Fig. 4.15d). For the semi-massive oxide, normalized La/Sm_N ranges from 0.96 to 1.88, with a mean of 1.42. The values of Gd/Yb_N range from 1.05 to 1.08, with a mean of 1.06. The Nb/Nb* values range from 0.34 to 0.66 and correspond to the negative anomaly observed with a mean of 0.50. The Ti/Ti* values range from 18.73 to 26.07 and correspond to the positive anomaly observed with a mean of 22.40 (Fig. 4.15b).

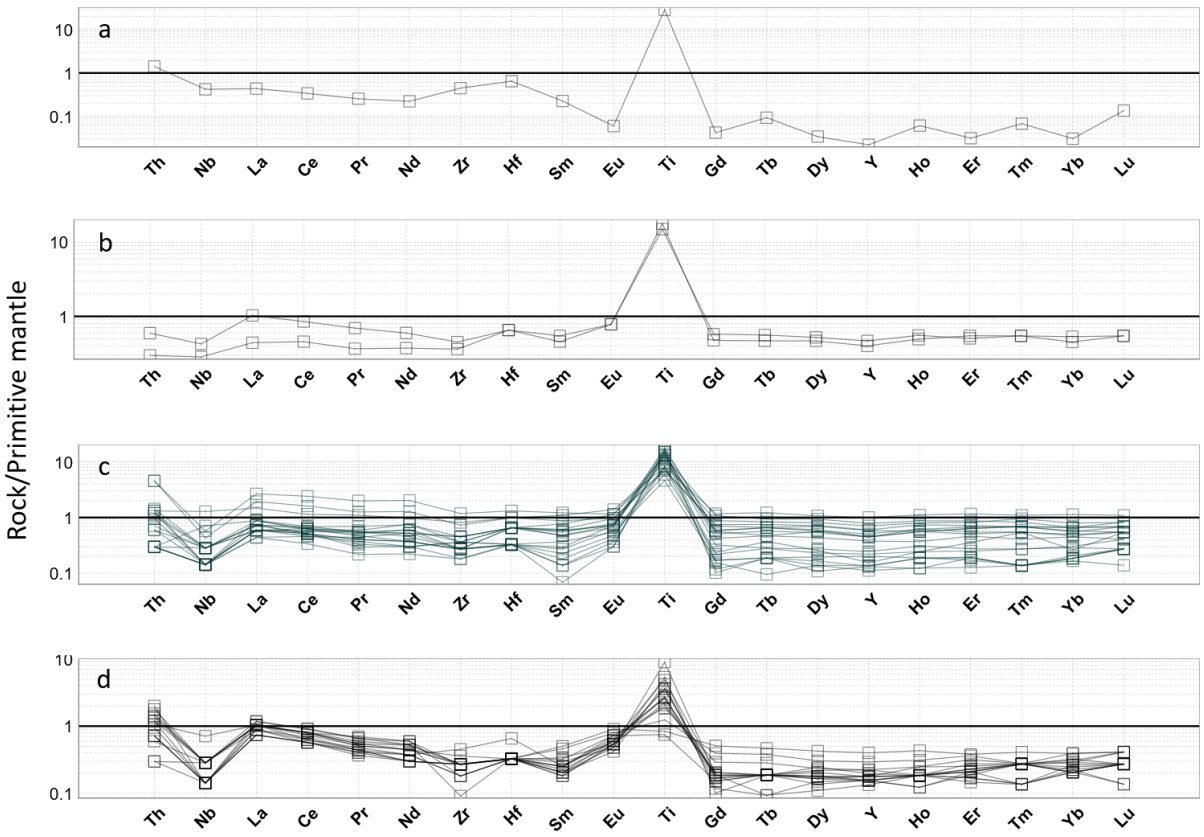

Figure 4.15. Primitive mantle normalized diagrams of the oxide category for the magnetite gabbro at Block Mine Intrusion, Lac des Iles. a) massive oxide. b) semi-massive oxide. c) heavily disseminated oxide. d) weakly disseminated oxide. Normalizing values from Sun and McDonough (1989).

4.4. Mineral Geochemistry

4.4.1. SEM

Energy dispersive spectrometry element maps and line scan profiles were used to distinguish mineral phases with high Fe and Ti contents, include their morphologies, and determine elemental concentrations. Compositional data for magnetite were obtained from 110 EDS analyses and for ilmenite from 98 EDS analyses are presented in Appendix E. Representative compositions are presented in Tables 4.4 and 4.5. The compositional ranges for magnetite varied from 46.66 to 97.6 wt. % FeO and 0.88 to 2.18 wt. % V_2O_5. The compositional ranges for ilmenite ranged from 29.8 to 54.6 wt. % TiO_2 and 33.3 to 91.01 wt. % FeO.

Table 4.4. Representative compositions of magnetite (EDS).

Sample	SB004	SB016	SB018	SB021
V_2O_5	1.58	1.53	1.04	1.81
FeO	88.78	94.03	75.52	82.22
TiO_2	0.96	0.68		1.18
Al_2O_3	0.64	0.81	6.31	2.4
SiO_2	0.25		12.05	2.27
CaO			1.87	
MgO			2.58	1.4
Cr_2O		0.54		
Na_2O			0.73	
ZnO				0.63
Total	92.22	97.58	100.1	91.9

Table 4.5. Representative compositions of ilmenite (EDS).

Sample	SB004	SB013	SB021	SB034
Texture	Trellis	sandwich	primary?	Sandwich
V_2O_5	1.1			1.32
FeO	62.74	47.15	48.22	72.63
TiO_2	17.98	44.85	48.73	19.58
Al_2O_3	8.97	4.73		4.6
SiO_2	3.79	0.75		
MnO		1.17	1.85	
MgO	2.7	0.78		0.74
Total	97.28	99.87	98.81	98.87

4.4.2. LA-ICP-MS

To determine the compositions of major and trace elements (Table 4.6), a total of 51 laser ablation line analyses were completed on magnetite samples from massive, semi-massive, heavily disseminated, and weakly disseminated oxide rocks. The compositions of the magnetite and ilmenite are listed in Appendix F and Table 4.6.

In magnetite, Fe, V, Ti, Al, Mg, Cr, Mn, Zn, Ga, Cu, Ni, and Si were detected in appreciable amounts, whereas P, Ca, Sc, Cu, Ge, As, Y, Zr, Nb, Mo, Sn, La, Yb, Hf, Ta, W, Ir, and Pb were limited to < ~10 ppm at maximum

when detected (Fig 4.16). Of all the elements analyzed in ilmenite, Fe, Ti, Mn, V, Mg, Al, Si, Ca, Sc, Co, Ni, Zn, Cr, and Zr were present in appreciable concentrations whereas P, Cu, Ga, Ge, As, Y, Nb, Mo, Sn, La, Yb, Hf, Ta, W, Ir, and Pb were limited to <~10 ppm at maximum when detected (Fig 4.17).

Table 4.6. Average compositions of magnetite and ilmenite grains analyzed from magnetite gabbro at Mine Block Intrusion (S.D.= standard deviation for the population).

Weight %	Magnetite				Ilmenite			
	Mean	S. D.	Minimum	Maximum	Mean	S. D.	Minimum	Maximum
MgO	0.188	0.159	0.001	0.626	0.315	0.406	0.020	1.504
Al_2O_3	0.736	0.537	0.139	2.382	0.160	0.178	0.004	0.891
SiO_2	0.358	0.263	0.000	0.948	0.202	0.230	0.002	1.191
P_2O_5	0.000	0.000	0.000	0.001	0.000	0.000	0.000	0.001
CaO	0.035	0.048	0.000	0.301	0.060	0.085	0.000	0.331
TiO_2	1.573	1.733	0.080	7.681	48.839	1.338	45.095	50.651
Cr_2O_3	0.203	0.187	0.000	0.621	0.026	0.026	0.000	0.113
MnO	0.065	0.056	0.010	0.246	1.596	0.392	1.053	2.475
FeO	90.262	1.976	84.998	92.910	45.525	1.674	42.881	52.340
V_2O_5	1.561	0.261	1.007	2.288	0.327	0.110	0.091	0.532

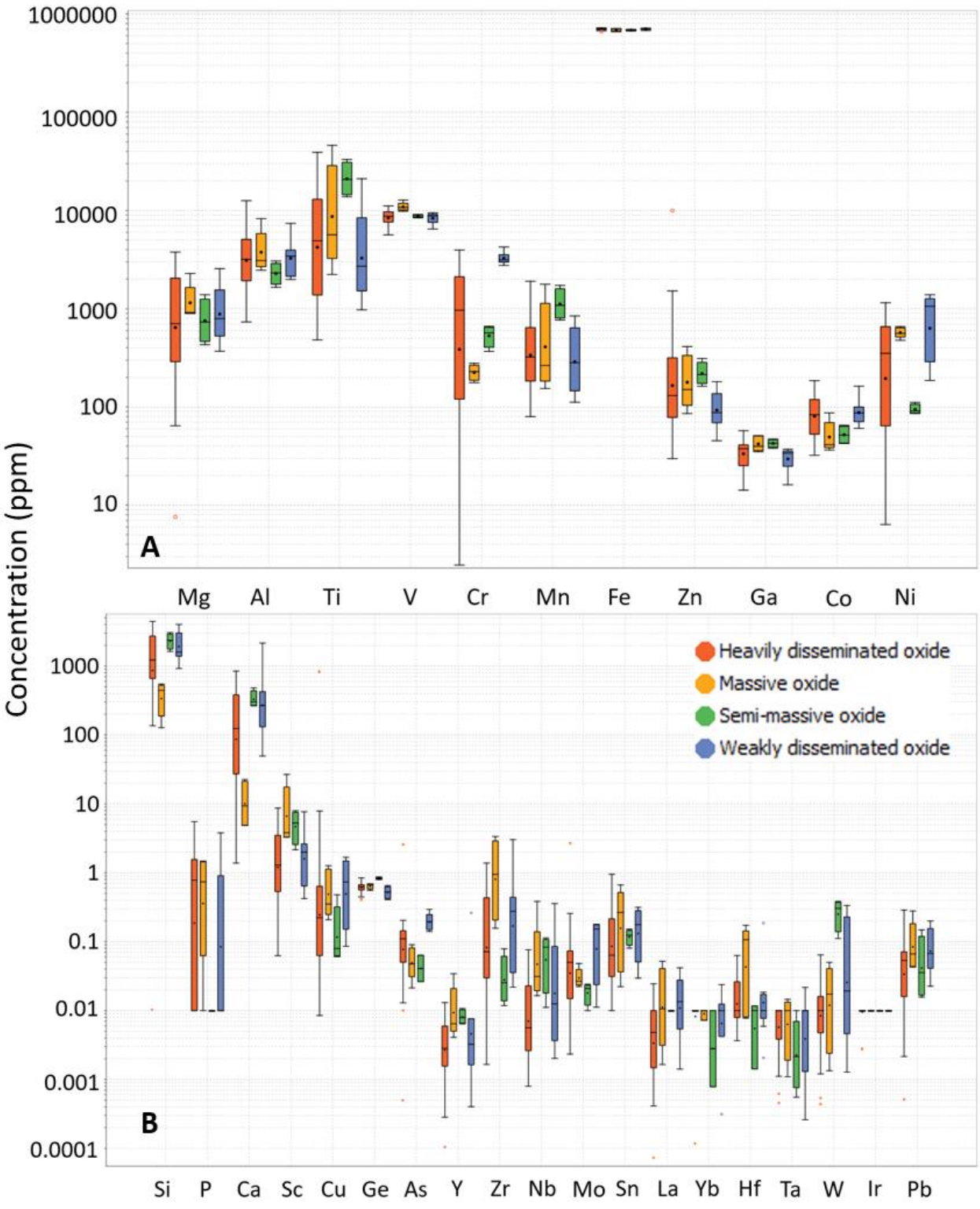

Figure 4.16. Box diagram of major (A) and trace elements (B) concentrations (ppm) for LDI magnetite.

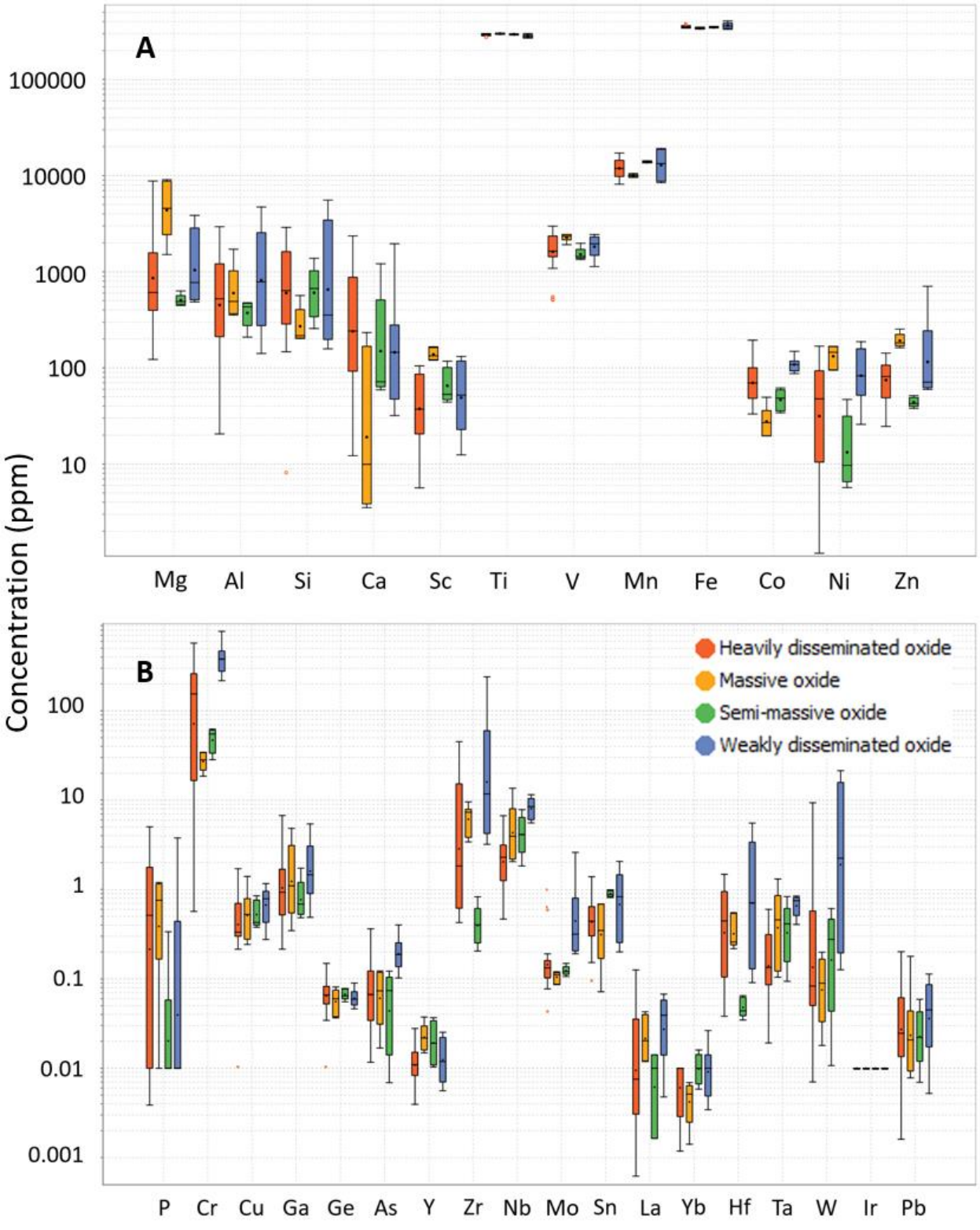

Figure 4.17. Box diagram of major (A) and trace elements (B) concentrations (ppm) for LDI ilmenite.

Figure 4.18 shows the average concentrations in ppm of V, Fe, Cr, Nb, Ti, and Ni in both magnetite and ilmenite, plotted against stratigraphic depth for the 14-902 drill core samples.

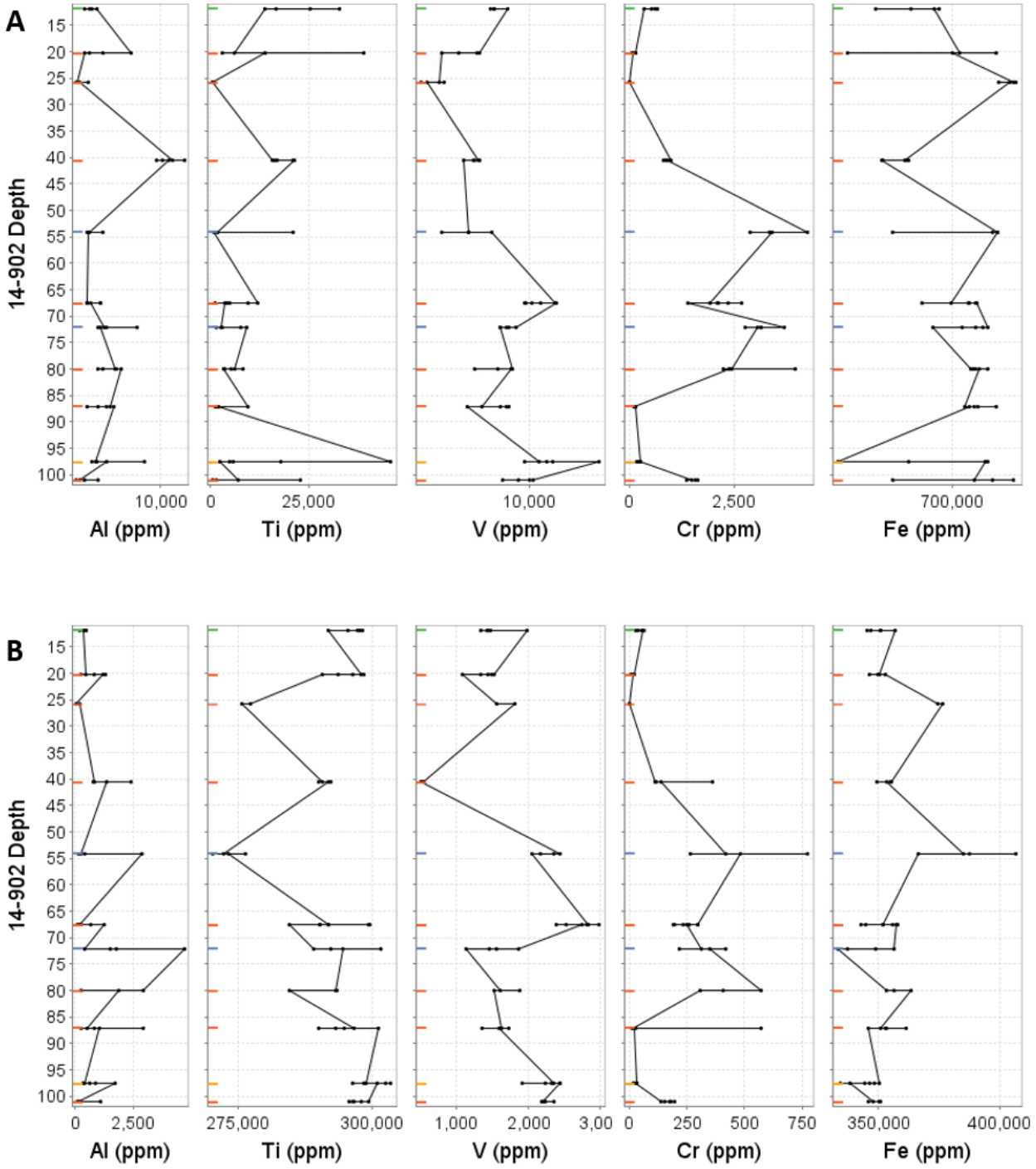

Figure 4.18. Profiles showing deposit-scale variations in Al, Ti, V, Cr, and Fe. Drill core 14-902. A. Magnetite. B. Ilmenite. Horizontal lines represent the variation in Fe-Ti oxide compositions within a single thin section.

Chapter 5 - Discussion

5.1. Field Observations

Oxide mineralization in the magnetite gabbronorite at the Mine Block Intrusion (MBI) can be separated into massive, semi-massive, weakly, and heavily disseminated oxides that have similar oxide and silicate mineralogy, mineral textures, alteration, and textural relationships. Massive and semi-massive iron oxide mineralization is observed in pods and bands along with plagioclase laths in gabbronorite throughout drill hole 14-902. The mineralization is fine- to coarse-grained and dominated by magnetite (up to 82 %). Weakly and heavily oxide disseminated mineralization is present in both drill holes and is fine- to coarse-grained and occurs interstitial to plagioclase and chlorite-altered pyroxenes. Contacts between massive to semi-massive mineralization styles and the host gabbronorite are sharp with disseminated oxide mineralization adjacent to the massive oxide zone within the host magnetite gabbronorite.

5.2. Petrography

Petrographic analysis revealed that the magnetite gabbronorite in the MBI at LDI rocks is composed of primary magmatic minerals. These minerals consist of plagioclase, orthopyroxene, magnetite in variable amounts, and trace sulfides. Plagioclase and clinopyroxene are generally similar in size and alternate as the predominant minerals, occurring as cumulates. Evidence for a cumulate origin in the magnetite gabbronorite in the MBI at LDI includes the presence of layering with alternating thin Fe-Ti oxides and silicate-rich layers consistent with the accumulation of crystals and compaction, and cumulus framework of touching grains, although it is not well-preserved due to alteration (Fig. 4.4). The observed alteration can be attributed to metamorphism within the regional greenschist facies since, in most analyzed samples, plagioclase is partially altered to sericite, and pyroxene has been partially to completely altered to tremolite-actinolite and talc, making it difficult to distinguish between orthopyroxene and clinopyroxene. Chlorite is an alteration product of pyroxene and plagioclase. The magnetite gabbronorite in the MBI exhibits similar mineral assemblages, alteration, and

cumulate characteristics to rocks described elsewhere within the MBI at LDI (Brugmann et al., 1989, 1997; Barnes and Gomwe, 2011; Djon and Barnes, 2012; Djon et al., 2018; Jonsson 2023).

Magnetite is interpreted to be a primary mineral based on its habit, as it is very fine- to coarse-grained and intergrown with the other silicates (Fig. 4.10). Magnetite occurrence (up to 80%) and the lack of foliation or association with the alteration assemblages also suggest a primary magmatic origin. Magnetite gabbronorite in the MBI at LDI shows a modal abundance variation rather than a textural one or changes in the mineralogy. This suggests a closed-system fractional crystallization since this results in a regular variation in mineral composition instead of significant textural variations, such as the development of resorption surfaces as evolved magmas interacted with earlier-formed crystals (Shahabi Far et al., 2019).

The occurrence of weakly and heavily oxide-disseminated, semi-massive, and massive Fe-Ti oxide V-rich mineralization in the gabbronorite in the Mine Block Intrusion associated with primitive plagioclase suggests they crystallized at early stages of differentiation, probably towards the lower parts of the intrusion as in Panzhiua (Pang et al., 2008), although, usually, magnetite horizons formed from Fe–Ti-rich highly evolved basaltic melts late in the evolution of the layered intrusion at higher levels in the stratigraphy are common in large mafic-layered intrusions (Mungall, 2014). Generally, in layered intrusions chromite typically occurs in the basal rocks, PGE mineralisation towards the middle; and magnetite horizons and vanadiferous magnetite form toward the top from Fe–Ti-rich highly evolved basaltic melts late in the evolution of the layered intrusion (Mungall, 2014). Although not all intrusions are well layered, a change from more ultramafic to more felsic upward is common (Cawthorn et al., 2005).

Magmatic deposits of Ti-Fe-V oxides consist of layers and lenses of massive, disseminated titanomagnetite or vanadium-magnetite, in differentiated gabbroic intrusions or Proterozoic anorthosite complexes, usually near or at the tops of the fractionated mafic stratigraphy (Pang et al., 2010; Pirajno and Hoatson, 2012). The host rocks are typically norite, gabbronorite, anorthosite, and troctolite. The principal ore mineral is titanomagnetite and (or) V-bearing magnetite (Pirajno and Hoatson, 2012). Associated minerals are ilmenite, hematite, spinel,

and sulfide minerals (pyrite, pyrrhotite, and chalcopyrite). Mafic–ultramafic complexes are associated with Large Igneous Provinces (LIP) and may also host Fe–Ti–V, and PGE in their gabbroic differentiates, for example, in Alaskan-style intrusions (Pirajno and Hoatson, 2012). The magnetite in the MBI gabbronorite at LDI could be considered a magmatic Fe-Ti-V oxide mineralization characterized by layered massive to disseminated vanadium-magnetite in a gabbroic intrusion.

5.3. Whole-Rock Geochemistry

The cumulate nature of the magnetite gabbronorite in the MBI makes it difficult to identify the parental magma, and due to its degree of alteration, quantitative mineral analysis is challenging. Loss on ignition (LOI) values for the magnetite gabbronorite range from 0.78 to 5.59 wt%, suggesting a low presence of volatiles despite the mineral alteration. The TAS diagram is based on the premise that alkalis and silica are the most abundant components in most igneous rocks. However, most of the rocks of the magnetite gabbro in MBI have high Fe-oxides and low silica contents; hence, some samples plot outside of the boundaries of the TAS diagram. Nevertheless, the MBI samples where Fe-oxides are weakly disseminated are classified as gabbro (Fig. 5.1). Overall, the rocks analyzed show a broadly gabbroic composition.

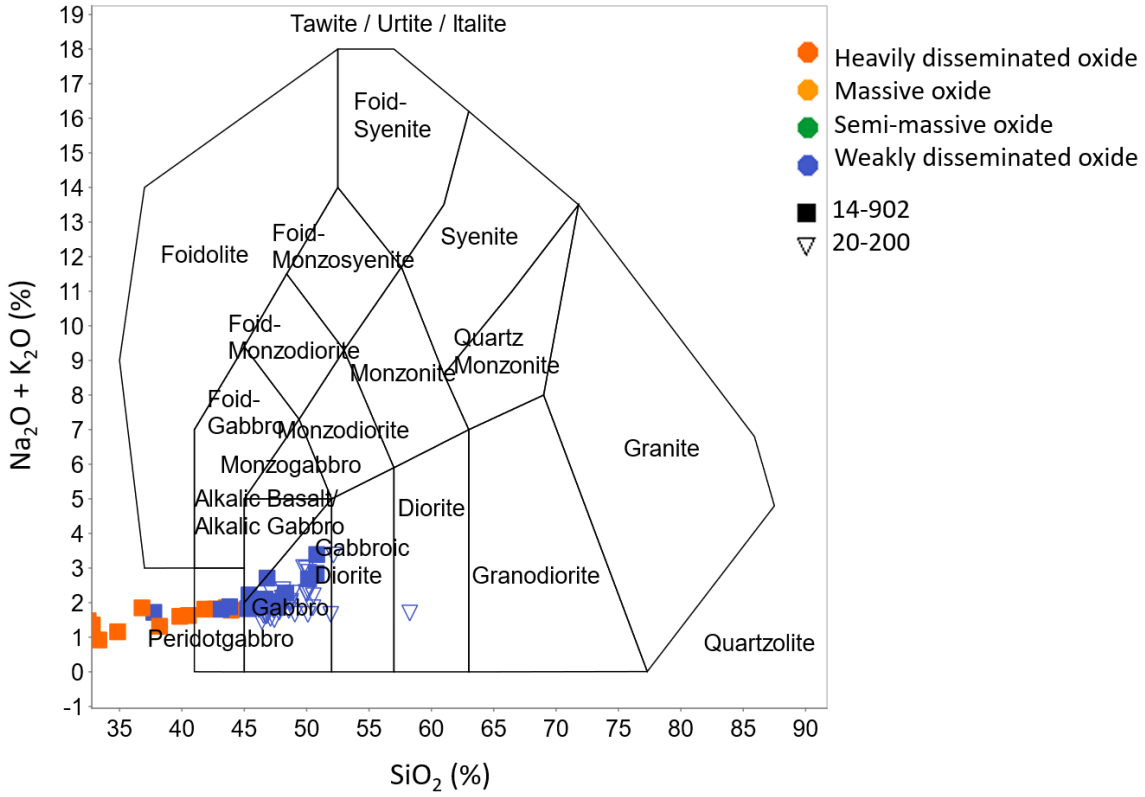

Figure 5.1. Total Alkali-Silica (TAS) discrimination diagram for plutonic rocks with rocks from MBI plotted (Middlemost, 1994).

To investigate the original rock types of the moderate and strongly altered rocks in the study, CIPW norms were calculated (Fig. 5.2). Most of the strongly and moderately altered rocks are norite and gabbronorite with minor gabbro, suggesting the predominance of orthopyroxenes over clinopyroxene, which is consistent with the petrographic observations made in the least altered rocks. This supports the work of Barnes and Gomwe (2011), who showed that the major element geochemistry in the MBI was consistent with most being plagioclase-orthopyroxene cumulates.

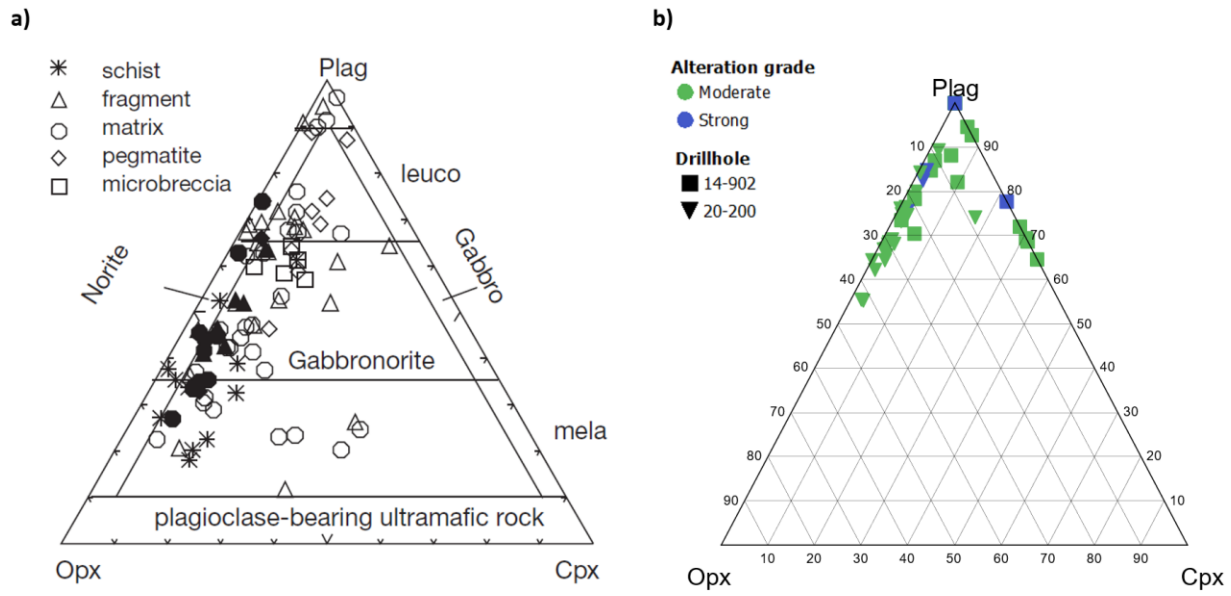

Figure 5.2. Rock classification based on CIPW norms. a) Roby, Twilight, and High-grade zones (Barnes and Gomwe, 2011). b) magnetite gabbronorite from the Mine Block Intrusion.

The normative calculations suggest the presence of minor clinopyroxene in some samples with a small number of samples plotting on the plagioclase/clinopyroxene axis. To assess this, Al_2O_3 versus MgO and CaO versus MgO were plotted. Whole rock geochemistry from weakly disseminated oxide samples (Fig. 5.3a) indicates that silicate phases are plagioclase and pyroxene. The CaO-MgO graph (Fig. 5.3b) suggests the predominance of orthopyroxene over clinopyroxene since the samples plotted on the plagioclase-orthopyroxene tie line which is consistent with the petrography.

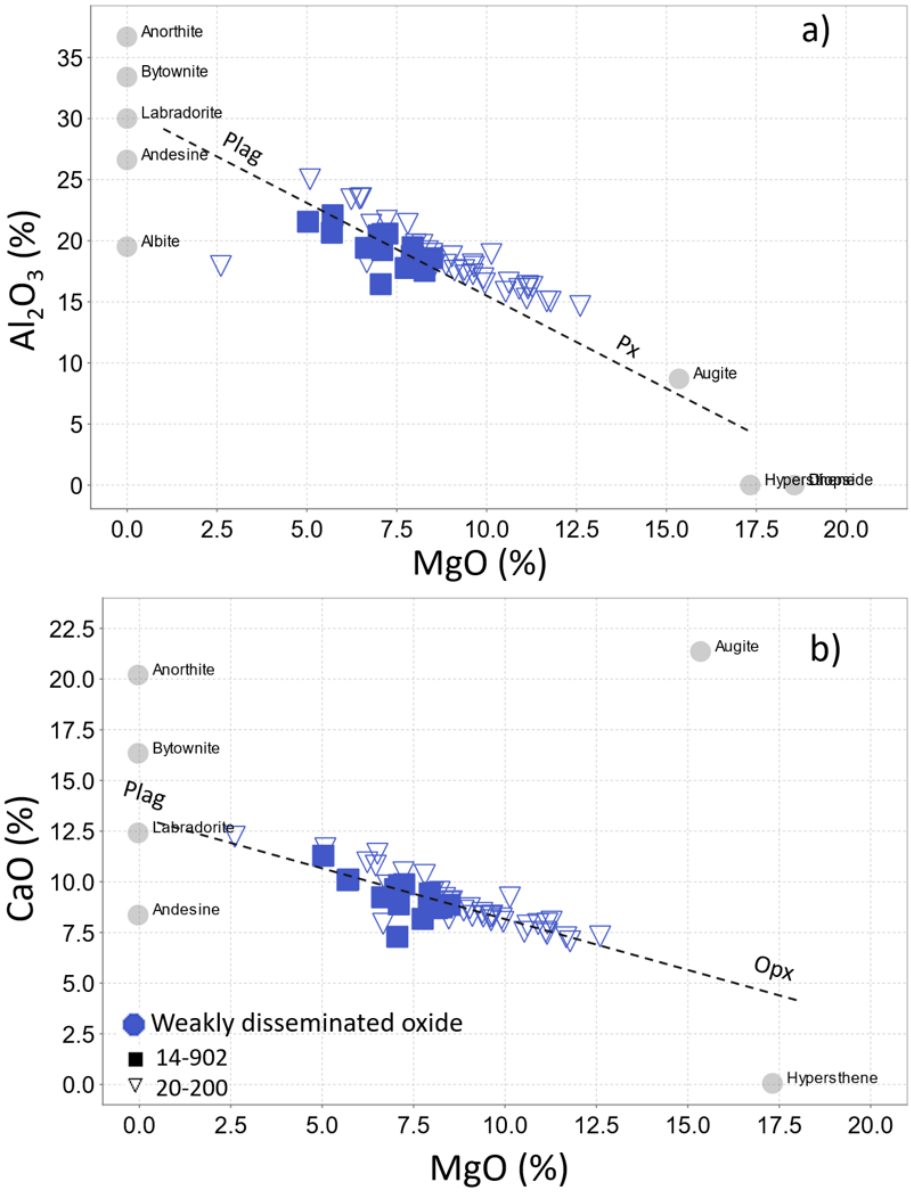

Figure 5.3. Major element chemistry of LDI magnetite gabbronorites. (a) Al_2O_3 vs. MgO; (b) CaO vs. MgO.

Binary diagrams of SiO_2 and Fe_2O_3 (Fig. 5.4) suggest that the fractionation is controlled by plagioclase (SiO_2-Al_2O_3; SiO_2-CaO), pyroxene (SiO_2-Fe_2O_3; Fe_2O_3-V_2O_5), and magnetite (SiO_2-Fe_2O_3; Fe_2O_3-TiO_2). Variations in whole-rock compositions show that most of the rocks lie on orthopyroxene-plagioclase tie lines. This is consistent with what is observed in the less altered rocks and with what is suggested by the calculated CIPW norms.

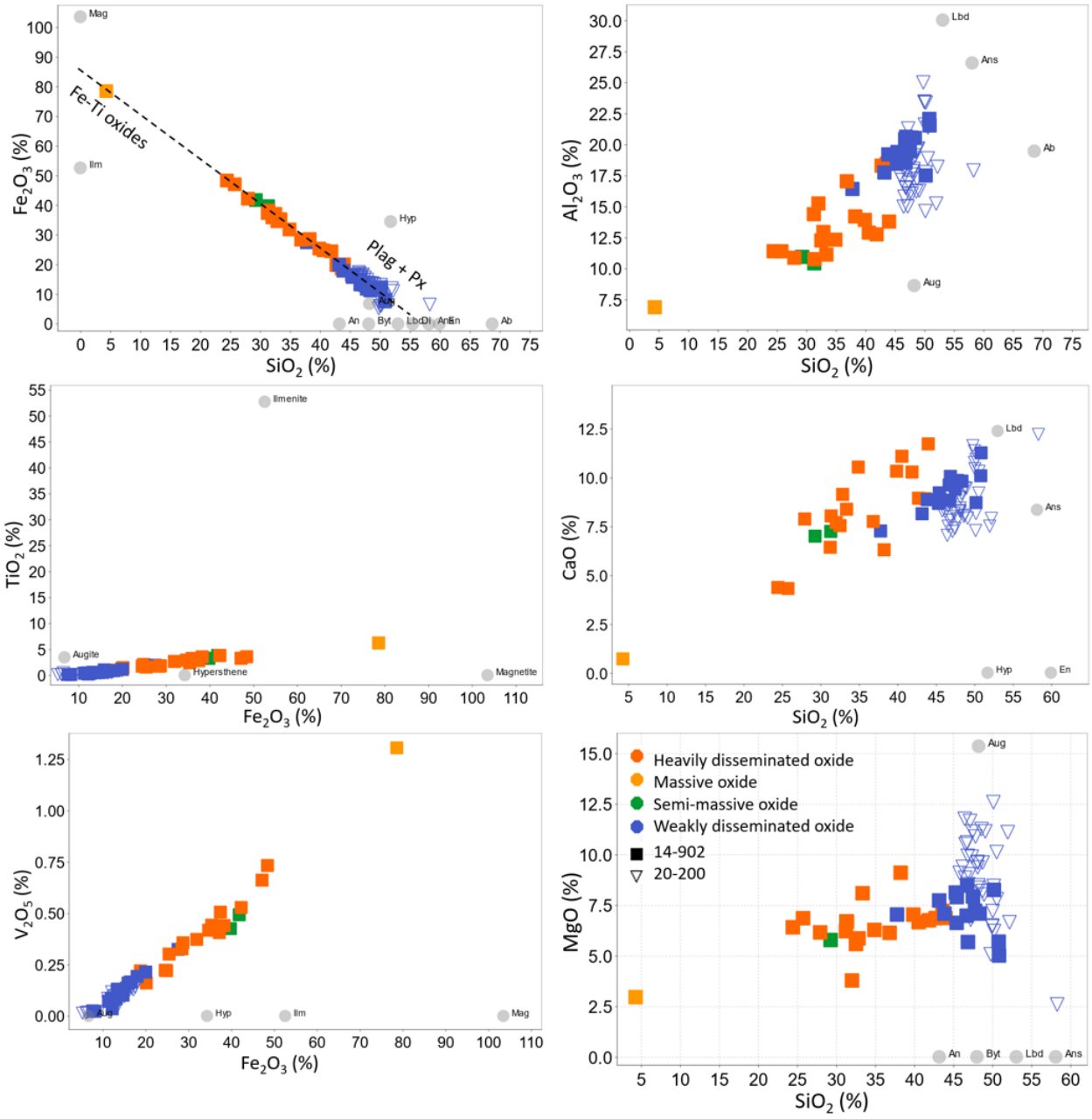

Figure 5.4. Binary variation diagrams of whole-rock geochemical analyses from the Mine Block Intrusion gabbronorite at LDI. Mineral compositions are indicated by gray circles. (Ab) Albite, (Ans) Andesine, (An) Anorthite, (Byt) Bytownite, (Lbd) Labradorite, (Aug) Augite, (Di) Diopside, (En) Enstatite, (Hyp) Hypersthene, (Mag) Magnetite, and (Ilm) Ilmenite.

As a convenient way to display the chemistry of magnetite-rich rocks and to see which elements increase due to the presence of oxides, the whole-rock chemical data is displayed on the diagram of Dare et al. (2014; Fig. 5.5). In the magnetite gabbronorite at LDI, incompatible lithophile elements such as Y, Zr, Nb, Hf, P, Sn, and Ta are depleted; Sc increases in heavily disseminated oxides, compared to weakly disseminated oxides since it is a compatible element in ilmenite, probably primary ilmenite. Compatible lithophile elements such as V, Co, Zn, and Ti are more abundant in heavily disseminated oxides than weakly disseminated oxides since they are compatible elements in magnetite. Chalcophile elements such as Cu and Ni are probably associated with sulfides, whose formation could be triggered by the oxide crystallization. Barnes and Gomwe (2011) suggested that positive anomalies of Sr, Eu, and Pb in samples from MBI at LDI could reflect the presence of cumulate plagioclase and the positive Sc anomaly was probably due to the presence of cumulate orthopyroxene.

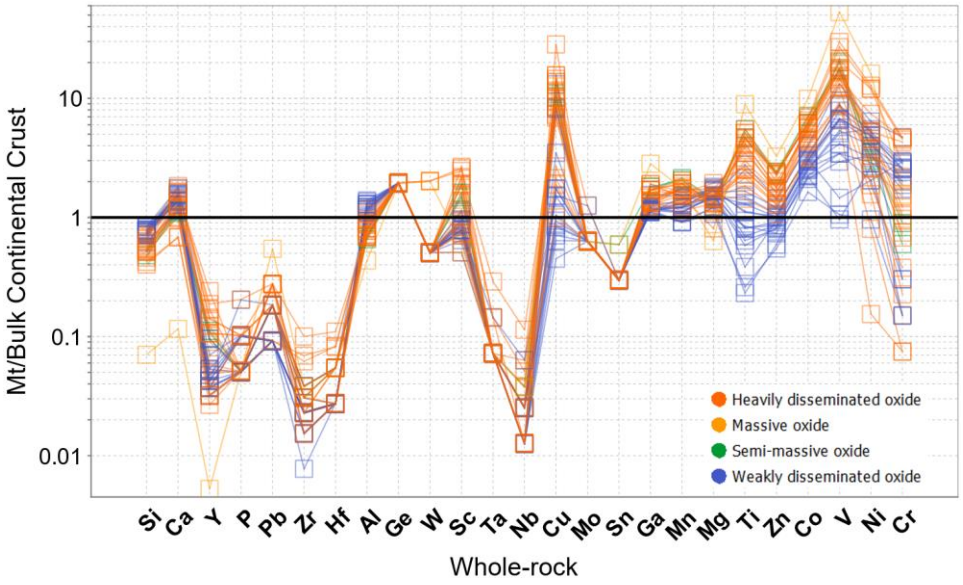

Figure 5.5. Multi-elemental diagram for magnetite gabbronorite in the MBI normalized to bulk continental crust (Adapted from Dare et al., 2014).

Plotting the magnetite gabbronorite samples from this study on the Th/Yb vs. Nb/Yb diagram (Pearce and Peate, 1995; Pearce, 2008; Fig. 5.6a) reveals that, similar to the samples from the Breccia and Norite domains of South LDI, they plot above the most depleted portion of the "mantle array", consistent with an influence from a depleted mantle source affected by subduction, as demonstrated by Jonsson (2023) in a study of the

norite and breccia domains in the South Lac des Iles Intrusive complex (Fig. 5.6a), or contamination by subduction modified crust or crustal material. Using a dataset of 478 samples from known post-Archean tectonic settings, Saccani (2015) identified a high level of distinction (>94%) between the MORB-OIB array and the volcanic arc array and proposed a discrimination diagram using absolute measures of Th and Nb normalized to N-MORB values of Sun and McDonough (1989). Plotting the weakly disseminated oxide samples from this study on Saccani's diagram (Fig. 5.6b), they plot in the volcanic arc array, consistent with the results of Figure 5.6a. Similarly, plotting the weakly disseminated oxide samples from the gabbronorite in the MBI on the V (ppm) vs. Ti (ppm)/1000 Vermeesch's diagram (Fig. 5.6c), they plot in the IAB (Island Arc Basalt) field, also suggesting a convergent plate setting.

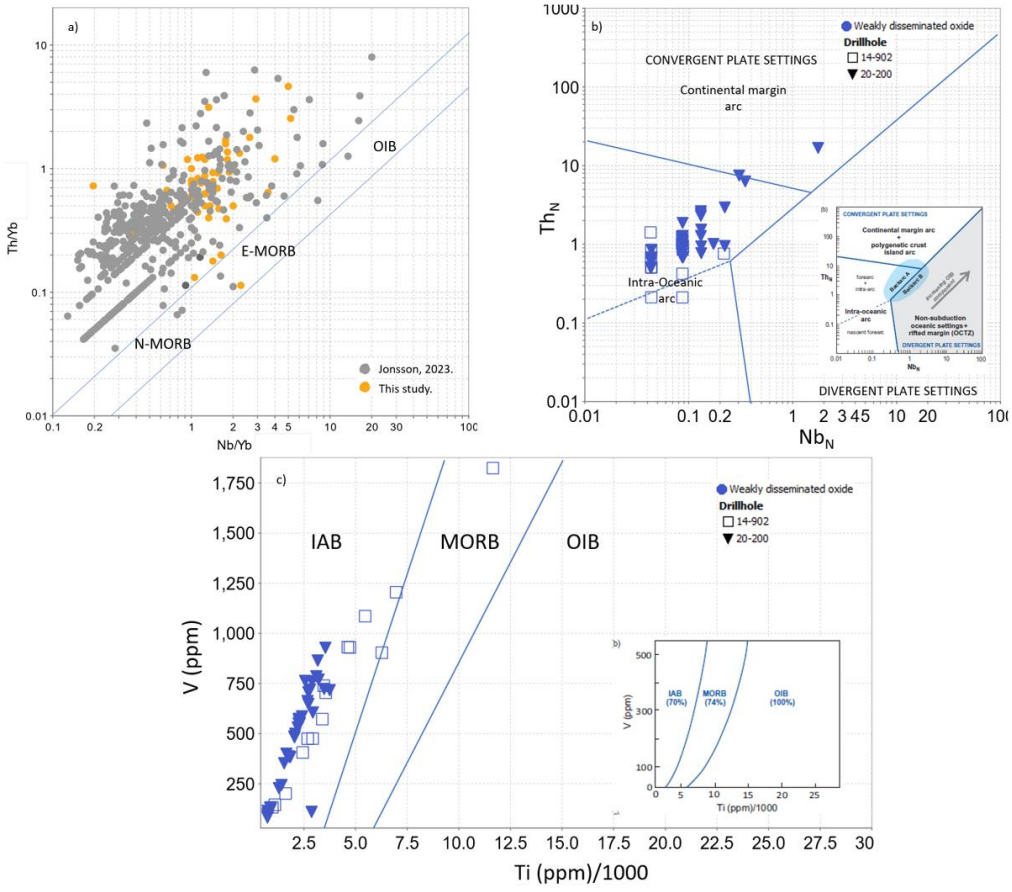

Figure 5.6. Tectonic discrimination bivariate plots. a) Th/Yb vs. Nb/Yb for Jonsson (2023) and this study. Mantle array (in grey) from Pearce et al. (2008). N-MORB, E-MORB, OIB compositions from Sun and McDonough (1989). Modified from Pearce (2008). b) Tectonic interpretation of weakly disseminated oxide samples from the gabbronorite in the MBI based on ophiolitic basaltic (Modified from Saccani 2015). c) Tectonic interpretation of weakly disseminated oxide samples from the gabbronorite in the MBI based on the island arc, mid-ocean ridge, and ocean island basalts discrimination diagram of Vermeesch (2006).

Taken together, the geochemical data is consistent with rocks having formed above a subduction zone or a mantle enriched by previous metasomatic event. This is consistent with recent studies that have argued for an arc setting for the LDI complex (Brugmann et al., 1997; Barnes and Gomwe, 2011; Djon et al., 2018) rather than the mantle plume origin proposed by Hinchey et al. (2005). The age of the LDI suite intrusions (2,699 Ma and 2,686 Ma) overlaps with regional, arc-related, intermediate to felsic intrusions that occur in both the southern Wabigoon Terrane and the northern Quetico Subprovince along the Shelby Lake Fault (Decharte et al., 2018) and suggests a possible genetic relationship between these contemporaneous magmatic events.

5.4. Mineral chemistry

Plagioclase

In general, despite the slight difference towards the lower part of the section (Fig. 4.6), the variation in the An-number (An_{74} to An_{59}) from samples of the magnetite gabbronorite in the MBI at LDI decreases up hole, suggesting a normal fractionation process. Sharp changes in mineral chemical compositions (e.g., Mg# of pyroxenes, An-content of plagioclase) across the igneous stratigraphy are generally thought to reflect changes in magma composition that arise from processes supplementary to progressive differentiation, such as magma injections (e. g., Namur et al., 2010; Polivchuk, 2017). Plagioclase identified within the magnetite gabbronorite of the MBI corresponds to labradorite-bytownite (An-number ranging from 0.59 to 0.74). This is consistent with the observations made by Barnes and Gomwe (2011), who noted that in the Roby, Twilight, and High-grade zones at South LDI, the orthopyroxene and plagioclase have fairly low Mg and An numbers (ranging from 0.64 to 0.71 and 0.58 to 0.66, respectively).

Plagioclase composition from the magnetite gabbronorite in the MBI at LDI is less evolved than observed in other systems such as the upper zone of the Bushveld which has a relatively evolved plagioclase composition (Cawthorn et al., 2005). In the Bushveld Complex in South Africa, plagioclase ranges from An_{80} in the critical

zone to An_{30} in the upper zone reflecting an almost complete range of differentiation products (Cawthorn et al., 2005). The An-number of plagioclase from samples of the MBI at LDI varies among An_{61}-An_{84} (Djon and Barnes 2012), An_{58}-An_{66} (Barnes and Gomwe 2011), and An_{64}-An_{71} (this study). The comparison of the plagioclase composition from LDI with well-studied layered intrusions suggests that saturation of Fe-Ti oxides in the MBI occurs at an early stage of differentiation compared with other mafic intrusions (Namur et al., 2010; Fig. 5.7). In most layered intrusions, the compositions of the silicate phases in equilibrium with the first liquidus Fe-Ti oxides are highly evolved indicating that saturation of Fe-Ti oxides in mafic layered intrusions commonly occurs at an advanced stage of differentiation (Namur et al., 2010).

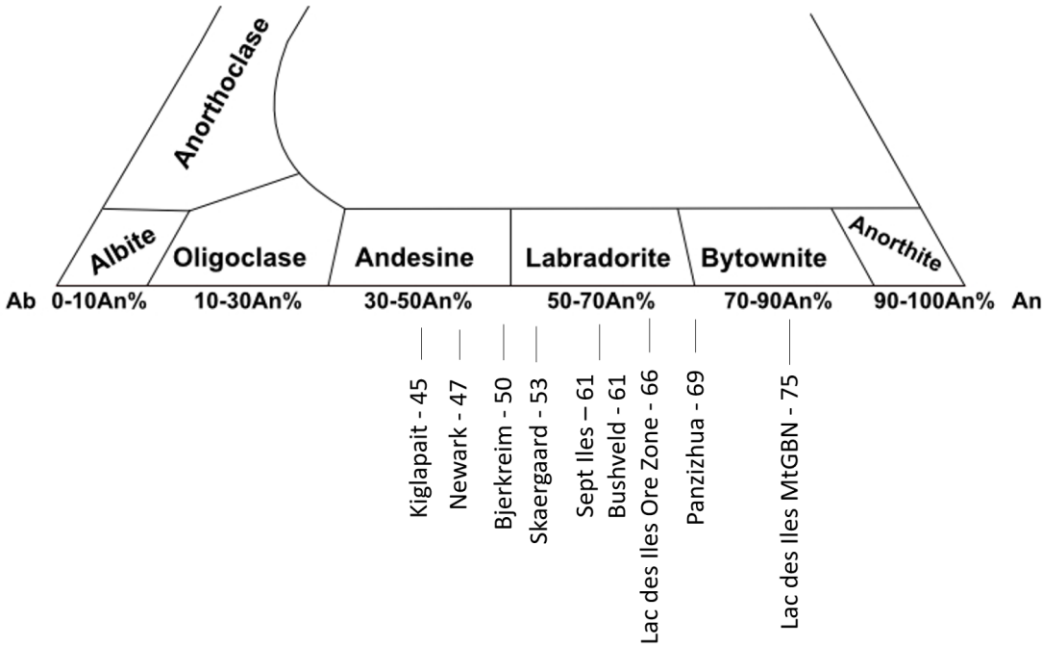

Figure 5.7. Plagioclase compositions of Fe-Ti oxide deposits.

Fe-Ti oxides and Al-spinel

Sub-solidus re-equilibration processes resulting from miscibility gaps in the system $FeO–Fe_2O_3–MgO–TiO_2–Al_2O_3$ can be preserved in Fe–Ti oxides. Exsolutions are responsible for a large variety of microscopic textures and the most common exsolutions result from the miscibility gaps in magnetite–ulvöspinel and hematite–ilmenite solid solutions (Charlier et al., 2015). Although subsolidus exsolution locally redistributes some of the

trace elements, the presence and type of exsolution minerals reflects the primary composition of the Fe-oxide that crystallized from the liquid (Dare et al., 2012). Fe-Ti oxides in the gabbronorite in the MBI at LDI display exsolutions that can be grouped into three main types: exsolution of Al-spinel in magnetite, exsolution of ilmenite in magnetite ($Spinel_{ss}$), and exsolution of hematite in ilmenite ($Ilm\text{-}Hem_{ss}$ — solid solution).

No exsolutions of Al-spinel were observed in the primary ilmenite, only in magnetite and in the ilmenite that exsolved from the magnetite, which indicates that Al went to titanomagnetite, not to the primary ilmenite. As well as the two-component solid solution of magnetite and ulvöspinel, pleonaste, an intermediate member of the hercynite-$spinel_{ss}$ series, is the most common representative of Al-spinel exsolutions in titanomagnetite, and, more rarely, in ilmenite (Gross, 2015). The diadochic substitution of Fe^{3+} for Al^{3+}, and Fe^{2+} for Mg^{2+} and Zn^{2+}, is responsible for the presence of $FeAl_2O_4$ (hercynite), $MgAl_2O_4$ (spinel), and $ZnAl_2O_4$ (gahnite) in solid solution (Arguin et al., 2018).

The most abundant exsolution in the magnetite in the MBI at LDI is granular-type ilmenite exsolution, followed by sandwich, and trellis-type ilmenite exsolutions. Magnetite in the MBI at LDI does not show cloth-like lamellae, but the preservation of these is relatively rare because under relatively oxidizing conditions, ulvöspinel is unstable and changes to ilmenite (Buddington and Lindsley 1964). Ilmenite exsolutions within magnetite can form through 1) exsolution of ulvöspinel at T<600°C, which forms ultra-fine, cloth-textured lamellae (Ramdohr 1953; Price 1981). The miscibility gap of ulvospinel (Usp)–Mt_{ss} (~600 °C) would separate an ulvospinel-rich phase from the $spinel_{(ss)}$ on slow cooling, in response to a decrease in the solubility of its solid solution state at lower temperatures, initially exsolving as ulvospinel (cloth-like lamellae) and becoming oxidized to ilmenite at a later stage (Arguin, 2008; Tan & Liu, 2016). Or, 2) exsolution of ulvöspinel at T>600°C. Buddington and Lindsley (1964) proposed that ilmenite exsolutions in magnetite could be ascribed to the oxidation of the ulvöspinel component at temperatures above the magnetite-ulvöspinel solvus. These authors also suggested that increasing degrees of diffusion during this oxy-exsolution process result in a systematic progression of ilmenite exsolution textures from the trellis-type texture of thin ilmenite lamellae; through the

sandwich-type texture of thick ilmenite lamellae; magnetite-hosted granular exsolutions; to external granular exsolutions (Arguin, 2018).

The absence of cloth-like ilmenite texture and the predominance of thick-lamellae textures (i.e., sandwich-type and external granules) in magnetite from the magnetite gabbronorite in the MBI at LDI suggests super-solvus ilmenite exsolution formed from titanomagnetite of the same composition. Coarse-grained granular exsolution features (such as granular ilmenite exsolutions), as well as Al-spinel exsolution in magnetite, occur at >750 °C (Buddington and Lindsley, 1964; Mucke, 2003). Buddington and Lindsley (1964) showed that at high temperatures, ilmenite tends to migrate to grain boundaries where it forms granular oxy-exsolutions, whereas, at lower temperatures and slower diffusion rates, ilmenite is prevented from leaving the host magnetite and instead remains as lamellae or granules inside the titanomagnetite (Dare at el., 2012). The predominance of granular-type ilmenite exsolutions in the MBI at LDI suggests that temperatures likely remained high, allowing its formation. Then, the temperature rapidly decreased, preventing the formation of sub-solvus ilmenite.

$Spinel_{ss}$ and $Ilm–Hem_{ss}$ can crystallize simultaneously from magmas at a wide range of O fugacities and temperatures (Buddington & Lindsley, 1964). Primary, euhedral to sub-euhedral ilmenite commonly crystallizes simultaneously with Ti-rich magnetite. A miscibility gap would separate a hematite-rich phase from an ilmenite-rich phase on cooling, and the ilmenite in many mafic-ultramafic intrusions thus contains hematite exsolutions (Tan & Liu, 2016). Coarse primary ilmenite grains with hematite lamellae in the MBI at LDI indicate primary ilmenite crystallization. When hematite content exceeds 7–9 wt.%, ilmenite may exsolve lenses of hematite, and it is called hemo-ilmenite (Charlier et al., 2015). In the MBI primary ilmenite could suggest a high TiO_2 concentration in the magma since, under common geological conditions, ilmenite and magnetite are present on the liquidus together with clinopyroxene when the TiO_2 concentration in the magma is over 4 wt% (Unganai et al., 2022 and references therein).

Grant (2020) evaluated the origin of coarse-grained ilmenite by using bulk rock Ti and Fe contents and compared it with the bulk rock composition of massive oxides from the Lac Tio Ti deposit (dominated by hemo-ilmenite), and the Buttercup Fe-Ti-V deposit (dominated by titanomagnetite with limited ilmenite exsolutions) so that ilmenite of samples displaying similar whole-rock Ti-Fe compositions to Buttercup probably formed through external granule exsolution of titanomagnetite, rather than by direct crystallization. The plot of the bulk rock data from samples of the gabbronorite in the MBI at LDI (Fig. 5.8) reveals a low titanium content closer to Buttercup composition even though they contain rare coarse-grained ilmenite, indicating they formed through exsolution of titanomagnetite rather than crystallized from a high-Ti magma. This suggests a high fO_2 of the magma since it allows the incorporation of approximately 7-9 wt.% hematite into the ilmenite structure (Grant 2020).

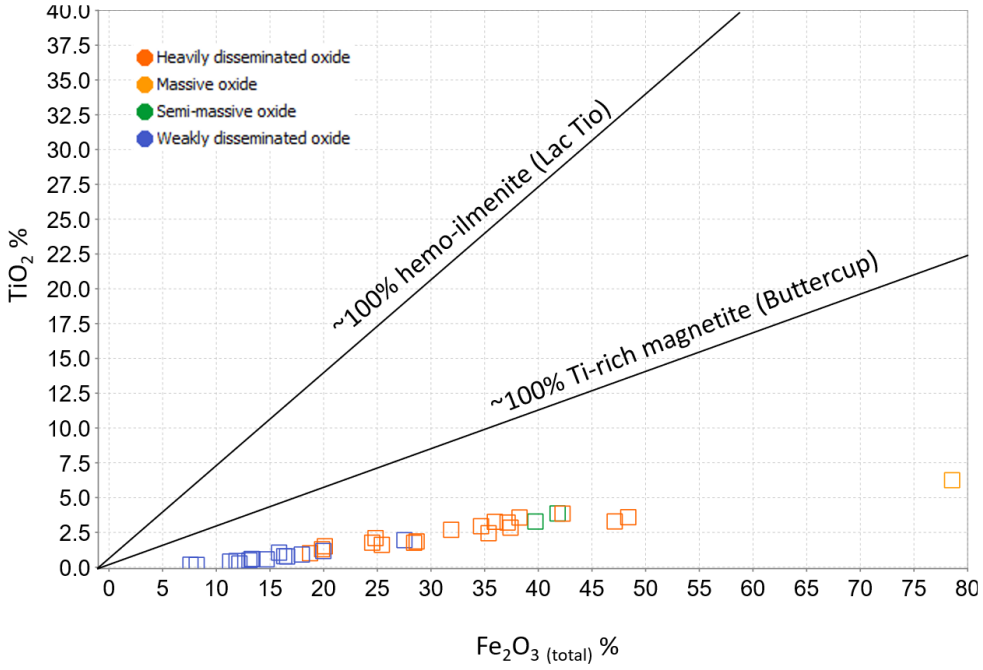

Figure 5.8. Comparison of bulk rock Ti and Fe contents from magnetite gabbronorite in the MBI at LDI with massive oxides from the Lac Tio Ti deposit (dominated by hemo-ilmenite), and Buttercup Fe-Ti-V deposit (dominated by titanomagnetite and low ilmenite exsolutions; Adapted from Grant, 2020).

All observed Fe-Ti oxide mineralization in the gabbronorite in the MBI at LDI is dominated by magnetite with less abundant primary ilmenite that shows hematite exsolutions throughout the studied section. The presence of these phases could suggest oxidizing conditions since it has been shown that the magnetite content of magnetite–ulvöspinel series and the hematite content of ilmenite–hematite series both increase with increasingly oxidizing conditions (Charlier et al., 2015, and reference therein).

During periods of slow cooling, as well as during metamorphism, Fe-Ti oxide minerals can undergo extensive sub-solidus re-equilibration with a net effect of purification towards their end-member compositions by means of inter-oxide, oxide-silicate, or intra-oxide re-equilibration (Pang et al., 2008; Dare et al., 2012; Nadoll et al., 2014; Valvasori, 2020). Therefore, it is important to establish if sub-solidus processes (post-cumulus evolution) have significantly modified the primary composition of the Fe-oxide. Knowledge of the primary composition of magnetite (titanomagnetite) is crucial for the reconstruction of fractionation processes. This composition was calculated as follows. The concentrations of elements in the Fe oxides (magnetite and ilmenite exsolutions) were obtained from a laser ablation line in such a way that magnetite segments and ilmenite segments can be chosen from the same grain. By using the images obtained by micro XRF, the area corresponding to ilmenite and magnetite throughout the thin section was obtained. The sum of the areas of magnetite and ilmenite correspond to the total area of Fe oxides in the thin section. By dividing the area of magnetite by the total area of Fe oxides, the area of the magnetite fraction is obtained and similarly by dividing the area of ilmenite by the total area of Fe oxides, the area of the ilmenite fraction is obtained. To obtain the concentration of an element in the titanomagnetite before the ilmenite exsolution for a thin section, multiply the fraction of magnetite by the content of that element in magnetite and add it to the result of multiplying the fraction of ilmenite by the content of that element in ilmenite.

Fe-Ti oxides from the MBI at LDI show intra-oxide re-equilibration processes with the ilmenite gaining Ti, Mn, Nb, Sc, and Zr and the magnetite gaining Fe, Cr, and V (Fig. 5.9). Upon cooling, coexisting Ti-magnetite and ilmenite undergo $Fe^{2+}Ti^{4+}$ for 2 Fe^{3+} exchange, with the magnetite gaining Fe^{3+} and the ilmenite gaining

$Fe^{2+}Ti^{4+}$, leading to natural "purification" of both minerals (Gross, 2015; Charlier et al., 2015). For example, adjacent Ti-magnetite and ilmenite may interact following the reaction $FeTi_2O_4$ (in magnetite) + Fe_2O_3 (in ilmenite) → Fe_3O_4 (in magnetite) + $FeTiO_3$ (in ilmenite; Buddington and Lindsley, 1964; Duchesne, 1972). In the Sept-Iles layered intrusion and, in the Lac St. Jean anorthosite, it has been demonstrated that, during co-crystallization of both Fe-Ti oxides, ilmenite preferentially incorporates HFSE, Sc, and W, whereas magnetite preferentially accommodates Al, Ga, Mg, Ni, and Cr (Méric, 2011; Néron, 2012 in Duran et al., 2016). The development of exsolutions in the magnetite grains in the gabbronorite of the MBI led to the local concentration of certain trace elements in either the host or the exsolved phase. Titanium, Mn, Nb, Sc, and Zr show higher concentrations in ilmenite since these elements go to ilmenite (by exsolution), so they are depleted in magnetite.

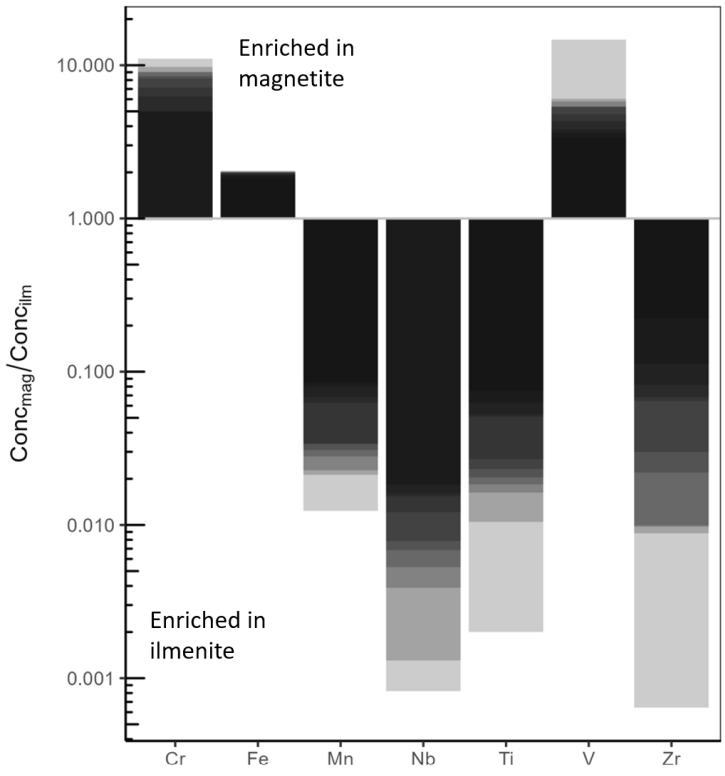

Figure 5.9. Bar graph displaying the partitioning behavior of trace elements between magnetite and ilmenite from the Mine Block Intrusion (MBI) at Lac des Iles (LDI), as quantified by the enrichment factor (ConcMag/ConcIlm).

When comparing Mg, Zn, and Co in titanomagnetite (prior to exsolution and oxidation) with magnetite (current), from samples of the MBI at LDI (red boxes in Fig. 5.10), they do not show a significant change, suggesting that there was no exchange of those elements due to re-equilibrium with silicates. The main effect of this re-equilibration with silicates is to drive down the MgO content of Fe–Ti oxides (Charlier et al., 2015). The concentration of (divalent) elements such as Mg, Zn, and Co usually show changes in magnetite due to re-equilibration with silicates.

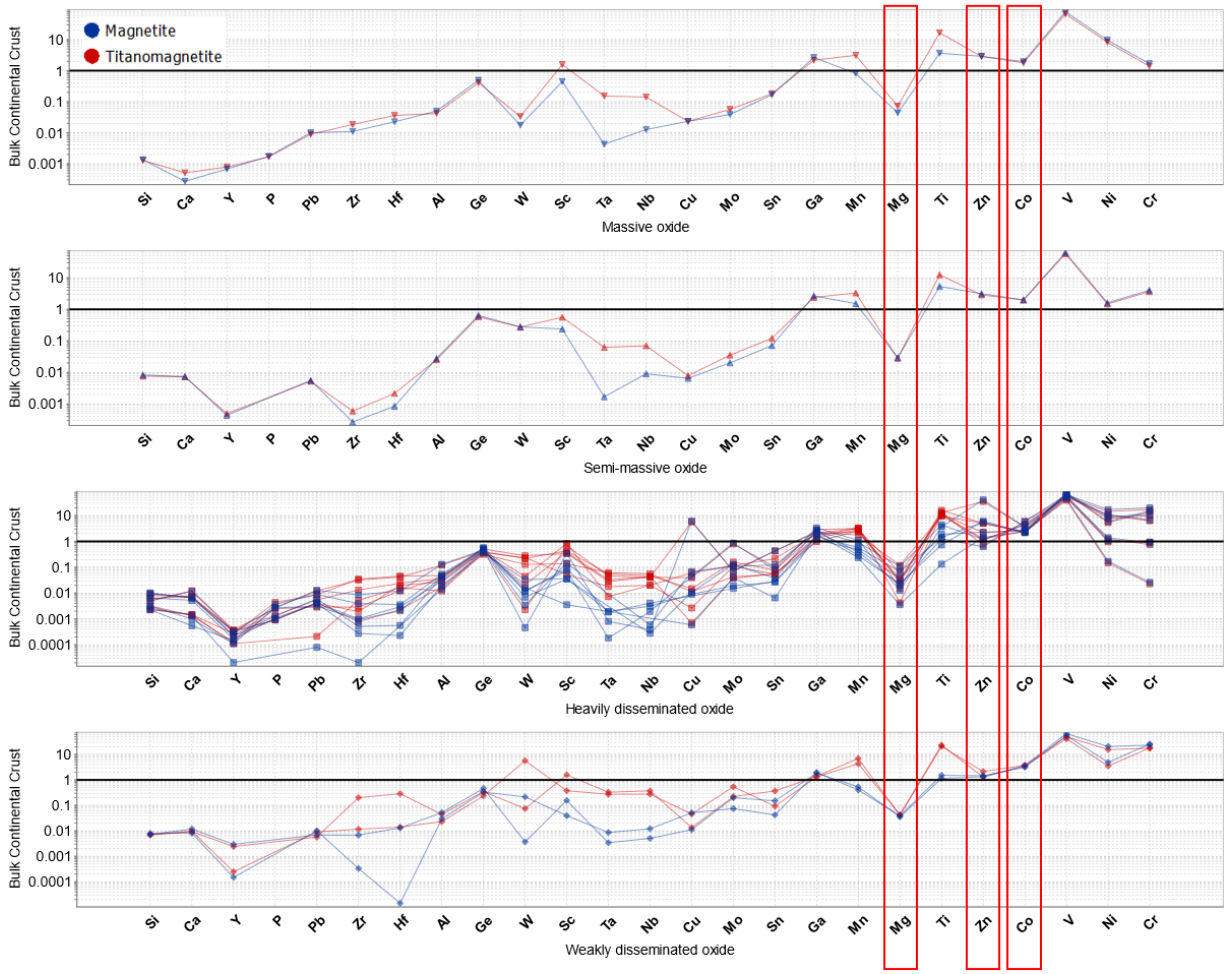

Figure 5.10. Bulk continental crust normalized multi-element diagram (based on Dare et al., 2012) of magnetite and titanomagnetite from the Mine Block Intrusion at Lac des Iles magnetite gabbronorite.

Although there is no evidence of sub-solidus re-equilibration between Fe-oxides and silicates which would suggest magnetite composition has not been modified, intra-oxide re-equilibration processes have occurred

indicating the importance of determining and utilizing the composition of primary titanomagnetite (before ilmenite exsolutions occurred).

Although the alteration observed in the petrography of the samples analyzed from the gabbronorite in the MBI at LDI could suggest a hydrothermal origin for the magnetite, the Ti content greater than 2%, ilmenite exsolutions, and the Ni/Cu ratios indicate that titanomagnetite from the LDI gabbronorite has an igneous origin. Magnetite from felsic rocks and hydrothermal magnetite generally has lower Ti (<2 wt.%) than magnetite from mafic-intermediate igneous rocks (Dare et al., 2019). Vanadium, Ni, and Cr are usually the most enriched elements in magmatic magnetite, whereas they are depleted in hydrothermal magnetite (Dare et al., 2014; Nadoll et al., 2014). Due to their abundance in silicate melts and/or high partitioning coefficients between magnetite and silicate melt at high temperatures, igneous magnetite generally has high Ti, Al, Mg, and Mn (Wen et al., 2017). Magmatic magnetite may also be enriched in some chalcophile elements, such as Pb, Cu, Mo, Sn, Zn, and Co (Dare et al., 2012, 2014). A number of diagrams have been proposed to discriminate magmatic and hydrothermal magnetite. For instance, Dare et al. (2019; Fig 5.11a) use the Ni/Cr ratio and Knipping et al. (2015; Fig 5.11b) use Ti and V contents. In both diagrams, magnetite samples from the gabbronorite at LDI fall within the range of igneous magnetite consistent with a magmatic origin and enrichment in vanadium.

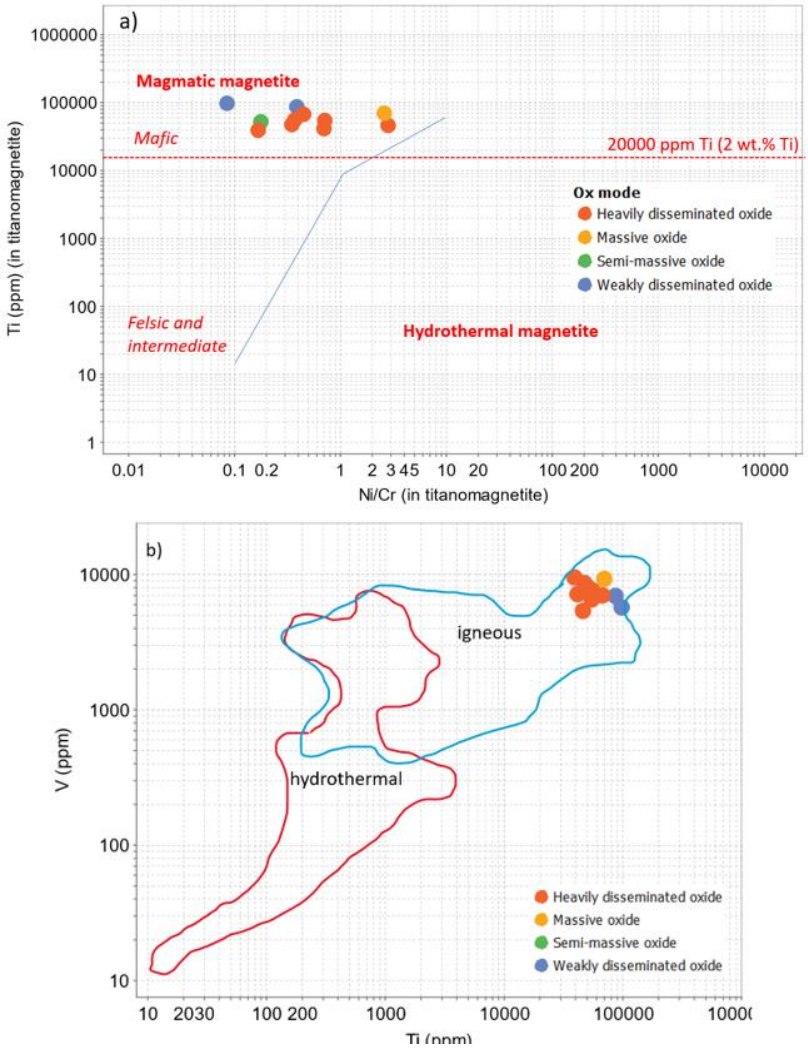

Figure 5.11. Plot of magnetite samples from the MBI at LDI in discrimination diagrams to identify magnetite from magmatic and hydrothermal origin. a) Plot of Ti (ppm) versus Ni/Cr ratio (un-normalized) in magnetite (Adapted from Dare et al., 2014). b) Plot of Concentration of Ti vs. V in magnetite. Blue area includes igneous formed magnetite, while red area is defined by hydrothermal magnetite (Adapted from Knipping et al, 2015).

To examine the effect of fractionation of a silicate melt on the trace element content of magnetite, Dare et al. (2014) analyzed Fe-oxides from the lowermost layers (Fe-Ti-V deposits) and the uppermost layers (Fe-Ti-P deposits) of massive magnetite in the Bushveld Complex and Sept Iles, and they reported that magnetite from V deposits (i.e., lowermost layers) has a more primitive signature (enriched in magnetite-compatible elements: Cr, Ni, V, Co, Mg; and depleted in magnetite-incompatible elements) than magnetite from the P deposits (i.e.,

uppermost layers), which has a more evolved signature (depleted in compatible but enriched in magnetite-incompatible elements (Ti, Mn, Sn, Mo, and HFSE — Nb, Ta, Sc, Zr, and Hf; Dare et al., 2014, 2019).

Dare et al. (2014) summarized variations observed in the trace element composition of magnetite relative to melt fractionation using well-characterized samples from various magmatic environments in a multielement variation diagram, where higher values for elements compatible with magnetite increase to the right. When samples from the magnetite gabbronorite in the MBI at LDI are plotted on this multielement variation diagram, the pattern of compatible elements such as V, Ni, and Cr shows a distribution from primitive to evolved magnetite (Fig. 5.12). This distribution allows for the observation of the effect of silicate magma fractionation on the trace elements within magnetite from MBI in LDI. Consequently, it suggests that magnetite at MBI crystallized from a magma of primitive composition (Fe-Ti-V) rather than from a more evolved magma (Fe-Ti-P), which is consistent with the absence of apatite and the low phosphorus contents observed in whole rock geochemistry.

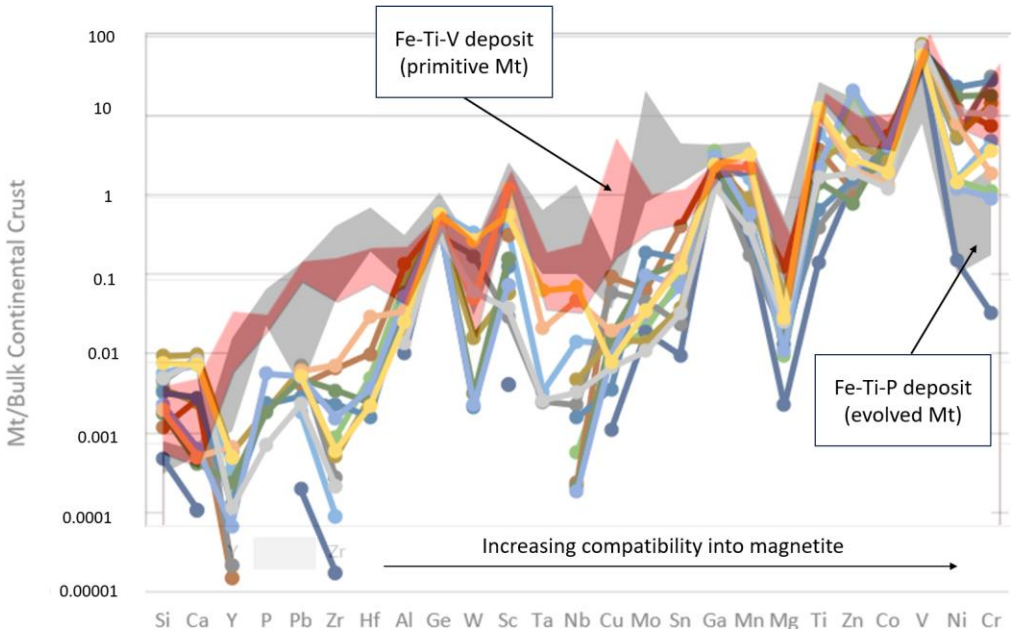

Figure 5.12. Multielement variation diagrams normalized to bulk continental crust (values from Rudnick and Gao, 2003) of magnetite from MDI at LDI, compared to magnetite (Mt), from magmatic magnetite from intermediate magmas (Fe-Ti-V deposits; pink field (Bushveld Complex, S. Africa), Fe-Ti-P deposits; gray field (Sept Iles, Canada; St. Charles de Bourget, Canada; Bushveld Complex: adapted from Dare et al., 2014).

Although fractionation of silicate magma is suggested in Figure 5.12 for samples from the gabbronorite in MBI at LDI, geochemically discriminating magnetite from Fe-Ti-V and Fe-Ti-P deposits is best performed using a small number of elements (Cr, Ni, V ± Ti, Mo, Ga, Nb, and Ta; Dare et al., 2014). The upward decrease of some of the compatible elements, such as Mg, Ni, V, and Cr in the gabbronorite from the MBI (Fig. 5.13), is consistent with the evolution of the composition of a silicate melt recorded by magnetite, since, generally, elements compatible during magnetite crystallization (Mg, Ni, Co, V, and Cr) are concentrated in more primitive magnetite from the lowermost layers (Ti-V deposits) and decrease up sequence in layered intrusions, with the lowest values in those from the uppermost (Ti-P deposits) magnetite layers (Dare et al., 2014; 2015).

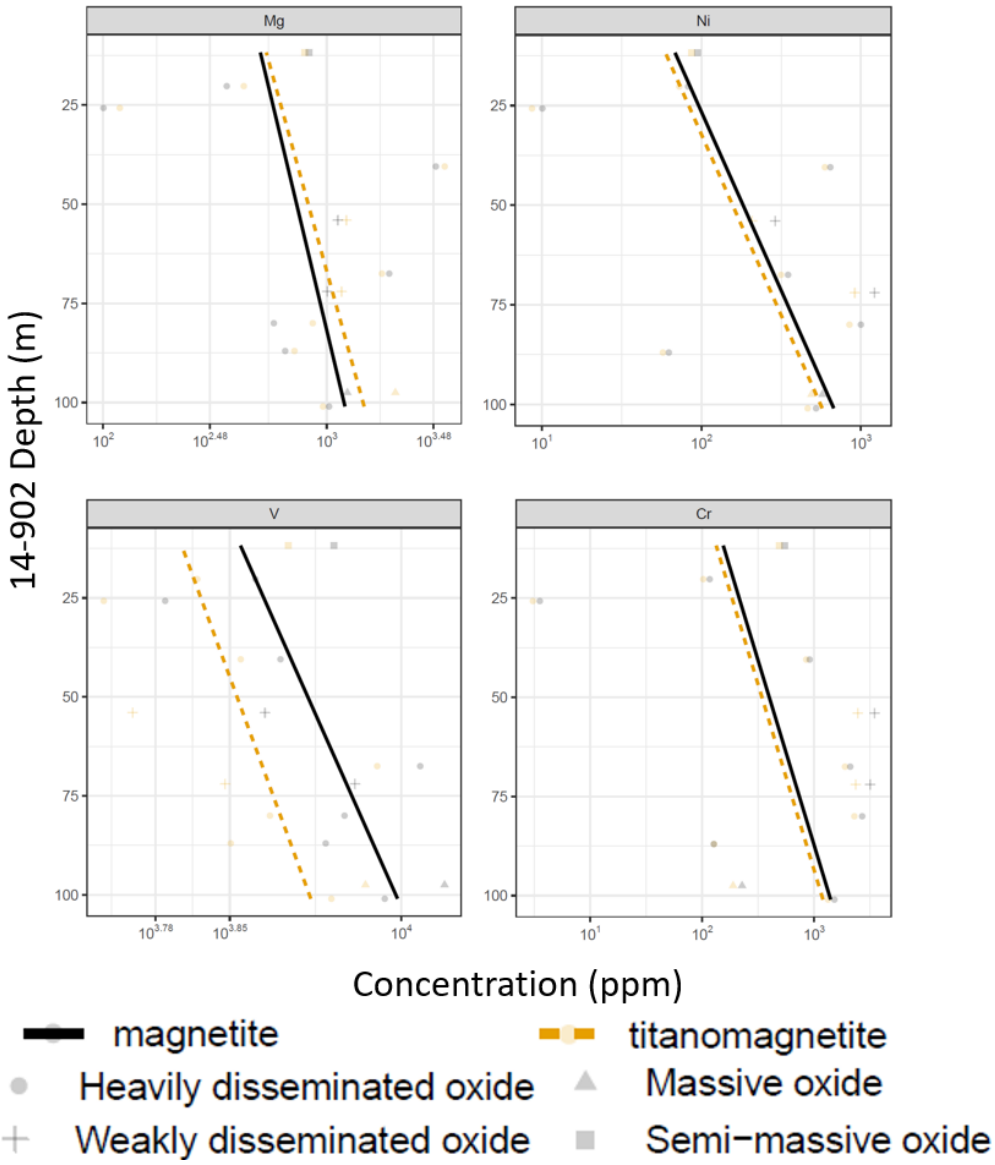

Figure 5.13. Magnetite-compatible elements from the Mine Block Intrusion (MB) at LDI (Lac des Iles). Lines represent regressions through the data.

Fractionation of the silicate melt to form the MBI magnetite gabbronorite in LDI is suggested in Figure 5.14 given the upward increase of some of the magnetite-incompatible elements such as Mo, Zn, Mn, and Ti, since, in general, during fractionation magnetite-incompatible elements (Ga, Ge, Hf, Mn, Mo, Nb, Sc, Sn, Ta, Ti, W, Zn, and Zr) increase up section and are concentrated in more evolved magnetite in the uppermost parts of the intrusions, even when trace amounts of immiscible sulfides formed (Dare et al., 2014; 2015).

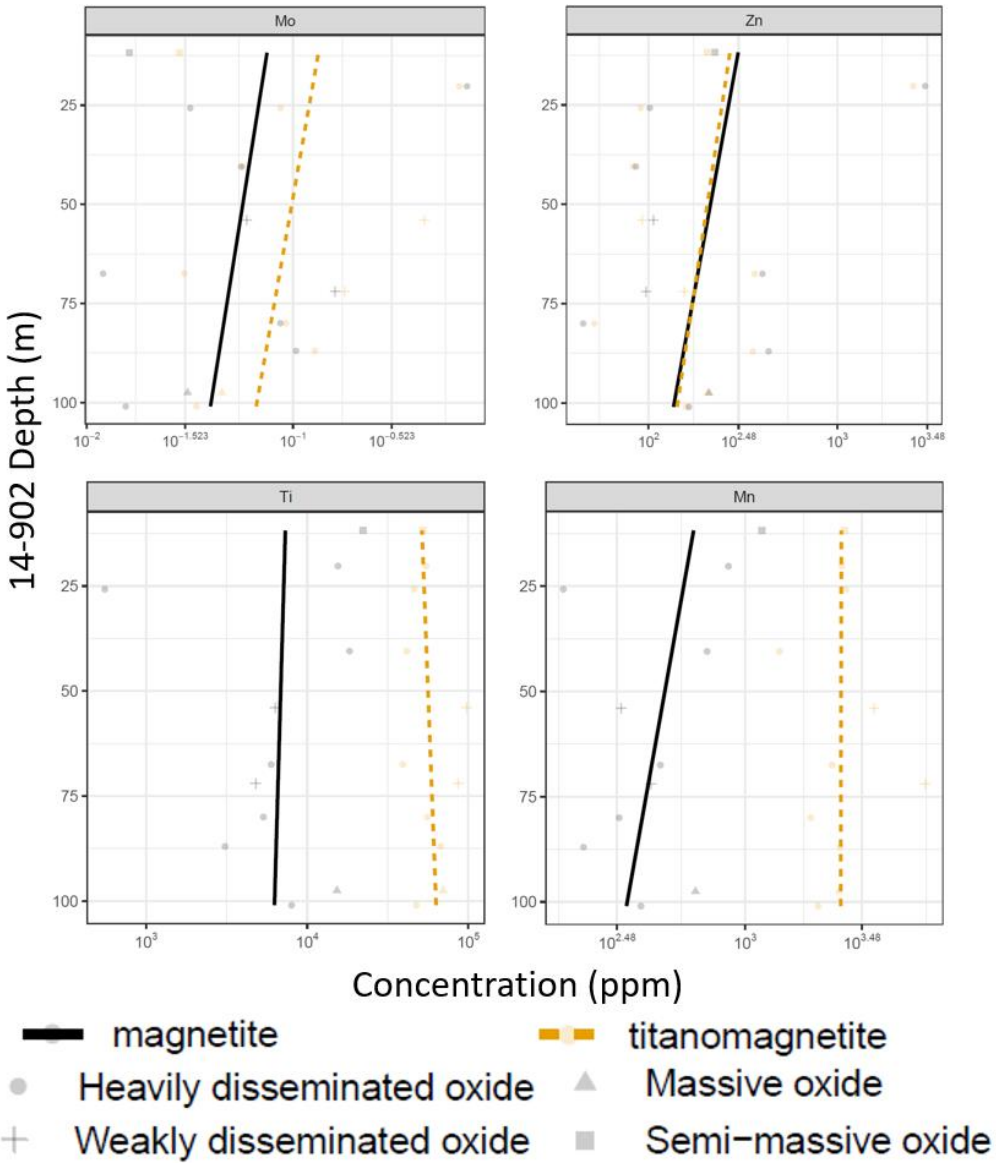

Figure 5.14. Magnetite-incompatible elements from the Mine Block Intrusion (MB) at LDI (Lac des Iles). Lines represent regressions through the data.

The upward decrease of elements compatible with magnetite, such as Mg, Ni, V, and Cr, and the upward increase of magnetite from elements incompatible with magnetite, such as Mo, Zn, Ti, and Mg, suggests fractional crystallization of the silicate melt from a less evolved melt to a more evolved one.

The variation in the An-number in plagioclase (Fig. 4.6) and the upward variations of compatible and incompatible elements in magnetite (Fig. 5.13 and 5.14) indicate normal fractionation processes in the magnetite

gabbronorite of the MBI at LDI. The crystallization of Fe-Ti oxides at a relatively early stage could have triggered the gravitational settling and sorting of Fe-Ti oxide crystals, driven by the strong density contrast between Fe-Ti oxides (~4.5-4.6 g/cm^3) and basaltic magma (~3.1-3.2 g/cm^3), which resulted in the cumulate textures observed in the magnetite gabbronorite in the MBI at LDI (Pang et al., 2010; Charlier et al., 2015).

As an alternative to fractional crystallization, liquid immiscibility has been proposed as one of the mechanisms responsible for the formation of Fe-Ti oxide deposits hosted in mafic-ultramafic rocks (Zhou et al., 2005; Charlier et al., 2015). This model involves the separation of highly evolved Fe–Ti-rich basaltic magmas (i.e., ferrobasalts) into a pair of immiscible silicate liquids. During phase separation, the denser Fe-rich melt ponds at the base of the magma chamber or even percolate down into the upper part of the cumulate pile. As the Fe-rich silicate liquid then crystallizes, it will leave Fe–Ti oxides (Ti magnetite or ilmenite) either as monomineralic layers concordant with layering, as downward-stepping sills and dikes cutting the previously formed silicate cumulates, or as poikilitic or net -textured oxide accumulations surrounding previously formed cumulus silicates (Mungall, 2014). Features described as the result of liquid immiscibility are not observed in the samples analyzed at LDI. Instead, textures in the magnetite gabbronorite of the MBI at LDI suggest that Fe-Ti oxides and silicates formed simultaneously. The continuous variation of the trace element contents in magnetite with depth without any sharp changes, as would be expected if the magma had split into two immiscible melts, also argues against the liquid immiscibility process as an explanation for the oxide crystallization in the rocks analyzed. In a basaltic magmatic system, the partitioning of magma into Si-rich melts and Fe-rich melts only occurs at the late stage of magma evolution, just above 1,000°C, and only plays a role during the later stages of basaltic magma fractionation (Ding et al., 2023). Although the multi-element variation diagram (Fig. 5.12) suggests magma fractionation in the MBI, it shows that fractionation has not evolved sufficiently to crystallize apatite, indicating that the magma was not in its last stage of evolution, making it unlikely that liquid immiscibility occurred (Charlier et al., 2015).

Magma mixing has been postulated as another Fe-Ti ore-forming mechanism (Hoatson and Keays, 1989; Li et al., 2002; Charlier et al., 2010). Cawthorn and Walraven (1998) showed that repetitive magma addition in the Lower Zone of the Bushveld Complex produced the layering and oscillations in the Mg-number in mineral and whole-rock compositions. The Mg-number from the magnetite gabbronorite at LDI does not show any rapid decrease (Fig. 5.15), suggesting no magma addition in the section studied at LDI. Evidence of magma mixing in layered intrusions also includes rhythmically alternating monomineralic layers of oxide and silicate minerals in sharp, straight contacts with the underlying layer and in sharp to gradational contact with the overlying layer, compositional reversal to more primitive mineral compositions as a result of a new magma influx, and large variations in compatible elements such as Mg, Mn, V, and Cr in Fe-Ti oxide minerals between layers (Valvasori, 2020). None of this evidence was observed in the rocks studied, indicating that magma mixing did not occur in the analyzed section of the magnetite gabbronorite in the MBI. Rhythmically alternating mono-mineralic layers of oxides and silicates in the magnetite gabbronorite at LDI were not observed. Although compatible elements in magnetite, such as Cr, Mg, and Co, show variations towards the middle of the studied section, they do not constitute reversal to more primitive mineral compositions.

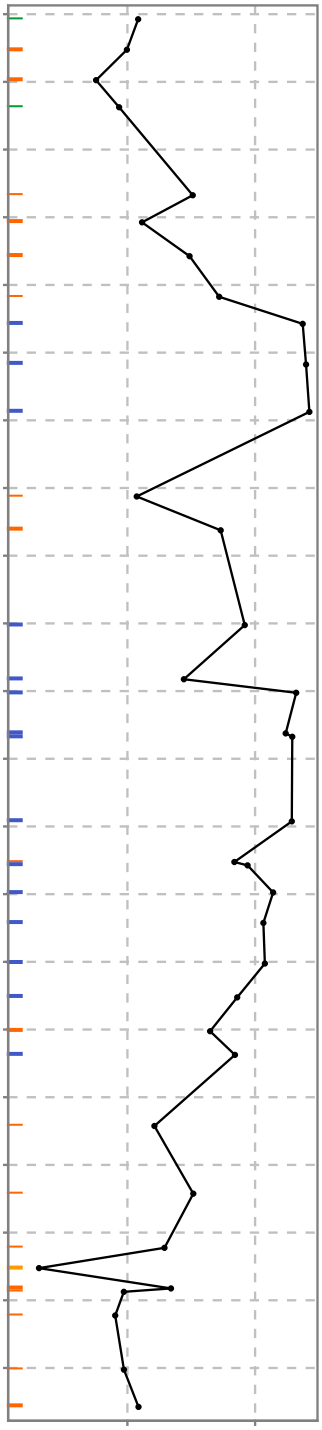

Figure 5.15. Magnetite gabbronorite magnesium number (whole rock) from the Mine Block Intrusion at LDI.

5.5. Economic potential of the Fe-Ti oxide mineralization

Various authors have proposed empirical magnetite discrimination diagrams with fields derived from in-situ analyses of magnetite from various types of ore deposits based on the principle that magnetite origin provides insight into the physicochemical conditions of magnetite formation and the mineral deposit it is associated with (Valvasori et al., 2020).

It has been shown that the Ni + Cr vs. Si + Mg plot (Dupuis and Beaudoin, 2011) is useful for identifying magnetite-bearing samples from Ni-Cu-PGE and Cr magmatic deposits versus those from all other deposit types (Boutroy et al., 2014; Fig. 5.16). The magnetite in the MBI gabbronorite at LDI can be considered as belonging to the Fe-Ti-V deposit group according to the classification scheme proposed by Dupuis and Beaudoin (2011; Figs. 5.16, 5.17). Iron oxide compositions that plot outside the Ni–Cu–PGE and the VMS fields belong to groups of samples from Iron–Oxide–Copper–Gold (IOCG), Kiruna-type, porphyry-Cu, Banded Iron Formation (BIF), skarn, Fe–Ti, and V. Magnetite samples analyzed by LA-ICP-MS of the MBI gabbronorite at LDI fall outside of the Ni-Cu-PGE field, suggesting they do not belong that kind of deposit (Fig. 5.16).

Dupuis and Beaudoin (2011) and Nadoll et al. (2014) proposed a scheme to discriminate magnetite from various geologic environments based on Ni/(Cr + Mn), Ca + Al + Mn (or Al + Mn) and Ti + V contents. By using that diagram, it is possible to distinguish magnetite in massive Fe-Ti-V ore (high Ti + V) from all other deposit types. Figure 5.17 indicates that magnetite samples analyzed by LA-ICP-MS of the MBI gabbronorite at LDI belong to the Fe-Ti-V deposit type.

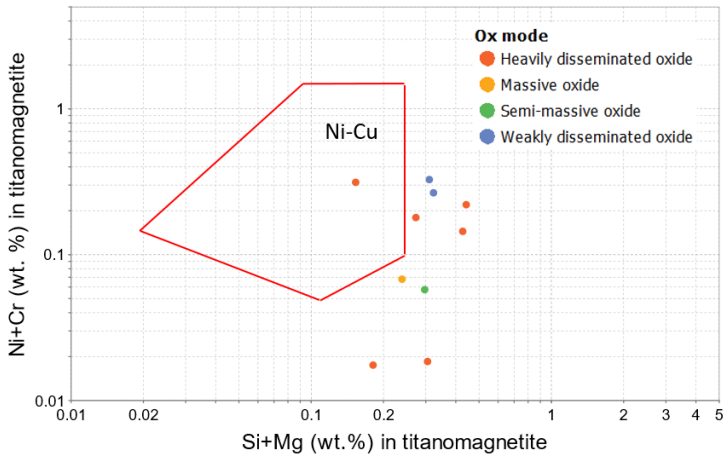

Figure 5.16. Ni+Cr vs. Si+Mg discriminant diagram of average Fe-oxide deposit composition for Ni-Cu deposits compared to other deposit types (Dupuis and Beaudoin, 2011).

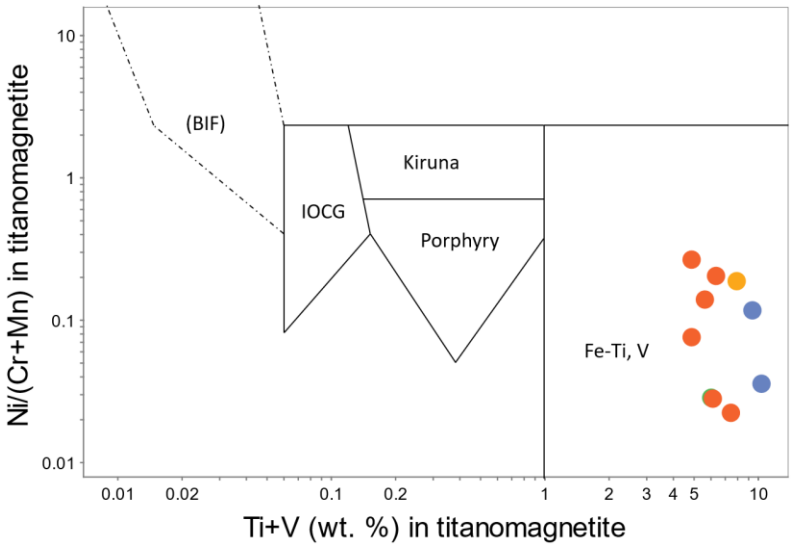

Figure 5.17. Ni/(Cr+Mn) vs. Ti+V discriminant diagram for average Fe-oxide compositions from Kiruna, IOCG, porphyry Cu, Fe-Ti-V, and BIF deposits (Dupuis and Beaudoin, 2011).

With about 26 Mt in reserves and an average bulk grade of about 0.5 wt.% V_2O_5, the Rhovan deposit in the Bushveld Complex of South Africa is the largest deposit mined for vanadium. Deposits in the Panzhihua region (China) contain resources of over 1300 Mt at about 0.3 wt.% V_2O_5 (Zhou et al., 2005).

Figure 5.18 compares V_2O_5 (wt.%) and Fe_2O_3 (wt.%) whole-rock from vanadiferous titanomagnetite of the Pazhihua and Rhovan (Bushveld) vanadium production mines with the vanadium content found in this study. The low-grade, high-tonnage Panzhihua mine in China has a vanadium oxide average bulk grade of 0.3 %, and the low-tonnage, high-grade production mines in the Bushveld, South Africa, has a vanadium oxide average bulk grade of 0.5 %. Although the data from this study has an average of 0.19 V_2O_5 (wt.%), in the MBI at the LDI mine, heavily disseminated, semi-massive, and massive oxides show a vanadium content above the average bulk grade of Panzhiua and the Lac Dore deposit in Canada or even higher than the Rhovan mine in the Bushveld deposit, which could suggest a V potential for the magnetite gabbronorite rocks at Lac des Iles if the tonnage is enough. The Lac Doré deposit is an example of an orthomagmatic oxide deposit in Canada. Resource estimates for the Lac Doré deposit total about 100 Mt at a grade of 0.49% V_2O_5 (wt.%), making it the largest undeveloped V deposit in North America (Kerr et al., 2013).

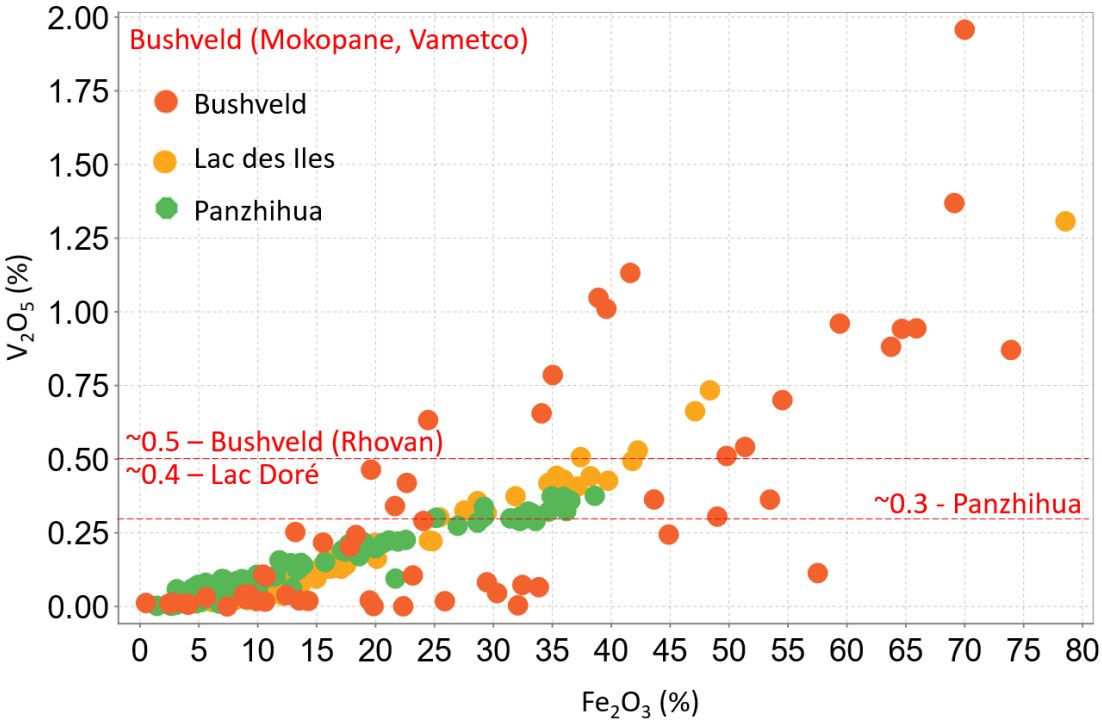

Figure 5.18. V2O5 (%) - Fe2O3 (%) bivariate whole-rock plot. Comparison of different deposits (Taken from Barnes et al., 2004; Song et al., 2013; Mathieu, 2019, Lac des Iles from this study) with V2O5 (%) grade reported from the Bushveld and Panzhihua mines.

The vanadium-rich magnetite gabbronorite in the MBI at the LDI possesses some features, including i) association with a subduction setting, whereas most V deposits are plume-related, ii) low-Ti magma, and iii) occurrences of mineralization associated with primitive silicates (plagioclase) in low stratigraphic positions that contrast with some characteristics of magmatic Fe–Ti oxide deposits worldwide summarized by Pang et al. (2010; Table 5.1).

Table 5.1. Characteristics of magmatic Fe-Ti oxide deposits worldwide (Modified from Pang et al., 2010).

Association	Host rock	Ore occurrence	Ore mineralogy	Example
Proterozoic anorthosite complexes	Anorthosite, leuconorite, leucogabbro, leucotroctolite	Cross-cutting, massive lenses with sharp contacts against host rocks	Hemo-ilmenite or titanomagnetite, with or without apatite	Tellnes (Norway), Lac Tio (Canada)
Upper parts of large layered complexes	Gabbronorite, ferrogabbronorite, ferrodiorite	Conformable, laterally extensive layers with either sharp or gradational contacts against host rocks	Titanomagnetite, with or without apatite	Bushveld (South Africa), Windimurra (Australia)
Lower parts of sub-volcanic intrusions associated with flood basalts	Gabbro, ferrogabbro, ultramafic cumulates	Conformable, massive lenses or layers with either sharp or gradational contacts against host rocks	Titanomagnetite, with or without ilmenite	Panzhihua (China), Hongge (China)
Lower parts of an intrusion in a subduction setting	Gabbro, Gabbronorite, and norite cumulates	Comfortable massive layers	Titanomagnetite, with or without ilmenite	Lac des Iles (Canada)

Chapter 6 - Conclusions

This study aimed to investigate the paragenesis of the magnetite gabbronorite in the Mine Block Intrusion at Lac des Iles and assess the possibility of V mineralization using petrography, whole rock geochemistry and laser ablation of magnetite.

The analyzed samples in the Mine Block Intrusion are layered, medium-grained gabbronorite rocks that consist of plagioclase (7 to 63 %), pyroxene (11 to 80 %), iron oxides (up to 81 %), and sulfides (up to 6%). Cumulate plagioclase and clinopyroxene, alternate as the predominant minerals. Fe-oxides mainly consist of magnetite, with lesser amounts of ilmenite. Disseminated, net-textured, and massive magnetite mineralization can be used to divide the gabbroic rocks into massive, semi-massive, weakly, and heavily disseminated oxides with similar oxide and silicate mineralogy, mineral textures, alteration, and textural relationships. In most analyzed samples, plagioclase is partially altered to sericite, and pyroxene has been partially to completely altered to tremolite-actinolite and talc, making it difficult to distinguish between orthopyroxene and clinopyroxene. Chlorite is an alteration product of pyroxene and plagioclase. The observed alteration can be attributed to regional metamorphism within the greenschist facies. Disseminated sulfides consist mainly of pyrite, with lesser chalcopyrite and pyrrhotite, and though they are ubiquitous, they are generally in low abundance.

Major element data indicate that the rocks have a broadly gabbroic composition with protoliths dominated by plagioclase, a predominance of orthopyroxenes over clinopyroxene, and titano-magnetite, which is consistent with the petrographic observations. Vanadium enrichment is observed in all rocks, although it is less in weakly disseminated oxide samples given the lower abundance of titanomagnetite. Compatible elements such as Cr, Ni, V, and Mg decrease in concentration up-section and are more abundant in heavily disseminated oxides than weakly disseminated oxides since they are compatible elements in magnetite (Dare et al., 2014). Scandium increases in heavily disseminated oxides, compared to weakly disseminated oxides, since it is a compatible element in ilmenite. Chalcophile elements such as Cu and Ni are probably associated with sulfides.

Plots of whole-rock geochemistry from samples of weakly disseminated oxides from the MBI are consistent with rocks derived from a depleted mantle source in a subduction-related setting (Vermeesch, 2006; Pearce, 2008; Saccani, 2015). This is consistent with the arc setting proposed for the Lac des Iles Complex by several authors (Brugmann et al., 1997; Barnes and Gomwe, 2010; Djon et al., 2018; Decharte et al., 2018; Jonsson, 2023).

Plagioclase composition decreases up hole, with no sharp change, suggesting a normal fractionation process that does not require magma injection events. Plagioclase identified within the magnetite gabbronorite of the MBI is labradorite-bytownite (An-number ranging from 0.58 to 0.75), which is less evolved than observed in other systems such as the upper zone of the Bushveld, which has a relatively evolved plagioclase composition (Cawthorn et al., 2005). This suggests that in the MBI Fe-Ti oxides occur at an early stage of differentiation compared with other mafic intrusions. EDS compositional data for pyroxene indicates the presence of clinopyroxene and orthopyroxene.

Fe-Ti oxides in the gabbronorite in the MBI at LDI display exsolutions that can be grouped into three main types: exsolution of Al-spinel in magnetite, exsolution of ilmenite in magnetite ($Spinel_{ss}$), and exsolution of hematite in ilmenite ($Ilm\text{-}Hem_{ss}$ — solid solution). Al-spinel exsolutions in magnetite can form at T_{max} of approximately 900°C, far higher than those at which cloth-textured intergrowths of magnetite and ulvöspinel start to form suggesting they formed before ulvöspinel exsolutions (Brown et al., 1957; Turnock and Eugster, 1962; Buddington and Lindsley, 1964). The most abundant exsolution in the magnetite in the MBI at LDI is granular-type ilmenite exsolution, followed by sandwich-, and trellis-type ilmenite exsolutions. The absence of cloth-like ilmenite texture and the predominance of thick-lamellae textures (i.e., sandwich-type and external granules) in magnetite suggest they formed at super-solvus temperature and that temperatures likely remained high (>750 °C), which allowed the ilmenite to migrate to grain boundaries where it formed granular oxy-exsolutions. Coarse primary ilmenite grains with hematite lamellae in the MBI at LDI indicate primary ilmenite

crystallization and suggest a high TiO_2 concentration in the magma. However, comparison with rocks dominated by hemo-ilmenite (Lac Tio deposit) and titanomagnetite (Buttercup Fe-Ti-V deposit) with low titanium contents suggests that the primary ilmenite crystallized from a low-Ti magma and granular ilmenite was formed through exsolution of titanomagnetite.

The Ni/Cu ratio, Ti content above 2%, along with the V, Ni, and Cr enrichment in the titanomagnetite from the MBI indicate its igneous origin. When plotting samples from the magnetite gabbronorite on the multielement variation diagram proposed by Dare et al. (2014), the effect of silicate magma fractionation on the trace elements within magnetite is observed. The diagram also suggests that magnetite at MBI crystallized from a magma of primitive composition (Fe-Ti-V) rather than from a more evolved magma (Fe-Ti-P), which aligns with the absence of apatite in petrography and the low P contents observed in whole rock geochemistry.

The upward decrease of some of the compatible elements, such as Mg, Ni, V, and Cr in the gabbronorite from the MBI, is consistent with the evolution of the composition of a silicate melt recorded by magnetite, since, generally, elements compatible during magnetite crystallization (Mg, Ni, Co, V, and Cr) are concentrated in more primitive magnetite from the lowermost layers (Ti-V deposits) and decrease up sequence in layered intrusions, with the lowest values in those from the uppermost (Ti-P deposits) magnetite layers. Fractionation of the silicate melt to form the MBI magnetite gabbronorite in LDI is also suggested, given the upward increase of some of the magnetite-incompatible elements such as Mo, Zn, Mn, and Ti, since, in general, during fractionation, magnetite-incompatible elements (Ga, Ge, Hf, Mn, Mo, Nb, Sc, Sn, Ta, Ti, W, Zn, and Zr) increase up section and are concentrated in more evolved magnetite in the uppermost parts of the intrusions. Plagioclase could have accumulated at the top of the magma chamber whereas the iron oxides would sink as they are denser, resulting in the cumulate textures observed in the magnetite gabbronorite in the MBI.

The magnetite in the MBI gabbronorite at LDI can be considered to belong to the Fe-Ti-V deposit group. The magnetite gabbronorite in the MBI is consistent with the type of hosted layered intrusions, characterized by

titanomagnetite as the dominant oxide mineral occurring in layers ranging from several tens of centimeters to several meters thick. Additionally, the oxide mineralization is associated with gabbronoritic cumulates. Although the data from this study has an average of 0.19 V_2O_5 (wt. %), several samples have concentrations above the Panzhihua mine V grade (0.3 wt.%) and outliers, corresponding to the massive oxide samples and some disseminated oxide samples from this study, have V concentrations above grade of the Rhovan (Bushveld Complex) vanadium mine (0.5 wt.%), which could suggest a vanadium potential for the magnetite gabbronorite rocks at Lac des Iles.

References

ALS. (2021). *Geochemistry Fee Schedule CAD*. ALS. https://www.alsglobal.com/

Arguin, J.-P., Pagé, P., Barnes, S.-J., Girard, R., & Duran, C. (2018). An integrated model for ilmenite, Al-spinel, and corundum exsolutions in titanomagnetite from oxide-rich layers of the Lac Doré Complex (Québec, Canada). *Minerals*, *8*(11), 476. https://doi.org/10.3390/min8110476

Bain, W. M., Hollings, P., Djon, L. M., Brzozowski, M. J., Layton-Matthews, D., & Dobosz, A. (2024). The geology, geochemistry, and magmatic evolution of the Legris Lake mafic–ultramafic complex, Ontario, Canada. *Mineralium Deposita*, *59*(1), 85–108. https://doi.org/10.1007/s00126-023-01183-x

Barnes, S.-J., & Gomwe, T. S. (2011). The Pd Deposits of the Lac des Iles Complex, Northwestern Ontario. In C. Li & E. M. Ripley (Eds.), *Magmatic Ni-Cu and PGE Deposits: Geology, Geochemistry, and Genesis* (Vol. 17, p. 0). Society of Economic Geologists. https://doi.org/10.5382/Rev.17

Boutroy, E., Dare, S. A. S., Beaudoin, G., Barnes, S.-J., & Lightfoot, P. C. (2014). Magnetite composition in Ni-Cu-PGE deposits worldwide: Application to mineral exploration. *Journal of Geochemical Exploration*, *145*, 64–81. https://doi.org/10.1016/j.gexplo.2014.05.010

Brugmann, G. E., Naldrett, A. J., & Macdonald, A. J. (1989). Magma mixing and constitution zone refining in the Lac des Iles Complex, Ontario; genesis of platinum-group element mineralization. *Economic Geology*, *84*(6), 1557–1573. https://doi.org/10.2113/gsecongeo.84.6.1557

Brügmann, G. E., Reischmann, T., Naldrett, A. J., & Sutcliffe, R. H. (1997). Roots of an Archean volcanic arc complex: The Lac des Iles area in Ontario, Canada. *Precambrian Research*, *81*(3–4), 223–239. https://doi.org/10.1016/S0301-9268(96)00036-8

Brzozowski, M. J., Samson, I. M., Gagnon, J. E., Good, D. J., & Linnen, R. L. (2021). Oxide mineralogy and trace element chemistry as an index to magma evolution and Marathon-type mineralization in the Eastern Gabbro of the alkaline Coldwell Complex, Canada. *Mineralium Deposita*, *56*(4), 621–642. https://doi.org/10.1007/s00126-020-00985-7

Buddington, A. F. and Lindsley, D. H. (1964). Iron-titanium oxide minerals and synthetic equivalents. *Journal of Petrology*, *5*(2), 310–357. https://doi.org/10.1093/petrology/5.2.310

Buss, B., Roney, C., Peck, D., Decharte, D., Marrs, G., Canosa, J., Hutton, K., Ritchie, L., & Therrien, L. (2017). *Feasibility Study Incorporating the Life of Mine Plan for Lac des Iles Mine* (NI 43-101 Technical Report 16378–2017; pp. 1–925). North American Palladium Ltd.

Card, K. D. (1990). A review of the Superior Province of the Canadian Shield, a product of Archean accretion. *Precambrian Research*, *48*(1–2), 99–156. https://doi.org/10.1016/0301-9268(90)90059-Y

Card, K., D., & Ciesielski, A. (1985). Subdivisions of the Superior Province of the Canadian Shield. *Geoscience Canada*, *13*(1), 5–13.

Cawthorn, R. G., Barnes, S. J., Ballhaus, C., & Malitch, K. N. (2005). Platinum Group Element, Chromium, and Vanadium Deposits in Mafic and Ultramafic Rocks. In J. W. Hedenquist, J. F. H. Thompson, R. J. Goldfarb, & J. P. Richards (Eds.), *One Hundredth Anniversary Volume* (p. 0). Society of Economic Geologists. https://doi.org/10.5382/AV100.09

Cawthorn, R. G. and Walraven, F. (1998). Emplacement and crystallization time for the Bushveld Complex. *Journal of Petrology*, *39*(9), 1669–1687. https://doi.org/10.1093/petroj/39.9.1669

Charlier, B., Namur, O., Bolle, O., Latypov, R., & Duchesne, J.-C. (2015). Fe–Ti–V–P ore deposits associated with Proterozoic massif-type anorthosites and related rocks. *Earth-Science Reviews*, *141*, 56–81. https://doi.org/10.1016/j.earscirev.2014.11.005

Charlier, B., Namur, O., Malpas, S., De Marneffe, C., Duchesne, J.-C., Auwera, J. V., & Bolle, O. (2010). Origin of the giant Allard Lake ilmenite ore deposit (Canada) by fractional crystallization, multiple magma pulses and mixing. *Lithos*, *117*(1–4), 119–134. https://doi.org/10.1016/j.lithos.2010.02.009

Chen, W. T., Zhou, M.-F., Gao, J.-F., & Hu, R. (2015). Geochemistry of magnetite from Proterozoic Fe-Cu deposits in the Kangdian metallogenic province, SW China. *Mineralium Deposita*, *50*(7), 795–809. https://doi.org/10.1007/s00126-014-0575-7

Dare, S. A. S., Ames, D. E., Lightfoot, P. C., Barnes, S.-J., & Beaudoin, G. (2015). Trace elements in Fe-oxide minerals from fertile and barren igneous complexes: Investigating their use as a vectoring tool for Ni-Cu-PGE sulphide mineralization. In D. E. Ames & M. G. Houlé (Eds.), *Targeted Geoscience Initiative 4: Canadian Nickel-Copper-Platinum Group Elements-Chromium Ore Systems—Fertility, Pathfinders, New and Revised Models, (ed.)* (pp. 177–185). Geological Survey of Canada.

Dare, S. A. S., Barnes, S.-J., & Beaudoin, G. (2012). Variation in trace element content of magnetite crystallized from a fractionating sulfide liquid, Sudbury, Canada: Implications for provenance discrimination. *Geochimica et Cosmochimica Acta*, *88*, 27–50. https://doi.org/10.1016/j.gca.2012.04.032

Dare, S. A. S., Barnes, S.-J., Beaudoin, G., Méric, J., Boutroy, E., & Potvin-Doucet, C. (2014). Trace elements in magnetite as petrogenetic indicators. *Mineralium Deposita*, *49*(7), 785–796. https://doi.org/10.1007/s00126-014-0529-0

Dare, S. A. S., Grant, M., Polivchuk, M., & Bethell, E. (2019). *Pathfinder mineral geochemistry for magmatic oxide and sulfide mineralization: Insights from trace elements in Fe- oxides determined by laser ablation ICP-MS*. 1–4.

Dare, S., Lightfoot, P., Barnes, S.-J., & Beaudoin, G. (2014). *Mineral chemistry and supporting databases for TGI4 project on "Trace elements in Fe-oxides from fertile and barren igneous complexes: Investigating their use as a vectoring tool in the intrusions that host Ni-Cu-PGE deposits"* (Open File 7538). Geological Survey of Canada.

Decharte, D., Hofton, T., & Marrs, G. (2018). *Feasibility Study for Lac des Iles Mine Incorporating Underground Mining of the Roby Zone* (p. 889). North American Palladium Ltd.

Ding, X., Chen, X., & Shao, Z. (2023). Was the Panzhihua large Fe-Ti oxide deposit, SW China, formed by silicate immiscibility? *Acta Geologica Sinica — English Edition*, *97*(5), 1451–1461. https://doi.org/10.1111/1755-6724.15003

Djon, M. L. N., & Barnes, S.-J. (2012). Changes in sulfides and platinum-group minerals with the degree of alteration in the Roby, Twilight, and High Grade Zones of the Lac des Iles Complex, Ontario, Canada. *Mineralium Deposita*, *47*(8), 875–896. https://doi.org/10.1007/s00126-012-0401-z

Djon, M. L., Olivo, G. R., Miller, J. D., Peck, D. C., & Joy, B. (2017). Stratiform platinum-group element mineralization in the layered Northern Ultramafic Center of the Lac des Iles Intrusive Complex, Ontario, Canada. *Ore Geology Reviews*, *90*, 697–722. https://doi.org/10.1016/j.oregeorev.2017.03.011

Djon, M. L., Peck, D. C., Olivo, G. R., Miller, J. D., & Joy, B. (2018). Contrasting styles of Pd-rich magmatic sulfide mineralization in the Lac des Iles Intrusive Complex, Ontario, Canada. *Economic Geology*, *113*(3), 741–767. https://doi.org/10.5382/econgeo.2018.4568

Duchesne, J.-C. (1972). Iron-titanium oxide minerals in the Bjerkrem-Sogndal Massif, South-western Norway. *Journal of Petrology*, *13*(1), 57–81. https://doi.org/10.1093/petrology/13.1.57

Duparc, Q., Dare, S. A. S., Cousineau, P. A., & Goutier, J. (2016). Magnetite Chemistry As A Provenance Indicator In Archean Metamorphosed Sedimentary Rocks. *Journal of Sedimentary Research*, *86*(5), 542–563. https://doi.org/10.2110/jsr.2016.36

Dupuis, C., & Beaudoin, G. (2011). Discriminant diagrams for iron oxide trace element fingerprinting of mineral deposit types. *Mineralium Deposita*, *46*(4), 319–335. https://doi.org/10.1007/s00126-011-0334-y

Duran, C. J., Barnes, S.-J., & Corkery, J. T. (2016). Trace element distribution in primary sulfides and Fe–Ti oxides from the sulfide-rich pods of the Lac des Iles Pd deposits, Western Ontario, Canada: Constraints on processes controlling the composition of the ore and the use of pentlandite compositions in exploration. *Journal of Geochemical Exploration*, *166*, 45–63. https://doi.org/10.1016/j.gexplo.2016.04.005

Duran, C. J., Barnes, S.-J., Mansur, E. T., Dare, S. A. S., Bédard, L. P., & Sluzhenikin, S. F. (2020). Magnetite chemistry by LA-ICP-MS records sulfide fractional crystallization in massive Nickel-Copper-Platinum group element ores from the Norilsk-Talnakh mining district (Siberia, Russia): Implications for trace element partitioning into magnetite. *Economic Geology*, *115*(6), 1245–1266. https://doi.org/10.5382/econgeo.4742

Gilligan, R., & Nikoloski, A. N. (2020). The extraction of vanadium from titanomagnetites and other sources. *Minerals Engineering*, *146*, 106106. https://doi.org/10.1016/j.mineng.2019.106106

Grant, M. (2020). *Formation of magmatic Fe-Ti-V-P deposits within the Lac St. Jean area Saguenay, Québec, Canada: Insights from trace element composition of Fe-oxides and apatite*. University of Ottawa.

Gross, G. A. (1995). Mafic Intrusion-Hosted Titanium-Iron. In O. R. Eckstrand, W. D. Sinclair, & R. I. Thorpe (Eds.), *Geology of Canadian Mineral Deposit Types* (Vol. 8, p. 0). Geological Society of America. https://doi.org/10.1130/DNAG-GNA-P1.573

Gustafsson, J. P. (2019). Vanadium geochemistry in the biogeosphere –speciation, solid-solution interactions, and ecotoxicity. *Applied Geochemistry*, *102*, 1–25. https://doi.org/10.1016/j.apgeochem.2018.12.027

Haggerty, S. E. (1991). Chapter 5. Oxide Textures - A Mini-Atlas. In D. H. Lindsley (Ed.), *Petrologic and Magnetic Significance* (pp. 129–220). De Gruyter. https://doi.org/doi:10.1515/9781501508684-008

Hinchey, J. G., Hattori, K. H., & Lavigne, M. J. (2005). Geology, petrology, and controls on PGE mineralization of the Southern Roby and Twilight zones, Lac des Iles mine, Canada. *Economic Geology*, *100*(1), 43–61. https://doi.org/10.2113/100.1.0043

Hoatson, D. M., & Keays, R. R. (1989). Formation of platiniferous sulfide horizons by crystal fractionation and magma mixing in the Munni Munni layered intrusion, West Pilbara Block, Western Australia. *Economic Geology*, *84*(7), 1775–1804. https://doi.org/10.2113/gsecongeo.84.7.1775

Hu, H., Lentz, D., Li, J.-W., McCarron, T., Zhao, X.-F., & Hall, D. (2015). Reequilibration processes in magnetite from Iron Skarn Deposits. *Economic Geology*, *110*(1), 1–8. https://doi.org/10.2113/econgeo.110.1.1

Huang, J.-H., Huang, F., Evans, L., & Glasauer, S. (2015). Vanadium: Global (bio)geochemistry. *Chemical Geology*, *417*, 68–89. https://doi.org/10.1016/j.chemgeo.2015.09.019

Impala Platinum Holdings Limited. (2022). *Mineral Resource and Mineral Reserve Statement as at 30 June 2022* (p. 107). Impala Platinum Holdings Limited.

Implats. (2022). *Mineral Resource and Mineral Reserve Statement as at 30 June 2022* (pp. 1–110). Implats.

Jonsson, J. (2023). *Petrogenesis of mineralized horizons in the Offset and Creek zones, Lac des Iles Complex, N. Ontario*. Lakehead University.

Kelley, K., Scott, C., Polyak, D., Seal, R., & Bradley, D. (2017). *Vanadium. Chapter U of Critical Mineral Resources of the United States—Economic and Environmental Geology and Prospects for Future Supply* (Professional Paper 1802–U; Professional Paper). U.S. Geological Survey Professional.

Kerr, A., Walsh, J. A., Sparkes, G. W., & Hinchey, J. G. (2013). *Vanadium potential in Newfoundland and Labrador: A review and assessment* (13–1; pp. 137–165). Newfoundland and Labrador Department of Natural Resources Geological Survey.

Klein, C., & Dutrow, B. (2007). *Manual of Mineral Science* (23rd Edition). Wiley.

Knipping, J. L., Bilenker, L. D., Simon, A. C., Reich, M., Barra, F., Deditius, A. P., Wälle, M., Heinrich, C. A., Holtz, F., & Munizaga, R. (2015). Trace elements in magnetite from massive iron oxide-apatite deposits indicate a combined formation by igneous and magmatic-hydrothermal processes. *Geochimica et Cosmochimica Acta*, *171*, 15–38. https://doi.org/10.1016/j.gca.2015.08.010

Kuzmich, B. (2014). *Petrogenesis of the Ferrogabbroic Intrusions and Associated Fe-Ti-V-P Mineralization within the McFaulds Greenstone belt, Superior Province, Canada*. Lakehead University.

Lattard, D. (1995). Experimental evidence for the exsolution of ilmenite from titaniferous spinel. *American Mineralogist*, *80*(9–10), 968–981. https://doi.org/10.2138/am-1995-9-1013

Lavigne, M. J., & Michaud, M. J. (2001). Geology of North American Palladium Ltd.'s Roby Zone Deposit, Lac des Iles. *Exploration and Mining Geology*, *10*(1–2), 1–17. https://doi.org/10.2113/10.1-2.1

Lavigne, M. J., Michaud, M. J., & Rickard, J. (2005). Discovery and geology of the Lac des Iles palladium deposits. In *Short Course 35, Oulu, Finland* (pp. 369–390). Mineralogical Association of Canada.

Lee, J., Yang, S., White, N. C., Shin, D., & Kim, E. (2022). Whole-rock geochemistry and mineral compositions of gabbroic rocks and the associated Fe–Ti (–V) oxide deposit in the Gonamsan intrusion, South Korea. *Ore Geology Reviews*, *148*, 105054. https://doi.org/10.1016/j.oregeorev.2022.105054

Li, C., Maier, W. D., & De Waal, S. A. (2002). The role of magma mixing in the genesis of PGE mineralization in the bushveld complex: Thermodynamic calculations and new interpretations—a reply. *Economic Geology*, *97*(3), 667–667. https://doi.org/10.2113/gsecongeo.97.3.667

Liu, C., Eleish, A., Hystad, G., Golden, J. J., Downs, R. T., Morrison, S. M., Hummer, D. R., Ralph, J. P., Fox, P., & Hazen, R. M. (2018). Analysis and visualization of vanadium mineral diversity and distribution. *American Mineralogist*, *103*(7), 1080–1086. https://doi.org/10.2138/am-2018-6274

MacTavish, A. D. (1999). *The mafic-ultramafic intrusions of the Atikokan-Quetico area, Northwestern Ontario* (Open File Report 5997; p. 127). Ontario Geological Survey.

McCracken, T., Kanhai, T., Bridson, P., McBride, W., Small, K., & Penna, D. (2013). *Technical Report Lac des Iles Mine, Ontario, Incorporating Prefeasibility Study Offset Zone Phase I* (NAP-43-101-Technical-Report-Feb-19-2013 1296780300-REP-R0001-05; pp. 1–594). North American Palladium Ltd.

Middlemost, E. A. K. (1994). Naming materials in the magma/igneous rock system. *Earth-Science Reviews*, *37*(3–4), 215–224. https://doi.org/10.1016/0012-8252(94)90029-9

Mucke, A. (2003). Magnetite, ilmenite and ulvite in rocks and ore deposits: Petrography, microprobe analyses and genetic implications. *Mineralogy and Petrology*, *77*(3–4), 215–234. https://doi.org/10.1007/s00710-002-0216-1

Mungall, J. E. (2014). 13.8—Geochemistry of Magmatic Ore Deposits. In H. D. Holland & K. K. Turekian (Eds.), *Treatise on Geochemistry (Second Edition)* (Second Edition, pp. 195–218). Elsevier. https://doi.org/10.1016/B978-0-08-095975-7.01108-6

Nadoll, P., Angerer, T., Mauk, J. L., French, D., & Walshe, J. (2014). The chemistry of hydrothermal magnetite: A review. *Ore Geology Reviews*, *61*, 1–32. https://doi.org/10.1016/j.oregeorev.2013.12.013

Nadoll, P., & Koenig, A. E. (2011). LA-ICP-MS of magnetite: Methods and reference materials. *Journal of Analytical Atomic Spectrometry*, *26*(9), 1872. https://doi.org/10.1039/c1ja10105f

Namur, O., Charlier, B., Toplis, M. J., Higgins, M. D., Liégeois, J.-P., & Vander Auwera, J. (2010). Crystallization sequence and magma chamber processes in the ferrobasaltic Sept Iles layered intrusion, Canada. *Journal of Petrology*, *51*(6), 1203–1236. https://doi.org/10.1093/petrology/egq016

Nesse, W. D. (2012). *Introduction to mineralogy* (2. Ed). Oxford Univ. Press.

Pang, K.-N., Zhou, M.-F., Lindsley, D., Zhao, D., & Malpas, J. (2008). Origin of Fe-Ti oxide ores in mafic intrusions: evidence from the Panzhihua Intrusion, SW China. *Journal of Petrology*, *49*(2), 295–313. https://doi.org/10.1093/petrology/egm082

Pang, K.-N., Zhou, M.-F., Qi, L., Shellnutt, G., Wang, C. Y., & Zhao, D. (2010). Flood basalt-related Fe–Ti oxide deposits in the Emeishan large igneous province, SW China. *Lithos*, *119*(1–2), 123–136. https://doi.org/10.1016/j.lithos.2010.06.003

Peck, D., & Djon, L. (2020). *The Lac des Iles Palladium Deposits*. North American Palladium.

Percival, J. A., Sanborn-Barrie, M., Skulski, T., Stott, G. M., Helmstaedt, H., & White, D. J. (2006). Tectonic evolution of the western Superior Province from NATMAP and Lithoprobe studies. *Canadian Journal of Earth Sciences*, *43*(7), 1085–1117. https://doi.org/10.1139/e06-062

Percival, J., Skulski, T., Sanborn-Barrie, M., Stott, G., Leclair, A., Corkery, T., & Boily, M. (2012). Geology and tectonic evolution of the Superior Province, Canada. In F. A. Cook & R. Clowes (Eds.), *Subdivisions of the Superior Province of the Canadian Shield* (1. Print, pp. 321–378). Geological Association of Canada.

Pirajno, F., & Hoatson, D. M. (2012). A review of Australia's Large Igneous Provinces and associated mineral systems: Implications for mantle dynamics through geological time. *Ore Geology Reviews*, *48*, 2–54. https://doi.org/10.1016/j.oregeorev.2012.04.007

Polivchuk, M. (2017). *The formation of vanadium deposits in the Archean Rivière Bell Complex, Quebec: Insights from Fe-Ti oxide chemistry.* [PhD Thesis]. University of Ottawa.

Price, G. D. (1981). Subsolidus phase relations in the titanomagnetite solid solution series. *American Mineralogist*, *66*(7–8), 751–758.

Ramdohr, P. (1953). Ulvoespinel and its significance in titaniferous iron ores. *Economic Geology*, *48*(8), 677–688. https://doi.org/10.2113/gsecongeo.48.8.677

Ripley, E. M., & Li, C. (2018). Chapter 3—Metallic Ore Deposits Associated With Mafic to Ultramafic Igneous Rocks. In S. K. Mondal & W. L. Griffin (Eds.), *Processes and Ore Deposits of Ultramafic-Mafic Magmas through Space and Time* (pp. 79–111). Elsevier. https://doi.org/10.1016/B978-0-12-811159-8.00004-4

Rudnick, R. L., & Gao, S. (2003). The Composition of the Continental Crust. In *Treatise on Geochemistry* (Vol. 3, pp. 1–64). Elsevier-Pergamon. http://dx.doi.org/10.1016/b0-08-043751-6/03016-4

Saccani, E. (2015). A new method of discriminating different types of post-Archean ophiolitic basalts and their tectonic significance using Th-Nb and Ce-Dy-Yb systematics. *Geoscience Frontiers*, *6*(4), 481–501. https://doi.org/10.1016/j.gsf.2014.03.006

Shahabi Far, M., Samson, I. M., Gagnon, J. E., Good, D. J., Linnen, R. L., & Ames, D. (2019). Evolution of a Conduit System at the Marathon PGE–Cu Deposit: Insights from Silicate Mineral Textures and Chemistry. *Journal of Petrology*, *60*(7), 1427–1460. https://doi.org/10.1093/petrology/egz035

Skinner, H. C. W., & Ehrlich, H. (2014). Biomineralization. In *Treatise on Geochemistry* (Second, pp. 105–162). Elsevier.

Stone, D., Fell, M., Daley, A., Nielsen, P., Schnieders, B., Scott, J., & Wagner, D. (2003). *Lac des Iles Area. Map P.3532* [Map]. Ontario Geological Survey.

Stott, G. M. (1997). The Superior Province, Canada. In *Greenstone Belts* (pp. 480–507). Clarendon Press – Oxford.

Stott, G. M., Corkery, M. T., Percival, J. A., Simard, M., & Goutier, J. (2010). *A revised terrane subdivision of the Superior Province; in Summary of Field Work and Other Activities 2010, Ontario Geological Survey, Open File Report 6260, p.20-1 to 20-10.*

Sun, S. -s., & McDonough, W. F. (1989). Chemical and isotopic systematics of oceanic basalts: Implications for mantle composition and processes. *Geological Society, London, Special Publications*, *42*(1), 313–345. https://doi.org/10.1144/GSL.SP.1989.042.01.19

Tan, W., Liu, P., He, H., Wang, C. Y., & Liang, X. (2016). Mineralogy and origin of exsolution in Ti-rich magnetite from different magmatic Fe-Ti oxide-bearing iIntrusions. *The Canadian Mineralogist*, *54*(3), 539–553. https://doi.org/10.3749/canmin.1400069

Tomlinson, K. Y., Davis, D. W., Stone, D., & Hart, T. R. (2003). U–Pb age and Nd isotopic evidence for Archean terrane development and crustal recycling in the south-central Wabigoon subprovince, Canada. *Contributions to Mineralogy and Petrology*, *144*(6), 684–702. https://doi.org/10.1007/s00410-002-0423-0

Toplis, M. J., & Carroll, M. R. (1995). An experimental study of the influence of oxygen fugacity on Fe-Ti oxide stability, phase relations, and mineral-melt equilibria in ferro-basaltic systems. *Journal of Petrology*, *36*(5), 1137–1170. https://doi.org/10.1093/petrology/36.5.1137

Turnock, A. C., & Eugster, H. P. (1962). Fe—Al Oxides: Phase Relationships below 1,000°C1. *Journal of Petrology*, *3*(3), 533–565. https://doi.org/10.1093/petrology/3.3.533

Unganai, D. A. B., Imai, A., Takahashi, R., Jamal, D. L., Agangi, A., Hoshide, T., & Sato, H. (2022). Genesis of magmatic ilmenite ores associated with the Mazua ultramafic intrusion, NE Mozambique. *Ore Geology Reviews*, *143*, 104760. https://doi.org/10.1016/j.oregeorev.2022.104760

Valvasori, A. A., Hanchar, J. M., Piercey, S. J., & Fonkwe, M. L. D. (2020). The origin and evolution of V-rich, magnetite dominated Fe-Ti oxide mineralization; Northwest River Anorthosite, south-central Labrador, Canada. *Mineralium Deposita*, *55*(3), 555–575. https://doi.org/10.1007/s00126-019-00892-6

Vermeesch, P. (2006). Tectonic discrimination diagrams revisited. *Geochemistry, Geophysics, Geosystems*, *7*(6), 2005GC001092. https://doi.org/10.1029/2005GC001092

Wen, G., Li, J.-W., Hofstra, A. H., Koenig, A. E., Lowers, H. A., & Adams, D. (2017). Hydrothermal reequilibration of igneous magnetite in altered granitic plutons and its implications for magnetite classification schemes: Insights from the Handan-Xingtai iron district, North China Craton. *Geochimica et Cosmochimica Acta*, *213*, 255–270. https://doi.org/10.1016/j.gca.2017.06.043

Winter, J. D. (2010). *An introduction to igneous and metamorphic petrology* (2. Ed., [international ed.]). Prentice Hall.

Xiong, F., Tao, Y., Liao, M., Liao, Y., & Ma, J. (2021). Liquid immiscibility in the Panzhihua intrusion, SW China: Evidence from ore textures and Fe–Ti oxide-rich globules in gabbros. *Journal of Asian Earth Sciences*, *209*, 104683. https://doi.org/10.1016/j.jseaes.2021.104683

Zhou, M.-F., Robinson, P. T., Lesher, C. M., Keays, R. R., Zhang, C.-J., & Malpas, J. (2005). Geochemistry, petrogenesis and metallogenesis of the Panzhihua gabbroic layered intrusion and associated Fe–Ti–V oxide deposits, Sichuan Province, SW China. *Journal of Petrology*, *46*(11), 2253–2280. https://doi.org/10.1093/petrology/egi054

Appendix A

Petrographic descriptions

LDI-21-SB001		**Drillhole 14-902**		**Depth 5.25 m**
Mineral (interpreted pre-alteration)	%	Mineral (actual)	%	Details
Plagioclase	15	Plagioclase	10	0.2-5.0 mm. Cumulate. Subhedral. Moderate alteration to patches of very fine-grained sericite occurring on the plagioclase grain and/or chlorite occurring as partial rims. Commonly weakly fractured.
		Sericite	4	
		Chlorite	1	
		Epidote	tr	
Pyroxene	39	Tremolite-actinolite	34	0.3-8.0 mm. Anhedral. Pyroxene is completely replaced by very fine-grained tremolite-actinolite±chlorite. Pre-alteration orthopyroxene/clinopyroxene proportion is not discernible.
		Chlorite	5	
Fe-Ti oxides	40	Magnetite		0.1-2.0 mm, interstitial grains in tremolite-actinolite, and clusters with sharp, jagged boundaries. Ilmenite observed as sandwich- and trellis-type lamellae exsolution from magnetite and anhedral granules grains at the magnetite borders.
		Ilmenite		
Sulfides	6	Pyrite	4	Mostly present as finely disseminated (<0.1 mm) monosulfide crystals of pyrite or chalcopyrite occurring within silicate alteration aggregates or filling fractures in silicates and Iron oxides.
		Chalcopyrite	2	
Comments: massive, cumulate. Variable crystal size, dominantly medium-grained, discontinuous chlorite-dominated veinlets occur on the long axis of the thin section. Semi-massive oxide.				

LDI-21-SB002		Drillhole 14-902		Depth 7.5 m
Mineral (interpreted pre-alteration)	%	Mineral (actual)	%	Details
Plagioclase	35	Plagioclase	26	Medium- to coarse-grained. anhedral to subhedral. Bending twinning. Weakly to moderately altered to patches and fracture fill of very fine-grained sericite±chlorite±epidote.
		Sericite	5	
		Chlorite	4	
		Epidote	tr	
Pyroxene	35	Tremolite-actinolite	30	0.2-2.0 mm. Primary pyroxene has been completely altered. Alteration

		Talc	1	occurs as fine-grained aggregates of tremolite-actinolite+chlorite±talc, and fine to very fine-grained rims and veinlets of chlorite. Chlorite alteration mostly occurs at boundaries to altered pyroxene.
		Chlorite	4	
Fe-Ti oxides	25	Magnetite		Medium- to coarse-grained. Subhedral. Occurring as interstitial grains in silicates. Sandwich- and granular ilmenite-type exsolutions.
		Ilmenite		
Sulfides	5	Pyrite	2.5	Very fine- to fine-grained. Subhedral to euhedral. Disseminated and occasionally filling fractures.
		Chalcopyrite	2.5	
Comments: massive, cumulate. Variable crystal size, dominantly medium-grained. Pre-alteration crystal boundaries and texture are very difficult to determine due to alteration. Moderate alteration. Heavily disseminated oxide. Gabbronorite.				

LDI-21-SB003		Drillhole 14-902		Depth 9.75 m
Mineral (interpreted pre-alteration)	%	Mineral (actual)	%	Details
Plagioclase	25	Plagioclase	24	Medium- to coarse-grained. Subhedral, tabular. Weakly fractured, showing only minor gritty sericite alteration and chlorite±epidote rims.
		Sericite	1	
		Chlorite	tr	
		Epidote	tr	
Pyroxene	35	Tremolite-actinolite	34	Medium- to coarse-grained. Anhedral to subhedral. Completely replaced by alteration minerals. Alteration is present as very tine to fine tremolite-actinolite±talc±chlorite.
		Chlorite	1	
Fe-Ti oxides	38	Magnetite		Disseminated, interstitial, anhedral magnetite. 4 mm veinlet of iron oxides along the thin section. Occasionally trellis-type ilmenite exsolution. Very fine to fine subhedral disseminated ilmenite grains within magnetite grains.
		Ilmenite		
Sulfides	2	Pyrite	1.5	Very fine. Anhedral. Disseminated and occasionally filling fractures.
		Chalcopyrite	tr	
		Pyrrhotite	tr	
Comments: massive, cumulate. Variable crystal size, dominantly medium-grained. Pre-alteration crystal boundaries and texture are very difficult to determine due to alteration. Moderate alteration. Heavily disseminated oxide. Gabbronorite.				

LDI-21-SB004		Drillhole 14-902		Depth 11.75 m
Mineral (interpreted pre-alteration)	%	Mineral (actual)	%	Details
Plagioclase	25	Plagioclase	20	Medium- to coarse-grained. Cumulate. Larger crystals tabular and subhedral to anhedral. Moderate alteration as rims and small patches of very fine-grained sericite.
		Sericite	4	
		Chlorite	1	
		Epidote	tr	
Pyroxene	30	Tremolite-actinolite	31	Medium- to coarse-grained. Anhedral to subhedral. Pyroxene is completely replaced by fine-grained tremolite-actinolite±chlorite.
		Chlorite	4	
Fe-Ti oxides	42	Magnetite		Medium- to coarse-grained, semi-massive with a banded appearance, commonly as aggregates. A few grains of magnetite show sandwich-type ilmenite exsolutions. Fine- to medium-grained subhedral disseminated ilmenite grains.
		Ilmenite		
Sulfides	3	Pyrite	2	Mostly present as finely disseminated crystals of anhedral pyrite and chalcopyrite occurring interstitial to silicate.
		Chalcopyrite	1	
Comments: Cumulate. Variable crystal size, dominantly medium-grained. Magnetite occurs semi-massive with a banded appearance, commonly as aggregates. Semi-massive oxide.				

LDI-21-SB005		Drillhole 14-902		Depth 18.25 m
Mineral (interpreted pre-alteration)	%	Mineral (actual)	%	Details
Plagioclase	45	Plagioclase	40	Fine- to medium-grained. Large tabular and subhedral to anhedral crystals. Very weak alteration as patches of fine-grained sericite and chlorite rims. A few grains are weakly fractured.
		Sericite	2	
		Chlorite	3	
Pyroxene	35	Tremolite-actinolite	32	Fine- to medium-grained. The degree of alteration masks pre-alteration crystal properties. Very fine-grained tremolite-actinolite±chlorite aggregates are present throughout.
		Chlorite	3	
Fe-Ti oxides	15	Magnetite		Medium-grained. Anhedral Interstitial grains. Magnetite is evenly disseminated in the thin section. Occasionally sandwich-type ilmenite
		Ilmenite		

				exsolution. Fine to medium subhedral disseminated ilmenite grains.
Sulfides	5	Pyrite	2	Very fine- to fine-grained. Disseminated monosulfide crystals and in contact with interstitial iron oxides.
		Chalcopyrite	3	
Comments: Dominantly medium-grained. Heavily disseminated oxide. Moderately altered. Gabbronorite.				

LDI-21-SB006		Drillhole 14-902		Depth 20.25 m
Mineral (interpreted pre-alteration)	%	Mineral (actual)	%	Details
Plagioclase	40	Plagioclase	39	Medium coarse-grained. Equant to rarely tabular, anhedral crystals occasionally weakly fractured. Alteration present as patches and rims of sericite±epidote±chlorite.
		Sericite	1	
		Chlorite	tr	
		Epidote	tr	
Pyroxene	35	Tremolite-actinolite	34	Fine- to medium-grained. Pyroxene has been completed replaced by tremolite-actinolite±talc±chlorite fine-grained alteration products.
		Chlorite	1	
		Talc	tr	
Fe-Ti oxides	20	Magnetite		Aggregates of fine- to medium-grained anhedral disseminated magnetite and ilmenite commonly surround the silicate. An anhedral iron oxide veinlet occurs in the thin section. Occasionally sandwich- and granular-type ilmenite exsolution.
		Ilmenite		
Sulfides	5	Pyrite	4	Finely disseminated pyrite crystals and rare interstitial pyrite±pyrrhotite±chalcopyrite crystals.
		Pyrrhotite	tr	
		Chalcopyrite	1	
Comments: Homogeneous, non-foliated. Heavily disseminated oxide. Moderately altered. Gabbronorite.				

LDI-21-SB007		Drillhole 14-902		Depth 22.75 m
Mineral (interpreted pre-alteration)	%	Mineral (actual)	%	Details
Plagioclase	35	Plagioclase	30	Coarse-grained. Cumulate. Large tabular and subhedral to anhedral crystals. Medium alteration as patches and rims of sericite±epidote±chlorite. weakly fractured, rare deformation twinning.
		Sericite	3	
		Chlorite	2	
		Epidote		

Pyroxene	50	Tremolite-actinolite	45	Fine- to coarse-grained. Large tabular and subhedral to anhedral crystals. High internal alteration to tremolite-actinolite±chlorite.
		Chlorite	5	
Fe-Ti oxides	13	Magnetite		Fine- to coarse-grained. predominantly as disseminated interstitial anhedral grains but also as anhedral magnetite veinlets. Ilmenite occurs occasionally as sandwich-type exsolution and as large anhedral grains.
		Ilmenite		
Sulfides	2	Pyrite	1	Very fine- to fine-grained. Monosulfide anhedral to subhedral disseminated pyrite and chalcopyrite. Minor aggregates of Pyrrhotite>Pyrite>Chalcopyrite.
		Pyrrhotite	1	
		Chalcopyrite	tr	
Comments: Massive. Cumulate. Variable crystal size, ranging from fine to coarse. Heavily disseminated oxide. Moderately altered. Gabbronorite.				

LDI-21-SB008		Drillhole 14-902		Depth 25.75 m
Mineral (interpreted pre-alteration)	%	Mineral (actual)	%	Details
Plagioclase	37	Plagioclase	30	Fine- to medium-grained. Cumulate. Equant to tabular. Anhedral to subhedral grains. Very fine patches of sericite±chlorite alteration and rims of chlorite±sericite with minor epidote proportional to proximity to altered pyroxene. Very weakly fractured.
		Sericite	2	
		Chlorite	4	
		Epidote	tr	
Pyroxene	48	Tremolite-actinolite	42	Fine- to coarse-grained size. Tabular, anhedral to subhedral grains. Very fine-grained tremolite-actinolite ±chlorite±talc aggregates are present throughout, with talc commonly occurring as a minor component.
		Chlorite	6	
Fe-Ti oxides	14	Magnetite		Magnetite and ilmenite are evenly distributed in the thin section, predominantly as disseminated fine to medium anhedral grains. Magnetite predominates over ilmenite. Magnetite with no exsolutions.
		Ilmenite		
Sulfides	1	Pyrite	tr	Very finely disseminated anhedral monosulfide pyrite or chalcopyrite crystals.
		Chalcopyrite	tr	

Comments: Massive. Cumulate. Heavily disseminated oxide. Moderately altered. Gabbronorite.

LDI-21-SB009		Drillhole 14-902		Depth 27.75 m
Mineral (interpreted pre-alteration)	%	Mineral (actual)	%	Details
Plagioclase	61	Plagioclase	54	Fine- to coarse-grained. Subhedral, equant to tabular. Alteration as patches of very fine to fine-grained sericite. Trace chlorite and epidote. Very weakly fractured, rare deformation twinning.
		Sericite	5	
		Chlorite	2	
		Epidote	tr	
Pyroxene	38	Tremolite-actinolite	33	Fine- to medium-grained. Equant and subhedral. Pre-alteration mineral properties are difficult to determine. Fine-grained tremolite-actinolite±chlorite.
		Chlorite	5	
Fe-Ti oxides	0.5	Magnetite		Very fine- to fine-grained. Interstitial, disseminated.
		Ilmenite		
Sulfides	0.5	Pyrite	tr	Very fine- to fine-grained. Interstitial, disseminated.
		Chalcopyrite	tr	
Comments: Massive. Cumulate. Variable crystal size, ranging from fine- to coarse-grained. Weakly disseminated oxide. Moderately altered. Gabbronorite.				

LDI-21-SB010		Drillhole 14-902		Depth 29.5 m
Mineral (interpreted pre-alteration)	%	Mineral (actual)	%	Details
Plagioclase	60	Plagioclase	55	Fine- to coarse-grained. Equant to tabular. Anhedral to subhedral grains. Alteration as patches of fine-grained sericite. Very weakly fractured, rare deformation twinning.
		Sericite	5	
Pyroxene	37	Tremolite-actinolite	37	Medium- to coarse-grained size. Pyroxene is completely replaced by tremolite-actinolite.
Fe-Ti oxides	2	Magnetite		Very finely disseminated, very fine-grained crystals rarely occurring as a minor component within silicate alteration aggregates.
Sulfides	1	Pyrite	tr	Mostly present as finely disseminated, very fine-grained monosulfide crystals of pyrite or chalcopyrite occurring within silicate alteration aggregates.
		Chalcopyrite	tr	
Comments: Massive. Cumulate. Weakly disseminated oxide. Moderately altered. Gabbronorite.				

LDI-21-SB011		Drillhole 14-902		Depth 30.75 m
Mineral (interpreted pre-alteration)	%	Mineral (actual)	%	Details
Plagioclase	33	Plagioclase	31	Fine- to medium-grained. Tabular. Subhedral. Medium sericite alteration, often more concentrated towards the center of the grain.
		Sericite	2	
		Chlorite	tr	
		Epidote	tr	
Pyroxene	66	Tremolite-actinolite	65	Medium-grained. Anhedral, generally equant to occasionally tabular. Alteration present as fine- to very fine-grained tremolite-actinolite aggregates throughout.
		Chlorite	1	
Fe-Ti oxides	0.8	Magnetite	tr	Very finely disseminated, very fine-grained crystals rarely occurring as a minor component.
Sulfides	0.2	Pyrite	tr	Mostly present as finely disseminated, very fine-grained monosulfide crystals occurring within silicate alteration aggregates.
		Chalcopyrite	tr	
Comments: Massive. Cumulate. Weakly disseminated oxide. Moderately altered. Gabbronorite.				

LDI-21-SB012		Drillhole 14-902		Depth 34.25 m
Mineral (interpreted pre-alteration)	%	Mineral (actual)	%	Details
Plagioclase	46	Plagioclase	42	Fine- to medium-grained size. Subhedral, equant to tabular. Alteration is generally weak, typically as patches of very fine-grained sericite.
		Sericite	4	
Pyroxene	53	Tremolite-actinolite	49	Fine- to medium-grained. Anhedral to subhedral, equant to tabular. High internal alteration to tremolite-actinolite±chlorite.
		Chlorite	4	
Fe-Ti oxides	0.7	Magnetite		Finely disseminated fine to very fine interstitial grains. Ilmenite occurring as very fine crystal associated to magnetite.
		Ilmenite		
Sulfides	0.3	Pyrite	tr	Finely disseminated, very fine-grained monosulfide crystals occurring within silicate alteration aggregates.
		Pyrrhotite	tr	
		Chalcopyrite	tr	
Comments: Holocrystalline, inequigranular, Variable crystal size, ranging from fine- to coarse-grained. Massive. Cumulate. Weakly disseminated oxide. Moderately altered. Gabbronorite.				

LDI-21-SB013		Drillhole 14-902		Depth 40.5 m
Mineral (interpreted pre-alteration)	%	Mineral (actual)	%	Details
Plagioclase	22	Plagioclase	19	Fine- to medium-grained. Equant to tabular. Subhedral. Alteration is generally very weak, typically as rims and small patches of very fine-grained sericite and chlorite. Larger plagioclase crystals occasionally partially or completely encircle magnetite crystals.
		Sericite	2	
		Chlorite	1	
Pyroxene	43.5	Tremolite-actinolite	40	Fine- to medium-grained size. Equant to tabular. Subhedral. Predominance of orthopyroxene over clinopyroxene. Minor amounts of replacement by alteration tremolite-actinolite as rims is common.
		Chlorite	3.5	
Fe-Ti oxides	33.8	Magnetite		Magnetite is evenly distributed in the thin section, predominantly as interstitial anhedral medium-grained grains. Trellis- and granular-type ilmenite exsolution. Occasionally fine- to coarse-grained subhedral ilmenite grains.
		Ilmenite		
Sulfides	0.7	Pyrite	tr	Very fine to fine-grained size finely disseminated grains. Pyrrhotite and chalcopyrite commonly intergrown.
		Pyrrhotite	tr	
		Chalcopyrite	tr	
Comments: Holocrystalline, inequigranular, variable crystal size, ranging from very fine- to coarse-grained. Massive. Cumulate. Heavily disseminated oxide. Weakly altered. Gabbronorite.				

LDI-21-SB014		Drillhole 14-902		Depth 43 m
Mineral (interpreted pre-alteration)	%	Mineral (actual)	%	Details
Plagioclase	30	Plagioclase	27	Fine- to coarse-grained size. Equant to tabular. Subhedral. Weakly altered, as patches of fine-grained sericite and rims of chlorite and minor epidote.
		Sericite	2	
		Chlorite	1	
		Epidote	tr	
Pyroxene	52	Tremolite-actinolite	49	Fine- to medium-grained size. Equant and subhedral, less commonly elongate and irregularly shaped. Predominance of orthopyroxene over clinopyroxene. Moderate amounts of replacement by tremolite-actinolite±chlorite around the rims is
		Chlorite	3	

				common. Larger pyroxene crystals occasionally completely encircle smaller plagioclase crystals.
Fe-Ti oxides	15	Magnetite		Magnetite occurs as disseminated, interstitial, anhedral grains and as a veinlet at a corner of the thin section with a semi-massive to massive texture with a banded appearance, commonly as aggregates. Occasionally trellis-type ilmenite exsolution. Very fine to fine subhedral disseminated ilmenite grains within magnetite grains.
		Ilmenite		
Sulfides	3	Pyrrhotite	2	Very fine-grained up to fine-grained subhedral or anhedral blebs of pyrrhotite and chalcopyrite, disseminated throughout sample. Minor very fine disseminated anhedral pyrite grains.
		Chalcopyrite	1	
		Pyrite	tr	
Comments: Massive. Cumulate. Variable crystal size, ranging from fine to coarse. Magnetite occurs semi-massive with a banded appearance, commonly as aggregates. Heavily disseminated oxide. Weakly altered. Gabbronorite.				

LDI-21-SB015		Drillhole 14-902		Depth 50 m
Mineral (interpreted pre-alteration)	%	Mineral (actual)	%	Details
Plagioclase	43	Plagioclase	39	Fine- to medium-grained size. Equant to tabular and subhedral to anhedral cumulate crystals. Alteration is very weak, as patches of very fine-grained sericite and chlorite thin partial rims. very weakly fractured.
		Sericite	3	
		Chlorite	1	
Pyroxene	53	Tremolite-actinolite	50	Fine- to medium-grained size. Equant to tabular and subhedral to anhedral. Alteration present as very fine to fine-grained tremolite-actinolite±chlorite aggregates.
		Chlorite	3	
Fe-Ti oxides	4	Magnetite		Magnetite is evenly distributed in the thin section, predominantly as disseminated and interstitial anhedral fine- to medium-grained size grains.. Fine to medium subhedral ilmenite grains.
		Ilmenite		
Sulfides	tr	Chalcopyrite	tr	Disseminated anhedral to subhedral monosulfide crystals
		Pyrite	tr	

				present interstitially and as inclusions in magnetite. Blebs of chalcopyrite and pyrite.
Comments: Massive. Cumulate. Variable crystal size, ranging from fine to coarse. Magnetite occurs weakly disseminated and evenly distributed. Moderately altered. Gabbronorite.				

LDI-21-SB016		Drillhole 14-902		Depth 54 m
Mineral (interpreted pre-alteration)	%	Mineral (actual)	%	Details
Plagioclase	60	Plagioclase	54	Fine- to medium-grained size. Equant to tabular and subhedral to anhedral cumulate crystals. Medium alteration as patches of very fine-grained sericite and chlorite rims. Minor epidote.
		Sericite	4	
		Chlorite	2	
		Epidote	tr	
Pyroxene	37	Tremolite-actinolite	36	Fine- to medium-grained size. Anhedral and irregularly shaped. High internal alteration to aggregates of tremolite-actinolite±chlorite.
		Chlorite	1	
Fe-Ti oxides	2	Magnetite		Anhedral to subhedral fine-grained disseminated magnetite and ilmenite grains. Fe oxides occur evenly distributed in the thin section. Magnetite without exsolutions.
		Ilmenite		
Sulfides	1	Chalcopyrite	tr	Very fine monosulfide grains.
		Pyrite	tr	
Comments: Massive. Cumulate. Variable crystal size. Magnetite occurs weakly disseminated and evenly distributed. Moderately altered. Gabbronorite.				

LDI-21-SB017		Drillhole 14-902		Depth 55 m
Mineral (interpreted pre-alteration)	%	Mineral (actual)	%	Details
Plagioclase	53.5	Plagioclase	53	Fine- to coarse-grained. Equant to tabular and subhedral to anhedral cumulate crystals. Very weakly fractured, rare deformation twinning. Alteration is weak as small patches of very fine-grained sericite.
		Sericite	0.5	
		Chlorite	tr	
Pyroxene	44.5	Tremolite-actinolite	44	Anhedral and irregularly shaped, fine- to medium-grained. Pyroxene is completely replaced by Very fine-grained tremolite-actinolite±talc±chlorite aggregates.
		Chlorite	0.5	
Fe-Ti oxides	1.6	Magnetite		

		Ilmenite		Very fine- to medium-grained anhedral disseminated smooth magnetite grains. Fine-grained anhedral and interstitial granular ilmenite, associated with magnetite. Very fine anhedral patchy exsolutions of ilmenite containing tiny blebs of magnetite.
Sulfides	0.4	Chalcopyrite	tr	Very fine-grained anhedral disseminated grains throughout the sample.
		Pyrite	tr	
Comments: Massive. Cumulate. Variable crystal size. Magnetite occurs weakly disseminated and evenly distributed. Granular ilmenite grains. Moderately altered. Gabbronorite.				

LDI-21-SB018		Drillhole 14-902		Depth 58.25 m
Mineral (interpreted pre-alteration)	%	Mineral (actual)	%	
Plagioclase	47.6	Plagioclase	47	Fine- to coarse-grained size. Subhedral. Equant to tabular. Very weakly fractured, rare deformation twinning. Weak alteration as patches or along the fracture planes of sericite.
		Sericite	0.6	
		Chlorite	tr	
Pyroxene	50	Tremolite-actinolite	49	Equant to tabular and subhedral to anhedral, fine- to medium-grained grains. Moderate alteration of orthopyroxene as rims and patches of very fine-grained tremolite-actinolite±talc±chlorite.
		Chlorite	1	
		Talc	tr	
Fe-Ti oxides	2	Magnetite	2	Very fine- to fine-grained anhedral disseminated interstitial smooth magnetite grains. Fine-grained anhedral, interstitial granular, and composite ilmenite, associated with magnetite.
		Ilmenite	tr	
Sulfides	0.4	Chalcopyrite	tr	Very fine-grained anhedral disseminated grains throughout the sample.
Comments: Massive. Cumulate. Variable crystal size. Magnetite occurs weakly disseminated and evenly distributed. Granular ilmenite grains. Moderately altered. Gabbronorite.				

LDI-21-SB019		Drillhole 14-902		Depth 58 m
Mineral (interpreted pre-alteration)	%	Mineral (actual)	%	

Plagioclase	58	Plagioclase	57	Very fine- to coarse-grained. Anhedral to subhedral tabular grains. Very weakly fractured, rare deformation twinning. Weak alteration as small patches of very fine-grained sericite. Plagioclase grains enclosing pyroxene and magnetite grains.
		Sericite	1	
		Chlorite	tr	
Pyroxene	40	Tremolite-actinolite	38	Anhedral to subhedral, fine- to medium-grained grains. Equant to elongated. Predominance of orthopyroxene over clinopyroxene. Medium to high alteration to patches of talc and rims of tremolite-actinolite±talc±chlorite. Pyroxene grains partially and completely exclosing plagioclase grains.
		Chlorite	1	
		Talc	1	
Fe-Ti oxides	1.8	Magnetite		Very fine- to fine-grained anhedral disseminated interstitial magnetite. Sandwich ilmenite exsolution and granular ilmenite.
		Ilmenite		
Sulfides	0.2	Chalcopyrite	tr	Very fine-grained anhedral disseminated grains throughout the sample.
Comments: Massive. Cumulate. Variable crystal size. Magnetite occurs weakly disseminated and evenly distributed. Granular ilmenite grains. Weakly altered. Gabbronorite.				

LDI-21-SB020		Drillhole 14-902		Depth 64.5 m
Mineral (interpreted pre-alteration)	%	Mineral (actual)	%	
Plagioclase	32	Plagioclase	31	Fine- to coarse-grained. Equant to tabular. Subhedral. Very weakly fractured, rare deformation twinning. Weak alteration as small patches of very fine-grained sericite and chlorite.
		Sericite	1	
		Chlorite	tr	
Pyroxene	65	Tremolite-actinolite	64	Anhedral to subhedral, fine- to medium-grained grains. Equant to elongated. Predominance of orthopyroxene over clinopyroxene. Medium to high alteration to patches of talc and rims of tremolite-actinolite±talc±chlorite. Pyroxene grains enclosing partially and completely plagioclase grains.
		Chlorite	1	
		Talc	tr	
Fe-Ti oxides	2.7	Magnetite		Very fine- to fine-grained anhedral disseminated interstitial smooth magnetite. Fine-grained anhedral,
		Ilmenite		

				interstitial granular, and composite ilmenite, associated with magnetite.
Sulfides	0.3	Chalcopyrite	tr	Very fine-grained anhedral disseminated grains throughout the sample.
Comments: Massive. Cumulate. Variable crystal size. Magnetite occurs weakly disseminated and evenly distributed. Granular ilmenite grains. Weakly altered. Gabbronorite.				

LDI-21-SB021		Drillhole 14-902		Depth 67.5 m
Mineral (interpreted pre-alteration)	%	Mineral (actual)	%	
Plagioclase	42	Plagioclase	41	Fine- to coarse-grained. Equant to tabular. Subhedral. Very weakly fractured, rare deformation twinning. Weak alteration as small patches of very fine-grained sericite and chlorite.
		Sericite	1	
		Chlorite	tr	
Pyroxene	44.7	Tremolite-actinolite	44	Pyroxene has been completely replaced by very fine to fine-grained tremolite-actinolite+talc±chlorite aggregates.
		Chlorite	1	
		Talc	0.7	
Fe-Ti oxides	13	Magnetite		Very fine- to fine-grained anhedral disseminated interstitial magnetite. Granular- sandwich-type ilmenite exsolution. Fine-grained ilmenite with hematite? exsolutions.
		Ilmenite		
Sulfides	0.3	Chalcopyrite	tr	Very fine-grained anhedral disseminated grains throughout the sample.
Comments: Massive. Cumulate. Variable crystal size. Magnetite occurs heavily disseminated and evenly distributed. Granular ilmenite grains. Moderately altered. Gabbronorite.				

LDI-21-SB022		Drillhole 14-902		Depth 67.75 m
Mineral (interpreted pre-alteration)	%	Mineral (actual)	%	
Plagioclase	63.5	Plagioclase	63	Fine- to medium-grained. Equant to tabular. Subhedral. Very weakly fractured, rare deformation twinning. Weak alteration as small patches of very fine-grained sericite and chlorite as rims at contact with pyroxenes. Plagioclase grains enclosing pyroxene grains.
		Sericite	0.5	
		Chlorite	tr	
Pyroxene	34.5	Tremolite-actinolite	5	Fine-grained. Anhedral to subhedral. Irregular shaped. Completely

		Chlorite	tr	replaced by alteration products, tremolite-actinolite±chlorite. Pyroxene grains enclosing sulfide grains.
Fe-Ti oxides	1.8	Magnetite		Fine-grained anhedral disseminated interstitial smooth magnetite. Fine-grained anhedral, interstitial granular, ilmenite, associated with magnetite. A few ilmenite grains are in contact with sulfides.
		Ilmenite		
Sulfides	0.2	Chalcopyrite	tr	Very fine-grained anhedral disseminated grains throughout the sample.
		Pyrite	tr	
Comments: Massive. Cumulate. Variable crystal size. Magnetite occurs weakly disseminated and evenly distributed. Granular ilmenite grains. Moderately altered. Gabbronorite.				

LDI-21-SB023		Drillhole 14-902		Depth 69.75 m
Mineral (interpreted pre-alteration)	%	Mineral (actual)	%	
Plagioclase	46.9	Plagioclase	46	Fine- to coarse-grained. Equant to tabular. Subhedral. Weakly altered to fine-grained sericite. Very weakly fractured, rare deformation twinning. Plagioclase grains enclosing pyroxene grains.
		Sericite	0.9	
		Chlorite	tr	
Orthopyroxene	48.8	Tremolite-actinolite	0.8	Fine-grained. Anhedral. Medium alteration to talc along the fractures and to tremolite-actinolite as rims. Traces of “blue” chlorite. Pyroxene grains enclosing plagioclase grains.
		Chlorite	tr	
Fe-Ti oxides	3.9	Magnetite		Fine-grained anhedral disseminated interstitial smooth magnetite. Fine-grained anhedral, interstitial granular, ilmenite, associated with magnetite.
		Ilmenite		
Sulfides	0.4	Chalcopyrite	tr	Very fine-grained anhedral disseminated grains throughout the sample.
		Pyrite	tr	
Comments: Massive. Cumulate. Variable crystal size. Magnetite occurs weakly disseminated and evenly distributed. Granular ilmenite grains. Weakly altered. Gabbronorite.				

LDI-21-SB024		Drillhole 14-902		Depth 72 m
Mineral (interpreted pre-alteration)	%	Mineral (actual)	%	
Plagioclase	51.8	Plagioclase	51	

		Sericite	0.8	Fine- to coarse-grained. Subhedral. Equant to tabular. Weakly altered to fine-grained sericite. Chlorite filling fractures. Very weakly fractured, rare deformation twinning. Plagioclase crystals partially or completely encircle pyroxene grains.
		Chlorite	tr	
Orthopyroxene	43.1	Tremolite-actinolite	0.5	Fine- to medium-grained. Subhedral. Equant to irregular shaped. Medium alteration of orthopyroxene as rims and patches of very fine-grained talc and tremolite-actinolite, chlorite as rims in contact with plagioclase.
		Talc	0.5	
		Chlorite	tr	
Fe-Ti oxides	4.8	Magnetite		Fine-grained anhedral disseminated interstitial magnetite. Few magnetite grains with sandwich-type ilmenite exsolution. Fine-grained anhedral, interstitial granular, ilmenite, associated with magnetite.
		Ilmenite		
Sulfides	0.3	Chalcopyrite	tr	Very fine-grained anhedral disseminated grains throughout the sample.
		Pyrite	tr	
Comments: Massive. Cumulate. Variable crystal size. Magnetite occurs weakly disseminated and evenly distributed. Granular ilmenite grains. Weakly altered. Gabbronorite.				

LDI-21-SB025		Drillhole 14-902		Depth 75 m
Mineral (interpreted pre-alteration)	%	Mineral (actual)	%	
Plagioclase	46.3	Plagioclase	46	Fine- to coarse-grained. Subhedral. Equant to tabular. Weakly altered to parches of fine-grained sericite. Chlorite filling fractures. Very weakly fractured, rare deformation twinning.
		Sericite	0.3	
		Chlorite	tr	
Orthopyroxene	48.3	Tremolite-actinolite	0.5	Fine-grained. Anhedral to subhedral. Medium alteration to talc and tremolite-actinolite along the fractures and to tremolite-actinolite as rims. Pyroxene grains enclosing plagioclase and magnetite grains.
		Talc	0.3	
		Chlorite	tr	
Fe-Ti oxides	5.1	Magnetite		Fine-grained anhedral disseminated interstitial magnetite. Few magnetite grains with sandwich-type ilmenite exsolution. Fine-grained anhedral, interstitial granular, ilmenite, associated with magnetite.
		Ilmenite		
Sulfides	0.3	Chalcopyrite	tr	

		Pyrite	tr	Very fine-grained anhedral disseminated grains throughout the sample.
Comments: Massive. Cumulate. Variable crystal size. Magnetite occurs weakly disseminated and evenly distributed. Granular ilmenite grains. Weakly altered. Gabbronorite.				

LDI-21-SB026		Drillhole 14-902		Depth 77.5 m
Mineral (interpreted pre-alteration)	%	Mineral (actual)	%	
Plagioclase	43.2	Plagioclase	43	Fine- to coarse-grained. Subhedral. Equant to tabular. Very weakly altered to parches of fine-grained sericite. Very weakly fractured, rare deformation twinning.
		Sericite	0.2	
		Chlorite	tr	
Orthopyroxene	47.6	Talc	tr	Fine-grained. Anhedral to subhedral. Medium alteration to chlorite and talc as rims. Pyroxene crystals partially or completely encircle plagioclase grains.
		Chlorite	tr	
Biotite	tr	Biotite	tr	Fine-grained. Subhedral platy disseminated crystals. Associated with orthopyroxene.
Fe-Ti oxides	8.3	Magnetite		Fine-grained anhedral disseminated interstitial magnetite. Few magnetite grains with sandwich-type ilmenite exsolution. Fine-grained anhedral, interstitial granular, ilmenite, associated with magnetite.
		Ilmenite		
Sulfides	0.9	Chalcopyrite	tr	Very fine-grained anhedral disseminated grains throughout the sample.
		Pyrite	tr	
Comments: Massive. Cumulate. Variable crystal size. Magnetite occurs weakly disseminated and evenly distributed. Granular ilmenite grains. Weakly altered. Gabbronorite.				

LDI-21-SB027		Drillhole 14-902		Depth 80 m
Mineral (interpreted pre-alteration)	%	Mineral (actual)	%	
Plagioclase	25.3	Plagioclase	25	Fine- to coarse-grained. Equant to tabular. Subhedral. Very weakly altered to parches of fine-grained sericite and traces of chlorite as rims at contact with pyroxenes. Very weakly fractured, rare deformation twinning.
		Sericite	1	
		Chlorite	tr	

Orthopyroxene	55.6	Tremolite-actinolite	55	Fine-grained. Anhedral. Low alteration to talc along the fractures and to tremolite-actinolite as rims. Traces of chlorite.
		Chlorite	0.6	
Fe-Ti oxides	18	Magnetite		Fine-grained anhedral disseminated interstitial magnetite. Few magnetite grains with granular-type ilmenite exsolution.
		Ilmenite		
Sulfides	1.1	Chalcopyrite	tr	Very fine-grained anhedral disseminated grains throughout the sample.
		Pyrite	tr	
Comments: Massive. Cumulate. Variable crystal size. Magnetite occurs heavily disseminated and evenly distributed. Granular ilmenite grains. Weakly altered. Gabbronorite.				

LDI-21-SB028		Drillhole 14-902		Depth 81.75 m
Mineral (interpreted pre-alteration)	%	Mineral (actual)	%	
Plagioclase	48	Plagioclase	48	Fine- to coarse-grained. Equant to tabular. Subhedral. Very weakly altered to patches of fine-grained sericite and traces of chlorite as rims at contact with pyroxenes. Very weakly fractured, rare deformation twinning. Plagioclase grains enclosing pyroxene grains.
		Sericite	tr	
		Chlorite	tr	
Orthopyroxene	45.7	Tremolite-actinolite	5	Fine-grained. Anhedral to subhedral. Low alteration to talc and tremolite-actinolite along the fractures and to tremolite-actinolite as rims. Pyroxene grains enclosing plagioclase and magnetite grains.
		Chlorite	0.7	
Fe-Ti oxides	6.3	Magnetite		Fine-grained anhedral disseminated interstitial magnetite. Magnetite grains with sandwich-type and internal granular ilmenite exsolution. Fine-grained anhedral, interstitial granular, ilmenite, associated with magnetite.
		Ilmenite		
Biotite	tr	Biotite	tr	Very fine-grained anhedral disseminated grains throughout the sample.
Sulfides	tr	Pyrite	tr	
		Chalcopyrite	tr	
Comments: Massive. Cumulate. Variable crystal size. Magnetite occurs weakly disseminated and evenly distributed. Granular ilmenite grains. Weakly altered. Gabbronorite.				

LDI-21-SB029		Drillhole 14-902		Depth 87 m
Mineral (interpreted pre-alteration)	%	Mineral (actual)	%	
Plagioclase	57.5	Plagioclase	52	Fine-grained. Equant to tabular. Subhedral. Plagioclase has been moderately replaced by very fine-grained chlorite±sericite. Very fine-grained sericite is dominant.
		Sericite	5	
		Chlorite	0.5	
Pyroxene	26.5	Tremolite-actinolite	26	Pyroxene has been completely replaced by very fine to fine-grained tremolite-actinolite+talc±chlorite aggregates.
		Chlorite	0.5	
Fe-Ti oxides	15.6	Magnetite		Fine-grained anhedral disseminated interstitial magnetite. Magnetite grains with sandwich-type and internal granular ilmenite exsolution.
		Ilmenite		
Sulfides	0.4	Pyrite	tr	Very fine-grained anhedral disseminated grains throughout the sample.
		Chalcopyrite	tr	
Comments: Massive. Cumulate. Variable crystal size. Magnetite occurs heavily disseminated and evenly distributed. Granular ilmenite grains. Strongly altered. Gabbronorite.				

LDI-21-SB030		Drillhole 14-902		Depth 89 m
Mineral (interpreted pre-alteration)	%	Mineral (actual)	%	
Plagioclase	16.2	Plagioclase		Crystal properties are difficult to discern due to strong alteration to chlorite rims and patches of sericite and/or chlorite. Appear to be fine- to coarse-grained and generally equant. Weakly fractured.
		Sericite	10	
		Chlorite	6	
Pyroxene	79.5	Tremolite-actinolite	78	Fine-grained. Ahnedral to subhedral. Irregular shaped. Completely replaced by alteration products, tremolite-actinolite±chlorite.
		Chlorite	1.5	
Fe-Ti oxides	4	Magnetite		Fine-grained anhedral disseminated interstitial magnetite. Sandwich-type ilmenite exsolution. Fine-grained anhedral, interstitial granular, ilmenite, associated with magnetite.
		Ilmenite		
Sulfides	0.3	Pyrite	tr	Very fine-grained anhedral disseminated aggregates throughout the sample.
		Chalcopyrite	tr	

Comments: Massive. Cumulate. Variable crystal size. Magnetite occurs weakly disseminated and evenly distributed. Granular ilmenite grains. Strongly altered. Gabbronorite.

LDI-21-SB031		Drillhole 14-902		Depth 92 m
Mineral (interpreted pre-alteration)	%	Mineral (actual)	%	
Plagioclase	31	Plagioclase	30	Fine- to coarse-grained. Equant to tabular. Subhedral. Very weakly altered to parches of fine-grained sericite.
		Sericite	1	
		Chlorite	tr	
Pyroxene	58	Tremolite-actinolite	58	Fine- to coarse-grained. Anhedral to subhedral. Completely replaced by alteration minerals. Alteration is present as very tine to fine tremolite-actinolite±chlorite.
		Chlorite	tr	
Fe-Ti oxides	10.9	Magnetite		Fine-grained anhedral disseminated interstitial magnetite. Magnetite grains with sandwich-type ilmenite exsolution. Fine-grained anhedral, interstitial granular ilmenite, associated with magnetite.
		Ilmenite		
Sulfides	0.1	Pyrite	tr	Very fine-grained anhedral disseminated aggregates throughout the sample.
		Chalcopyrite	tr	
Comments: Sharp contact between very fine and fine to coarse gabbronorite. Massive. Cumulate. Variable crystal size. Magnetite occurs heavily disseminated and evenly distributed. Granular ilmenite grains. Moderately altered. Gabbronorite.				

LDI-21-SB032		Drillhole 14-902		Depth 99 m
Mineral (interpreted pre-alteration)	%	Mineral (actual)	%	
Plagioclase	33.2	Plagioclase	33	Fine-grained. Equant to tabular. Subhedral. Very weakly altered to parches of fine-grained sericite, chlorite, and traces of epidote.
		Sericite	0.2	
		Chlorite	tr	
Pyroxene	46.5	Tremolite-actinolite	46	Fine- to coarse-grained. Anhedral to subhedral. Completely replaced by alteration minerals. Alteration is present as very tine to fine tremolite-actinolite±chlorite.
		Chlorite	0.5	
Fe-Ti oxides	20	Magnetite		Fine-grained anhedral disseminated interstitial magnetite. Magnetite grains with sandwich-type ilmenite exsolution. Fine-grained anhedral,
		Ilmenite		

				interstitial granular ilmenite, associated with magnetite.
Sulfides	0.3	Pyrite	tr	Very fine-grained anhedral disseminated aggregates throughout the sample.
		Chalcopyrite	tr	
Comments: Massive. Cumulate. Variable crystal size. Magnetite occurs heavily disseminated and evenly distributed. Granular ilmenite grains. Moderate alteration grade. Gabbronorite.				

LDI-21-SB033		Drillhole 14-902		Depth 96 m
Mineral (interpreted pre-alteration)	%	Mineral (actual)	%	
Plagioclase	22.3	Plagioclase	22	Fine- to coarse-grained. Equant to tabular. Subhedral. Very weakly altered to parches of fine-grained sericite. Very weakly fractured, rare deformation twinning.
		Sericite	0.3	
		Chlorite	tr	
Pyroxene	54.6	Tremolite-actinolite	54	Fine- to coarse-grained. Anhedral to subhedral. Completely replaced by alteration minerals. Alteration is present as very tine to fine tremolite-actinolite±chlorite.
		Chlorite	0.6	
Fe-Ti oxides	22.4	Magnetite		Fine-grained anhedral disseminated interstitial magnetite. Magnetite grains with trellis- and sandwich-type ilmenite exsolution. Fine-grained anhedral, interstitial granular ilmenite, with hematite? Exsolutions, associated with magnetite.
		Ilmenite		
Sulfides	0.7	Pyrite	tr	Very fine-grained anhedral disseminated aggregates throughout the sample.
		Chalcopyrite	tr	
Comments: Massive. Cumulate. Variable crystal size. Magnetite occurs heavily disseminated and evenly distributed. Granular ilmenite grains. Moderately altered. Gabbronorite.				

LDI-21-SB034		Drillhole 14-902		Depth 97.5 m
Mineral (interpreted pre-alteration)	%	Mineral (actual)	%	
Plagioclase	7	Sericite	5	Completely replaced by alteration minerals.
		Chlorite	2	
Pyroxene	11	Tremolite-actinolite	9	Completely replaced by alteration minerals.
		Chlorite	2	
Fe-Ti oxides	81.8	Magnetite		Coarse-grained. Anhedral to subhedral. Equant to tabular. Trellis-
		Ilmenite		

				and granular-type ilmenite exsolutions. Fine anhedral spinel exsolutions. Triple junction texture.
Sulfides	0.2	Pyrite	tr	Very fine-grained anhedral disseminated aggregates throughout the sample.
		Chalcopyrite	tr	
Comments: Massive. Variable crystal size. Magnetite occurs heavily disseminated and evenly distributed. Trellis- and granular-type ilmenite exsolutions. Strongly altered. Massive oxide.				

LDI-21-SB035		Drillhole 14-902		Depth 99.25
Mineral (interpreted pre-alteration)	%	Mineral (actual)	%	
Plagioclase	30.2	Plagioclase	30	Fine- to coarse-grained. Equant to tabular. Anhedral to subhedral. Weak alteration to parches of sericite. Weakly fractured with chlorite filling fractures.
		Sericite	0.2	
		Chlorite	tr	
Pyroxene	54.3	Tremolite-actinolite	54	Fine- to coarse-grained. Equant to tabular. Subhedral. Pyroxene is completely replaced by tabular aggregates of tremolite-actinolite, and chlorite as rims in contact with plagioclase. Weakly fractured with chlorite filling fractures. Pyroxene encloses fine grains of Fe-Ti oxides.
		Chlorite	tr	
Fe-Ti oxides	14.3	Magnetite		Occur as bands and disseminate. Interstitial. Fine- to coarse-grained. Subhedral. Trellis-type and granular ilmenite exsolutions.
		Ilmenite		
Sulfides	1.2	Pyrite	tr	Very fine-grained anhedral disseminated aggregates throughout the sample.
		Chalcopyrite	tr	
Comments: Massive. Cumulate. Variable crystal size. Magnetite occurs heavily disseminated and as bands. Granular ilmenite and trellis-type ilmenite exsolutions. Moderately altered. Gabbronorite.				

LDI-21-SB036		Drillhole 14-902		Depth 101 m
Mineral (interpreted pre-alteration)	%	Mineral (actual)	%	
Plagioclase	30	Plagioclase	29	Fine- to coarse-grained. Equant to tabular. Anhedral to subhedral. Weak alteration to parches of sericite. Weakly fractured with chlorite filling fractures.
		Sericite	tr	
		Chlorite	tr	

Pyroxene	43.5	Tremolite-actinolite	43	Fine- to coarse-grained. Equant to tabular. Subhedral. Pyroxene is completely replaced by tabular aggregates of tremolite-actinolite, and chlorite as rims in contact with plagioclase.
		Chlorite	0.5	
Fe-Ti oxides	26	Magnetite		Fine-grained anhedral disseminated interstitial magnetite. Magnetite grains sandwich-type ilmenite exsolution. Fine-grained anhedral, interstitial granular ilmenite.
		Ilmenite		
Sulfides	0.5	Pyrite	tr	Very fine-grained anhedral disseminated aggregates throughout the sample.
Comments: Massive. Cumulate. Variable crystal size. Magnetite occurs heavily disseminated and as bands. Granular ilmenite and trellis-type ilmenite exsolutions. Moderately altered. Gabbronorite.				

LDI-21-SB037		Drillhole 14-902		Depth 105 m
Mineral (interpreted pre-alteration)	%	Mineral (actual)	%	
Plagioclase	38.5	Plagioclase	38	Fine- to coarse-grained. Equant to tabular. Anhedral to subhedral. Weak alteration to parches of sericite.
		Sericite	tr	
		Chlorite	tr	
Pyroxene	48.5	Tremolite-actinolite	48	Fine-grained. Anhedral to subhedral. Pyroxene is completely replaced by tabular aggregates of tremolite-actinolite. Pyroxene grains enclosing plagioclase and magnetite grains.
		Chlorite	tr	
Fe-Ti oxides	12.5	Magnetite		Occur as bands and disseminate. Interstitial. Fine- to coarse-grained. Subhedral. Trellis-type and granular ilmenite exsolutions. Magnetite grains with 120° triple junction texture.
		Ilmenite		
Sulfides	0.5	Pyrite	tr	Very fine-grained anhedral disseminated aggregates throughout the sample.
		Chalcopyrite	tr	
Comments: Massive. Cumulate. Variable crystal size. Magnetite occurs heavily disseminated and as bands. Granular ilmenite and trellis-type ilmenite exsolutions. Moderately altered. Gabbronorite.				

LDI-21-SB038		Drillhole 14-902		Depth 107.75
Mineral (interpreted pre-alteration)	%	Mineral (actual)	%	
Plagioclase	31.5	Plagioclase	30	Fine- to coarse-grained. Equant to tabular. Anhedral to subhedral. Moderate alteration to patches of sericite and chlorite as rims and filling fractures. Plagioclase grains enclosing pyroxene grains.
		Sericite	1.5	
		Chlorite	tr	
Pyroxene	39	Tremolite-actinolite	38	Fine-coarse grained. Anhedral to subhedral. Completely replaced by alteration minerals. Alteration is present as very tine to fine tremolite-actinolite±chlorite.
		Chlorite	1	
Fe-Ti oxides	29	Magnetite		Occur as bands and disseminate. Interstitial. Fine- to coarse-grained. Subhedral. Granular ilmenite exsolutions. Coarse ilmenite grains with exsolutions (hematite?)
		Ilmenite		
Sulfides	0.5	Pyrite	tr	Very fine-grained anhedral disseminated aggregates throughout the sample.
		Chalcopyrite	tr	
Comments: Massive. Cumulate. Variable crystal size. Magnetite occurs heavily disseminated and as bands. Granular ilmenite and trellis-type ilmenite exsolutions. Strongly altered. Gabbronorite.				

LDI-21-SB041		Drillhole	14-902	Depth
Mineral (interpreted pre-alteration)		Mineral (actual)		
Plagioclase	53.2	Plagioclase		Plagioclase has been strongly replaced by very fine-grained chlorite±sericite. Pre-alteration plagioclase size appears to have been fine. Very fine-grained sericite is dominant.
		Sericite		
		Chlorite		
Pyroxene	46.6	Tremolite-actinolite		Pyroxene has been completely replaced by very fine to fine-grained tremolite-actinolite+talc±chlorite aggregates
		Chlorite		
Comments: Massive. Variable crystal size. Pre-alteration texture not discernible. Fe-Ti oxides and sulfides occur very rare and disseminated. Strongly altered. Gabbronorite.				

LDI-21-SB042		Drillhole	14-902	Depth
Mineral (interpreted pre-alteration)		Mineral (actual)		
Plagioclase	69	Plagioclase		Plagioclase has been strongly replaced by very fine-grained chlorite±sericite. Pre-alteration plagioclase size appears to have been fine. Very fine-grained sericite is dominant.
		Sericite		
		Chlorite		
Pyroxene	30.8	Tremolite-actinolite		Pyroxene has been completely replaced by very fine to fine-grained tremolite-actinolite+talc±chlorite aggregates
		Chlorite		
		Chalcopyrite		
Comments: Massive. Variable crystal size. Disseminated traces of very fine Fe-Ti oxides and sulfides. Strongly altered. Gabbronorite.				

LDI-21-SB041		Drillhole 20-200		Depth 419 m
Mineral (interpreted pre-alteration)	%	Mineral (actual)	%	Details
Plagioclase	53.2	Plagioclase	49	Medium- to coarse-grained. Cumulate. Subhedral. Strong alteration to patches of very fine-grained sericite occurring on the plagioclase grain and/or chlorite occurring as partial rims.
		Sericite	3	
		Chlorite	1	
		Epidote	tr	
Pyroxene	46.6	Tremolite-actinolite	40	Medium- to coarse-grained. Anhedral. Pyroxene is completely replaced by very fine-grained tremolite-actinolite±chlorite. Pre-alteration orthopyroxene/clinopyroxene proportion is not discernible.
		Chlorite	6	
Fe-Ti oxides	0.08	Magnetite	tr	0.1-2.0 mm, occurring as interstitial grains in tremolite-actinolite, and clusters with sharp, jagged boundaries. Ilmenite observed as sandwich- and trellis-type lamellae exsolution from magnetite and anhedral granules grains at the magnetite borders.

Sulfides	0.1	Pyrite	tr	Mostly present as finely disseminated (<0.1 mm) monosulfide crystals occurring within silicate alteration aggregates or filling fractures in silicates and Iron oxides.
Comments: Gabbronorite. Medium- to coarse-grained. Strongly altered. Weakly disseminated oxide.				

LDI-21-SB042		Drillhole 20-200		Depth 426 m
Mineral (interpreted pre-alteration)	%	Mineral (actual)	%	Details
Plagioclase	69	Plagioclase	60	Medium to coarse-grained. anhedral to subhedral. Weakly to moderately altered to patches of very fine-grained sericite±chlorite±epidote.
		Sericite	5	
		Chlorite	4	
		Epidote	tr	
Pyroxene	30.8	Tremolite-actinolite	29	Medium- to coarse-grained. Primary pyroxene has been completely altered. Alteration occurs as fine-grained aggregates of tremolite-actinolite+talc± chlorite, and fine to very fine-grained rims of chlorite. Chlorite alteration mostly occurs at boundaries to altered pyroxene.
		Talc	1	
		Chlorite	tr	
Fe-Ti oxides	0.05	Magnetite	tr	Very fine- to fine-grained. Subhedral. Occurring as interstitial grains in silicates.
Sulfides	0.2	Pyrite	tr	Very fine to fine. Subhedral to euhedral. Disseminated.
Comments: Massive, cumulate. Variable crystal size, dominantly coarse-grained. Pre-alteration crystal boundaries and texture are very difficult to determine due to alteration. Strongly altered. Gabbronorite. Weakly disseminated oxide.				

LDI-21-SB047		Drillhole 20-200		Depth 466 m
Mineral (interpreted pre-alteration)	%	Mineral (actual)	%	Details
Plagioclase	44	Plagioclase	43	Medium- to coarse-grained. Subhedral, tabular. Weakly fractured. Showing only minor gritty sericite alteration and traces of chlorite±epidote rims.
		Sericite	1	
Pyroxene	50	Tremolite-actinolite	49	Medium to coarse-grained. Anhedral to subhedral.
		Chlorite	1	

				Alteration is present as very tine to fine tremolite-actinolite.
Fe-Ti oxides	5.5	Magnetite	5	Disseminated, interstitial, anhedral magnetite. Occasionally trellis-type ilmenite exsolution. Very fine to fine subhedral disseminated ilmenite grains within magnetite grains.
		Ilmenite	tr	
Sulfides	0.5	Pyrite	tr	Very fine. Anhedral. Disseminated.
Comments: massive, cumulate. Variable crystal size, dominantly medium-grained. Gabbronorite. Weakly disseminated oxide. Weakly altered.				

LDI-21-SB050		Drillhole 20-200		Depth 487 m
Mineral (interpreted pre-alteration)	%	Mineral (actual)	%	Details
Plagioclase	51.5	Plagioclase	51	Medium to coarse-grained. Cumulate. larger crystals tabular and subhedral to anhedral. Low alteration as rims and small patches of very fine-grained sericite.
		Sericite	tr	
Pyroxene	41.5	Tremolite-actinolite	20	Medium to coarse-grained. Anhedral to subhedral. Orthopyroxene is partially replaced by fine-grained tremolite-actinolite.
		Chlorite	tr	
Fe-Ti oxides	6.1	Magnetite		Fine-grained. Disseminated. A few grains of magnetite show sandwich-type ilmenite exsolutions.
Sulfides	0.9	Pyrite	tr	Mostly present as finely disseminated crystals of anhedral pyrite occurring interstitial to silicate.
Comments: Cumulate. Variable crystal size, dominantly medium-grained. Gabbronorite. Weakly disseminated oxide. Weakly altered.				

LDI-21-SB051		Drillhole 20-200		Depth 491 m
Mineral (interpreted pre-alteration)	%	Mineral (actual)	%	Details
Plagioclase	44	Plagioclase	41	Fine- to medium-grained size. Large tabular and subhedral to anhedral crystals. Very weak alteration as patches of fine-grained sericite.
		Sericite	3	
Pyroxene	50	Orthopyroxene	20	Fine- to medium-grained size orthopyroxene grains. Very fine-grained tremolite-actinolite alteration towards the center of the section.
		Tremolite-actinolite	30	

Fe-Ti oxides	5	Magnetite	5	Medium-grained size. Anhedral Interstitial grains. Magnetite is evenly disseminated in the thin section.
Sulfides	1	Pyrite	1	Very fine- to fine-grained. Occur as disseminated monosulfide crystals.
Comments: Massive. Cumulate. Dominantly medium-grained. Gabbronorite. Weakly disseminated oxide. Weakly altered.				

LDI-21-SB052		Drillhole 20-200		Depth 493 m
Mineral (interpreted pre-alteration)	%	Mineral (actual)	%	Details
Plagioclase	43	Plagioclase	42	Medium- to coarse-grained. Larger crystals tabular and subhedral to anhedral. Alteration present as patches of sericite.
		Sericite	tr	
Pyroxene	51	Tremolite-actinolite	51	Fine- to coarse-grained. Orthopyroxene has been replaced by tremolite-actinolite±chlorite fine-grained alteration products.
		Chlorite	tr	
Fe-Ti oxides	5.7	Magnetite		Aggregates of fine to medium-grained anhedral disseminated commonly surround the silicate. Occasionally sandwich- and granular-type ilmenite exsolution.
Sulfides	0.3	Pyrite	tr	Finely disseminated pyrite crystals.
Comments: Massive. Gabbronorite. Weakly disseminated oxide. Weakly altered.				

LDI-21-SB055		Drillhole 20-200		Depth 512 m
Mineral (interpreted pre-alteration)	%	Mineral (actual)	%	Details
Plagioclase	51	Plagioclase	49	Coarse-grained. Cumulate. Large tabular and subhedral to anhedral crystals. Low alteration as patches sericite.
		Sericite	2	
Pyroxene	46	Tremolite-actinolite	45	Medium- to coarse-grained. Large tabular and subhedral to anhedral crystals. Orthopyroxene with low alteration to tremolite-actinolite±chlorite.
		Chlorite	1	

Fe-Ti oxides	3	Magnetite	3	Fine- to medium-grained. predominantly as disseminated interstitial anhedral grains. Ilmenite occurs occasionally as sandwich-type exsolution.
Comments: Massive. Cumulate. Gabbronorite. Weakly disseminated oxide. Weakly altered.				

LDI-21-SB059		Drillhole 20-200		Depth 540 m
Mineral (interpreted pre-alteration)	%	Mineral (actual)	%	Details
Plagioclase	35	Plagioclase	30	Medium- to coarse-grained. Cumulate. Equant to tabular. Anhedral to subhedral grains. Patches of sericite±chlorite alteration and rims of chlorite±sericite with minor epidote proportional to proximity to altered pyroxene.
		Sericite	2	
		Chlorite	3	
		Epidote	tr	
Pyroxene	64	Tremolite-actinolite	58	Coarse-grained. Tabular, anhedral to subhedral grains. Very fine-grained tremolite-actinolite ±chlorite±talc aggregates are present throughout, with talc commonly occurring as a minor component.
		Chlorite	6	
Fe-Ti oxides	0.5	Magnetite		Magnetite and ilmenite are evenly distributed in the thin section, predominantly as disseminated fine to medium anhedral grains. Magnetite predominates over ilmenite.
		Ilmenite		
Sulfides	0.5	Pyrite	tr	Very finely disseminated anhedral monosulfide pyrite crystals.
Comments: Massive. Cumulate. Gabbronorite. Weakly disseminated oxide. Moderately altered.				

LDI-21-SB061		Drillhole 20-200		Depth 548 m
Mineral (interpreted pre-alteration)	%	Mineral (actual)	%	Details
Plagioclase	35	Plagioclase	28	Fine- to coarse-grained. Subhedral, equant to tabular. Alteration as patches of very fine to fine-grained sericite. Trace chlorite and epidote.
		Sericite	4	
		Chlorite	2	
		Epidote	tr	
Pyroxene	59	Tremolite-actinolite	54	Fine- to coarse-grained. Pre-alteration mineral properties are difficult to determine. Fine-grained tremolite-actinolite±chlorite.
		Chlorite	5	

Fe-Ti oxides	6	Magnetite	6	Very fine- to fine-grained size. Interstitial, disseminated.
Comments: Massive. Cumulate. Variable crystal size, ranging from fine- to coarse-grained. Gabbronorite. Weakly disseminated oxide. Moderately altered.				

LDI-21-SB062		Drillhole 20-200		Depth 556 m
Mineral (interpreted pre-alteration)	%	Mineral (actual)	%	Details
Plagioclase	30	Plagioclase	25	Fine- to coarse-grained. Equant to tabular. Anhedral to subhedral grains. Alteration as patches of fine-grained sericite. Very weakly fractured, rare deformation twinning.
		Sericite	5	
Pyroxene	70	Tremolite-actinolite	70	Medium- to coarse-grained. Pyroxene is completely replaced by tremolite-actinolite.
Comments: Massive. Cumulate. Gabbronorite. Strongly altered.				

LDI-21-SB063		Drillhole 20-200		Depth 562 m
Mineral (interpreted pre-alteration)	%	Mineral (actual)	%	Details
Plagioclase	36.8	Plagioclase	31	Fine- to medium-grained. Tabular. Subhedral. Medium sericite alteration throughout the section.
		Sericite	2	
		Chlorite	tr	
		Epidote	tr	
Pyroxene	60	Tremolite-actinolite	59	Medium-grained. Anhedral, generally equant to occasionally tabular. Alteration present as fine to very fine-grained tremolite-actinolite aggregates throughout.
		Chlorite	1	
Fe-Ti oxides	3	Magnetite	3	Very finely disseminated, very fine-grained crystals.
Sulfides	0.2	Pyrite	tr	Mostly present as finely disseminated, very fine-grained monosulfide crystals occurring within silicate alteration aggregates.
Comments: Massive. Cumulate. Gabbronorite. Weakly disseminated oxide. Moderately altered.				

LDI-21-SB064		Drillhole 20-200		Depth 566 m
Mineral (interpreted pre-alteration)	%	Mineral (actual)	%	Details
Plagioclase	38	Plagioclase	35	

		Sericite	3	Medium- to coarse-grained. Subhedral, equant to tabular. Alteration is generally weak, typically as patches of very fine-grained sericite.
Pyroxene	58	Tremolite-actinolite	54	Medium- to coarse-grained. Anhedral to subhedral, equant to tabular. High internal alteration to tremolite-actinolite±chlorite.
		Chlorite	4	
Fe-Ti oxides	4	Magnetite	4	Finely disseminated fine to very fine interstitial grains.
Comments: Holocrystalline, medium- to coarse-grained size. Massive. Cumulate. Gabbronorite. Weakly disseminated oxide. Moderately altered.				

LDI-21-SB065		Drillhole 20-200		Depth 577 m
Mineral (interpreted pre-alteration)	%	Mineral (actual)	%	Details
Plagioclase	49	Plagioclase	46	Fine- to coarse-grained. Equant to tabular. Subhedral. Alteration is very weak as small patches of very fine-grained sericite and chlorite.
		Sericite	2	
		Chlorite	1	
Pyroxene	45	Tremolite-actinolite	42	Fine- to medium-grained. Equant to tabular. Subhedral. Replacement by alteration tremolite-actinolite as rims is common.
		Chlorite	3	
Fe-Ti oxides	5.4	Magnetite	5	Magnetite is evenly distributed in the thin section, predominantly as interstitial anhedral medium-grained grains. Trellis- and granular-type ilmenite exsolution.
Sulfides	0.6	Pyrite	tr	Very fine- to fine-grained finely disseminated grains.
Comments: Holocrystalline, inequigranular, Variable crystal size, ranging from fine- to coarse-grained. Massive. Cumulate. Gabbronorite. Weakly disseminated oxide. Weakly altered.				

LDI-21-SB066		Drillhole 20-200		Depth 578 m
Mineral (interpreted pre-alteration)	%	Mineral (actual)	%	Details
Plagioclase	46	Plagioclase	27	Medium- to coarse-grained. Equant to tabular. Subhedral. Alteration is weak, as patches of fine-grained sericite and rims of chlorite.
		Sericite	2	

Pyroxene	47	Tremolite-actinolite	49	Medium- to coarse-grained. Equant and subhedral. Predominance of orthopyroxene. Moderate amounts of replacement by tremolite-actinolite±chlorite.
		Chlorite	3	
Fe-Ti oxides	6.3	Magnetite		Magnetite occurs as disseminated, interstitial, anhedral grains. Occasionally trellis-type ilmenite exsolution.
Sulfides	0.7	Pyrite	tr	Very fine-grained up to fine-grained subhedral pyrite disseminated throughout the sample.
Comments: Massive. Cumulate. Gabbronorite. Weakly disseminated oxide. Weakly altered.				

LDI-21-SB067		Drillhole 20-200		Depth 584 m
Mineral (interpreted pre-alteration)	%	Mineral (actual)	%	Details
Plagioclase	51	Plagioclase	48	Fine- to coarse-grained. Equant to tabular and subhedral to anhedral cumulate crystals. Alteration is very weak, as patches of very fine-grained sericite and chlorite thin partial rims. very weakly fractured.
		Sericite	3	
		Chlorite	tr	
Pyroxene	42.5	Tremolite-actinolite	42	Medium- to coarse-grained. Equant to tabular and subhedral to anhedral. Alteration present as very fine to fine-grained tremolite-actinolite±chlorite aggregates.
		Chlorite	tr	
Fe-Ti oxides	6.2	Magnetite		Magnetite is evenly distributed in the thin section, predominantly as disseminated and interstitial anhedral fine- to medium-grained size grains.
Sulfides	0.3	Pyrite	tr	Disseminated anhedral to subhedral monosulfide crystals present interstitially.
Comments: Massive. Cumulate. Variable crystal size, ranging from fine to coarse. Gabbronorite. Weakly disseminated oxide. Moderately altered.				

LDI-21-SB069		Drillhole 20-200		Depth 595 m
Mineral (interpreted pre-alteration)	%	Mineral (actual)	%	Details
Plagioclase	44	Plagioclase	54	Medium- to coarse-grained. Equant to tabular and subhedral to anhedral
		Sericite	4	

		Chlorite	tr	cumulate crystals. Medium alteration as patches of very fine-grained sericite and chlorite rims.
Pyroxene	51	Tremolite-actinolite	50	Medium- to coarse-grained. Anhedral and irregularly shaped. High internal alteration to aggregates of tremolite-actinolite±chlorite.
		Chlorite	1	
Fe-Ti oxides	4.1	Magnetite		Anhedral to subhedral fine-grained disseminated magnetite evenly distributed in the thin section.
Sulfides	0.9	Pyrite	tr	Very fine monosulfide grains
Comments: Massive. Cumulate. Variable crystal size. Gabbronorite. Magnetite occurs weakly disseminated and evenly distributed. Weakly altered.				

LDI-21-SB073		Drillhole 20-200		Depth 613 m
Mineral (interpreted pre-alteration)	%	Mineral (actual)	%	Details
Plagioclase	42.9	Plagioclase	42	Fine- to coarse-grained. Equant to tabular and subhedral to anhedral cumulate crystals. Very weakly fractured, rare deformation twinning. Alteration is weak as small patches of very fine-grained sericite.
		Sericite	tr	
Pyroxene	49.6	Tremolite-actinolite	49	Anhedral and irregularly shaped, fine- to medium-grained. Pyroxene is completely replaced by very fine-grained tremolite-actinolite aggregates.
		Chlorite	tr	
Fe-Ti oxides	6.6	Magnetite		Very fine- to fine-grained anhedral disseminated smooth magnetite grains.
Sulfides	0.9	Pyrite	tr	Very fine-grained anhedral disseminated grains throughout the sample.
Comments: Massive. Cumulate. Variable crystal size. Magnetite occurs weakly disseminated and evenly distributed. Moderately altered. Gabbronorite.				

LDI-21-SB074		Drillhole 20-200		Depth 615 m
Mineral (interpreted pre-alteration)	%	Mineral (actual)	%	
Plagioclase	35	Plagioclase	35	Medium- to coarse-grained. Subhedral. Equant to tabular. Very
		Sericite	tr	

				weakly fractured. Weak alteration as patches.
Pyroxene	58.3	Tremolite-actinolite	58	Equant to tabular and subhedral to anhedral, fine- to coarse-grained grains. Medium alteration of pyroxene as rims and patches of very fine-grained tremolite-actinolite±talc±chlorite.
		Chlorite	tr	
		Talc	tr	
Fe-Ti oxides	6.1	Magnetite		Very fine- to fine-grained anhedral disseminated interstitial smooth magnetite grains.
Sulfides	0.9	Pyrite	tr	Very fine-grained anhedral disseminated grains throughout the sample.
Comments: Massive. Cumulate. Variable crystal size. Magnetite occurs weakly disseminated and evenly distributed. Weakly altered. Gabbronorite.				

LDI-21-SB075		Drillhole 20-200		Depth m
Mineral (interpreted pre-alteration)	%	Mineral (actual)	%	
Plagioclase	60.2	Plagioclase	59	Medium- to coarse-grained. Anhedral to subhedral tabular grains. Very weakly fractured, rare deformation twinning. Weak alteration as small patches of very fine-grained sericite.
		Sericite	tr	
		Chlorite	tr	
Pyroxene	35	Tremolite-actinolite	34	Anhedral to subhedral, Medium- to coarse-grained grains. Equant to elongated. Medium to high alteration to patches of talc and rims of tremolite-actinolite±talc±chlorite.
		Chlorite	tr	
		Talc	tr	
Fe-Ti oxides	4.3	Magnetite		Very fine- to fine-grained anhedral disseminated interstitial magnetite.
Sulfides	0.5	Pyrite	tr	Very fine-grained anhedral disseminated grains throughout the sample.
Comments: Massive. Cumulate. Variable crystal size. Magnetite occurs weakly disseminated and evenly distributed. Weakly altered. Gabbronorite.				

Appendix B

Magnetic susceptibility

ID Hole	North	East	Domain	From	to	Kappa
14-902	5449569	309799.4	Magnetite Norite	0	0.25	354.9
14-902	5449569	309799.4	Magnetite Norite	0.25	0.5	340.9
14-902	5449569	309799.4	Magnetite Norite	0.5	0.75	320.2
14-902	5449569	309799.4	Magnetite Norite	0.75	1	269.3
14-902	5449569	309799.4	Magnetite Norite	1	1.25	462.5
14-902	5449569	309799.4	Magnetite Norite	1.25	1.5	359.2
14-902	5449569	309799.4	Magnetite Norite	1.5	1.75	277.4
14-902	5449569	309799.4	Magnetite Norite	1.75	2	244.8
14-902	5449569	309799.4	Magnetite Norite	2	2.25	340.0
14-902	5449569	309799.4	Magnetite Norite	2.25	2.5	294.6
14-902	5449569	309799.4	Magnetite Norite	2.5	2.75	551.6
14-902	5449569	309799.4	Magnetite Norite	2.75	3	355.5
14-902	5449569	309799.4	Magnetite Norite	3	3.25	413.6
14-902	5449569	309799.4	Magnetite Norite	3.25	3.5	336.3
14-902	5449569	309799.4	Magnetite Norite	3.5	3.75	175.1
14-902	5449569	309799.4	Magnetite Norite	3.75	4	397.0
14-902	5449569	309799.4	Magnetite Norite	4	4.25	465.3
14-902	5449569	309799.4	Magnetite Norite	4.25	4.5	223.0
14-902	5449569	309799.4	Magnetite Norite	4.5	4.75	250.0
14-902	5449569	309799.4	Magnetite Norite	4.75	5	813.1
14-902	5449569	309799.4	Magnetite Norite	5	5.25	643.4
14-902	5449569	309799.4	Magnetite Norite	5.25	5.5	444.3
14-902	5449569	309799.4	Magnetite Norite	5.5	5.75	957.1
14-902	5449569	309799.4	Magnetite Norite	5.75	6	534.3
14-902	5449569	309799.4	Magnetite Norite	6	6.25	363.7
14-902	5449569	309799.4	Magnetite Norite	6.25	6.5	295.0
14-902	5449569	309799.4	Magnetite Norite	6.5	6.75	361.8
14-902	5449569	309799.4	Magnetite Norite	6.75	7	336.8
14-902	5449569	309799.4	Magnetite Norite	7	7.25	402.3
14-902	5449569	309799.4	Magnetite Norite	7.25	7.5	474.8
14-902	5449569	309799.4	Magnetite Gabbronorite	7.5	7.75	796.1
14-902	5449569	309799.4	Magnetite Gabbronorite	7.75	8	485.5
14-902	5449569	309799.4	Magnetite Gabbronorite	8	8.25	297.5

ID Hole	North	East	Domain	From	to	Kappa
14-902	5449569	309799.4	Magnetite Gabbronorite	8.25	8.5	772.0
14-902	5449569	309799.4	Magnetite Gabbronorite	8.5	8.75	498.0
14-902	5449569	309799.4	Magnetite Gabbronorite	8.75	9	434.8
14-902	5449569	309799.4	Magnetite Gabbronorite	9	9.25	202.5
14-902	5449569	309799.4	Magnetite Gabbronorite	9.25	9.5	1266.6
14-902	5449569	309799.4	Magnetite Gabbronorite	9.5	9.75	1075.2
14-902	5449569	309799.4	Magnetite Gabbronorite	9.75	10	144.5
14-902	5449569	309799.4	Magnetite Gabbronorite	10	10.25	369.0
14-902	5449569	309799.4	Magnetite Gabbronorite	10.25	10.5	311.0
14-902	5449569	309799.4	Magnetite Gabbronorite	10.5	10.75	208.8
14-902	5449569	309799.4	Magnetite Gabbronorite	10.75	11	100.3
14-902	5449569	309799.4	Magnetite Gabbronorite	11	11.25	754.2
14-902	5449569	309799.4	Magnetite Gabbronorite	11.25	11.5	314.2
14-902	5449569	309799.4	Magnetite Gabbronorite	11.5	11.75	218.3
14-902	5449569	309799.4	Magnetite Gabbro	11.75	12	1189.7
14-902	5449569	309799.4	Magnetite Gabbro	12	12.25	374.9
14-902	5449569	309799.4	Magnetite Gabbro	12.25	12.5	207.8
14-902	5449569	309799.4	Magnetite Gabbro	12.5	12.75	557.1
14-902	5449569	309799.4	Magnetite Gabbro	12.75	13	1279.9
14-902	5449569	309799.4	Magnetite Gabbro	13	13.25	124.7
14-902	5449569	309799.4	Magnetite Gabbro	13.25	13.5	133.4
14-902	5449569	309799.4	Magnetite Gabbro	13.5	13.75	111.5
14-902	5449569	309799.4	Magnetite Gabbro	13.75	14	276.1
14-902	5449569	309799.4	Magnetite Gabbro	14	14.25	279.4
14-902	5449569	309799.4	Magnetite Gabbro	14.25	14.5	288.6
14-902	5449569	309799.4	Magnetite Gabbro	14.5	14.75	381.5
14-902	5449569	309799.4	Magnetite Gabbro	14.75	15	360.5
14-902	5449569	309799.4	Magnetite Gabbro	15	15.25	266.7
14-902	5449569	309799.4	Magnetite Gabbro	15.25	15.5	256.0
14-902	5449569	309799.4	Magnetite Gabbro	15.5	15.75	284.1
14-902	5449569	309799.4	Magnetite Gabbro	15.75	16	132.2
14-902	5449569	309799.4	Magnetite Gabbro	16	16.25	218.8
14-902	5449569	309799.4	Magnetite Gabbro	16.25	16.5	82.0
14-902	5449569	309799.4	Magnetite Gabbro	16.5	16.75	109.2
14-902	5449569	309799.4	Magnetite Gabbro	16.75	17	241.5
14-902	5449569	309799.4	Magnetite Gabbro	17	17.25	252.6
14-902	5449569	309799.4	Magnetite Gabbro	17.25	17.5	16.9

ID Hole	North	East	Domain	From	to	Kappa
14-902	5449569	309799.4	Magnetite Gabbro	17.5	17.75	201.1
14-902	5449569	309799.4	Magnetite Gabbro	17.75	18	138.2
14-902	5449569	309799.4	Magnetite Gabbro	18	18.25	27.6
14-902	5449569	309799.4	Vari-textured Gabbro	18.25	18.5	13.8
14-902	5449569	309799.4	Vari-textured Gabbro	18.5	18.75	255.1
14-902	5449569	309799.4	Vari-textured Gabbro	18.75	19	227.4
14-902	5449569	309799.4	Vari-textured Gabbro	19	19.25	338.5
14-902	5449569	309799.4	Vari-textured Gabbro	19.25	19.5	293.2
14-902	5449569	309799.4	Vari-textured Gabbro	19.5	19.75	410.0
14-902	5449569	309799.4	Vari-textured Gabbro	19.75	20	242.6
14-902	5449569	309799.4	Vari-textured Gabbro	20	20.25	151.8
14-902	5449569	309799.4	Vari-textured Gabbro	20.25	20.5	266.7
14-902	5449569	309799.4	Vari-textured Gabbro	20.5	20.75	564.9
14-902	5449569	309799.4	Vari-textured Gabbro	20.75	21	395.1
14-902	5449569	309799.4	Vari-textured Gabbro	21	21.25	204.0
14-902	5449569	309799.4	Vari-textured Gabbro	21.25	21.5	275.2
14-902	5449569	309799.4	Vari-textured Gabbro	21.5	21.75	388.7
14-902	5449569	309799.4	Vari-textured Gabbro	21.75	22	526.2
14-902	5449569	309799.4	Vari-textured Gabbro	22	22.25	234.3
14-902	5449569	309799.4	Vari-textured Gabbro	22.25	22.5	386.2
14-902	5449569	309799.4	Vari-textured Gabbro	22.5	22.75	260.2
14-902	5449569	309799.4	Vari-textured Gabbro	22.75	23	536.4
14-902	5449569	309799.4	Vari-textured Gabbro	23	23.25	433.5
14-902	5449569	309799.4	Vari-textured Gabbro	23.25	23.5	253.8
14-902	5449569	309799.4	Magnetite Gabbro	23.5	23.75	90.0
14-902	5449569	309799.4	Magnetite Gabbro	23.75	24	235.5
14-902	5449569	309799.4	Magnetite Gabbro	24	24.25	263.5
14-902	5449569	309799.4	Magnetite Gabbro	24.25	24.5	193.7
14-902	5449569	309799.4	Magnetite Gabbro	24.5	24.75	109.1
14-902	5449569	309799.4	Magnetite Gabbro	24.75	25	143.1
14-902	5449569	309799.4	Magnetite Gabbro	25	25.25	190.3
14-902	5449569	309799.4	Magnetite Gabbro	25.25	25.5	92.7
14-902	5449569	309799.4	Magnetite Gabbro	25.5	25.75	163.7
14-902	5449569	309799.4	Magnetite Gabbro	25.75	26	68.6
14-902	5449569	309799.4	Magnetite Gabbro	26	26.25	181.1
14-902	5449569	309799.4	Magnetite Gabbro	26.25	26.5	121.3
14-902	5449569	309799.4	Magnetite Gabbro	26.5	26.75	34.8

ID Hole	North	East	Domain	From	to	Kappa
14-902	5449569	309799.4	Magnetite Gabbro	26.75	27	4.4
14-902	5449569	309799.4	Magnetite Gabbro	27	27.25	3.3
14-902	5449569	309799.4	Magnetite Gabbro	27.25	27.5	6.9
14-902	5449569	309799.4	Magnetite Gabbro	27.5	27.75	2.3
14-902	5449569	309799.4	Magnetite Gabbro	27.75	28	2.2
14-902	5449569	309799.4	Magnetite Gabbro	28	28.25	2.2
14-902	5449569	309799.4	Magnetite Gabbro	28.25	28.5	2.7
14-902	5449569	309799.4	Magnetite Gabbro	28.5	28.75	1.6
14-902	5449569	309799.4	Magnetite Gabbro	28.75	29	0.9
14-902	5449569	309799.4	Magnetite Gabbro	29	29.25	1.3
14-902	5449569	309799.4	Magnetite Gabbro	29.25	29.5	1.1
14-902	5449569	309799.4	Vari-textured Gabbro	29.5	29.75	2.6
14-902	5449569	309799.4	Vari-textured Gabbro	29.75	30	1.3
14-902	5449569	309799.4	Vari-textured Gabbro	30	30.25	6.4
14-902	5449569	309799.4	Vari-textured Gabbro	30.25	30.5	2.4
14-902	5449569	309799.4	Vari-textured Gabbro	30.5	30.75	3.2
14-902	5449569	309799.4	Vari-textured Gabbro	30.75	31	1.3
14-902	5449569	309799.4	Magnetite Gabbro	31	31.25	3.2
14-902	5449569	309799.4	Magnetite Gabbro	31.25	31.5	3.4
14-902	5449569	309799.4	Magnetite Gabbro	31.5	31.75	173.0
14-902	5449569	309799.4	Magnetite Gabbro	31.75	32	16.8
14-902	5449569	309799.4	Magnetite Gabbro	32	32.25	301.5
14-902	5449569	309799.4	Magnetite Gabbro	32.25	32.5	35.0
14-902	5449569	309799.4	Magnetite Gabbro	32.5	32.75	51.2
14-902	5449569	309799.4	Magnetite Gabbro	32.75	33	3.5
14-902	5449569	309799.4	Magnetite Gabbro	33	33.25	6.9
14-902	5449569	309799.4	Magnetite Gabbro	33.25	33.5	157.4
14-902	5449569	309799.4	Magnetite Gabbro	33.5	33.75	68.3
14-902	5449569	309799.4	Magnetite Gabbro	33.75	34	4.3
14-902	5449569	309799.4	Magnetite Gabbro	34	34.25	6.0
14-902	5449569	309799.4	Magnetite Gabbro	34.25	34.5	4.5
14-902	5449569	309799.4	Magnetite Gabbro	34.5	34.75	10.4
14-902	5449569	309799.4	Magnetite Gabbro	34.75	35	3.7
14-902	5449569	309799.4	Magnetite Gabbro	35	35.25	124.3
14-902	5449569	309799.4	Magnetite Gabbro	35.25	35.5	161.9
14-902	5449569	309799.4	Magnetite Gabbro	35.5	35.75	406.3
14-902	5449569	309799.4	Magnetite Gabbro	35.75	36	189.0

ID Hole	North	East	Domain	From	to	Kappa
14-902	5449569	309799.4	Magnetite Gabbro	36	36.25	268.6
14-902	5449569	309799.4	Magnetite Gabbro	36.25	36.5	239.9
14-902	5449569	309799.4	Magnetite Gabbro	36.5	36.75	231.6
14-902	5449569	309799.4	Magnetite Gabbro	36.75	37	214.5
14-902	5449569	309799.4	Magnetite Gabbro	37	37.25	185.4
14-902	5449569	309799.4	Magnetite Gabbro	37.25	37.5	179.5
14-902	5449569	309799.4	Magnetite Gabbro	37.5	37.75	157.3
14-902	5449569	309799.4	Magnetite Gabbro	37.75	38	215.4
14-902	5449569	309799.4	Magnetite Gabbro	38	38.25	231.9
14-902	5449569	309799.4	Magnetite Gabbro	38.25	38.5	320.0
14-902	5449569	309799.4	Magnetite Gabbro	38.5	38.75	1205.1
14-902	5449569	309799.4	Magnetite Gabbro	38.75	39	153.3
14-902	5449569	309799.4	Magnetite Gabbro	39	39.25	259.7
14-902	5449569	309799.4	Magnetite Gabbro	39.25	39.5	334.1
14-902	5449569	309799.4	Magnetite Gabbro	39.5	39.75	195.9
14-902	5449569	309799.4	Magnetite Gabbro	39.75	40	174.3
14-902	5449569	309799.4	Magnetite Gabbro	40	40.25	181.7
14-902	5449569	309799.4	Magnetite Norite	40.25	40.5	136.5
14-902	5449569	309799.4	Magnetite Norite	40.5	40.75	243.2
14-902	5449569	309799.4	Magnetite Norite	40.75	41	497.8
14-902	5449569	309799.4	Magnetite Norite	41	41.25	683.6
14-902	5449569	309799.4	Magnetite Norite	41.25	41.5	358.3
14-902	5449569	309799.4	Magnetite Norite	41.5	41.75	1123.8
14-902	5449569	309799.4	Magnetite Norite	41.75	42	869.8
14-902	5449569	309799.4	Magnetite Gabbronorite	42	42.25	564.8
14-902	5449569	309799.4	Magnetite Gabbronorite	42.25	42.5	515.3
14-902	5449569	309799.4	Magnetite Gabbronorite	42.5	42.75	1027.0
14-902	5449569	309799.4	Magnetite Gabbronorite	42.75	43	1281.2
14-902	5449569	309799.4	Magnetite Gabbronorite	43	43.25	1062.6
14-902	5449569	309799.4	Magnetite Gabbronorite	43.25	43.5	141.4
14-902	5449569	309799.4	Magnetite Gabbronorite	43.5	43.75	230.0
14-902	5449569	309799.4	Magnetite Gabbronorite	43.75	44	200.5
14-902	5449569	309799.4	Magnetite Gabbronorite	44	44.25	156.7
14-902	5449569	309799.4	Magnetite Gabbronorite	44.25	44.5	27.6
14-902	5449569	309799.4	Magnetite Norite	44.5	44.75	127.2
14-902	5449569	309799.4	Magnetite Norite	44.75	45	67.3
14-902	5449569	309799.4	Magnetite Norite	45	45.25	74.0

ID Hole	North	East	Domain	From	to	Kappa
14-902	5449569	309799.4	Magnetite Norite	45.25	45.5	66.9
14-902	5449569	309799.4	Magnetite Norite	45.5	45.75	130.8
14-902	5449569	309799.4	Magnetite Norite	45.75	46	58.9
14-902	5449569	309799.4	Magnetite Norite	46	46.25	121.9
14-902	5449569	309799.4	Magnetite Norite	46.25	46.5	44.2
14-902	5449569	309799.4	Magnetite Norite	46.5	46.75	183.1
14-902	5449569	309799.4	Magnetite Norite	46.75	47	125.3
14-902	5449569	309799.4	Magnetite Norite	47	47.25	72.7
14-902	5449569	309799.4	Magnetite Norite	47.25	47.5	101.9
14-902	5449569	309799.4	Magnetite Norite	47.5	47.75	96.1
14-902	5449569	309799.4	Magnetite Norite	47.75	48	33.3
14-902	5449569	309799.4	Magnetite Norite	48	48.25	99.0
14-902	5449569	309799.4	Magnetite Norite	48.25	48.5	147.6
14-902	5449569	309799.4	Magnetite Norite	48.5	48.75	116.9
14-902	5449569	309799.4	Magnetite Norite	48.75	49	194.5
14-902	5449569	309799.4	Magnetite Norite	49	49.25	101.0
14-902	5449569	309799.4	Magnetite Norite	49.25	49.5	105.9
14-902	5449569	309799.4	Magnetite Norite	49.5	49.75	167.1
14-902	5449569	309799.4	Magnetite Norite	49.75	50	67.7
14-902	5449569	309799.4	Magnetite Norite	50	50.25	65.1
14-902	5449569	309799.4	Magnetite Norite	50.25	50.5	88.9
14-902	5449569	309799.4	Magnetite Norite	50.5	50.75	34.1
14-902	5449569	309799.4	Magnetite Norite	50.75	51	61.6
14-902	5449569	309799.4	Magnetite Norite	51	51.25	154.9
14-902	5449569	309799.4	Magnetite Norite	51.25	51.5	217.8
14-902	5449569	309799.4	Magnetite Norite	51.5	51.75	189.1
14-902	5449569	309799.4	Magnetite Norite	51.75	52	64.2
14-902	5449569	309799.4	Magnetite Norite	52	52.25	178.3
14-902	5449569	309799.4	Magnetite Norite	52.25	52.5	95.7
14-902	5449569	309799.4	Magnetite Norite	52.5	52.75	149.3
14-902	5449569	309799.4	Magnetite Norite	52.75	53	248.3
14-902	5449569	309799.4	Magnetite Norite	53	53.25	211.9
14-902	5449569	309799.4	Magnetite Norite	53.25	53.5	389.0
14-902	5449569	309799.4	Magnetite Norite	53.5	53.75	524.7
14-902	5449569	309799.4	Magnetite Norite	53.75	54	502.5
14-902	5449569	309799.4	Magnetite Norite	54	54.25	139.4
14-902	5449569	309799.4	Magnetite Gabbro	54.25	54.5	49.4

ID Hole	North	East	Domain	From	to	Kappa
14-902	5449569	309799.4	Magnetite Gabbro	54.5	54.75	39.5
14-902	5449569	309799.4	Magnetite Gabbro	54.75	55	18.2
14-902	5449569	309799.4	Magnetite Gabbro	55	55.25	31.5
14-902	5449569	309799.4	Magnetite Gabbro	55.25	55.5	72.6
14-902	5449569	309799.4	Magnetite Gabbro	55.5	55.75	55.6
14-902	5449569	309799.4	Magnetite Gabbro	55.75	56	38.5
14-902	5449569	309799.4	Magnetite Norite	56	56.25	36.5
14-902	5449569	309799.4	Magnetite Norite	56.25	56.5	22.8
14-902	5449569	309799.4	Magnetite Norite	56.5	56.75	49.4
14-902	5449569	309799.4	Magnetite Norite	56.75	57	11.9
14-902	5449569	309799.4	Magnetite Norite	57	57.25	59.6
14-902	5449569	309799.4	Magnetite Norite	57.25	57.5	27.3
14-902	5449569	309799.4	Magnetite Norite	57.5	57.75	77.1
14-902	5449569	309799.4	Magnetite Norite	57.75	58	58.8
14-902	5449569	309799.4	Magnetite Norite	58	58.25	46.6
14-902	5449569	309799.4	Magnetite Norite	58.25	58.5	52.0
14-902	5449569	309799.4	Magnetite Norite	58.5	58.75	33.2
14-902	5449569	309799.4	Magnetite Norite	58.75	59	120.0
14-902	5449569	309799.4	Magnetite Norite	59	59.25	79.2
14-902	5449569	309799.4	Magnetite Norite	59.25	59.5	67.4
14-902	5449569	309799.4	Magnetite Norite	59.5	59.75	41.8
14-902	5449569	309799.4	Magnetite Norite	59.75	60	19.0
14-902	5449569	309799.4	Magnetite Norite	60	60.25	99.8
14-902	5449569	309799.4	Magnetite Norite	60.25	60.5	72.0
14-902	5449569	309799.4	Magnetite Norite	60.5	60.75	85.3
14-902	5449569	309799.4	Magnetite Norite	60.75	61	27.7
14-902	5449569	309799.4	Magnetite Norite	61	61.25	75.8
14-902	5449569	309799.4	Magnetite Norite	61.25	61.5	61.0
14-902	5449569	309799.4	Magnetite Norite	61.5	61.75	10.4
14-902	5449569	309799.4	Magnetite Norite	61.75	62	4.8
14-902	5449569	309799.4	Magnetite Norite	62	62.25	72.6
14-902	5449569	309799.4	Magnetite Norite	62.25	62.5	74.8
14-902	5449569	309799.4	Magnetite Norite	62.5	62.75	15.3
14-902	5449569	309799.4	Magnetite Norite	62.75	63	100.3
14-902	5449569	309799.4	Magnetite Norite	63	63.25	119.7
14-902	5449569	309799.4	Magnetite Norite	63.25	63.5	104.1
14-902	5449569	309799.4	Magnetite Norite	63.5	63.75	27.5

ID Hole	North	East	Domain	From	to	Kappa
14-902	5449569	309799.4	Magnetite Norite	63.75	64	85.5
14-902	5449569	309799.4	Magnetite Norite	64	64.25	89.7
14-902	5449569	309799.4	Magnetite Norite	64.25	64.5	72.3
14-902	5449569	309799.4	Magnetite Norite	64.5	64.75	59.2
14-902	5449569	309799.4	Magnetite Norite	64.75	65	77.5
14-902	5449569	309799.4	Magnetite Norite	65	65.25	116.9
14-902	5449569	309799.4	Magnetite Norite	65.25	65.5	73.6
14-902	5449569	309799.4	Magnetite Norite	65.5	65.75	46.4
14-902	5449569	309799.4	Magnetite Norite	65.75	66	103.7
14-902	5449569	309799.4	Magnetite Norite	66	66.25	20.0
14-902	5449569	309799.4	Magnetite Norite	66.25	66.5	21.4
14-902	5449569	309799.4	Magnetite Norite	66.5	66.75	29.9
14-902	5449569	309799.4	Magnetite Norite	66.75	67	141.4
14-902	5449569	309799.4	Magnetite Norite	67	67.25	272.8
14-902	5449569	309799.4	Magnetite Norite	67.25	67.5	192.0
14-902	5449569	309799.4	Magnetite Norite	67.5	67.75	30.6
14-902	5449569	309799.4	Magnetite Gabbro	67.75	68	16.5
14-902	5449569	309799.4	Magnetite Gabbro	68	68.25	120.4
14-902	5449569	309799.4	Magnetite Gabbro	68.25	68.5	51.1
14-902	5449569	309799.4	Magnetite Gabbro	68.5	68.75	96.9
14-902	5449569	309799.4	Magnetite Gabbro	68.75	69	186.1
14-902	5449569	309799.4	Magnetite Gabbro	69	69.25	131.6
14-902	5449569	309799.4	Magnetite Gabbro	69.25	69.5	5.1
14-902	5449569	309799.4	Magnetite Gabbro	69.5	69.75	138.4
14-902	5449569	309799.4	Magnetite Norite	69.75	70	100.7
14-902	5449569	309799.4	Magnetite Norite	70	70.25	72.2
14-902	5449569	309799.4	Magnetite Norite	70.25	70.5	64.6
14-902	5449569	309799.4	Magnetite Norite	70.5	70.75	82.3
14-902	5449569	309799.4	Magnetite Norite	70.75	71	46.2
14-902	5449569	309799.4	Magnetite Norite	71	71.25	55.9
14-902	5449569	309799.4	Magnetite Norite	71.25	71.5	82.9
14-902	5449569	309799.4	Magnetite Norite	71.5	71.75	36.1
14-902	5449569	309799.4	Magnetite Norite	71.75	72	153.9
14-902	5449569	309799.4	Magnetite Norite	72	72.25	116.8
14-902	5449569	309799.4	Magnetite Norite	72.25	72.5	118.5
14-902	5449569	309799.4	Magnetite Norite	72.5	72.75	28.3
14-902	5449569	309799.4	Magnetite Norite	72.75	73	20.0

ID Hole	North	East	Domain	From	to	Kappa
14-902	5449569	309799.4	Magnetite Norite	73	73.25	23.8
14-902	5449569	309799.4	Magnetite Norite	73.25	73.5	26.2
14-902	5449569	309799.4	Magnetite Norite	73.5	73.75	81.6
14-902	5449569	309799.4	Magnetite Norite	73.75	74	135.3
14-902	5449569	309799.4	Magnetite Norite	74	74.25	44.2
14-902	5449569	309799.4	Magnetite Norite	74.25	74.5	80.7
14-902	5449569	309799.4	Magnetite Norite	74.5	74.75	65.1
14-902	5449569	309799.4	Magnetite Norite	74.75	75	57.3
14-902	5449569	309799.4	Magnetite Norite	75	75.25	144.1
14-902	5449569	309799.4	Magnetite Norite	75.25	75.5	226.7
14-902	5449569	309799.4	Magnetite Norite	75.5	75.75	62.7
14-902	5449569	309799.4	Magnetite Norite	75.75	76	191.7
14-902	5449569	309799.4	Magnetite Norite	76	76.25	171.8
14-902	5449569	309799.4	Magnetite Norite	76.25	76.5	136.6
14-902	5449569	309799.4	Magnetite Norite	76.5	76.75	76.9
14-902	5449569	309799.4	Magnetite Norite	76.75	77	92.6
14-902	5449569	309799.4	Magnetite Norite	77	77.25	153.4
14-902	5449569	309799.4	Magnetite Norite	77.25	77.5	353.2
14-902	5449569	309799.4	Magnetite Norite	77.5	77.75	23.7
14-902	5449569	309799.4	Magnetite Norite	77.75	78	159.6
14-902	5449569	309799.4	Magnetite Norite	78	78.25	95.8
14-902	5449569	309799.4	Magnetite Norite	78.25	78.5	11.9
14-902	5449569	309799.4	Magnetite Norite	78.5	78.75	138.4
14-902	5449569	309799.4	Magnetite Norite	78.75	79	178.3
14-902	5449569	309799.4	Magnetite Norite	79	79.25	176.6
14-902	5449569	309799.4	Magnetite Norite	79.25	79.5	240.7
14-902	5449569	309799.4	Magnetite Norite	79.5	79.75	156.1
14-902	5449569	309799.4	Magnetite Norite	79.75	80	13.5
14-902	5449569	309799.4	Magnetite Norite	80	80.25	140.1
14-902	5449569	309799.4	Magnetite Norite	80.25	80.5	146.2
14-902	5449569	309799.4	Magnetite Norite	80.5	80.75	208.9
14-902	5449569	309799.4	Magnetite Norite	80.75	81	430.7
14-902	5449569	309799.4	Magnetite Norite	81	81.25	69.0
14-902	5449569	309799.4	Magnetite Norite	81.25	81.5	37.7
14-902	5449569	309799.4	Magnetite Norite	81.5	81.75	116.9
14-902	5449569	309799.4	Magnetite Norite	81.75	82	370.5
14-902	5449569	309799.4	Magnetite Norite	82	82.25	356.1

ID Hole	North	East	Domain	From	to	Kappa
14-902	5449569	309799.4	Magnetite Norite	82.25	82.5	166.8
14-902	5449569	309799.4	Magnetite Norite	82.5	82.75	161.0
14-902	5449569	309799.4	Magnetite Norite	82.75	83	295.7
14-902	5449569	309799.4	Magnetite Norite	83	83.25	142.5
14-902	5449569	309799.4	Magnetite Norite	83.25	83.5	270.9
14-902	5449569	309799.4	Magnetite Norite	83.5	83.75	150.7
14-902	5449569	309799.4	Magnetite Norite	83.75	84	123.9
14-902	5449569	309799.4	Magnetite Norite	84	84.25	129.0
14-902	5449569	309799.4	Magnetite Norite	84.25	84.5	120.4
14-902	5449569	309799.4	Magnetite Norite	84.5	84.75	381.0
14-902	5449569	309799.4	Magnetite Norite	84.75	85	340.4
14-902	5449569	309799.4	Magnetite Norite	85	85.25	232.6
14-902	5449569	309799.4	Magnetite Gabbronorite	85.25	85.5	17.2
14-902	5449569	309799.4	Magnetite Gabbronorite	85.5	85.75	102.1
14-902	5449569	309799.4	Magnetite Gabbronorite	85.75	86	132.9
14-902	5449569	309799.4	Magnetite Gabbronorite	86	86.25	249.1
14-902	5449569	309799.4	Magnetite Gabbronorite	86.25	86.5	219.3
14-902	5449569	309799.4	Magnetite Gabbronorite	86.5	86.75	238.8
14-902	5449569	309799.4	Magnetite Gabbronorite	86.75	87	12.7
14-902	5449569	309799.4	Magnetite Gabbronorite	87	87.25	292.4
14-902	5449569	309799.4	Magnetite Norite	87.25	87.5	867.6
14-902	5449569	309799.4	Magnetite Norite	87.5	87.75	180.0
14-902	5449569	309799.4	Magnetite Norite	87.75	88	299.5
14-902	5449569	309799.4	Magnetite Norite	88	88.25	31.8
14-902	5449569	309799.4	Magnetite Norite	88.25	88.5	98.5
14-902	5449569	309799.4	Magnetite Norite	88.5	88.75	33.4
14-902	5449569	309799.4	Magnetite Norite	88.75	89	193.1
14-902	5449569	309799.4	Magnetite Norite	89	89.25	341.1
14-902	5449569	309799.4	Magnetite Norite	89.25	89.5	630.0
14-902	5449569	309799.4	Magnetite Norite	89.5	89.75	40.7
14-902	5449569	309799.4	Magnetite Norite	89.75	90	13.4
14-902	5449569	309799.4	Magnetite Norite	90	90.25	29.4
14-902	5449569	309799.4	Magnetite Norite	90.25	90.5	77.6
14-902	5449569	309799.4	Magnetite Norite	90.5	90.75	407.4
14-902	5449569	309799.4	Magnetite Norite	90.75	91	75.2
14-902	5449569	309799.4	Magnetite Norite	91	91.25	532.0
14-902	5449569	309799.4	Magnetite Gabbronorite	91.25	91.5	184.8

ID Hole	North	East	Domain	From	to	Kappa
14-902	5449569	309799.4	Magnetite Gabbronorite	91.5	91.75	12.9
14-902	5449569	309799.4	Magnetite Gabbronorite	91.75	92	21.6
14-902	5449569	309799.4	Magnetite Gabbronorite	92	92.25	25.8
14-902	5449569	309799.4	Magnetite Gabbronorite	92.25	92.5	251.1
14-902	5449569	309799.4	Magnetite Gabbronorite	92.5	92.75	288.2
14-902	5449569	309799.4	Magnetite Gabbronorite	92.75	93	539.9
14-902	5449569	309799.4	Magnetite Gabbronorite	93	93.25	366.7
14-902	5449569	309799.4	Magnetite Norite	93.25	93.5	236.2
14-902	5449569	309799.4	Magnetite Norite	93.5	93.75	174.9
14-902	5449569	309799.4	Magnetite Norite	93.75	94	197.7
14-902	5449569	309799.4	Magnetite Norite	94	94.25	555.5
14-902	5449569	309799.4	Magnetite Norite	94.25	94.5	3.6
14-902	5449569	309799.4	Magnetite Norite	94.5	94.75	75.8
14-902	5449569	309799.4	Magnetite Norite	94.75	95	83.5
14-902	5449569	309799.4	Magnetite Norite	95	95.25	238.3
14-902	5449569	309799.4	Magnetite Norite	95.25	95.5	107.8
14-902	5449569	309799.4	Magnetite Norite	95.5	95.75	51.4
14-902	5449569	309799.4	Magnetite Norite	95.75	96	213.1
14-902	5449569	309799.4	Magnetite Norite	96	96.25	375.7
14-902	5449569	309799.4	Magnetite Norite	96.25	96.5	840.2
14-902	5449569	309799.4	Magnetite Norite	96.5	96.75	308.0
14-902	5449569	309799.4	Magnetite Norite	96.75	97	696.3
14-902	5449569	309799.4	Magnetite Norite	97	97.25	2000.0
14-902	5449569	309799.4	Magnetite Norite	97.25	97.5	1000.2
14-902	5449569	309799.4	Magnetite Norite	97.5	97.75	1129.7
14-902	5449569	309799.4	Magnetite Norite	97.75	98	857.8
14-902	5449569	309799.4	Magnetite Norite	98	98.25	1110.0
14-902	5449569	309799.4	Magnetite Norite	98.25	98.5	376.9
14-902	5449569	309799.4	Magnetite Norite	98.5	98.75	934.1
14-902	5449569	309799.4	Magnetite Norite	98.75	99	950.2
14-902	5449569	309799.4	Magnetite Norite	99	99.25	1076.7
14-902	5449569	309799.4	Magnetite Norite	99.25	99.5	54.0
14-902	5449569	309799.4	Magnetite Norite	99.5	99.75	791.3
14-902	5449569	309799.4	Magnetite Norite	99.75	100	901.3
14-902	5449569	309799.4	Magnetite Norite	100	100.25	934.8
14-902	5449569	309799.4	Magnetite Norite	100.25	100.5	839.5
14-902	5449569	309799.4	Magnetite Norite	100.5	100.75	582.0

ID Hole	North	East	Domain	From	to	Kappa
14-902	5449569	309799.4	Magnetite Norite	100.75	101	261.7
14-902	5449569	309799.4	Magnetite Norite	101	101.25	774.5
14-902	5449569	309799.4	Magnetite Norite	101.25	101.5	1006.2
14-902	5449569	309799.4	Magnetite Norite	101.5	101.75	409.6
14-902	5449569	309799.4	Magnetite Norite	101.75	102	615.8
14-902	5449569	309799.4	Magnetite Norite	102	102.25	278.1
14-902	5449569	309799.4	Magnetite Norite	102.25	102.5	336.5
14-902	5449569	309799.4	Magnetite Norite	102.5	102.75	209.0
14-902	5449569	309799.4	Magnetite Norite	102.75	103	241.2
14-902	5449569	309799.4	Magnetite Norite	103	103.25	232.5
14-902	5449569	309799.4	Magnetite Norite	103.25	103.5	304.1
14-902	5449569	309799.4	Magnetite Norite	103.5	103.75	400.0
14-902	5449569	309799.4	Magnetite Norite	103.75	104	383.1
14-902	5449569	309799.4	Magnetite Norite	104	104.25	293.8
14-902	5449569	309799.4	Magnetite Norite	104.25	104.5	386.2
14-902	5449569	309799.4	Magnetite Norite	104.5	104.75	399.0
14-902	5449569	309799.4	Magnetite Norite	104.75	105	311.8
14-902	5449569	309799.4	Magnetite Gabbro	105	105.25	59.4
14-902	5449569	309799.4	Magnetite Gabbro	105.25	105.5	75.5
14-902	5449569	309799.4	Magnetite Gabbro	105.5	105.75	804.5
14-902	5449569	309799.4	Magnetite Gabbro	105.75	106	476.2
14-902	5449569	309799.4	Magnetite Gabbro	106	106.25	416.8
14-902	5449569	309799.4	Magnetite Gabbro	106.25	106.5	
14-902	5449569	309799.4	Magnetite Gabbro	106.5	106.75	
14-902	5449569	309799.4	Magnetite Gabbro	106.75	107	
14-902	5449569	309799.4	Magnetite Gabbro	107	107.25	
14-902	5449569	309799.4	Magnetite Gabbro	107.25	107.5	
14-902	5449569	309799.4	Magnetite Gabbro	107.5	107.75	
14-902	5449569	309799.4	Magnetite Gabbro	107.75	108	1103.2
20-200	5449588	309496	Gabbro	406	406.5	8.3
20-200	5449588	309496	Gabbro	406.25	406.75	1.1
20-200	5449588	309496	Gabbro	406.5	407	2.6
20-200	5449588	309496	Gabbro	406.75	407.25	2.7
20-200	5449588	309496	Gabbro	407	407.5	2.2
20-200	5449588	309496	Gabbro	407.25	407.75	2.2
20-200	5449588	309496	Gabbro	407.5	408	1.1
20-200	5449588	309496	Gabbro	407.75	408.25	2.2

ID Hole	North	East	Domain	From	to	Kappa
20-200	5449588	309496	Gabbro	408	408.5	4.0
20-200	5449588	309496	Gabbro	408.25	408.75	1.2
20-200	5449588	309496	Gabbro	408.5	409	2.0
20-200	5449588	309496	Gabbro	408.75	409.25	3.8
20-200	5449588	309496	Gabbro	409	409.5	6.3
20-200	5449588	309496	Gabbro	409.25	409.75	5.5
20-200	5449588	309496	Gabbro	409.5	410	66.2
20-200	5449588	309496	Gabbro	409.75	410.25	2.8
20-200	5449588	309496	Gabbro	410	410.5	2.9
20-200	5449588	309496	Gabbro	410.25	410.75	15.0
20-200	5449588	309496	Gabbro	410.5	411	15.1
20-200	5449588	309496	Gabbro	410.75	411.25	1.9
20-200	5449588	309496	Gabbro	411	411.5	12.1
20-200	5449588	309496	Gabbro	411.25	411.75	1.3
20-200	5449588	309496	Gabbro	411.5	412	2.7
20-200	5449588	309496	Gabbro	411.75	412.25	3.8
20-200	5449588	309496	Gabbro	412	412.5	1.1
20-200	5449588	309496	Gabbro	412.25	412.75	1.5
20-200	5449588	309496	Gabbro	412.5	413	2.2
20-200	5449588	309496	Gabbro	412.75	413.25	3.8
20-200	5449588	309496	Gabbro	413	413.5	2.9
20-200	5449588	309496	Gabbro	413.25	413.75	2.0
20-200	5449588	309496	Gabbro	413.5	414	3.1
20-200	5449588	309496	Gabbro	413.75	414.25	3.7
20-200	5449588	309496	Gabbro	414	414.5	6.1
20-200	5449588	309496	Gabbro	414.25	414.75	1.4
20-200	5449588	309496	Gabbro	414.5	415	3.7
20-200	5449588	309496	Gabbro	414.75	415.25	3.8
20-200	5449588	309496	Gabbro	415	415.5	17.2
20-200	5449588	309496	Gabbro	415.25	415.75	26.3
20-200	5449588	309496	Gabbro	415.5	416	61.3
20-200	5449588	309496	Gabbro	415.75	416.25	51.6
20-200	5449588	309496	Gabbro	416	416.5	13.0
20-200	5449588	309496	Gabbro	416.25	416.75	0.4
20-200	5449588	309496	Gabbro	416.5	417	0.4
20-200	5449588	309496	Gabbro	416.75	417.25	0.6
20-200	5449588	309496	Gabbro	417	417.5	1.7

ID Hole	North	East	Domain	From	to	Kappa
20-200	5449588	309496	Gabbro	417.25	417.75	0.9
20-200	5449588	309496	Gabbro	417.5	418	1.8
20-200	5449588	309496	Gabbro	417.75	418.25	1.2
20-200	5449588	309496	Gabbro	418	418.5	1.4
20-200	5449588	309496	Gabbro	418.25	418.75	0.5
20-200	5449588	309496	Gabbro	418.5	419	0.5
20-200	5449588	309496	Gabbro	418.75	419.25	0.3
20-200	5449588	309496	Gabbro	419	419.5	2.1
20-200	5449588	309496	Gabbro	419.25	419.75	18.5
20-200	5449588	309496	Gabbro	419.5	420	0.8
20-200	5449588	309496	Gabbro	419.75	420.25	59.5
20-200	5449588	309496	Gabbro	420	420.5	0.6
20-200	5449588	309496	Gabbro	420.25	420.75	0.5
20-200	5449588	309496	Gabbro	420.5	421	0.8
20-200	5449588	309496	Gabbro	420.75	421.25	0.4
20-200	5449588	309496	Gabbro	421	421.5	1.9
20-200	5449588	309496	Gabbro	421.25	421.75	0.7
20-200	5449588	309496	Gabbro	421.5	422	0.4
20-200	5449588	309496	Gabbro	421.75	422.25	0.6
20-200	5449588	309496	Gabbro	422	422.5	1.7
20-200	5449588	309496	Gabbro	422.25	422.75	0.7
20-200	5449588	309496	Gabbro	422.5	423	0.9
20-200	5449588	309496	Gabbro	422.75	423.25	1.0
20-200	5449588	309496	Gabbro	423	423.5	0.9
20-200	5449588	309496	Gabbro	423.25	423.75	0.9
20-200	5449588	309496	Gabbro	423.5	424	0.8
20-200	5449588	309496	Gabbro	423.75	424.25	0.8
20-200	5449588	309496	Gabbro	424	424.5	1.9
20-200	5449588	309496	Gabbro	424.25	424.75	0.4
20-200	5449588	309496	Gabbro	424.5	425	0.3
20-200	5449588	309496	Gabbro	424.75	425.25	0.5
20-200	5449588	309496	Gabbro	425	425.5	1.7
20-200	5449588	309496	Gabbro	425.25	425.75	0.9
20-200	5449588	309496	Gabbro	425.5	426	0.6
20-200	5449588	309496	Gabbro	425.75	426.25	0.5
20-200	5449588	309496	Gabbro	426	426.5	1.1
20-200	5449588	309496	Gabbro	426.25	426.75	0.6

ID Hole	North	East	Domain	From	to	Kappa
20-200	5449588	309496	Gabbro	426.5	427	0.8
20-200	5449588	309496	Gabbro	426.75	427.25	0.5
20-200	5449588	309496	Gabbro	427	427.5	0.5
20-200	5449588	309496	Gabbro	427.25	427.75	0.6
20-200	5449588	309496	Gabbro	427.5	428	0.9
20-200	5449588	309496	Gabbro	427.75	428.25	0.9
20-200	5449588	309496	Gabbro	428	428.5	1.0
20-200	5449588	309496	Gabbro	428.25	428.75	0.6
20-200	5449588	309496	Gabbro	428.5	429	0.8
20-200	5449588	309496	Gabbro	428.75	429.25	1.0
20-200	5449588	309496	Gabbro	429	429.5	0.9
20-200	5449588	309496	Gabbro	429.25	429.75	0.9
20-200	5449588	309496	Gabbro	429.5	430	0.7
20-200	5449588	309496	Gabbro	429.75	430.25	0.9
20-200	5449588	309496	Gabbro	430	430.5	2.5
20-200	5449588	309496	Gabbro	430.25	430.75	1.1
20-200	5449588	309496	Gabbro	430.5	431	0.9
20-200	5449588	309496	Gabbro	430.75	431.25	3.4
20-200	5449588	309496	Gabbro	431	431.5	3.8
20-200	5449588	309496	Gabbro	431.25	431.75	1.3
20-200	5449588	309496	Gabbro	431.5	432	1.8
20-200	5449588	309496	Gabbro	431.75	432.25	2.2
20-200	5449588	309496	Gabbro	432	432.5	1.2
20-200	5449588	309496	Gabbro	432.25	432.75	1.2
20-200	5449588	309496	Gabbro	432.5	433	0.9
20-200	5449588	309496	Gabbro	432.75	433.25	2.4
20-200	5449588	309496	Gabbro	433	433.5	1.5
20-200	5449588	309496	Gabbro	433.25	433.75	2.4
20-200	5449588	309496	Gabbro	433.5	434	0.7
20-200	5449588	309496	Gabbro	433.75	434.25	3.0
20-200	5449588	309496	Gabbro	434	434.5	1.3
20-200	5449588	309496	Gabbro	434.25	434.75	2.2
20-200	5449588	309496	Gabbro	434.5	435	1.3
20-200	5449588	309496	Norite	434.75	435.25	1.5
20-200	5449588	309496	Norite	435	435.5	1.3
20-200	5449588	309496	Norite	435.25	435.75	14.2
20-200	5449588	309496	Norite	435.5	436	2.4

ID Hole	North	East	Domain	From	to	Kappa
20-200	5449588	309496	Norite	435.75	436.25	1.7
20-200	5449588	309496	Norite	436	436.5	2.2
20-200	5449588	309496	Norite	436.25	436.75	8.0
20-200	5449588	309496	Norite	436.5	437	2.2
20-200	5449588	309496	Norite	436.75	437.25	2.4
20-200	5449588	309496	Norite	437	437.5	4.6
20-200	5449588	309496	Norite	437.25	437.75	25.7
20-200	5449588	309496	Norite	437.5	438	12.7
20-200	5449588	309496	Norite	437.75	438.25	35.0
20-200	5449588	309496	Norite	438	438.5	6.4
20-200	5449588	309496	Norite	438.25	438.75	30.9
20-200	5449588	309496	Norite	438.5	439	3.7
20-200	5449588	309496	Norite	438.75	439.25	6.5
20-200	5449588	309496	Norite	439	439.5	13.0
20-200	5449588	309496	Norite	439.25	439.75	21.8
20-200	5449588	309496	Norite	439.5	440	2.5
20-200	5449588	309496	Norite	439.75	440.25	4.2
20-200	5449588	309496	Norite	440	440.5	2.0
20-200	5449588	309496	Norite	440.25	440.75	1.3
20-200	5449588	309496	Norite	440.5	441	18.9
20-200	5449588	309496	Norite	440.75	441.25	11.6
20-200	5449588	309496	Norite	441	441.5	21.0
20-200	5449588	309496	Norite	441.25	441.75	26.0
20-200	5449588	309496	Norite	441.5	442	1.2
20-200	5449588	309496	Norite	441.75	442.25	9.6
20-200	5449588	309496	Norite	442	442.5	9.0
20-200	5449588	309496	Norite	442.25	442.75	26.9
20-200	5449588	309496	Norite	442.5	443	1.2
20-200	5449588	309496	Norite	442.75	443.25	6.7
20-200	5449588	309496	Norite	443	443.5	9.7
20-200	5449588	309496	Norite	443.25	443.75	10.9
20-200	5449588	309496	Norite	443.5	444	9.2
20-200	5449588	309496	Norite	443.75	444.25	1.2
20-200	5449588	309496	Norite	444	444.5	1.1
20-200	5449588	309496	Norite	444.25	444.75	2.4
20-200	5449588	309496	Norite	444.5	445	1.6
20-200	5449588	309496	Norite	444.75	445.25	0.4

ID Hole	North	East	Domain	From	to	Kappa
20-200	5449588	309496	Norite	445	445.5	1.3
20-200	5449588	309496	Norite	445.25	445.75	3.7
20-200	5449588	309496	Norite	445.5	446	4.8
20-200	5449588	309496	Norite	445.75	446.25	2.8
20-200	5449588	309496	Norite	446	446.5	2.6
20-200	5449588	309496	Norite	446.25	446.75	2.0
20-200	5449588	309496	Norite	446.5	447	2.0
20-200	5449588	309496	Norite	446.75	447.25	6.2
20-200	5449588	309496	Norite	447	447.5	1.5
20-200	5449588	309496	Norite	447.25	447.75	6.2
20-200	5449588	309496	Norite	447.5	448	14.9
20-200	5449588	309496	Norite	447.75	448.25	24.9
20-200	5449588	309496	Norite	448	448.5	8.7
20-200	5449588	309496	Norite	448.25	448.75	31.8
20-200	5449588	309496	Norite	448.5	449	5.4
20-200	5449588	309496	Norite	448.75	449.25	2.7
20-200	5449588	309496	Norite	449	449.5	1.7
20-200	5449588	309496	Norite	449.25	449.75	5.9
20-200	5449588	309496	Norite	449.5	450	26.6
20-200	5449588	309496	Norite	449.75	450.25	9.3
20-200	5449588	309496	Norite	450	450.5	5.8
20-200	5449588	309496	Norite	450.25	450.75	21.2
20-200	5449588	309496	Norite	450.5	451	12.8
20-200	5449588	309496	Norite	450.75	451.25	8.8
20-200	5449588	309496	Norite	451	451.5	10.3
20-200	5449588	309496	Norite	451.25	451.75	10.3
20-200	5449588	309496	Norite	451.5	452	16.3
20-200	5449588	309496	Norite	451.75	452.25	9.6
20-200	5449588	309496	Norite	452	452.5	14.4
20-200	5449588	309496	Norite	452.25	452.75	17.3
20-200	5449588	309496	Norite	452.5	453	10.8
20-200	5449588	309496	Norite	452.75	453.25	16.2
20-200	5449588	309496	Norite	453	453.5	11.6
20-200	5449588	309496	Norite	453.25	453.75	10.3
20-200	5449588	309496	Norite	453.5	454	8.4
20-200	5449588	309496	Norite	453.75	454.25	9.5
20-200	5449588	309496	Norite	454	454.5	6.1

ID Hole	North	East	Domain	From	to	Kappa
20-200	5449588	309496	Norite	454.25	454.75	19.4
20-200	5449588	309496	Norite	454.5	455	12.3
20-200	5449588	309496	Magnetite Norite	454.75	455.25	18.8
20-200	5449588	309496	Magnetite Norite	455	455.5	36.2
20-200	5449588	309496	Magnetite Norite	455.25	455.75	22.5
20-200	5449588	309496	Magnetite Norite	455.5	456	38.0
20-200	5449588	309496	Magnetite Norite	455.75	456.25	47.0
20-200	5449588	309496	Magnetite Norite	456	456.5	63.6
20-200	5449588	309496	Magnetite Norite	456.25	456.75	65.0
20-200	5449588	309496	Magnetite Norite	456.5	457	87.0
20-200	5449588	309496	Magnetite Norite	456.75	457.25	82.9
20-200	5449588	309496	Magnetite Norite	457	457.5	132.0
20-200	5449588	309496	Magnetite Norite	457.25	457.75	44.8
20-200	5449588	309496	Magnetite Norite	457.5	458	16.3
20-200	5449588	309496	Magnetite Norite	457.75	458.25	92.9
20-200	5449588	309496	Magnetite Norite	458	458.5	78.3
20-200	5449588	309496	Magnetite Norite	458.25	458.75	33.0
20-200	5449588	309496	Magnetite Norite	458.5	459	41.8
20-200	5449588	309496	Magnetite Norite	458.75	459.25	53.4
20-200	5449588	309496	Magnetite Norite	459	459.5	41.3
20-200	5449588	309496	Magnetite Norite	459.25	459.75	21.5
20-200	5449588	309496	Magnetite Norite	459.5	460	60.9
20-200	5449588	309496	Magnetite Norite	459.75	460.25	50.4
20-200	5449588	309496	Magnetite Norite	460	460.5	78.2
20-200	5449588	309496	Magnetite Norite	460.25	460.75	45.1
20-200	5449588	309496	Magnetite Norite	460.5	461	60.8
20-200	5449588	309496	Magnetite Norite	460.75	461.25	37.4
20-200	5449588	309496	Magnetite Norite	461	461.5	108.0
20-200	5449588	309496	Magnetite Norite	461.25	461.75	76.9
20-200	5449588	309496	Magnetite Norite	461.5	462	100.0
20-200	5449588	309496	Magnetite Norite	461.75	462.25	36.5
20-200	5449588	309496	Magnetite Norite	462	462.5	88.2
20-200	5449588	309496	Magnetite Norite	462.25	462.75	92.9
20-200	5449588	309496	Magnetite Norite	462.5	463	82.0
20-200	5449588	309496	Magnetite Norite	462.75	463.25	26.8
20-200	5449588	309496	Magnetite Norite	463	463.5	32.1
20-200	5449588	309496	Magnetite Norite	463.25	463.75	110.0

ID Hole	North	East	Domain	From	to	Kappa
20-200	5449588	309496	Magnetite Norite	463.5	464	46.1
20-200	5449588	309496	Magnetite Norite	463.75	464.25	96.4
20-200	5449588	309496	Magnetite Norite	464	464.5	136.0
20-200	5449588	309496	Magnetite Norite	464.25	464.75	114.0
20-200	5449588	309496	Magnetite Norite	464.5	465	87.1
20-200	5449588	309496	Magnetite Norite	464.75	465.25	77.8
20-200	5449588	309496	Magnetite Norite	465	465.5	43.9
20-200	5449588	309496	Magnetite Norite	465.25	465.75	171.0
20-200	5449588	309496	Magnetite Norite	465.5	466	37.3
20-200	5449588	309496	Magnetite Norite	465.75	466.25	62.8
20-200	5449588	309496	Magnetite Norite	466	466.5	117.0
20-200	5449588	309496	Magnetite Norite	466.25	466.75	55.5
20-200	5449588	309496	Magnetite Norite	466.5	467	166.0
20-200	5449588	309496	Magnetite Norite	466.75	467.25	128.0
20-200	5449588	309496	Magnetite Norite	467	467.5	75.1
20-200	5449588	309496	Magnetite Norite	467.25	467.75	32.5
20-200	5449588	309496	Magnetite Norite	467.5	468	27.4
20-200	5449588	309496	Magnetite Norite	467.75	468.25	38.6
20-200	5449588	309496	Magnetite Norite	468	468.5	30.0
20-200	5449588	309496	Magnetite Norite	468.25	468.75	74.4
20-200	5449588	309496	Magnetite Norite	468.5	469	82.4
20-200	5449588	309496	Magnetite Norite	468.75	469.25	103.0
20-200	5449588	309496	Magnetite Norite	469	469.5	98.5
20-200	5449588	309496	Magnetite Norite	469.25	469.75	114.0
20-200	5449588	309496	Magnetite Norite	469.5	470	139.0
20-200	5449588	309496	Magnetite Norite	469.75	470.25	80.5
20-200	5449588	309496	Magnetite Norite	470	470.5	85.6
20-200	5449588	309496	Magnetite Norite	470.25	470.75	130.0
20-200	5449588	309496	Magnetite Norite	470.5	471	84.3
20-200	5449588	309496	Magnetite Norite	470.75	471.25	107.0
20-200	5449588	309496	Magnetite Norite	471	471.5	55.3
20-200	5449588	309496	Magnetite Norite	471.25	471.75	66.0
20-200	5449588	309496	Magnetite Norite	471.5	472	65.4
20-200	5449588	309496	Magnetite Norite	471.75	472.25	168.0
20-200	5449588	309496	Magnetite Norite	472	472.5	163.0
20-200	5449588	309496	Magnetite Norite	472.25	472.75	61.4
20-200	5449588	309496	Magnetite Norite	472.5	473	178.0

ID Hole	North	East	Domain	From	to	Kappa
20-200	5449588	309496	Magnetite Norite	472.75	473.25	67.9
20-200	5449588	309496	Magnetite Norite	473	473.5	144.0
20-200	5449588	309496	Magnetite Norite	473.25	473.75	132.0
20-200	5449588	309496	Magnetite Norite	473.5	474	86.6
20-200	5449588	309496	Magnetite Norite	473.75	474.25	77.8
20-200	5449588	309496	Magnetite Norite	474	474.5	104.0
20-200	5449588	309496	Magnetite Norite	474.25	474.75	105.0
20-200	5449588	309496	Magnetite Norite	474.5	475	96.1
20-200	5449588	309496	Magnetite Norite	474.75	475.25	128.0
20-200	5449588	309496	Magnetite Norite	475	475.5	107.0
20-200	5449588	309496	Magnetite Norite	475.25	475.75	67.1
20-200	5449588	309496	Magnetite Norite	475.5	476	69.8
20-200	5449588	309496	Magnetite Norite	475.75	476.25	93.4
20-200	5449588	309496	Magnetite Norite	476	476.5	96.8
20-200	5449588	309496	Magnetite Norite	476.25	476.75	92.1
20-200	5449588	309496	Magnetite Norite	476.5	477	63.3
20-200	5449588	309496	Magnetite Norite	476.75	477.25	57.9
20-200	5449588	309496	Magnetite Norite	477	477.5	75.2
20-200	5449588	309496	Magnetite Norite	477.25	477.75	38.4
20-200	5449588	309496	Magnetite Norite	477.5	478	84.0
20-200	5449588	309496	Magnetite Norite	477.75	478.25	50.0
20-200	5449588	309496	Magnetite Norite	478	478.5	69.6
20-200	5449588	309496	Magnetite Norite	478.25	478.75	103.0
20-200	5449588	309496	Magnetite Norite	478.5	479	47.5
20-200	5449588	309496	Magnetite Norite	478.75	479.25	30.2
20-200	5449588	309496	Magnetite Norite	479	479.5	39.5
20-200	5449588	309496	Magnetite Norite	479.25	479.75	49.8
20-200	5449588	309496	Magnetite Norite	479.5	480	34.4
20-200	5449588	309496	Magnetite Norite	479.75	480.25	50.0
20-200	5449588	309496	Magnetite Norite	480	480.5	40.2
20-200	5449588	309496	Magnetite Norite	480.25	480.75	77.7
20-200	5449588	309496	Magnetite Norite	480.5	481	73.1
20-200	5449588	309496	Magnetite Norite	480.75	481.25	83.0
20-200	5449588	309496	Magnetite Norite	481	481.5	21.9
20-200	5449588	309496	Magnetite Norite	481.25	481.75	16.3
20-200	5449588	309496	Magnetite Norite	481.5	482	60.9
20-200	5449588	309496	Magnetite Norite	481.75	482.25	84.8

ID Hole	North	East	Domain	From	to	Kappa
20-200	5449588	309496	Magnetite Norite	482	482.5	70.9
20-200	5449588	309496	Magnetite Norite	482.25	482.75	80.0
20-200	5449588	309496	Magnetite Norite	482.5	483	20.2
20-200	5449588	309496	Magnetite Norite	482.75	483.25	82.2
20-200	5449588	309496	Magnetite Norite	483	483.5	36.0
20-200	5449588	309496	Magnetite Norite	483.25	483.75	51.4
20-200	5449588	309496	Magnetite Norite	483.5	484	86.0
20-200	5449588	309496	Magnetite Norite	483.75	484.25	29.2
20-200	5449588	309496	Magnetite Norite	484	484.5	31.6
20-200	5449588	309496	Magnetite Norite	484.25	484.75	42.6
20-200	5449588	309496	Magnetite Norite	484.5	485	70.7
20-200	5449588	309496	Magnetite Norite	484.75	485.25	86.2
20-200	5449588	309496	Magnetite Norite	485	485.5	110.0
20-200	5449588	309496	Magnetite Norite	485.25	485.75	98.9
20-200	5449588	309496	Magnetite Norite	485.5	486	96.8
20-200	5449588	309496	Magnetite Norite	485.75	486.25	88.1
20-200	5449588	309496	Magnetite Norite	486	486.5	88.0
20-200	5449588	309496	Magnetite Norite	486.25	486.75	129.0
20-200	5449588	309496	Magnetite Norite	486.5	487	108.0
20-200	5449588	309496	Magnetite Norite	486.75	487.25	87.2
20-200	5449588	309496	Magnetite Norite	487	487.5	209.0
20-200	5449588	309496	Magnetite Norite	487.25	487.75	82.6
20-200	5449588	309496	Magnetite Norite	487.5	488	66.0
20-200	5449588	309496	Magnetite Norite	487.75	488.25	90.2
20-200	5449588	309496	Magnetite Norite	488	488.5	120.0
20-200	5449588	309496	Magnetite Norite	488.25	488.75	53.5
20-200	5449588	309496	Magnetite Norite	488.5	489	64.4
20-200	5449588	309496	Magnetite Norite	488.75	489.25	169.0
20-200	5449588	309496	Magnetite Norite	489	489.5	236.0
20-200	5449588	309496	Magnetite Norite	489.25	489.75	235.0
20-200	5449588	309496	Magnetite Norite	489.5	490	114.0
20-200	5449588	309496	Magnetite Norite	489.75	490.25	227.0
20-200	5449588	309496	Magnetite Norite	490	490.5	97.5
20-200	5449588	309496	Magnetite Norite	490.25	490.75	167.0
20-200	5449588	309496	Magnetite Norite	490.5	491	86.6
20-200	5449588	309496	Magnetite Norite	490.75	491.25	61.6
20-200	5449588	309496	Magnetite Norite	491	491.5	144.0

ID Hole	North	East	Domain	From	to	Kappa
20-200	5449588	309496	Magnetite Norite	491.25	491.75	174.0
20-200	5449588	309496	Magnetite Norite	491.5	492	196.0
20-200	5449588	309496	Magnetite Norite	491.75	492.25	182.0
20-200	5449588	309496	Magnetite Norite	492	492.5	184.0
20-200	5449588	309496	Magnetite Norite	492.25	492.75	100.0
20-200	5449588	309496	Magnetite Norite	492.5	493	178.0
20-200	5449588	309496	Magnetite Norite	492.75	493.25	192.0
20-200	5449588	309496	Magnetite Norite	493	493.5	224.0
20-200	5449588	309496	Magnetite Norite	493.25	493.75	246.0
20-200	5449588	309496	Magnetite Norite	493.5	494	149.0
20-200	5449588	309496	Magnetite Norite	493.75	494.25	151.0
20-200	5449588	309496	Magnetite Norite	494	494.5	187.0
20-200	5449588	309496	Magnetite Norite	494.25	494.75	144.0
20-200	5449588	309496	Magnetite Norite	494.5	495	104.0
20-200	5449588	309496	Magnetite Norite	494.75	495.25	181.0
20-200	5449588	309496	Magnetite Norite	495	495.5	108.0
20-200	5449588	309496	Magnetite Norite	495.25	495.75	109.0
20-200	5449588	309496	Magnetite Norite	495.5	496	108.0
20-200	5449588	309496	Magnetite Norite	495.75	496.25	82.6
20-200	5449588	309496	Magnetite Norite	496	496.5	73.9
20-200	5449588	309496	Magnetite Norite	496.25	496.75	82.8
20-200	5449588	309496	Magnetite Norite	496.5	497	37.2
20-200	5449588	309496	Magnetite Norite	496.75	497.25	65.8
20-200	5449588	309496	Magnetite Norite	497	497.5	53.8
20-200	5449588	309496	Magnetite Norite	497.25	497.75	31.5
20-200	5449588	309496	Magnetite Norite	497.5	498	38.5
20-200	5449588	309496	Magnetite Norite	497.75	498.25	85.2
20-200	5449588	309496	Magnetite Norite	498	498.5	95.6
20-200	5449588	309496	Magnetite Norite	498.25	498.75	49.2
20-200	5449588	309496	Magnetite Norite	498.5	499	36.2
20-200	5449588	309496	Magnetite Norite	498.75	499.25	43.7
20-200	5449588	309496	Magnetite Norite	499	499.5	64.4
20-200	5449588	309496	Magnetite Norite	499.25	499.75	34.8
20-200	5449588	309496	Magnetite Norite	499.5	500	70.8
20-200	5449588	309496	Magnetite Norite	499.75	500.25	47.9
20-200	5449588	309496	Magnetite Norite	500	500.5	46.6
20-200	5449588	309496	Magnetite Norite	500.25	500.75	99.1

ID Hole	North	East	Domain	From	to	Kappa
20-200	5449588	309496	Magnetite Norite	500.5	501	25.4
20-200	5449588	309496	Magnetite Norite	500.75	501.25	133.0
20-200	5449588	309496	Magnetite Norite	501	501.5	114.0
20-200	5449588	309496	Magnetite Norite	501.25	501.75	70.1
20-200	5449588	309496	Magnetite Norite	501.5	502	97.6
20-200	5449588	309496	Magnetite Norite	501.75	502.25	87.9
20-200	5449588	309496	Magnetite Norite	502	502.5	96.3
20-200	5449588	309496	Magnetite Norite	502.25	502.75	104.0
20-200	5449588	309496	Magnetite Norite	502.5	503	109.0
20-200	5449588	309496	Magnetite Norite	502.75	503.25	76.7
20-200	5449588	309496	Magnetite Norite	503	503.5	91.7
20-200	5449588	309496	Magnetite Norite	503.25	503.75	60.8
20-200	5449588	309496	Magnetite Norite	503.5	504	61.3
20-200	5449588	309496	Magnetite Norite	503.75	504.25	82.7
20-200	5449588	309496	Magnetite Norite	504	504.5	73.3
20-200	5449588	309496	Magnetite Norite	504.25	504.75	37.0
20-200	5449588	309496	Magnetite Norite	504.5	505	24.9
20-200	5449588	309496	Magnetite Norite	504.75	505.25	69.1
20-200	5449588	309496	Magnetite Norite	505	505.5	59.1
20-200	5449588	309496	Magnetite Norite	505.25	505.75	35.3
20-200	5449588	309496	Magnetite Norite	505.5	506	50.7
20-200	5449588	309496	Magnetite Norite	505.75	506.25	56.0
20-200	5449588	309496	Magnetite Norite	506	506.5	49.3
20-200	5449588	309496	Magnetite Norite	506.25	506.75	56.7
20-200	5449588	309496	Magnetite Norite	506.5	507	61.6
20-200	5449588	309496	Magnetite Norite	506.75	507.25	47.8
20-200	5449588	309496	Magnetite Norite	507	507.5	19.0
20-200	5449588	309496	Magnetite Norite	507.25	507.75	77.0
20-200	5449588	309496	Magnetite Norite	507.5	508	73.9
20-200	5449588	309496	Magnetite Norite	507.75	508.25	38.0
20-200	5449588	309496	Magnetite Norite	508	508.5	46.5
20-200	5449588	309496	Magnetite Norite	508.25	508.75	68.2
20-200	5449588	309496	Magnetite Norite	508.5	509	81.1
20-200	5449588	309496	Magnetite Norite	508.75	509.25	81.7
20-200	5449588	309496	Magnetite Norite	509	509.5	172.0
20-200	5449588	309496	Magnetite Norite	509.25	509.75	77.5
20-200	5449588	309496	Magnetite Norite	509.5	510	82.8

ID Hole	North	East	Domain	From	to	Kappa
20-200	5449588	309496	Magnetite Norite	509.75	510.25	58.4
20-200	5449588	309496	Magnetite Norite	510	510.5	122.0
20-200	5449588	309496	Magnetite Norite	510.25	510.75	118.0
20-200	5449588	309496	Magnetite Norite	510.5	511	110.0
20-200	5449588	309496	Magnetite Norite	510.75	511.25	5.1
20-200	5449588	309496	Magnetite Norite	511	511.5	58.8
20-200	5449588	309496	Magnetite Norite	511.25	511.75	128.0
20-200	5449588	309496	Magnetite Norite	511.5	512	73.7
20-200	5449588	309496	Magnetite Norite	511.75	512.25	124.0
20-200	5449588	309496	Magnetite Norite	512	512.5	206.0
20-200	5449588	309496	Magnetite Norite	512.25	512.75	130.0
20-200	5449588	309496	Magnetite Norite	512.5	513	141.0
20-200	5449588	309496	Magnetite Norite	512.75	513.25	139.0
20-200	5449588	309496	Magnetite Norite	513	513.5	42.6
20-200	5449588	309496	Magnetite Norite	513.25	513.75	99.7
20-200	5449588	309496	Magnetite Norite	513.5	514	108.0
20-200	5449588	309496	Magnetite Norite	513.75	514.25	166.0
20-200	5449588	309496	Magnetite Norite	514	514.5	59.8
20-200	5449588	309496	Magnetite Norite	514.25	514.75	104.0
20-200	5449588	309496	Magnetite Norite	514.5	515	82.8
20-200	5449588	309496	Magnetite Norite	514.75	515.25	79.9
20-200	5449588	309496	Magnetite Norite	515	515.5	74.8
20-200	5449588	309496	Magnetite Norite	515.25	515.75	39.2
20-200	5449588	309496	Magnetite Norite	515.5	516	65.3
20-200	5449588	309496	Magnetite Norite	515.75	516.25	41.3
20-200	5449588	309496	Magnetite Norite	516	516.5	59.1
20-200	5449588	309496	Magnetite Norite	516.25	516.75	43.9
20-200	5449588	309496	Magnetite Norite	516.5	517	56.1
20-200	5449588	309496	Magnetite Norite	516.75	517.25	50.1
20-200	5449588	309496	Magnetite Norite	517	517.5	25.4
20-200	5449588	309496	Magnetite Norite	517.25	517.75	29.0
20-200	5449588	309496	Magnetite Norite	517.5	518	23.3
20-200	5449588	309496	Magnetite Norite	517.75	518.25	74.1
20-200	5449588	309496	Magnetite Norite	518	518.5	39.0
20-200	5449588	309496	Magnetite Norite	518.25	518.75	44.1
20-200	5449588	309496	Magnetite Norite	518.5	519	18.5
20-200	5449588	309496	Magnetite Norite	518.75	519.25	6.3

ID Hole	North	East	Domain	From	to	Kappa
20-200	5449588	309496	Magnetite Norite	519	519.5	45.1
20-200	5449588	309496	Magnetite Norite	519.25	519.75	55.7
20-200	5449588	309496	Magnetite Norite	519.5	520	58.5
20-200	5449588	309496	Magnetite Norite	519.75	520.25	28.9
20-200	5449588	309496	Magnetite Norite	520	520.5	57.8
20-200	5449588	309496	Magnetite Norite	520.25	520.75	82.1
20-200	5449588	309496	Magnetite Norite	520.5	521	88.0
20-200	5449588	309496	Magnetite Norite	520.75	521.25	78.5
20-200	5449588	309496	Magnetite Norite	521	521.5	39.4
20-200	5449588	309496	Magnetite Norite	521.25	521.75	137.0
20-200	5449588	309496	Magnetite Norite	521.5	522	38.6
20-200	5449588	309496	Magnetite Norite	521.75	522.25	55.1
20-200	5449588	309496	Magnetite Norite	522	522.5	50.9
20-200	5449588	309496	Magnetite Norite	522.25	522.75	86.7
20-200	5449588	309496	Magnetite Norite	522.5	523	80.0
20-200	5449588	309496	Magnetite Norite	522.75	523.25	61.8
20-200	5449588	309496	Magnetite Norite	523	523.5	89.1
20-200	5449588	309496	Magnetite Norite	523.25	523.75	91.4
20-200	5449588	309496	Magnetite Norite	523.5	524	15.6
20-200	5449588	309496	Magnetite Norite	523.75	524.25	115.0
20-200	5449588	309496	Magnetite Norite	524	524.5	103.0
20-200	5449588	309496	Magnetite Norite	524.25	524.75	69.5
20-200	5449588	309496	Magnetite Norite	524.5	525	48.5
20-200	5449588	309496	Magnetite Norite	524.75	525.25	74.6
20-200	5449588	309496	Magnetite Norite	525	525.5	61.2
20-200	5449588	309496	Magnetite Norite	525.25	525.75	70.7
20-200	5449588	309496	Magnetite Norite	525.5	526	49.5
20-200	5449588	309496	Magnetite Norite	525.75	526.25	81.6
20-200	5449588	309496	Magnetite Norite	526	526.5	57.7
20-200	5449588	309496	Magnetite Norite	526.25	526.75	66.1
20-200	5449588	309496	Magnetite Norite	526.5	527	49.6
20-200	5449588	309496	Magnetite Norite	526.75	527.25	68.2
20-200	5449588	309496	Magnetite Norite	527	527.5	72.9
20-200	5449588	309496	Magnetite Norite	527.25	527.75	25.9
20-200	5449588	309496	Magnetite Norite	527.5	528	18.2
20-200	5449588	309496	Magnetite Norite	527.75	528.25	10.1
20-200	5449588	309496	Magnetite Norite	528	528.5	54.8

ID Hole	North	East	Domain	From	to	Kappa
20-200	5449588	309496	Magnetite Norite	528.25	528.75	25.2
20-200	5449588	309496	Magnetite Norite	528.5	529	47.0
20-200	5449588	309496	Magnetite Norite	528.75	529.25	18.6
20-200	5449588	309496	Magnetite Norite	529	529.5	42.7
20-200	5449588	309496	Magnetite Norite	529.25	529.75	40.6
20-200	5449588	309496	Magnetite Norite	529.5	530	61.4
20-200	5449588	309496	Magnetite Norite	529.75	530.25	59.2
20-200	5449588	309496	Magnetite Norite	530	530.5	44.8
20-200	5449588	309496	Magnetite Norite	530.25	530.75	22.4
20-200	5449588	309496	Magnetite Norite	530.5	531	22.0
20-200	5449588	309496	Magnetite Norite	530.75	531.25	44.9
20-200	5449588	309496	Magnetite Norite	531	531.5	111.0
20-200	5449588	309496	Magnetite Norite	531.25	531.75	88.1
20-200	5449588	309496	Magnetite Norite	531.5	532	39.5
20-200	5449588	309496	Magnetite Norite	531.75	532.25	64.3
20-200	5449588	309496	Magnetite Norite	532	532.5	51.9
20-200	5449588	309496	Magnetite Norite	532.25	532.75	33.1
20-200	5449588	309496	Magnetite Norite	532.5	533	51.0
20-200	5449588	309496	Norite	532.75	533.25	19.0
20-200	5449588	309496	Norite	533	533.5	11.3
20-200	5449588	309496	Norite	533.25	533.75	17.1
20-200	5449588	309496	Norite	533.5	534	17.7
20-200	5449588	309496	Norite	533.75	534.25	8.7
20-200	5449588	309496	Norite	534	534.5	52.0
20-200	5449588	309496	Norite	534.25	534.75	23.6
20-200	5449588	309496	Norite	534.5	535	29.1
20-200	5449588	309496	Norite	534.75	535.25	20.9
20-200	5449588	309496	Norite	535	535.5	22.9
20-200	5449588	309496	Norite	535.25	535.75	27.9
20-200	5449588	309496	Norite	535.5	536	61.9
20-200	5449588	309496	Norite	535.75	536.25	33.3
20-200	5449588	309496	Norite	536	536.5	37.2
20-200	5449588	309496	Norite	536.25	536.75	35.1
20-200	5449588	309496	Norite	536.5	537	53.5
20-200	5449588	309496	Norite	536.75	537.25	47.6
20-200	5449588	309496	Norite	537	537.5	39.9
20-200	5449588	309496	Norite	537.25	537.75	42.1

ID Hole	North	East	Domain	From	to	Kappa
20-200	5449588	309496	Norite	537.5	538	28.0
20-200	5449588	309496	Norite	537.75	538.25	23.3
20-200	5449588	309496	Norite	538	538.5	33.2
20-200	5449588	309496	Norite	538.25	538.75	25.1
20-200	5449588	309496	Norite	538.5	539	26.1
20-200	5449588	309496	Norite	538.75	539.25	40.8
20-200	5449588	309496	Norite	539	539.5	37.0
20-200	5449588	309496	Norite	539.25	539.75	50.6
20-200	5449588	309496	Norite	539.5	540	19.5
20-200	5449588	309496	Norite	539.75	540.25	26.6
20-200	5449588	309496	Norite	540	540.5	36.3
20-200	5449588	309496	Norite	540.25	540.75	3.8
20-200	5449588	309496	Norite	540.5	541	37.6
20-200	5449588	309496	Norite	540.75	541.25	37.2
20-200	5449588	309496	Norite	541	541.5	14.9
20-200	5449588	309496	Norite	541.25	541.75	31.9
20-200	5449588	309496	Norite	541.5	542	21.7
20-200	5449588	309496	Norite	541.75	542.25	20.2
20-200	5449588	309496	Norite	542	542.5	28.8
20-200	5449588	309496	Norite	542.25	542.75	23.4
20-200	5449588	309496	Norite	542.5	543	25.1
20-200	5449588	309496	Norite	542.75	543.25	15.8
20-200	5449588	309496	Norite	543	543.5	28.9
20-200	5449588	309496	Norite	543.25	543.75	17.9
20-200	5449588	309496	Norite	543.5	544	25.1
20-200	5449588	309496	Norite	543.75	544.25	23.3
20-200	5449588	309496	Norite	544	544.5	15.6
20-200	5449588	309496	Norite	544.25	544.75	28.7
20-200	5449588	309496	Norite	544.5	545	17.4
20-200	5449588	309496	Norite	544.75	545.25	31.1
20-200	5449588	309496	Norite	545	545.5	49.4
20-200	5449588	309496	Norite	545.25	545.75	10.5
20-200	5449588	309496	Norite	545.5	546	19.6
20-200	5449588	309496	Norite	545.75	546.25	21.7
20-200	5449588	309496	Norite	546	546.5	27.2
20-200	5449588	309496	Norite	546.25	546.75	22.0
20-200	5449588	309496	Norite	546.5	547	4.4

ID Hole	North	East	Domain	From	to	Kappa
20-200	5449588	309496	Norite	546.75	547.25	6.3
20-200	5449588	309496	Norite	547	547.5	3.3
20-200	5449588	309496	Norite	547.25	547.75	20.7
20-200	5449588	309496	Norite	547.5	548	22.0
20-200	5449588	309496	Norite	547.75	548.25	42.0
20-200	5449588	309496	Norite	548	548.5	50.0
20-200	5449588	309496	Norite	548.25	548.75	190.0
20-200	5449588	309496	Norite	548.5	549	32.2
20-200	5449588	309496	Norite	548.75	549.25	152.0
20-200	5449588	309496	Norite	549	549.5	21.3
20-200	5449588	309496	Norite	549.25	549.75	7.6
20-200	5449588	309496	Norite	549.5	550	43.6
20-200	5449588	309496	Norite	549.75	550.25	18.0
20-200	5449588	309496	Norite	550	550.5	8.8
20-200	5449588	309496	Norite	550.25	550.75	7.3
20-200	5449588	309496	Norite	550.5	551	4.7
20-200	5449588	309496	Norite	550.75	551.25	7.0
20-200	5449588	309496	Norite	551	551.5	8.4
20-200	5449588	309496	Norite	551.25	551.75	11.5
20-200	5449588	309496	Norite	551.5	552	7.1
20-200	5449588	309496	Norite	551.75	552.25	33.8
20-200	5449588	309496	Norite	552	552.5	4.6
20-200	5449588	309496	Norite	552.25	552.75	75.2
20-200	5449588	309496	Norite	552.5	553	6.2
20-200	5449588	309496	Norite	552.75	553.25	17.1
20-200	5449588	309496	Norite	553	553.5	4.4
20-200	5449588	309496	Norite	553.25	553.75	13.5
20-200	5449588	309496	Norite	553.5	554	2.5
20-200	5449588	309496	Norite	553.75	554.25	15.5
20-200	5449588	309496	Norite	554	554.5	16.4
20-200	5449588	309496	Norite	554.25	554.75	32.1
20-200	5449588	309496	Norite	554.5	555	23.1
20-200	5449588	309496	Norite	554.75	555.25	18.9
20-200	5449588	309496	Norite	555	555.5	22.5
20-200	5449588	309496	Norite	555.25	555.75	23.2
20-200	5449588	309496	Norite	555.5	556	21.1
20-200	5449588	309496	Norite	555.75	556.25	20.9

ID Hole	North	East	Domain	From	to	Kappa
20-200	5449588	309496	Norite	556	556.5	16.0
20-200	5449588	309496	Norite	556.25	556.75	1.6
20-200	5449588	309496	Norite	556.5	557	20.7
20-200	5449588	309496	Norite	556.75	557.25	19.3
20-200	5449588	309496	Norite	557	557.5	20.3
20-200	5449588	309496	Norite	557.25	557.75	20.3
20-200	5449588	309496	Norite	557.5	558	17.4
20-200	5449588	309496	Norite	557.75	558.25	26.3
20-200	5449588	309496	Norite	558	558.5	12.8
20-200	5449588	309496	Norite	558.25	558.75	14.7
20-200	5449588	309496	Norite	558.5	559	17.7
20-200	5449588	309496	Norite	558.75	559.25	23.2
20-200	5449588	309496	Norite	559	559.5	23.4
20-200	5449588	309496	Norite	559.25	559.75	19.5
20-200	5449588	309496	Norite	559.5	560	21.8
20-200	5449588	309496	Norite	559.75	560.25	21.7
20-200	5449588	309496	Norite	560	560.5	16.5
20-200	5449588	309496	Norite	560.25	560.75	23.4
20-200	5449588	309496	Norite	560.5	561	24.9
20-200	5449588	309496	Norite	560.75	561.25	24.2
20-200	5449588	309496	Norite	561	561.5	7.7
20-200	5449588	309496	Norite	561.25	561.75	37.3
20-200	5449588	309496	Norite	561.5	562	9.9
20-200	5449588	309496	Norite	561.75	562.25	8.0
20-200	5449588	309496	Magnetite Norite	562	562.5	36.1
20-200	5449588	309496	Magnetite Norite	562.25	562.75	49.0
20-200	5449588	309496	Magnetite Norite	562.5	563	66.1
20-200	5449588	309496	Magnetite Norite	562.75	563.25	179.0
20-200	5449588	309496	Magnetite Norite	563	563.5	92.9
20-200	5449588	309496	Magnetite Norite	563.25	563.75	1.8
20-200	5449588	309496	Magnetite Norite	563.5	564	10.7
20-200	5449588	309496	Magnetite Norite	563.75	564.25	10.0
20-200	5449588	309496	Magnetite Norite	564	564.5	12.2
20-200	5449588	309496	Magnetite Norite	564.25	564.75	13.5
20-200	5449588	309496	Magnetite Norite	564.5	565	46.8
20-200	5449588	309496	Magnetite Norite	564.75	565.25	23.0
20-200	5449588	309496	Magnetite Norite	565	565.5	26.4

ID Hole	North	East	Domain	From	to	Kappa
20-200	5449588	309496	Magnetite Norite	565.25	565.75	15.4
20-200	5449588	309496	Magnetite Norite	565.5	566	64.4
20-200	5449588	309496	Magnetite Norite	565.75	566.25	78.1
20-200	5449588	309496	Magnetite Norite	566	566.5	8.3
20-200	5449588	309496	Magnetite Norite	566.25	566.75	51.7
20-200	5449588	309496	Magnetite Norite	566.5	567	172.0
20-200	5449588	309496	Magnetite Norite	566.75	567.25	84.2
20-200	5449588	309496	Magnetite Norite	567	567.5	90.1
20-200	5449588	309496	Magnetite Norite	567.25	567.75	83.9
20-200	5449588	309496	Magnetite Norite	567.5	568	7.3
20-200	5449588	309496	Magnetite Norite	567.75	568.25	98.9
20-200	5449588	309496	Magnetite Norite	568	568.5	42.9
20-200	5449588	309496	Magnetite Norite	568.25	568.75	35.0
20-200	5449588	309496	Magnetite Norite	568.5	569	42.2
20-200	5449588	309496	Magnetite Norite	568.75	569.25	38.0
20-200	5449588	309496	Magnetite Norite	569	569.5	66.6
20-200	5449588	309496	Magnetite Norite	569.25	569.75	52.4
20-200	5449588	309496	Magnetite Norite	569.5	570	34.1
20-200	5449588	309496	Magnetite Norite	569.75	570.25	87.5
20-200	5449588	309496	Magnetite Norite	570	570.5	56.8
20-200	5449588	309496	Magnetite Norite	570.25	570.75	76.8
20-200	5449588	309496	Magnetite Norite	570.5	571	66.5
20-200	5449588	309496	Magnetite Norite	570.75	571.25	52.1
20-200	5449588	309496	Magnetite Norite	571	571.5	88.2
20-200	5449588	309496	Magnetite Norite	571.25	571.75	72.8
20-200	5449588	309496	Magnetite Norite	571.5	572	73.7
20-200	5449588	309496	Magnetite Norite	571.75	572.25	37.3
20-200	5449588	309496	Magnetite Norite	572	572.5	75.6
20-200	5449588	309496	Magnetite Norite	572.25	572.75	66.2
20-200	5449588	309496	Magnetite Norite	572.5	573	50.6
20-200	5449588	309496	Magnetite Norite	572.75	573.25	75.7
20-200	5449588	309496	Magnetite Norite	573	573.5	29.7
20-200	5449588	309496	Magnetite Norite	573.25	573.75	59.9
20-200	5449588	309496	Magnetite Norite	573.5	574	71.7
20-200	5449588	309496	Magnetite Norite	573.75	574.25	67.6
20-200	5449588	309496	Magnetite Norite	574	574.5	56.8
20-200	5449588	309496	Magnetite Norite	574.25	574.75	51.8

ID Hole	North	East	Domain	From	to	Kappa
20-200	5449588	309496	Magnetite Norite	574.5	575	59.3
20-200	5449588	309496	Magnetite Norite	574.75	575.25	80.8
20-200	5449588	309496	Magnetite Norite	575	575.5	38.1
20-200	5449588	309496	Magnetite Norite	575.25	575.75	36.8
20-200	5449588	309496	Magnetite Norite	575.5	576	65.7
20-200	5449588	309496	Magnetite Norite	575.75	576.25	59.4
20-200	5449588	309496	Magnetite Norite	576	576.5	51.0
20-200	5449588	309496	Magnetite Norite	576.25	576.75	66.1
20-200	5449588	309496	Magnetite Norite	576.5	577	81.4
20-200	5449588	309496	Magnetite Norite	576.75	577.25	75.7
20-200	5449588	309496	Magnetite Norite	577	577.5	131.0
20-200	5449588	309496	Magnetite Norite	577.25	577.75	212.0
20-200	5449588	309496	Magnetite Norite	577.5	578	59.3
20-200	5449588	309496	Magnetite Norite	577.75	578.25	65.8
20-200	5449588	309496	Magnetite Norite	578	578.5	360.0
20-200	5449588	309496	Magnetite Norite	578.25	578.75	263.0
20-200	5449588	309496	Magnetite Norite	578.5	579	117.0
20-200	5449588	309496	Magnetite Norite	578.75	579.25	190.0
20-200	5449588	309496	Magnetite Norite	579	579.5	53.4
20-200	5449588	309496	Magnetite Norite	579.25	579.75	7.2
20-200	5449588	309496	Magnetite Norite	579.5	580	60.4
20-200	5449588	309496	Magnetite Norite	579.75	580.25	18.2
20-200	5449588	309496	Magnetite Norite	580	580.5	58.8
20-200	5449588	309496	Magnetite Norite	580.25	580.75	30.4
20-200	5449588	309496	Magnetite Norite	580.5	581	27.2
20-200	5449588	309496	Magnetite Norite	580.75	581.25	16.3
20-200	5449588	309496	Magnetite Norite	581	581.5	20.5
20-200	5449588	309496	Magnetite Norite	581.25	581.75	8.2
20-200	5449588	309496	Magnetite Norite	581.5	582	8.7
20-200	5449588	309496	Magnetite Norite	581.75	582.25	33.4
20-200	5449588	309496	Magnetite Norite	582	582.5	34.3
20-200	5449588	309496	Magnetite Norite	582.25	582.75	31.9
20-200	5449588	309496	Magnetite Norite	582.5	583	63.4
20-200	5449588	309496	Magnetite Norite	582.75	583.25	75.8
20-200	5449588	309496	Magnetite Norite	583	583.5	57.0
20-200	5449588	309496	Magnetite Norite	583.25	583.75	46.9
20-200	5449588	309496	Magnetite Norite	583.5	584	43.7

ID Hole	North	East	Domain	From	to	Kappa
20-200	5449588	309496	Magnetite Norite	583.75	584.25	57.7
20-200	5449588	309496	Magnetite Norite	584	584.5	208.0
20-200	5449588	309496	Magnetite Norite	584.25	584.75	159.0
20-200	5449588	309496	Magnetite Norite	584.5	585	70.8
20-200	5449588	309496	Magnetite Norite	584.75	585.25	140.0
20-200	5449588	309496	Magnetite Norite	585	585.5	85.1
20-200	5449588	309496	Magnetite Norite	585.25	585.75	113.0
20-200	5449588	309496	Magnetite Norite	585.5	586	127.0
20-200	5449588	309496	Magnetite Norite	585.75	586.25	114.0
20-200	5449588	309496	Magnetite Norite	586	586.5	92.6
20-200	5449588	309496	Magnetite Norite	586.25	586.75	116.0
20-200	5449588	309496	Magnetite Norite	586.5	587	110.0
20-200	5449588	309496	Magnetite Norite	586.75	587.25	142.0
20-200	5449588	309496	Magnetite Norite	587	587.5	117.0
20-200	5449588	309496	Magnetite Norite	587.25	587.75	122.0
20-200	5449588	309496	Magnetite Norite	587.5	588	96.6
20-200	5449588	309496	Magnetite Norite	587.75	588.25	111.0
20-200	5449588	309496	Magnetite Norite	588	588.5	65.1
20-200	5449588	309496	Magnetite Norite	588.25	588.75	67.6
20-200	5449588	309496	Magnetite Norite	588.5	589	62.9
20-200	5449588	309496	Magnetite Norite	588.75	589.25	17.1
20-200	5449588	309496	Magnetite Norite	589	589.5	106.0
20-200	5449588	309496	Magnetite Norite	589.25	589.75	87.7
20-200	5449588	309496	Magnetite Norite	589.5	590	49.6
20-200	5449588	309496	Magnetite Norite	589.75	590.25	65.1
20-200	5449588	309496	Magnetite Norite	590	590.5	56.7
20-200	5449588	309496	Magnetite Norite	590.25	590.75	35.8
20-200	5449588	309496	Magnetite Norite	590.5	591	51.4
20-200	5449588	309496	Magnetite Norite	590.75	591.25	52.3
20-200	5449588	309496	Magnetite Norite	591	591.5	69.7
20-200	5449588	309496	Magnetite Norite	591.25	591.75	52.9
20-200	5449588	309496	Magnetite Norite	591.5	592	91.1
20-200	5449588	309496	Magnetite Norite	591.75	592.25	81.3
20-200	5449588	309496	Magnetite Norite	592	592.5	157.0
20-200	5449588	309496	Magnetite Norite	592.25	592.75	136.0
20-200	5449588	309496	Magnetite Norite	592.5	593	95.4
20-200	5449588	309496	Magnetite Norite	592.75	593.25	76.7

ID Hole	North	East	Domain	From	to	Kappa
20-200	5449588	309496	Magnetite Norite	593	593.5	86.0
20-200	5449588	309496	Magnetite Norite	593.25	593.75	140.0
20-200	5449588	309496	Magnetite Norite	593.5	594	121.0
20-200	5449588	309496	Magnetite Norite	593.75	594.25	86.3
20-200	5449588	309496	Magnetite Norite	594	594.5	13.6
20-200	5449588	309496	Magnetite Norite	594.25	594.75	42.4
20-200	5449588	309496	Magnetite Norite	594.5	595	124.0
20-200	5449588	309496	Magnetite Norite	594.75	595.25	143.0
20-200	5449588	309496	Magnetite Norite	595	595.5	138.0
20-200	5449588	309496	Magnetite Norite	595.25	595.75	220.0
20-200	5449588	309496	Magnetite Norite	595.5	596	158.0
20-200	5449588	309496	Magnetite Norite	595.75	596.25	97.2
20-200	5449588	309496	Magnetite Norite	596	596.5	195.0
20-200	5449588	309496	Magnetite Norite	596.25	596.75	140.0
20-200	5449588	309496	Magnetite Norite	596.5	597	74.3
20-200	5449588	309496	Magnetite Norite	596.75	597.25	110.0
20-200	5449588	309496	Magnetite Norite	597	597.5	134.0
20-200	5449588	309496	Magnetite Norite	597.25	597.75	122.0
20-200	5449588	309496	Magnetite Norite	597.5	598	64.0
20-200	5449588	309496	Magnetite Norite	597.75	598.25	45.2
20-200	5449588	309496	Magnetite Norite	598	598.5	36.6
20-200	5449588	309496	Magnetite Norite	598.25	598.75	96.5
20-200	5449588	309496	Magnetite Norite	598.5	599	44.9
20-200	5449588	309496	Magnetite Norite	598.75	599.25	42.2
20-200	5449588	309496	Magnetite Norite	599	599.5	67.0
20-200	5449588	309496	Magnetite Norite	599.25	599.75	85.0
20-200	5449588	309496	Magnetite Norite	599.5	600	65.3
20-200	5449588	309496	Magnetite Norite	599.75	600.25	73.3
20-200	5449588	309496	Magnetite Norite	600	600.5	60.1
20-200	5449588	309496	Magnetite Norite	600.25	600.75	58.8
20-200	5449588	309496	Magnetite Norite	600.5	601	81.9
20-200	5449588	309496	Magnetite Norite	600.75	601.25	103.0
20-200	5449588	309496	Magnetite Norite	601	601.5	114.0
20-200	5449588	309496	Magnetite Norite	601.25	601.75	116.0
20-200	5449588	309496	Magnetite Norite	601.5	602	110.0
20-200	5449588	309496	Magnetite Norite	601.75	602.25	81.5
20-200	5449588	309496	Magnetite Norite	602	602.5	96.9

ID Hole	North	East	Domain	From	to	Kappa
20-200	5449588	309496	Magnetite Norite	602.25	602.75	52.6
20-200	5449588	309496	Magnetite Norite	602.5	603	71.4
20-200	5449588	309496	Magnetite Norite	602.75	603.25	44.0
20-200	5449588	309496	Magnetite Norite	603	603.5	45.5
20-200	5449588	309496	Magnetite Norite	603.25	603.75	65.6
20-200	5449588	309496	Magnetite Norite	603.5	604	86.4
20-200	5449588	309496	Magnetite Norite	603.75	604.25	105.0
20-200	5449588	309496	Magnetite Norite	604	604.5	41.2
20-200	5449588	309496	Magnetite Norite	604.25	604.75	26.2
20-200	5449588	309496	Magnetite Norite	604.5	605	62.0
20-200	5449588	309496	Magnetite Norite	604.75	605.25	46.1
20-200	5449588	309496	Magnetite Norite	605	605.5	37.9
20-200	5449588	309496	Magnetite Norite	605.25	605.75	98.3
20-200	5449588	309496	Magnetite Norite	605.5	606	58.2
20-200	5449588	309496	Magnetite Norite	605.75	606.25	101.0
20-200	5449588	309496	Magnetite Norite	606	606.5	33.4
20-200	5449588	309496	Magnetite Norite	606.25	606.75	49.5
20-200	5449588	309496	Magnetite Norite	606.5	607	53.0
20-200	5449588	309496	Magnetite Norite	606.75	607.25	89.6
20-200	5449588	309496	Magnetite Norite	607	607.5	48.0
20-200	5449588	309496	Magnetite Norite	607.25	607.75	29.2
20-200	5449588	309496	Magnetite Norite	607.5	608	38.1
20-200	5449588	309496	Magnetite Norite	607.75	608.25	35.2
20-200	5449588	309496	Magnetite Norite	608	608.5	16.2
20-200	5449588	309496	Magnetite Norite	608.25	608.75	16.0
20-200	5449588	309496	Magnetite Norite	608.5	609	87.5
20-200	5449588	309496	Magnetite Norite	608.75	609.25	50.6
20-200	5449588	309496	Magnetite Norite	609	609.5	54.5
20-200	5449588	309496	Magnetite Norite	609.25	609.75	66.4
20-200	5449588	309496	Magnetite Norite	609.5	610	45.3
20-200	5449588	309496	Magnetite Norite	609.75	610.25	73.0
20-200	5449588	309496	Magnetite Norite	610	610.5	58.8
20-200	5449588	309496	Magnetite Norite	610.25	610.75	61.8
20-200	5449588	309496	Magnetite Norite	610.5	611	45.3
20-200	5449588	309496	Magnetite Norite	610.75	611.25	36.0
20-200	5449588	309496	Magnetite Norite	611	611.5	74.6
20-200	5449588	309496	Magnetite Norite	611.25	611.75	70.4

ID Hole	North	East	Domain	From	to	Kappa
20-200	5449588	309496	Magnetite Norite	611.5	612	59.4
20-200	5449588	309496	Magnetite Norite	611.75	612.25	76.9
20-200	5449588	309496	Magnetite Norite	612	612.5	124.0
20-200	5449588	309496	Magnetite Norite	612.25	612.75	103.0
20-200	5449588	309496	Magnetite Norite	612.5	613	116.0
20-200	5449588	309496	Magnetite Norite	612.75	613.25	97.9
20-200	5449588	309496	Magnetite Norite	613	613.5	111.0
20-200	5449588	309496	Magnetite Norite	613.25	613.75	131.0
20-200	5449588	309496	Magnetite Norite	613.5	614	237.0
20-200	5449588	309496	Magnetite Norite	613.75	614.25	165.0
20-200	5449588	309496	Magnetite Norite	614	614.5	274.0
20-200	5449588	309496	Magnetite Norite	614.25	614.75	125.0
20-200	5449588	309496	Magnetite Norite	614.5	615	111.0
20-200	5449588	309496	Magnetite Norite	614.75	615.25	106.0
20-200	5449588	309496	Magnetite Norite	615	615.5	98.8
20-200	5449588	309496	Magnetite Norite	615.25	615.75	89.8
20-200	5449588	309496	Magnetite Norite	615.5	616	101.0
20-200	5449588	309496	Magnetite Norite	615.75	616.25	78.8
20-200	5449588	309496	Magnetite Norite	616	616.5	81.0
20-200	5449588	309496	Magnetite Norite	616.25	616.75	68.3
20-200	5449588	309496	Magnetite Norite	616.5	617	68.8
20-200	5449588	309496	Magnetite Norite	616.75	617.25	89.0
20-200	5449588	309496	Magnetite Norite	617	617.5	91.5
20-200	5449588	309496	Magnetite Norite	617.25	617.75	43.9
20-200	5449588	309496	Magnetite Norite	617.5	618	189.0

Appendix C

Plagioclase EDS analyses

Thin section	Na_2O %	Al_2O_3 %	SiO_2 %	K_2O %	CaO %	FeO %	Total
SB008	4.3	30.0	50.6	bdl	12.0	bdl	96.9
SB008	4.4	31.3	51.8	bdl	12.4	bdl	99.9
SB008	4.5	30.7	52.2	bdl	12.1	bdl	99.5
SB008	4.8	30.7	52.5	bdl	12.2	0.3	100.5
SB008	4.5	30.7	52.1	bdl	12.3	bdl	99.6
SB008	4.7	30.5	52.6	bdl	12.0	bdl	99.8
SB021	3.6	32.3	49.8	bdl	14.0	bdl	99.6
SB021	4.3	30.7	50.7	bdl	13.5	0.3	99.5
SB021	3.3	32.9	49.2	bdl	14.5	bdl	99.8
SB021	3.2	33.4	48.7	bdl	14.9	bdl	100.2
SB024	3.5	31.6	50.1	bdl	14.5	0.3	100.0
SB024	3.2	32.8	49.4	bdl	14.4	0.4	100.1
SB024	1.6	34.9	45.7	bdl	17.5	0.4	100.1
SB024	3.6	32.0	50.1	0.1	13.8	bdl	99.5
SB024	3.0	32.6	48.9	0.2	15.5	0.4	100.7
SB024	3.0	32.9	48.8	bdl	15.2	0.7	100.5
SB027	3.1	30.4	48.0	0.0	14.7	0.3	96.4
SB027	3.2	30.1	48.0	0.0	14.9	0.0	95.7
SB027	3.5	30.9	50.5	0.0	14.9	0.0	99.8
SB027	3.0	30.9	47.7	0.0	15.4	0.0	97.0
SB029	3.9	29.8	50.8	0.0	13.7	0.0	98.2
SB029	3.9	28.5	49.1	0.4	12.7	1.6	96.2
SB029	3.9	29.6	50.7	0.0	13.1	0.0	97.2
SB029	3.8	29.9	50.5	0.0	13.8	0.0	97.9
SB029	4.1	29.9	52.1	0.0	13.4	0.0	99.5
SB036	3.4	30.4	50.1	0.0	14.7	0.0	98.6
SB036	3.8	31.0	51.7	0.0	14.5	0.0	101.0
SB036	3.8	31.0	51.7	0.0	14.3	0.0	100.8
SB036	4.4	30.1	51.8	0.0	13.2	0.3	99.9

* bdl (below detection limit)

Pyroxene EDS analyses

Thin section	Na_2O (%)	MgO (%)	Al_2O_3 (%)	SiO_2 (%)	CaO (%)	TiO_2 (%)	MnO (%)	FeO (%)	Total
SB027	bdl	24	3	51	1.0	bdl	0.4	18.0	97.2
SB027	bdl	24	2	52	1.2	0.4	0.4	19.1	99.6
SB027	bdl	25	3	52	0.7	0.3	bdl	18.7	99.6
SB029	bdl	16	4	53	13.0	1.2	bdl	12.3	99.0
SB029	1.2	16	8	49	12.8	0.9	bdl	10.8	99.4
SB029	bdl	16	4	53	13.0	bdl	bdl	12.2	99.4
SB029	bdl	15	5	52	12.3	bdl	bdl	15.5	99.3
SB029	bdl	18	3	56	13.3	bdl	bdl	8.8	99.5
SB036	0.4	17	3	55	12.6	bdl	bdl	12.2	99.4
SB036	0.5	17	3	54	12.3	bdl	bdl	12.5	99.1
SB024	bdl	23	3	51	2.1	0.3	bdl	20.9	100.0
SB024	bdl	24	2	52	0.6	0.3	bdl	21.2	100.4
SB024	bdl	24	3	51	1.4	bdl	0.3	20.8	99.7
SB024	bdl	24	2	52	1.2	bdl	bdl	20.9	100.4

* bdl (below detection limit)

Appendix D

Whole-rock Geochemistry

All values are reported as anhydrous.

	SB001	SB002	SB003	SB004	SB005	SB006	SB007	SB008	SB009	SB010	SB011	SB012	SB013
Drillhole	14-902	14-902	14-902	14-902	14-902	14-902	14-902	14-902	14-902	14-902	14-902	14-902	14-902
From (m)	5.25	7.5	9.75	11.75	18.25	20.25	22.75	25.75	27.75	29.5	30.75	34.25	40.5
To (m)	5.5	7.75	10	12	18.5	20.5	23	26	28	29.75	31	34.5	40.75
SiO_2 (wt%)	31.28	32.49	31.98	29.24	41.84	31.33	40.52	43.95	50.81	51.35	50.15	50.77	31.21
Al_2O_3 (wt%)	10.44	12.30	15.28	10.96	12.78	10.78	12.92	13.81	21.56	19.92	17.53	22.09	14.40
Fe_2O_3 (wt%)	39.73	37.14	35.95	41.80	24.52	38.25	24.83	20.11	7.59	9.19	12.15	8.17	37.41
CaO (wt%)	7.26	7.56	7.72	7.02	10.30	8.06	11.11	11.74	11.29	8.91	8.74	10.11	6.45
MgO (wt%)	6.71	5.60	3.80	5.80	6.77	6.71	6.68	6.88	5.03	7.48	8.27	5.72	6.23
Na_2O (wt%)	0.98	1.41	1.74	0.98	1.67	0.98	1.55	1.66	3.04	2.63	2.46	2.68	1.17
K_2O (wt%)	0.07	0.07	0.07	0.10	0.14	0.07	0.08	0.12	0.35	0.20	0.23	0.17	0.05
Cr_2O_3 (wt%)	0.01	0.01	0.02	0.02	0.00	0.02	0.00	0.00	0.01	0.01	0.01	0.00	0.05
TiO_2 (wt%)	3.28	3.21	3.26	3.86	1.76	3.57	2.09	1.50	0.18	0.16	0.27	0.16	2.84
MnO (wt%)	0.21	0.19	0.15	0.21	0.18	0.20	0.19	0.18	0.09	0.11	0.14	0.09	0.15
P_2O_5 (wt%)	0.01	0.01	0.01	0.01	0.01	0.01	0.01	0.01	0.01	0.01	0.01	0.01	0.01
SrO (wt%)	0.01	0.02	0.02	0.01	0.02	0.01	0.02	0.02	0.04	0.03	0.03	0.03	0.02
BaO (wt%)	0.01	0.01	0.01	0.01	0.01	0.01	0.01	0.01	0.01	0.01	0.01	0.01	0.01
V_2O_5 (wt%)	0.43	0.41	0.43	0.49	0.22	0.44	0.22	0.16	0.03	0.02	0.04	0.02	0.51
LOI (wt%)	0.83	0.89	0.96	0.94	1.44	0.96	0.6	1.17	1.28	2.31	2.26	1.33	0.02
Mg#	0.27	0.25	0.19	0.23	0.38	0.28	0.37	0.43	0.59	0.64	0.60	0.61	0.27
Ba (ppm)	16.74	22.10	24.23	26.15	36.64	15.75	22.94	25.60	74.65	59.97	48.30	44.19	17.60
Ce (ppm)	1.51	1.11	0.91	0.81	2.03	1.11	1.21	1.01	1.42	3.17	1.43	1.22	0.60
Cr (ppm)	80.68	100.90	131.27	121.16	20.30	141.37	10.06	10.12	20.26	30.70	40.93	20.27	390.08
Cs (ppm)	0.66	0.71	0.79	1.10	1.00	0.56	0.57	0.60	1.81	1.76	1.62	0.83	0.12
Dy (ppm)	0.38	0.32	0.20	0.34	0.79	0.42	0.59	0.53	0.31	0.24	0.23	0.10	0.08
Er (ppm)	0.24	0.22	0.13	0.26	0.56	0.32	0.39	0.34	0.18	0.16	0.17	0.09	0.09
Eu (ppm)	0.13	0.11	0.12	0.13	0.23	0.13	0.19	0.16	0.15	0.16	0.13	0.12	0.07
Ga (ppm)	27.23	27.14	29.08	28.88	21.41	27.26	21.23	19.73	17.83	17.50	17.91	17.74	30.41
Gd (ppm)	0.34	0.25	0.19	0.28	0.70	0.35	0.52	0.45	0.30	0.30	0.24	0.09	0.07
Ge (ppm)	2.52	2.52	2.52	2.52	2.54	2.52	2.52	2.53	2.53	2.56	2.56	2.53	2.50
Hf (ppm)	0.20	0.20	0.10	0.20	0.30	0.20	0.20	0.20	0.10	0.10	0.10	0.10	0.10
Ho (ppm)	0.09	0.06	0.05	0.08	0.18	0.10	0.13	0.12	0.07	0.05	0.05	0.02	0.02
La (ppm)	0.71	0.61	0.50	0.30	1.01	0.50	0.50	0.40	0.71	1.74	0.72	0.61	0.30
Lu (ppm)	0.04	0.03	0.02	0.04	0.08	0.04	0.06	0.05	0.03	0.03	0.03	0.02	0.02
Nb (ppm)	0.30	0.50	0.20	0.20	0.91	0.20	0.10	0.10	0.20	0.20	0.20	0.10	0.10

	SB001	SB002	SB003	SB004	SB005	SB006	SB007	SB008	SB009	SB010	SB011	SB012	SB013
Nd (ppm)	0.81	0.71	0.50	0.50	1.32	0.71	1.01	0.81	0.81	1.43	0.72	0.51	0.30
Pr (ppm)	0.19	0.15	0.11	0.10	0.30	0.15	0.19	0.15	0.19	0.36	0.16	0.12	0.06
Rb (ppm)	1.51	1.31	1.31	3.74	3.65	1.31	1.21	3.04	10.74	7.16	8.08	2.84	0.30
Sm (ppm)	0.24	0.21	0.13	0.20	0.49	0.24	0.34	0.27	0.22	0.32	0.20	0.11	0.08
Sn (ppm)	1.01	0.50	0.50	0.50	0.51	0.50	0.50	0.51	0.51	0.51	0.51	0.51	0.50
Sr (ppm)	110.93	142.27	198.42	117.12	166.43	120.67	157.95	190.22	279.58	240.48	217.98	271.61	149.53
Ta (ppm)	0.05	0.05	0.05	0.05	0.20	0.05	0.10	0.05	0.05	0.05	0.05	0.05	0.05
Tb (ppm)	0.06	0.05	0.03	0.05	0.13	0.07	0.09	0.08	0.05	0.04	0.04	0.02	0.02
Th (ppm)	0.05	0.03	0.03	0.03	0.11	0.05	0.03	0.03	0.03	0.48	0.11	0.10	0.03
Tm (ppm)	0.04	0.03	0.02	0.04	0.08	0.05	0.07	0.05	0.03	0.02	0.02	0.02	0.01
U (ppm)	0.03	0.03	0.03	0.03	0.08	0.03	0.03	0.03	0.03	0.03	0.07	0.03	0.03
V (ppm)	2390.04	2280.36	2413.37	2766.52	1253.33	2473.93	1242.45	907.58	145.87	121.77	201.60	132.77	2840.57
W (ppm)	0.50	0.50	0.50	0.50	2.03	0.50	0.50	2.02	0.51	0.51	0.51	0.51	0.50
Y (ppm)	2.12	1.72	1.11	1.82	4.57	2.32	3.22	2.73	1.82	1.23	1.33	0.71	0.60
Yb (ppm)	0.26	0.22	0.14	0.22	0.56	0.28	0.39	0.32	0.19	0.15	0.19	0.10	0.09
Zr (ppm)	5.04	5.05	3.03	4.04	9.13	5.05	5.03	3.04	2.03	2.05	1.02	2.03	2.00
As (ppm)	0.20	0.30	0.30	0.30	0.30	0.20	0.10	0.20	0.30	0.51	0.31	0.20	0.10
Bi_ppm	0.12	0.08	0.02	0.18	0.11	0.02	0.01	0.02	0.04	0.04	0.08	0.03	0.10
Hg (ppm)	0.00	0.00	0.00	0.00	0.00	0.00	0.00	0.00	0.00	0.00	0.00	0.00	0.00
In (ppm)	0.01	0.01	0.01	0.01	0.01	0.00	0.01	0.00	0.00	0.00	0.00	0.00	0.02
Re (ppm)	0.00	0.00	0.00	0.00	0.00	0.00	0.00	0.00	0.00	0.00	0.00	0.00	0.00
Sb (ppm)	0.03	0.03	0.03	0.03	0.03	0.03	0.03	0.03	0.03	0.03	0.03	0.03	0.03
Se (ppm)	0.81	0.91	1.01	0.50	0.71	1.01	0.30	0.20	0.30	0.41	0.51	0.61	1.10
Te (ppm)	0.02	0.05	0.05	0.03	0.06	0.04	0.01	0.01	0.03	0.02	0.04	0.03	0.09
Tl (ppm)	0.04	0.03	0.03	0.04	0.03	0.02	0.01	0.01	0.01	0.02	0.03	0.02	0.01
Ag (ppm)	0.25	0.25	0.25	0.25	0.25	0.25	0.25	0.25	0.25	0.26	0.26	0.25	0.60
Cd (ppm)	0.81	1.11	0.81	0.81	0.51	0.71	0.50	0.25	0.25	0.26	0.26	0.25	0.60
Co (ppm)	188.58	162.45	141.37	165.59	111.63	165.60	104.63	83.98	43.56	59.35	81.87	58.78	149.03
Cu (ppm)	294.47	371.31	369.58	278.67	223.26	252.44	72.43	57.67	94.20	101.31	228.21	220.94	766.15
Li (ppm)	10.08	10.09	10.10	10.10	10.15	10.10	10.06	10.12	10.13	10.23	10.23	10.13	5.00
Mo (ppm)	0.50	1.01	0.50	0.50	0.51	0.50	0.50	0.51	0.51	0.51	0.51	0.51	0.50
Ni (ppm)	177.49	221.98	230.23	210.01	92.35	288.79	47.28	9.11	56.73	85.96	120.76	158.10	708.14
Pb (ppm)	2.02	2.02	2.02	2.02	1.01	2.02	2.01	2.02	2.03	1.02	1.02	1.01	3.00
Sc (ppm)	35.30	25.23	22.22	32.31	53.79	46.45	58.35	56.66	18.23	15.35	24.56	11.15	17.00
Zn (ppm)	173.45	170.52	144.40	166.60	100.47	164.59	117.71	92.07	39.51	62.42	68.57	42.57	132.03

	SB014	SB015	SB016	SB017	SB018	SB019	SB020	SB021	SB022	SB023	SB024	SB025	SB026
Drillhole	14-902	14-902	14-902	14-902	14-902	14-902	14-902	14-902	14-902	14-902	14-902	14-902	14-902
From (m)	43	50	54	55	58.25	58	64.5	67.5	67.75	69.75	72	75	77.5
To (m)	43.25	50.25	54.25	55.25	58.5	58.25	64.75	67.75	68	70	72.25	75.25	77.75
SiO_2 (wt%)	42.69	45.38	37.75	48.33	47.75	46.73	47.47	43.57	46.83	46.67	45.40	45.27	43.83
Al_2O_3 (wt%)	18.32	19.42	16.45	20.55	20.59	18.57	19.48	18.47	20.65	20.45	18.76	18.48	19.23
Fe_2O_3 (wt%)	19.85	15.85	27.53	11.29	11.89	14.69	13.09	18.73	13.29	13.36	16.33	16.60	17.97
CaO (wt%)	8.96	9.24	7.29	9.84	9.88	8.86	9.42	8.94	10.08	9.64	8.76	8.70	8.89
MgO (wt%)	6.88	6.64	7.05	7.10	7.24	8.49	7.94	7.23	5.70	7.00	7.92	8.14	7.10
Na_2O (wt%)	1.71	2.02	1.45	2.09	1.90	1.71	1.76	1.73	2.49	1.96	1.70	1.71	1.77
K_2O (wt%)	0.11	0.20	0.27	0.19	0.13	0.17	0.13	0.12	0.21	0.14	0.14	0.12	0.11
Cr_2O_3 (wt%)	0.04	0.04	0.09	0.03	0.04	0.05	0.05	0.04	0.01	0.05	0.05	0.05	0.05
TiO_2 (wt%)	1.29	1.05	1.94	0.41	0.45	0.57	0.49	1.00	0.59	0.58	0.79	0.77	0.91
MnO (wt%)	0.13	0.12	0.15	0.12	0.11	0.13	0.12	0.12	0.09	0.11	0.12	0.13	0.11
P_2O_5 (wt%)	0.00	0.01	0.01	0.01	0.01	0.01	0.02	0.01	0.01	0.01	0.01	0.01	0.01
SrO (wt%)	0.02	0.03	0.02	0.03	0.02	0.02	0.02	0.02	0.03	0.03	0.03	0.02	0.02
BaO (wt%)	0.00	0.01	0.01	0.01	0.00	0.01	0.01	0.01	0.01	0.01	0.01	0.01	0.01
V_2O_5 (wt%)	0.21	0.16	0.33	0.07	0.08	0.10	0.08	0.22	0.13	0.13	0.17	0.17	0.19
LOI (wt%)	0.02	1.41	1.31	1.8	1.02	1.32	1.53	2.09	1.95	0.94	0.55	0.02	0.52
Mg#	0.43	0.48	0.36	0.58	0.57	0.56	0.57	0.46	0.49	0.54	0.52	0.52	0.47
Ba (ppm)	32.81	64.30	56.64	49.08	38.79	36.68	34.43	35.86	50.08	44.72	43.24	37.21	36.79
Ce (ppm)	1.10	1.12	1.01	1.63	1.11	1.01	1.02	1.23	1.02	1.41	1.41	1.60	1.41
Cr (ppm)	270.05	253.55	638.35	234.21	272.74	354.66	396.05	296.27	40.80	343.24	341.89	350.07	382.00
Cs (ppm)	0.59	1.36	2.31	1.40	0.92	1.08	0.96	0.97	1.30	2.04	1.90	0.62	1.07
Dy (ppm)	0.17	0.16	0.08	0.17	0.12	0.13	0.12	0.14	0.13	0.13	0.15	0.18	0.11
Er (ppm)	0.12	0.13	0.08	0.15	0.10	0.12	0.10	0.09	0.08	0.11	0.07	0.11	0.10
Eu (ppm)	0.10	0.10	0.08	0.12	0.09	0.10	0.09	0.09	0.10	0.11	0.09	0.09	0.07
Ga (ppm)	21.60	19.37	24.72	18.23	18.38	17.73	18.79	19.92	18.46	18.78	18.40	18.40	19.20
Gd (ppm)	0.13	0.12	0.11	0.17	0.12	0.09	0.11	0.10	0.10	0.11	0.10	0.11	0.07
Ge (ppm)	2.50	2.54	2.53	2.55	2.53	2.53	2.54	2.55	2.55	2.52	2.51	2.50	2.51
Hf (ppm)	0.10	0.20	0.10	0.10	0.10	0.10	0.10	0.10	0.10	0.10	0.10	0.10	0.10
Ho (ppm)	0.04	0.03	0.03	0.04	0.03	0.04	0.03	0.03	0.03	0.03	0.03	0.03	0.03
La (ppm)	0.60	0.71	0.61	0.81	0.61	0.51	0.51	0.61	0.51	0.71	0.70	0.80	0.70
Lu (ppm)	0.03	0.03	0.02	0.03	0.02	0.02	0.02	0.02	0.01	0.02	0.02	0.02	0.01
Nb (ppm)	0.20	0.51	0.20	0.20	0.10	0.10	0.10	0.10	0.10	0.10	0.20	0.10	0.20

	SB014	SB015	SB016	SB017	SB018	SB019	SB020	SB021	SB022	SB023	SB024	SB025	SB026
Nd (ppm)	0.50	0.51	0.41	0.71	0.40	0.41	0.41	0.61	0.51	0.61	0.60	0.80	0.70
Pr (ppm)	0.13	0.13	0.11	0.18	0.12	0.12	0.10	0.15	0.11	0.15	0.14	0.18	0.15
Rb (ppm)	1.60	4.36	7.19	4.48	2.53	3.55	2.54	2.35	5.41	3.53	3.52	1.90	2.51
Sm (ppm)	0.12	0.11	0.09	0.14	0.10	0.09	0.08	0.16	0.11	0.11	0.08	0.15	0.09
Sn (ppm)	0.50	0.51	0.51	0.51	0.51	0.51	0.51	0.51	0.51	0.50	0.50	0.50	0.50
Sr (ppm)	208.04	227.18	188.97	247.45	234.35	209.76	222.40	204.33	278.44	248.34	225.25	217.04	220.15
Ta (ppm)	0.05	0.10	0.05	0.05	0.05	0.05	0.05	0.05	0.05	0.05	0.05	0.05	0.05
Tb (ppm)	0.03	0.02	0.01	0.03	0.02	0.02	0.02	0.02	0.02	0.02	0.02	0.02	0.01
Th (ppm)	0.06	0.09	0.05	0.10	0.06	0.06	0.03	0.11	0.06	0.08	0.12	0.17	0.15
Tm (ppm)	0.02	0.02	0.01	0.02	0.02	0.02	0.02	0.01	0.01	0.02	0.01	0.02	0.01
U (ppm)	0.03	0.03	0.05	0.03	0.03	0.03	0.03	0.03	0.03	0.03	0.03	0.03	0.03
V (ppm)	1175.23	903.64	1823.86	406.31	474.77	572.53	475.26	1236.17	703.76	738.97	930.14	931.19	1085.68
W (ppm)	0.50	0.51	0.51	0.51	0.51	0.51	0.51	0.51	0.51	0.50	0.50	0.50	0.50
Y (ppm)	1.00	1.01	0.61	1.02	0.71	0.81	0.81	0.92	0.71	0.81	0.80	0.90	0.70
Yb (ppm)	0.15	0.14	0.10	0.15	0.12	0.14	0.10	0.09	0.10	0.10	0.13	0.16	0.11
Zr (ppm)	3.00	5.07	3.04	3.05	3.03	3.04	3.05	3.06	2.04	3.03	3.02	3.00	3.02
As (ppm)	0.10	0.41	0.30	0.20	0.30	0.30	0.61	0.31	0.61	0.20	0.20	0.20	0.05
Bi_ppm	0.04	0.01	0.02	0.02	0.01	0.01	0.01	0.01	0.02	0.01	0.01	0.01	0.01
Hg (ppm)	0.00	0.00	0.00	0.00	0.00	0.00	0.00	0.00	0.00	0.00	0.00	0.00	0.00
In (ppm)	0.01	0.00	0.01	0.00	0.00	0.00	0.00	0.00	0.00	0.00	0.00	0.00	0.00
Re (ppm)	0.00	0.00	0.00	0.00	0.00	0.00	0.00	0.00	0.00	0.00	0.00	0.00	0.00
Sb (ppm)	0.03	0.03	0.03	0.03	0.03	0.03	0.03	0.03	0.03	0.03	0.03	0.03	0.03
Se (ppm)	0.50	0.10	0.10	0.20	0.20	0.30	0.30	0.10	0.71	0.30	0.10	0.20	0.20
Te (ppm)	0.03	0.01	0.01	0.01	0.01	0.01	0.01	0.01	0.06	0.01	0.01	0.01	0.01
Tl (ppm)	0.01	0.01	0.04	0.01	0.01	0.01	0.01	0.01	0.01	0.01	0.02	0.01	0.01
Ag (ppm)	0.25	0.25	0.25	0.25	0.25	0.25	0.25	0.26	0.25	0.25	0.25	0.25	0.25
Cd (ppm)	0.25	0.25	0.25	0.25	0.25	0.25	0.25	0.26	0.25	0.25	0.25	0.25	0.25
Co (ppm)	91.02	74.04	106.39	56.01	59.60	71.95	69.06	85.82	66.30	67.64	79.44	80.02	78.41
Cu (ppm)	196.04	40.57	25.33	22.40	23.23	12.16	17.26	51.08	353.92	28.27	47.26	47.01	19.10
Li (ppm)	5.00	10.14	10.13	10.18	10.10	10.13	10.16	20.43	10.20	5.05	5.03	5.00	5.03
Mo (ppm)	0.50	0.51	0.51	0.51	0.51	0.51	0.51	0.51	0.51	0.50	0.50	0.50	0.50
Ni (ppm)	311.06	254.56	376.93	195.52	170.71	185.44	120.85	192.07	324.34	236.23	285.58	284.06	289.52
Pb (ppm)	1.00	2.03	1.01	1.02	1.01	1.01	2.03	1.02	1.02	1.01	1.01	1.00	1.01
Sc (ppm)	21.00	17.24	17.23	16.29	17.17	20.27	19.29	20.43	17.34	14.13	19.11	21.00	17.09
Zn (ppm)	85.02	77.08	104.37	59.06	57.58	65.87	61.95	76.62	53.04	61.58	71.39	74.02	72.38

	SB027	SB028	SB029	SB030	SB031	SB032	SB033	SB034	SB035	SB036	SB037	SB038	SB039
Drillhole	14-902	14-902	14-902	14-902	14-902	14-902	14-902	14-902	14-902	14-902	14-902	14-902	20-200
From (m)	80	81.75	87	89	92	99	96	97.5	99.25	101	105	107.75	409
To (m)	80.25	82	87.25	89.25	92.25	99.25	96.25	97.75	99.5	101.25	105.25	108	410
SiO_2 (wt%)	38.21	43.15	34.85	36.41	39.83	33.34	36.80	4.26	25.71	24.40	27.90	32.82	49.96
Al_2O_3 (wt%)	14.23	17.77	12.35	12.38	13.95	11.15	17.06	6.91	11.42	11.43	10.90	12.97	23.48
Fe_2O_3 (wt%)	28.66	19.97	31.88	29.44	25.42	35.36	28.43	78.56	47.12	48.38	42.26	34.67	6.10
CaO (wt%)	6.33	8.17	10.56	10.77	10.34	8.40	7.77	0.74	4.34	4.40	7.90	9.16	11.38
MgO (wt%)	9.12	7.75	6.29	7.15	7.05	8.11	6.15	2.98	6.87	6.42	6.17	5.88	6.51
Na_2O (wt%)	1.20	1.66	1.05	1.17	1.45	0.84	1.62	0.06	0.91	1.00	0.70	1.11	2.11
K_2O (wt%)	0.12	0.15	0.11	0.15	0.15	0.08	0.23	0.02	0.07	0.11	0.07	0.25	0.19
Cr_2O_3 (wt%)	0.09	0.05	0.00	0.03	0.01	0.08	0.03	0.04	0.09	0.09	0.03	0.01	0.02
TiO_2 (wt%)	1.85	1.16	2.69	2.31	1.61	2.44	1.76	6.25	3.29	3.59	3.85	2.94	0.12
MnO (wt%)	0.16	0.14	0.17	0.19	0.15	0.17	0.11	0.18	0.15	0.16	0.19	0.16	0.08
P_2O_5 (wt%)	0.01	0.01	0.02	0.01	0.01	0.01	0.01	0.01	0.01	0.01	0.01	0.01	0.01
SrO (wt%)	0.02	0.02	0.02	0.01	0.01	0.01	0.02	0.01	0.01	0.01	0.01	0.02	0.03
BaO (wt%)	0.01	0.01	0.01	0.01	0.01	0.01	0.01	0.01	0.01	0.01	0.01	0.01	0.01
V_2O_5 (wt%)	0.36	0.22	0.37	0.32	0.30	0.44	0.33	1.31	0.66	0.73	0.53	0.42	0.02
LOI (wt%)	0.13	0.44	1.69	1.99	2.09	1.75	2.55	0.02	1.38	1.45	1.19	1.51	1.18
Mg#	0.41	0.46	0.30	0.35	0.38	0.34	0.32	0.08	0.24	0.23	0.24	0.27	0.70
Ba (ppm)	28.04	40.48	26.04	35.62	42.39	22.70	50.39	3.10	23.02	29.03	13.06	44.99	52.43
Ce (ppm)	0.90	1.31	4.27	2.65	2.86	1.12	0.82	0.60	0.91	0.91	0.81	1.02	2.02
Cr (ppm)	630.82	401.76	30.52	204.14	51.08	580.11	164.22	210.04	608.48	629.25	202.42	91.39	141.70
Cs (ppm)	1.02	1.10	0.56	1.02	0.73	0.59	1.18	0.11	0.79	1.20	0.37	0.92	1.00
Dy (ppm)	0.19	0.13	0.69	0.94	0.51	0.42	0.10	0.03	0.12	0.10	0.45	0.40	0.20
Er (ppm)	0.17	0.10	0.42	0.57	0.31	0.24	0.08	0.02	0.09	0.06	0.30	0.26	0.19
Eu (ppm)	0.08	0.08	0.19	0.21	0.16	0.12	0.06	0.01	0.05	0.05	0.12	0.12	0.16
Ga (ppm)	21.53	19.79	23.50	20.31	20.33	22.29	21.86	45.21	27.38	30.55	27.12	24.27	15.59
Gd (ppm)	0.14	0.06	0.64	0.79	0.42	0.34	0.09	0.03	0.10	0.06	0.34	0.30	0.25
Ge (ppm)	2.50	2.51	2.54	2.55	2.55	2.54	2.57	2.50	2.54	2.54	2.53	2.54	2.53
Hf (ppm)	0.10	0.10	0.41	0.31	0.31	0.20	0.10	0.20	0.10	0.10	0.20	0.20	0.20
Ho (ppm)	0.04	0.02	0.14	0.17	0.09	0.09	0.03	0.01	0.03	0.02	0.09	0.10	0.06
La (ppm)	0.50	0.70	1.83	1.02	1.33	0.41	0.41	0.30	0.41	0.41	0.30	0.41	1.11
Lu (ppm)	0.04	0.02	0.06	0.07	0.05	0.04	0.01	0.01	0.02	0.02	0.05	0.04	0.03
Nb (ppm)	0.20	0.20	0.41	0.10	0.31	0.10	0.10	0.30	0.20	0.20	0.10	0.10	0.20

	SB027	SB028	SB029	SB030	SB031	SB032	SB033	SB034	SB035	SB036	SB037	SB038	SB039
Nd (ppm)	0.50	0.60	2.75	1.84	1.74	1.02	0.41	0.30	0.41	0.41	0.71	0.81	0.91
Pr (ppm)	0.11	0.14	0.55	0.36	0.35	0.16	0.10	0.07	0.09	0.08	0.12	0.14	0.26
Rb (ppm)	2.80	3.41	1.83	2.65	3.06	2.44	6.67	0.40	2.54	3.04	1.01	5.89	3.54
Sm (ppm)	0.10	0.13	0.54	0.50	0.39	0.25	0.06	0.10	0.06	0.03	0.26	0.21	0.16
Sn (ppm)	0.50	0.50	0.51	0.51	0.51	0.51	0.51	1.00	0.51	0.51	0.51	0.51	0.51
Sr (ppm)	138.68	215.95	153.62	129.63	132.80	109.92	149.34	18.80	73.63	73.18	110.32	142.17	245.95
Ta (ppm)	0.05	0.05	0.10	0.05	0.05	0.05	0.05	0.05	0.05	0.05	0.05	0.05	0.05
Tb (ppm)	0.04	0.02	0.10	0.13	0.07	0.05	0.01	0.01	0.02	0.02	0.07	0.06	0.03
Th (ppm)	0.09	0.13	0.39	0.38	0.39	0.10	0.05	0.12	0.10	0.12	0.08	0.03	0.14
Tm (ppm)	0.04	0.02	0.06	0.07	0.05	0.04	0.01	0.01	0.01	0.01	0.05	0.04	0.02
U (ppm)	0.03	0.03	0.06	0.03	0.07	0.03	0.03	0.03	0.03	0.03	0.03	0.03	0.03
V (ppm)	2002.61	1205.29	2095.69	1776.02	1695.71	2483.27	1837.19	7321.52	3711.74	4110.45	2965.51	2345.78	91.09
W (ppm)	0.50	0.50	0.51	1.02	0.51	0.51	0.51	2.00	0.51	0.51	0.51	0.51	0.51
Y (ppm)	0.70	0.70	3.56	4.70	2.66	2.04	0.62	0.10	0.61	0.51	2.02	2.03	1.42
Yb (ppm)	0.13	0.11	0.33	0.52	0.33	0.24	0.08	0.02	0.10	0.09	0.27	0.23	0.16
Zr (ppm)	3.00	4.02	13.23	6.12	8.17	4.07	2.05	5.00	4.06	4.06	3.04	4.06	6.07
As (ppm)	0.30	0.40	0.31	0.41	0.41	0.31	0.31	0.20	0.10	0.20	0.40	0.41	0.71
Bi_ppm	0.01	0.02	0.03	0.04	0.03	0.06	0.10	0.08	0.05	0.14	0.01	0.03	0.01
Hg (ppm)	0.00	0.00	0.00	0.00	0.00	0.00	0.00	0.00	0.00	0.00	0.00	0.00	0.00
In (ppm)	0.01	0.00	0.01	0.01	0.00	0.00	0.01	0.03	0.01	0.01	0.00	0.00	0.00
Re (ppm)	0.00	0.00	0.00	0.00	0.00	0.00	0.00	0.00	0.00	0.00	0.00	0.01	0.00
Sb (ppm)	0.03	0.03	0.03	0.03	0.03	0.03	0.03	0.03	0.03	0.03	0.03	0.03	0.03
Se (ppm)	0.10	0.30	0.81	0.82	0.92	0.71	1.33	0.60	0.20	0.51	0.40	1.22	0.10
Te (ppm)	0.01	0.02	0.07	0.07	0.07	0.05	0.09	0.04	0.05	0.05	0.02	0.06	0.01
Tl (ppm)	0.01	0.01	0.01	0.01	0.01	0.01	0.01	0.01	0.01	0.01	0.01	0.01	0.01
Ag (ppm)	0.25	0.25	0.61	0.26	0.26	0.25	0.26	0.25	0.25	0.25	0.25	0.25	0.25
Cd (ppm)	0.25	0.25	0.61	0.71	0.26	0.25	0.51	0.25	0.61	0.91	0.61	0.51	0.25
Co (ppm)	122.16	88.39	152.60	113.30	134.84	161.82	148.82	264.05	173.42	183.70	162.95	155.37	39.47
Cu (ppm)	27.04	41.18	277.73	245.99	271.72	231.03	421.83	340.07	313.37	392.78	186.23	420.41	16.19
Li (ppm)	10.01	5.02	10.17	10.21	10.22	10.18	10.26	10.00	20.28	20.30	10.12	10.15	10.12
Mo (ppm)	0.50	1.00	0.51	1.02	0.51	0.51	0.51	0.50	0.51	0.51	0.51	0.51	0.51
Ni (ppm)	436.57	308.35	153.62	203.12	110.32	308.37	301.75	951.20	710.91	753.08	150.81	268.09	173.08
Pb (ppm)	2.00	2.01	3.05	1.02	1.02	2.04	2.05	6.00	3.04	3.04	3.04	3.05	1.01
Sc (ppm)	16.02	19.08	47.81	46.95	41.88	33.59	19.50	13.00	11.16	16.24	40.48	41.64	12.15
Zn (ppm)	117.15	87.38	114.96	109.22	93.98	126.20	103.66	234.05	160.23	167.46	175.10	127.95	37.45

	SB040	SB041	SB042	SB043	SB044	SB045	SB046	SB047	SB048	SB049	SB050	SB051	SB052
Drillhole	20-200	20-200	20-200	20-200	20-200	20-200	20-200	20-200	20-200	20-200	20-200	20-200	20-200
From (m)	415	419	426	426	439	443	457	466	473	478	487	491	493
To (m)	416	420	427	427	440	444	458	467	474	479	488	492	494
SiO_2 (wt%)	58.26	49.96	50.17	49.75	50.54	50.51	47.00	47.19	47.41	50.15	48.05	46.73	46.42
Al_2O_3 (wt%)	17.93	23.44	23.39	25.03	21.38	18.90	18.72	21.31	16.07	17.79	17.87	16.57	15.01
Fe_2O_3 (wt%)	6.51	6.07	6.10	5.22	7.46	9.04	13.99	12.00	15.72	12.49	13.38	15.92	17.49
CaO (wt%)	12.22	10.79	10.95	11.65	10.33	9.22	8.70	9.81	7.42	8.18	8.33	7.84	7.06
MgO (wt%)	2.61	6.47	6.23	5.09	7.81	10.13	9.04	6.79	11.15	8.46	9.65	10.61	11.78
Na_2O (wt%)	1.63	2.31	2.21	2.60	1.95	1.76	1.73	2.10	1.37	2.09	1.86	1.49	1.31
K_2O (wt%)	0.07	0.67	0.67	0.41	0.25	0.09	0.15	0.18	0.14	0.23	0.27	0.13	0.14
Cr_2O_3 (wt%)	0.01	0.02	0.02	0.01	0.02	0.02	0.06	0.02	0.06	0.05	0.05	0.07	0.07
TiO_2 (wt%)	0.48	0.12	0.13	0.12	0.12	0.14	0.45	0.45	0.48	0.38	0.37	0.47	0.52
MnO (wt%)	0.07	0.09	0.08	0.07	0.10	0.13	0.13	0.10	0.15	0.13	0.14	0.15	0.17
P_2O_5 (wt%)	0.12	0.01	0.01	0.01	0.01	0.01	0.01	0.00	0.01	0.01	0.01	0.00	0.01
SrO (wt%)	0.08	0.03	0.02	0.03	0.02	0.02	0.02	0.03	0.02	0.02	0.02	0.02	0.02
BaO (wt%)	0.01	0.02	0.02	0.01	0.01	0.01	0.01	0.01	0.01	0.01	0.01	0.00	0.00
V_2O_5 (wt%)	0.02	0.02	0.02	0.01	0.02	0.02	0.13	0.12	0.14	0.10	0.10	0.13	0.14
LOI (wt%)	2.44	3.15	2.69	2.14	1.74	1.8	1.96	0.79	1.63	1.8	1.66	0.06	0.06
Mg#	0.47	0.70	0.69	0.68	0.70	0.71	0.59	0.55	0.61	0.60	0.61	0.59	0.60
Ba (ppm)	34.13	173.44	186.67	115.97	61.07	39.41	48.44	53.62	38.42	62.82	57.14	35.22	32.52
Ce (ppm)	33.92	2.06	1.85	1.94	1.93	1.63	1.63	1.71	1.42	5.60	1.83	1.30	1.00
Cr (ppm)	71.74	144.53	123.42	102.18	162.85	183.32	428.29	181.41	437.04	325.82	325.36	480.29	440.26
Cs (ppm)	0.36	3.29	3.06	2.34	1.33	1.31	1.71	1.18	4.84	1.98	1.90	0.72	0.63
Dy (ppm)	2.17	0.22	0.22	0.27	0.23	0.24	0.17	0.22	0.18	0.27	0.26	0.15	0.17
Er (ppm)	0.92	0.15	0.17	0.22	0.19	0.16	0.10	0.12	0.11	0.17	0.20	0.16	0.09
Eu (ppm)	0.92	0.19	0.15	0.17	0.13	0.10	0.11	0.12	0.10	0.13	0.10	0.09	0.08
Ga (ppm)	20.39	16.93	16.25	17.98	15.06	13.95	17.34	18.34	15.65	15.68	15.86	16.01	14.61
Gd (ppm)	2.89	0.25	0.24	0.18	0.17	0.16	0.15	0.12	0.15	0.42	0.16	0.13	0.10
Ge (ppm)	2.56	2.58	2.57	2.55	2.54	2.55	2.55	2.52	2.54	2.55	2.54	2.50	2.50
Hf (ppm)	2.36	0.10	0.21	0.10	0.20	0.10	0.10	0.20	0.20	0.61	0.10	0.10	0.10
Ho (ppm)	0.38	0.04	0.05	0.05	0.02	0.05	0.02	0.03	0.05	0.07	0.04	0.03	0.04
La (ppm)	16.19	1.03	1.03	1.02	1.02	0.92	1.02	1.01	0.91	2.95	1.12	0.70	0.60
Lu (ppm)	0.11	0.03	0.04	0.01	0.02	0.03	0.03	0.03	0.04	0.03	0.02	0.03	0.02
Nb (ppm)	4.10	0.21	0.21	0.20	0.20	0.10	0.20	0.40	0.30	0.81	0.31	0.20	0.10

	SB040	SB041	SB042	SB043	SB044	SB045	SB046	SB047	SB048	SB049	SB050	SB051	SB052
Nd (ppm)	18.24	0.93	0.62	0.92	0.81	0.81	0.61	0.71	0.51	1.93	0.61	0.60	0.50
Pr (ppm)	4.01	0.24	0.25	0.25	0.21	0.16	0.16	0.19	0.15	0.56	0.20	0.13	0.12
Rb (ppm)	1.74	18.58	18.10	11.24	6.92	2.44	4.79	5.14	7.01	6.31	8.54	3.10	3.60
Sm (ppm)	3.55	0.02	0.07	0.24	0.15	0.10	0.15	0.20	0.20	0.34	0.16	0.06	0.13
Sn (ppm)	1.02	0.52	0.51	0.51	0.51	0.51	0.51	0.50	0.51	0.51	0.51	0.50	0.50
Sr (ppm)	623.11	261.19	250.95	290.18	240.20	203.18	203.95	244.90	164.65	195.49	189.63	173.60	149.59
Ta (ppm)	0.20	0.05	0.05	0.05	0.05	0.05	0.05	0.05	0.05	0.10	0.05	0.05	0.05
Tb (ppm)	0.43	0.04	0.04	0.07	0.04	0.03	0.03	0.03	0.02	0.03	0.02	0.02	0.02
Th (ppm)	2.01	0.08	0.11	0.11	0.13	0.10	0.15	0.12	0.32	0.75	0.15	0.09	0.06
Tm (ppm)	0.13	0.02	0.03	0.01	0.03	0.01	0.01	0.02	0.02	0.03	0.03	0.02	0.02
U (ppm)	0.47	0.03	0.03	0.03	0.03	0.03	0.03	0.03	0.03	0.20	0.05	0.03	0.03
V (ppm)	109.66	100.14	88.45	81.74	115.01	131.38	705.65	662.15	760.25	551.86	551.08	719.43	785.47
W (ppm)	1.02	1.03	0.51	0.51	0.51	1.02	0.51	0.50	0.51	0.51	0.51	0.50	0.50
Y (ppm)	10.66	1.24	1.13	1.23	1.53	1.43	1.12	1.11	1.22	1.93	1.42	1.10	1.10
Yb (ppm)	0.79	0.19	0.15	0.14	0.14	0.15	0.18	0.10	0.25	0.16	0.16	0.19	0.22
Zr (ppm)	87.11	5.16	5.14	5.11	6.11	5.09	5.10	5.04	5.08	16.29	5.08	4.00	3.00
As (ppm)	0.41	0.10	0.10	0.10	0.10	0.05	0.10	0.05	0.20	0.10	0.20	0.10	0.10
Bi_ppm	0.04	0.03	0.01	0.01	0.01	0.01	0.01	0.01	0.01	0.01	0.01	0.01	0.01
Hg (ppm)	0.00	0.00	0.00	0.00	0.00	0.00	0.00	0.00	0.00	0.00	0.00	0.00	0.00
In (ppm)	0.01	0.00	0.00	0.00	0.00	0.00	0.00	0.00	0.01	0.00	0.00	0.00	0.00
Re (ppm)	0.00	0.00	0.00	0.00	0.00	0.00	0.00	0.00	0.00	0.00	0.00	0.00	0.00
Sb (ppm)	0.03	0.03	0.03	0.03	0.03	0.03	0.03	0.03	0.03	0.03	0.03	0.03	0.03
Se (ppm)	0.20	0.10	0.10	0.10	0.10	0.10	0.10	0.10	0.10	0.10	0.10	0.10	0.10
Te (ppm)	0.01	0.01	0.01	0.01	0.01	0.01	0.01	0.01	0.01	0.01	0.01	0.01	0.01
Tl (ppm)	0.01	0.02	0.01	0.01	0.01	0.01	0.01	0.01	0.05	0.03	0.02	0.01	0.01
Ag (ppm)	0.26	0.26	0.26	0.26	0.25	0.25	0.25	0.25	0.25	0.25	0.25	0.25	0.25
Cd (ppm)	0.26	0.26	0.26	0.26	0.25	0.25	0.25	0.25	0.25	0.25	0.25	0.50	0.50
Co (ppm)	19.47	41.30	40.11	32.70	50.89	65.18	83.62	68.53	96.56	76.36	83.37	95.06	105.06
Cu (ppm)	65.59	10.32	11.31	8.17	10.18	6.11	8.16	10.08	7.11	12.22	9.15	8.00	8.00
Li (ppm)	10.25	20.65	10.28	10.22	10.18	10.18	10.20	5.04	10.16	10.18	10.17	5.00	5.00
Mo (ppm)	0.51	0.52	0.51	0.51	0.51	0.51	0.51	0.50	0.51	1.02	0.51	0.50	1.00
Ni (ppm)	64.57	179.63	168.67	133.85	203.56	262.76	466.01	243.90	356.75	269.82	298.93	354.21	394.24
Pb (ppm)	3.07	3.10	2.06	2.04	2.04	1.02	3.06	2.02	1.02	2.04	3.05	2.00	1.00
Sc (ppm)	11.27	11.36	11.31	9.20	14.25	24.44	23.45	14.11	24.39	17.31	21.35	21.01	20.01
Zn (ppm)	35.87	40.26	37.02	29.63	42.75	55.00	63.22	55.43	78.26	66.18	66.09	75.04	82.05

	SB053	SB054	SB055	SB056	SB057	SB058	SB059	SB060	SB061	SB062	SB063	SB064	SB065
Drillhole	20-200	20-200	20-200	20-200	20-200	20-200	20-200	20-200	20-200	20-200	20-200	20-200	20-200
From (m)	507	509	512	521	526	531	540	542	548	556	562	566	577
To (m)	508	510	513	522	527	532	541	543	549	557	563	567	578
SiO_2 (wt%)	48.10	48.70	47.10	47.80	48.57	49.05	50.10	51.93	52.15	50.01	47.33	48.08	46.88
Al_2O_3 (wt%)	18.06	17.25	15.02	16.05	16.22	16.30	14.65	15.26	18.22	21.63	16.93	17.60	17.95
Fe_2O_3 (wt%)	13.01	13.75	16.70	14.98	13.62	13.37	13.22	12.04	11.11	8.11	15.07	13.95	14.91
CaO (wt%)	8.28	8.10	7.26	7.91	8.03	7.94	7.31	7.53	7.93	10.46	8.19	8.46	9.04
MgO (wt%)	9.61	9.62	11.67	10.91	11.27	11.16	12.60	11.11	6.67	7.22	9.91	9.38	8.55
Na_2O (wt%)	1.94	1.64	1.32	1.47	1.47	1.43	1.29	1.31	2.62	2.05	1.54	1.59	1.78
K_2O (wt%)	0.43	0.34	0.22	0.25	0.31	0.24	0.37	0.35	0.75	0.19	0.25	0.26	0.16
Cr_2O_3 (wt%)	0.05	0.06	0.06	0.06	0.04	0.05	0.05	0.05	0.04	0.02	0.15	0.10	0.06
TiO_2 (wt%)	0.34	0.38	0.43	0.37	0.28	0.26	0.22	0.24	0.34	0.15	0.45	0.40	0.49
MnO (wt%)	0.13	0.13	0.16	0.15	0.15	0.15	0.16	0.14	0.11	0.10	0.14	0.14	0.14
P_2O_5 (wt%)	0.01	0.01	0.02	0.01	0.01	0.01	0.01	0.01	0.01	0.01	0.01	0.01	0.00
SrO (wt%)	0.02	0.01	0.02	0.03	0.02	0.03	0.02	0.02	0.03	0.03	0.02	0.02	0.03
BaO (wt%)	0.01	0.01	0.01	0.01	0.01	0.01	0.01	0.01	0.02	0.01	0.01	0.01	0.01
V_2O_5 (wt%)	0.09	0.10	0.14	0.09	0.07	0.06	0.04	0.04	0.09	0.02	0.12	0.10	0.11
LOI (wt%)	3.47	1.6	0.59	0.96	1.61	2.32	2.19	3.47	1.74	1.36	1.64	2.17	0.37
Mg#	0.62	0.61	0.61	0.62	0.65	0.65	0.68	0.67	0.57	0.66	0.59	0.60	0.56
Ba (ppm)	78.72	66.06	47.48	41.30	48.38	50.89	70.14	82.95	196.36	50.38	54.40	61.03	36.94
Ce (ppm)	2.07	2.54	1.71	2.02	1.32	1.33	1.74	3.73	4.99	1.72	1.63	1.74	2.01
Cr (ppm)	352.18	426.82	432.58	333.23	325.26	317.40	316.96	321.02	305.23	141.92	1057.55	766.76	381.40
Cs (ppm)	2.22	1.66	0.92	1.65	1.45	1.80	1.77	2.20	4.37	1.14	1.80	1.50	0.53
Dy (ppm)	0.26	0.24	0.21	0.24	0.18	0.16	0.22	0.31	0.24	0.24	0.18	0.22	0.26
Er (ppm)	0.25	0.17	0.22	0.18	0.14	0.22	0.26	0.54	0.18	0.13	0.11	0.17	0.27
Eu (ppm)	0.08	0.11	0.09	0.09	0.07	0.12	0.09	0.11	0.14	0.09	0.10	0.09	0.07
Ga (ppm)	16.47	16.46	16.30	14.34	14.74	14.23	13.60	13.77	18.72	17.33	18.30	18.61	15.16
Gd (ppm)	0.21	0.15	0.15	0.15	0.19	0.11	0.24	0.58	0.25	0.16	0.19	0.17	0.31
Ge (ppm)	2.59	2.54	2.51	2.52	2.54	2.56	2.56	2.59	2.54	2.53	2.54	2.56	2.51
Hf (ppm)	0.10	0.20	0.10	0.10	0.10	0.10	0.20	0.21	0.51	0.20	0.10	0.20	0.20
Ho (ppm)	0.04	0.04	0.05	0.04	0.03	0.03	0.05	0.07	0.05	0.05	0.05	0.05	0.07
La (ppm)	1.55	1.32	1.51	1.62	0.71	0.61	0.92	2.80	2.85	0.91	0.81	1.02	1.81
Lu (ppm)	0.01	0.03	0.03	0.03	0.04	0.03	0.03	0.03	0.04	0.01	0.03	0.04	0.03
Nb (ppm)	0.52	0.30	0.20	0.20	0.10	0.10	0.31	0.52	0.71	0.20	0.20	0.31	0.20

	SB053	SB054	SB055	SB056	SB057	SB058	SB059	SB060	SB061	SB062	SB063	SB064	SB065
Nd (ppm)	0.62	0.91	0.70	0.81	0.51	0.51	0.72	1.24	1.53	0.71	0.61	0.82	0.80
Pr (ppm)	0.21	0.25	0.22	0.21	0.14	0.17	0.20	0.32	0.42	0.21	0.18	0.20	0.18
Rb (ppm)	14.19	10.47	7.34	7.07	8.84	7.47	10.74	9.32	19.94	5.68	9.66	10.12	3.61
Sm (ppm)	0.12	0.17	0.20	0.12	0.10	0.11	0.09	0.33	0.33	0.22	0.16	0.17	0.12
Sn (ppm)	0.52	0.51	0.50	0.50	0.51	0.51	0.51	0.52	0.51	0.51	0.51	0.51	0.50
Sr (ppm)	187.48	184.45	160.46	158.03	165.17	164.84	157.97	152.74	248.25	245.31	187.61	199.87	175.14
Ta (ppm)	0.05	0.05	0.05	0.05	0.05	0.05	0.05	0.10	0.10	0.05	0.05	0.10	0.05
Tb (ppm)	0.03	0.04	0.03	0.04	0.02	0.03	0.03	0.05	0.05	0.03	0.04	0.02	0.05
Th (ppm)	0.11	0.27	0.11	0.12	0.06	0.08	0.11	0.35	0.90	0.12	0.22	0.18	0.15
Tm (ppm)	0.01	0.01	0.02	0.03	0.03	0.03	0.04	0.04	0.02	0.02	0.02	0.01	0.02
U (ppm)	0.06	0.08	0.03	0.06	0.03	0.03	0.03	0.07	0.30	0.03	0.05	0.06	0.05
V (ppm)	481.66	573.16	762.54	530.14	399.46	352.21	228.00	243.35	486.33	125.70	647.75	585.80	605.23
W (ppm)	1.04	1.02	1.01	1.01	0.51	0.51	0.51	1.04	3.05	5.07	0.51	0.51	1.00
Y (ppm)	1.24	1.22	1.31	1.31	1.02	1.13	1.53	1.97	1.42	1.32	1.22	1.23	1.51
Yb (ppm)	0.29	0.17	0.19	0.18	0.18	0.24	0.22	0.20	0.24	0.22	0.18	0.19	0.20
Zr (ppm)	4.14	7.11	4.02	6.06	3.05	10.24	5.11	6.21	19.33	5.07	5.08	7.16	6.02
As (ppm)	0.31	0.30	0.30	0.10	0.20	0.20	0.51	0.31	0.31	0.10	0.10	0.31	0.10
Bi_ppm	0.02	0.01	0.01	0.01	0.01	0.01	0.01	0.01	0.14	0.01	0.01	0.01	0.01
Hg (ppm)	0.01	0.00	0.01	0.00	0.00	0.00	0.00	0.00	0.01	0.00	0.00	0.00	0.00
In (ppm)	0.00	0.00	0.01	0.00	0.01	0.00	0.00	0.01	0.01	0.00	0.00	0.00	0.00
Re (ppm)	0.00	0.00	0.00	0.00	0.00	0.00	0.00	0.00	0.00	0.00	0.00	0.00	0.00
Sb (ppm)	0.03	0.03	0.03	0.03	0.03	0.03	0.03	0.03	0.03	0.03	0.03	0.03	0.03
Se (ppm)	0.10	0.10	0.20	0.10	0.10	0.10	0.20	0.10	0.10	0.10	0.10	0.10	0.20
Te (ppm)	0.01	0.01	0.01	0.01	0.01	0.01	0.01	0.01	0.02	0.01	0.01	0.01	0.01
Tl (ppm)	0.02	0.03	0.01	0.02	0.02	0.02	0.02	0.02	0.08	0.01	0.03	0.02	0.02
Ag (ppm)	0.26	0.25	0.25	0.25	0.25	0.26	0.26	0.26	0.25	0.25	0.25	0.26	0.25
Cd (ppm)	0.26	0.25	0.25	0.25	0.25	0.26	0.26	0.26	0.25	0.25	0.25	0.26	0.25
Co (ppm)	78.72	82.31	103.62	92.90	87.41	83.96	88.95	81.81	62.06	54.74	88.47	81.79	83.31
Cu (ppm)	19.68	16.26	8.05	10.10	11.18	8.19	12.27	10.36	14.24	30.41	17.29	29.65	62.23
Li (ppm)	20.72	10.16	10.06	10.10	10.16	10.24	10.22	10.36	10.17	10.14	10.17	10.22	10.04
Mo (ppm)	0.52	0.51	0.50	0.50	0.51	0.51	0.51	0.52	1.02	0.51	0.51	1.02	0.50
Ni (ppm)	293.14	308.94	386.30	346.36	320.18	303.06	332.29	299.27	269.62	173.34	324.38	279.10	312.15
Pb (ppm)	2.07	1.02	2.01	2.02	4.07	2.05	3.07	2.07	4.07	2.03	1.02	3.07	3.01
Sc (ppm)	21.75	18.29	21.13	28.27	20.33	24.57	24.54	21.75	15.26	13.18	21.35	25.56	27.10
Zn (ppm)	62.15	64.02	77.46	73.71	70.13	65.53	73.62	66.27	59.01	43.59	69.15	66.45	70.26

	SB066	SB067	SB068	SB069	SB070	SB071	SB072	SB073	SB075
Drillhole	20-200	20-200	20-200	20-200	20-200	20-200	20-200	20-200	20-200
From (m)	578	584	592	595	598	608	611	613	617
To (m)	579	585	593	596	599	609	612	614	618
SiO_2 (wt%)	46.18	45.78	46.81	46.54	48.89	48.28	48.71	46.47	48.17
Al_2O_3 (wt%)	17.15	17.55	16.50	15.82	19.70	19.14	19.67	18.03	18.93
Fe_2O_3 (wt%)	16.41	16.58	16.25	17.08	11.12	12.25	11.36	15.46	12.71
CaO (wt%)	8.28	8.31	8.02	7.53	9.46	9.20	9.50	8.58	8.99
MgO (wt%)	9.40	9.10	9.95	10.53	8.03	8.36	8.21	8.87	8.49
Na_2O (wt%)	1.58	1.60	1.44	1.42	1.96	1.84	1.86	1.62	1.89
K_2O (wt%)	0.22	0.25	0.18	0.21	0.32	0.37	0.17	0.22	0.24
Cr_2O_3 (wt%)	0.07	0.06	0.07	0.06	0.05	0.04	0.04	0.05	0.04
TiO_2 (wt%)	0.53	0.59	0.58	0.62	0.30	0.35	0.31	0.54	0.38
MnO (wt%)	0.15	0.13	0.16	0.15	0.12	0.13	0.12	0.13	0.12
P_2O_5 (wt%)	0.01	0.01	0.01	0.01	0.01	0.01	0.01	0.01	0.01
SrO (wt%)	0.02	0.03	0.02	0.02	0.03	0.02	0.03	0.03	0.02
BaO (wt%)	0.00	0.01	0.01	0.01	0.01	0.01	0.01	0.01	0.01
V_2O_5 (wt%)	0.15	0.17	0.13	0.13	0.07	0.09	0.07	0.14	0.10
LOI (wt%)	1.18	1.6	1.47	0.8	1.31	1.82	0.87	0.6	2.4
Mg#	0.56	0.55	0.57	0.58	0.61	0.60	0.61	0.56	0.60
Ba (ppm)	42.09	56.61	38.15	49.80	61.00	69.37	46.61	46.78	72.74
Ce (ppm)	1.42	1.83	1.22	1.31	2.23	1.73	1.41	1.21	1.84
Cr (ppm)	536.24	406.51	466.76	453.63	374.95	315.76	282.48	362.18	307.35
Cs (ppm)	1.34	1.38	1.09	0.94	1.64	1.77	1.16	1.10	3.26
Dy (ppm)	0.16	0.28	0.14	0.21	0.21	0.17	0.10	0.11	0.15
Er (ppm)	0.09	0.24	0.12	0.12	0.12	0.14	0.15	0.11	0.08
Eu (ppm)	0.09	0.09	0.06	0.05	0.09	0.10	0.15	0.10	0.09
Ga (ppm)	19.22	19.00	17.15	17.94	18.34	19.25	17.96	18.31	19.67
Gd (ppm)	0.14	0.18	0.18	0.14	0.21	0.20	0.09	0.19	0.18
Ge (ppm)	2.53	2.54	2.54	2.52	2.53	2.55	2.52	2.52	2.56
Hf (ppm)	0.20	0.10	0.10	0.20	0.10	0.10	0.10	0.20	0.20
Ho (ppm)	0.04	0.06	0.05	0.06	0.05	0.04	0.04	0.03	0.07
La (ppm)	0.81	1.93	0.51	0.71	1.22	0.92	0.81	0.70	1.02
Lu (ppm)	0.02	0.02	0.02	0.02	0.02	0.02	0.04	0.03	0.03
Nb (ppm)	0.20	0.20	0.10	0.20	0.30	0.20	0.10	0.10	0.31

	SB066	SB067	SB068	SB069	SB070	SB071	SB072	SB073	SB075
Nd (ppm)	0.51	0.81	0.41	0.60	0.81	0.61	0.61	0.60	0.72
Pr (ppm)	0.12	0.20	0.13	0.12	0.23	0.19	0.16	0.12	0.19
Rb (ppm)	8.60	8.44	5.78	6.25	9.42	12.94	4.64	7.04	8.81
Sm (ppm)	0.08	0.12	0.09	0.10	0.21	0.12	0.13	0.13	0.20
Sn (ppm)	0.51	0.51	0.51	0.50	0.51	0.51	0.50	0.50	0.51
Sr (ppm)	190.72	191.06	175.04	183.47	233.08	223.07	236.07	207.25	224.36
Ta (ppm)	0.05	0.05	0.05	0.05	0.05	0.05	0.05	0.05	0.05
Tb (ppm)	0.02	0.05	0.02	0.02	0.05	0.03	0.03	0.03	0.04
Th (ppm)	0.08	0.12	0.07	0.10	0.29	0.13	0.06	0.08	0.09
Tm (ppm)	0.02	0.02	0.01	0.02	0.01	0.02	0.02	0.01	0.02
U (ppm)	0.03	0.03	0.03	0.07	0.09	0.05	0.03	0.03	0.03
V (ppm)	864.05	927.86	722.47	716.73	386.09	499.10	382.36	769.64	565.52
W (ppm)	0.51	1.02	1.01	0.50	0.51	0.51	0.50	0.50	0.51
Y (ppm)	1.11	1.32	1.01	1.11	1.22	1.02	1.01	0.91	1.23
Yb (ppm)	0.16	0.21	0.14	0.16	0.17	0.17	0.13	0.16	0.19
Zr (ppm)	4.05	5.08	4.06	6.05	4.05	5.09	4.04	4.02	5.12
As (ppm)	0.20	0.10	0.30	0.30	0.20	0.20	0.10	0.20	0.20
Bi_ppm	0.01	0.01	0.01	0.05	0.01	0.01	0.01	0.01	0.01
Hg (ppm)	0.00	0.00	0.00	0.00	0.00	0.00	0.00	0.00	0.00
In (ppm)	0.01	0.01	0.00	0.01	0.00	0.00	0.00	0.01	0.00
Re (ppm)	0.00	0.00	0.00	0.00	0.00	0.00	0.00	0.00	0.00
Sb (ppm)	0.03	0.03	0.03	0.03	0.03	0.03	0.03	0.03	0.03
Se (ppm)	0.10	0.10	0.10	0.20	0.10	0.10	0.10	0.10	0.10
Te (ppm)	0.01	0.01	0.01	0.01	0.01	0.01	0.01	0.01	0.01
Tl (ppm)	0.03	0.02	0.02	0.02	0.04	0.02	0.01	0.02	0.02
Ag (ppm)	0.25	0.25	0.25	0.25	0.25	0.25	0.25	0.25	0.26
Cd (ppm)	0.25	0.25	0.25	0.25	0.25	0.25	0.25	0.25	0.26
Co (ppm)	90.05	88.42	93.35	96.77	65.87	70.28	68.60	88.53	75.81
Cu (ppm)	15.18	33.54	13.19	19.15	20.27	16.30	13.12	12.07	9.22
Li (ppm)	10.12	10.16	10.15	10.08	10.13	10.19	10.09	10.06	20.49
Mo (ppm)	0.51	0.51	1.01	0.50	1.01	0.51	0.50	0.50	1.02
Ni (ppm)	349.06	369.92	382.54	405.24	252.33	274.00	239.10	333.01	276.61
Pb (ppm)	3.04	1.02	2.03	3.02	3.04	1.02	2.02	2.01	1.02
Sc (ppm)	18.21	20.33	25.37	19.15	13.17	15.28	18.16	18.11	16.39
Zn (ppm)	72.85	70.12	77.12	78.63	55.74	61.11	57.51	76.46	68.64

Appendix E – EDS Magnetite

Sample	V_2O_5 (%)	FeO (%)	TiO_2 (%)	Al_2O_3 (%)	SiO_2 (%)	CaO (%)	MgO (%)	Cr_2O (%)	Na_2O (%)	ZnO (%)	Total
SB002	2.1	97.4	bdl	bdl	0.4	bdl	bdl	bdl	bdl	bdl	99.9
SB002	1.8	98.0	bdl	bdl	bdl	bdl	bdl	bdl	bdl	bdl	99.8
SB002	1.3	97.9	bdl	0.5	bdl	bdl	bdl	bdl	bdl	bdl	99.7
SB002	1.7	98.1	bdl	bdl	bdl	bdl	bdl	bdl	bdl	bdl	99.7
SB002	2.1	97.4	bdl	bdl	bdl	0.4	bdl	bdl	bdl	bdl	99.9
SB004	1.3	83.7	14.9	bdl	bdl	bdl	bdl	bdl	bdl	bdl	99.9
SB004	1.7	97.8	bdl	bdl	bdl	0.3	bdl	bdl	bdl	bdl	99.8
SB004	1.6	89.3	7.8	0.6	0.4	bdl	bdl	bdl	bdl	bdl	99.5
SB004	1.6	97.2	0.2	bdl	bdl	bdl	bdl	bdl	bdl	bdl	99.0
SB004	1.7	97.6	0.2	bdl	bdl	bdl	bdl	bdl	bdl	bdl	99.6
SB004	1.8	97.3	0.3	0.3	bdl	bdl	bdl	bdl	bdl	bdl	99.6
SB004	1.7	97.1	0.5	0.7	bdl	bdl	bdl	bdl	bdl	bdl	99.9
SB004	1.8	95.9	0.6	1.0	bdl	bdl	bdl	bdl	bdl	bdl	99.2
SB004	1.7	95.5	1.3	0.7	0.3	bdl	bdl	bdl	bdl	bdl	99.2
SB004	1.8	96.2	0.7	0.6	bdl	bdl	bdl	bdl	bdl	bdl	99.3
SB004	1.8	97.3	bdl	0.5	bdl	bdl	bdl	bdl	bdl	bdl	99.5
SB004	1.8	96.6	0.3	1.3	bdl	bdl	bdl	bdl	bdl	bdl	100.1
SB006	1.6	56.9	bdl	10.0	13.8	15.5	2.2	bdl	bdl	bdl	99.9
SB006	1.6	97.4	0.4	0.4	bdl	bdl	bdl	bdl	bdl	bdl	99.6
SB006	1.5	97.8	0.3	bdl	bdl	bdl	bdl	bdl	bdl	bdl	99.6
SB006	1.5	97.1	0.4	0.3	bdl	bdl	bdl	bdl	bdl	bdl	99.4
SB006	1.6	97.7	bdl	bdl	bdl	bdl	bdl	bdl	bdl	bdl	99.3
SB006	1.8	98.2	bdl	0.3	0.3	bdl	bdl	bdl	bdl	bdl	100.6
SB006	1.2	96.3	0.6	1.6	bdl	bdl	bdl	bdl	bdl	bdl	99.1
SB006	1.5	98.6	bdl	0.3	bdl	bdl	bdl	bdl	bdl	bdl	100.3
SB006	1.5	97.6	bdl	0.7	bdl	bdl	bdl	bdl	bdl	bdl	99.8
SB006	1.5	98.9	bdl	bdl	bdl	bdl	bdl	bdl	bdl	bdl	100.4
SB006	1.4	97.8	bdl	0.3	0.3	bdl	bdl	bdl	bdl	bdl	99.8
SB006	1.4	98.1	0.3	bdl	bdl	bdl	bdl	bdl	bdl	bdl	99.8
SB008	1.3	99.4	bdl	bdl	bdl	bdl	bdl	bdl	bdl	bdl	100.7
SB008	1.0	98.9	bdl	bdl	bdl	bdl	bdl	bdl	bdl	bdl	99.8
SB008	1.5	99.7	bdl	bdl	bdl	bdl	bdl	bdl	bdl	bdl	101.2
SB008	0.9	94.7	bdl	bdl	bdl	bdl	bdl	bdl	bdl	bdl	95.7
SB008	0.9	100.1	bdl	bdl	bdl	bdl	bdl	bdl	bdl	bdl	101.0
SB008	1.3	98.0	bdl	0.4	bdl	bdl	bdl	bdl	bdl	bdl	99.7

Sample	V_2O_5 (%)	FeO (%)	TiO_2 (%)	Al_2O_3 (%)	SiO_2 (%)	CaO (%)	MgO (%)	Cr_2O (%)	Na_2O (%)	ZnO (%)	Total
SB008	1.3	97.7	bdl	bdl	0.4	bdl	bdl	bdl	bdl	bdl	99.4
SB008	1.3	97.7	bdl	bdl	bdl	bdl	bdl	bdl	bdl	bdl	99.0
SB008	1.6	99.0	bdl	bdl	bdl	bdl	bdl	bdl	bdl	bdl	100.6
SB008	1.3	97.7	bdl	bdl	bdl	bdl	bdl	bdl	bdl	bdl	99.0
SB008	1.2	99.2	bdl	bdl	bdl	bdl	bdl	bdl	bdl	bdl	100.4
SB008	1.1	97.6	bdl	bdl	0.4	bdl	bdl	bdl	bdl	bdl	99.1
SB008	0.9	98.5	bdl	bdl	bdl	bdl	bdl	bdl	bdl	bdl	99.5
SB008	0.9	98.9	bdl	bdl	bdl	bdl	bdl	bdl	bdl	bdl	99.8
SB008	1.2	96.4	bdl	1.2	bdl	bdl	bdl	bdl	bdl	bdl	98.7
SB008	1.2	98.1	bdl	bdl	bdl	bdl	bdl	bdl	bdl	bdl	99.3
SB013	1.9	95.6	0.9	1.3	bdl	bdl	bdl	bdl	bdl	bdl	99.6
SB013	1.9	97.1	0.6	0.5	bdl	bdl	bdl	bdl	bdl	bdl	100.1
SB013	1.9	96.5	0.5	0.3	0.5	bdl	bdl	bdl	bdl	bdl	99.7
SB013	1.9	98.1	bdl	0.5	bdl	bdl	bdl	bdl	bdl	bdl	100.4
SB013	1.8	97.3	0.4	0.6	bdl	bdl	bdl	bdl	bdl	bdl	100.0
SB013	1.7	96.7	0.7	0.6	bdl	bdl	bdl	bdl	bdl	bdl	99.5
SB013	1.9	96.7	0.3	0.9	bdl	bdl	bdl	bdl	bdl	bdl	99.8
SB013	1.8	96.9	0.8	0.8	bdl	bdl	bdl	bdl	bdl	bdl	100.3
SB013	1.8	96.7	0.4	0.5	bdl	bdl	bdl	bdl	bdl	bdl	99.5
SB016	2.0	96.9	bdl	0.5	bdl	bdl	bdl	bdl	bdl	bdl	99.4
SB016	1.6	96.0	0.7	0.8	bdl	bdl	bdl	0.6	bdl	bdl	99.6
SB016	1.4	98.5	bdl	bdl	bdl	bdl	bdl	bdl	bdl	bdl	100.0
SB016	1.3	97.0	bdl	1.4	bdl	bdl	bdl	bdl	bdl	bdl	99.7
SB018	1.7	94.6	bdl	1.5	1.5	0.5	bdl	bdl	bdl	bdl	99.8
SB018	1.6	97.7	bdl	bdl	0.3	bdl	bdl	bdl	bdl	bdl	99.5
SB018	1.5	97.5	bdl	0.3	bdl	bdl	bdl	0.9	bdl	bdl	100.2
SB018	1.7	96.8	bdl	1.4	bdl	bdl	bdl	bdl	bdl	bdl	99.9
SB018	1.6	98.1	bdl	bdl	bdl	bdl	bdl	bdl	bdl	bdl	99.8
SB018	2.1	97.5	bdl	0.5	bdl	bdl	bdl	bdl	bdl	bdl	100.0
SB018	1.7	98.2	bdl	bdl	bdl	bdl	bdl	bdl	bdl	bdl	99.9
SB018	1.5	98.8	bdl	bdl	bdl	bdl	bdl	bdl	bdl	bdl	100.3
SB018	1.6	98.3	bdl	0.3	bdl	bdl	bdl	bdl	bdl	bdl	100.1
SB018	1.5	97.5	bdl	0.4	bdl	bdl	bdl	bdl	bdl	bdl	99.3
SB018	1.5	97.8	bdl	0.3	bdl	0.2	bdl	bdl	bdl	bdl	99.8
SB018	1.0	75.5	bdl	6.3	12.5	1.9	2.6	bdl	0.7	bdl	100.1
SB021	2.1	97.5	bdl	bdl	bdl	bdl	bdl	bdl	bdl	bdl	99.6
SB021	1.8	97.2	bdl	0.9	0.3	bdl	bdl	bdl	bdl	bdl	100.2

Sample	V_2O_5 (%)	FeO (%)	TiO_2 (%)	Al_2O_3 (%)	SiO_2 (%)	CaO (%)	MgO (%)	Cr_2O (%)	Na_2O (%)	ZnO (%)	Total
SB021	2.0	97.5	bdl	bdl	bdl	bdl	bdl	bdl	bdl	bdl	99.5
SB021	2.1	97.5	bdl	bdl	bdl	bdl	bdl	bdl	bdl	bdl	99.6
SB021	2.2	98.2	bdl	bdl	bdl	bdl	bdl	bdl	bdl	bdl	100.3
SB021	2.2	97.4	bdl	bdl	bdl	bdl	bdl	bdl	bdl	bdl	99.6
SB021	2.1	97.7	bdl	bdl	bdl	bdl	bdl	bdl	bdl	bdl	99.8
SB021	2.0	97.5	bdl	bdl	bdl	bdl	bdl	bdl	bdl	bdl	99.6
SB021	2.1	97.0	bdl	bdl	bdl	bdl	bdl	bdl	bdl	bdl	99.1
SB021	2.0	95.1	0.8	1.1	bdl	bdl	bdl	bdl	bdl	bdl	98.9
SB021	2.1	97.6	bdl	bdl	bdl	bdl	bdl	bdl	bdl	bdl	99.7
SB021	2.2	97.3	bdl	bdl	bdl	bdl	bdl	bdl	bdl	bdl	99.5
SB021	2.1	97.6	bdl	bdl	bdl	bdl	bdl	bdl	bdl	bdl	99.6
SB021	2.2	97.0	bdl	bdl	bdl	bdl	bdl	bdl	bdl	bdl	99.2
SB021	2.1	97.6	bdl	bdl	bdl	bdl	bdl	bdl	bdl	bdl	99.7
SB021	1.0	99.0	bdl	bdl	bdl	bdl	bdl	bdl	bdl	bdl	100.0
SB021	2.2	98.0	bdl	bdl	bdl	bdl	bdl	bdl	bdl	bdl	100.2
SB021	2.0	97.7	bdl	bdl	bdl	bdl	bdl	bdl	bdl	bdl	99.7
SB021	1.8	80.4	1.2	2.4	2.2	bdl	1.4	bdl	bdl	0.6	89.9
SB021	2.0	97.7	bdl	bdl	bdl	bdl	bdl	bdl	bdl	bdl	99.7
SB021	2.2	97.2	bdl	bdl	bdl	bdl	bdl	bdl	bdl	bdl	99.4
SB021	2.3	97.0	bdl	bdl	bdl	bdl	bdl	bdl	bdl	bdl	99.4
SB024	1.0	75.7	bdl	bdl	bdl	bdl	bdl	bdl	bdl	bdl	76.6
SB024	1.1	75.3	bdl	bdl	0.3	bdl	bdl	bdl	bdl	bdl	76.6
SB024	0.9	75.5	bdl	bdl	bdl	bdl	bdl	0.4	bdl	bdl	76.9
SB024	1.0	76.1	bdl	bdl	bdl	bdl	bdl	bdl	bdl	bdl	77.1
SB033	2.1	96.9	bdl	bdl	bdl	bdl	bdl	bdl	bdl	bdl	99.0
SB033	2.0	97.8	bdl	bdl	bdl	bdl	bdl	bdl	bdl	bdl	99.8
SB033	1.9	95.4	0.5	0.4	0.7	0.6	bdl	bdl	bdl	bdl	99.5
SB033	2.1	94.9	bdl	1.3	1.3	bdl	0.5	bdl	bdl	bdl	100.1
SB033	2.3	97.4	bdl	bdl	bdl	bdl	bdl	bdl	bdl	bdl	99.7
SB033	1.9	97.8	bdl	bdl	bdl	bdl	bdl	bdl	bdl	bdl	99.7
SB034	1.9	97.6	bdl	bdl	bdl	bdl	bdl	bdl	bdl	bdl	99.5
SB034	1.8	94.6	0.2	3.5	bdl	bdl	bdl	bdl	bdl	bdl	100.1
SB034	1.9	97.8	bdl	bdl	bdl	bdl	bdl	bdl	bdl	bdl	99.8
SB034	2.0	98.1	bdl	0.3	bdl	bdl	bdl	bdl	bdl	bdl	100.4
SB034	2.1	97.7	bdl	0.6	bdl	bdl	bdl	bdl	bdl	bdl	100.4
SB034	2.3	98.0	bdl	bdl	bdl	bdl	bdl	bdl	bdl	bdl	100.4
SB034	1.9	97.9	bdl	bdl	bdl	bdl	bdl	bdl	bdl	bdl	99.8

Sample	V_2O_5 (%)	FeO (%)	TiO_2 (%)	Al_2O_3 (%)	SiO_2 (%)	CaO (%)	MgO (%)	Cr_2O (%)	Na_2O (%)	ZnO (%)	Total
SB034	1.6	87.4	0.2	0.8	bdl	bdl	bdl	bdl	bdl	bdl	90.0

* bdl (below detection limit)

Appendix E – EDS Ilmenite

Sample	V_2O_5 (%)	FeO (%)	TiO_2 (%)	Al_2O_3 (%)	SiO_2 (%)	CaO (%)	MnO (%)	MgO (%)	Total
SB002	bdl	46.8	51.6	bdl	0.6	0.5	1.9	bdl	101.4
SB002	bdl	47.1	52.2	bdl	bdl	bdl	1.8	bdl	101.0
SB002	0.4	46.6	52.6	bdl	bdl	bdl	1.9	bdl	101.5
SB002	bdl	60.2	36.9	bdl	0.9	0.4	1.3	bdl	99.6
SB002	bdl	48.3	53.4	bdl	bdl	bdl	1.5	bdl	103.1
SB004	bdl	46.4	53.3	bdl	bdl	bdl	1.7	bdl	101.4
SB004	0.4	47.5	51.7	bdl	bdl	bdl	1.6	bdl	101.1
SB004	0.4	41.8	45.8	bdl	bdl	bdl	1.5	bdl	89.5
SB004	bdl	45.6	50.0	0.4	0.6	bdl	1.8	bdl	98.4
SB004	bdl	49.9	49.6	bdl	bdl	bdl	1.7	bdl	95.3
SB004	0.6	44.8	48.2	bdl	bdl	bdl	1.5	bdl	95.1
SB004	bdl	46.9	51.9	bdl	bdl	bdl	1.7	bdl	100.5
SB004	1.1	62.7	18.0	9.0	3.8	bdl	bdl	2.7	97.3
SB004	bdl	40.8	47.4	bdl	bdl	bdl	1.2	0.8	90.1
SB004	bdl	44.2	50.8	bdl	bdl	bdl	1.3	0.7	97.0
SB004	bdl	50.5	49.4	bdl	bdl	bdl	bdl	1.4	101.3
SB004	bdl	48.1	51.0	bdl	bdl	bdl	1.8	bdl	100.9
SB004	bdl	46.7	53.5	0.3	0.3	bdl	1.4	bdl	102.8
SB004	bdl	45.1	51.6	bdl	bdl	bdl	1.2	bdl	97.9
SB004	bdl	45.3	53.7	bdl	bdl	bdl	1.3	0.9	101.1
SB004	1.6	91.0	0.3	0.5	bdl	bdl	bdl	bdl	93.5
SB006	bdl	47.2	53.2	bdl	bdl	bdl	1.7	bdl	102.2
SB006	bdl	46.1	50.3	bdl	bdl	bdl	1.4	bdl	97.8
SB006	bdl	44.5	48.9	0.4	0.5	bdl	1.5	bdl	95.8
SB006	bdl	47.9	51.9	bdl	0.2	bdl	1.5	bdl	101.6
SB006	bdl	47.9	51.9	bdl	bdl	bdl	1.6	bdl	101.4
SB006	0.4	46.2	52.2	bdl	bdl	bdl	1.7	bdl	100.5
SB006	bdl	46.9	52.7	0.3	bdl	bdl	2.0	bdl	102.0
SB006	bdl	47.9	52.9	bdl	bdl	bdl	1.9	bdl	102.6

Sample	V_2O_5 (%)	FeO (%)	TiO_2 (%)	Al_2O_3 (%)	SiO_2 (%)	CaO (%)	MnO (%)	MgO (%)	Total
SB008	bdl	50.7	52.9	0.4	bdl	bdl	2.1	bdl	106.0
SB008	bdl	49.8	52.4	bdl	0.3	bdl	2.0	bdl	104.5
SB008	bdl	51.5	50.5	bdl	bdl	bdl	2.1	bdl	104.6
SB008	bdl	51.5	50.3	bdl	bdl	bdl	2.2	bdl	104.0
SB008	bdl	51.7	52.8	bdl	bdl	bdl	2.3	bdl	106.8
SB008	bdl	50.4	52.9	bdl	bdl	0.4	2.0	bdl	105.6
SB008	bdl	52.4	49.9	bdl	bdl	bdl	2.2	bdl	104.5
SB008	0.5	51.8	53.0	bdl	bdl	bdl	2.2	bdl	107.5
SB008	bdl	51.3	52.5	bdl	bdl	bdl	2.2	bdl	106.0
SB008	bdl	51.8	50.6	bdl	0.3	bdl	2.3	bdl	105.0
SB008	bdl	51.1	51.6	bdl	bdl	bdl	2.0	bdl	104.2
SB013	bdl	47.3	54.2	bdl	bdl	bdl	1.2	bdl	102.6
SB013	bdl	47.2	44.9	4.7	0.8	bdl	1.2	0.8	99.9
SB013	bdl	45.6	54.2	bdl	bdl	bdl	1.4	1.0	102.2
SB013	bdl	40.5	47.4	bdl	bdl	bdl	1.2	0.7	89.7
SB013	bdl	46.1	54.6	bdl	bdl	bdl	1.3	bdl	102.0
SB013	bdl	43.5	50.7	bdl	0.2	bdl	1.2	0.7	96.4
SB013	bdl	43.9	50.6	bdl	bdl	bdl	1.2	0.9	96.5
SB013	bdl	46.0	50.5	bdl	bdl	bdl	1.2	1.0	102.8
SB013	bdl	46.5	54.4	bdl	bdl	bdl	1.3	0.8	103.1
SB016	bdl	47.3	48.8	bdl	bdl	bdl	1.5	bdl	97.6
SB016	bdl	49.2	46.7	bdl	bdl	bdl	1.5	bdl	97.4
SB016	0.4	50.1	47.7	bdl	bdl	bdl	1.3	bdl	99.4
SB018	bdl	75.2	23.2	bdl	bdl	bdl	bdl	bdl	98.4
SB018	bdl	45.6	48.4	bdl	bdl	bdl	1.4	bdl	95.4
SB018	bdl	48.2	52.7	bdl	bdl	bdl	1.4	bdl	102.2
SB018	bdl	49.8	51.3	bdl	bdl	bdl	1.4	bdl	102.5
SB018	bdl	48.3	53.9	bdl	bdl	bdl	1.4	bdl	103.5
SB018	bdl	48.7	52.0	bdl	bdl	bdl	1.4	bdl	102.1
SB018	bdl	48.4	52.4	bdl	bdl	bdl	1.6	bdl	102.3
SB018	bdl	50.2	50.6	bdl	bdl	bdl	1.4	bdl	102.2
SB021	bdl	46.5	53.7	bdl	bdl	bdl	2.5	bdl	102.7
SB021	bdl	47.3	48.4	bdl	bdl	bdl	2.0	bdl	97.7
SB021	0.6	55.3	44.0	bdl	bdl	bdl	bdl	bdl	105.6
SB021	bdl	48.2	48.7	bdl	bdl	bdl	1.9	bdl	98.8
SB021	bdl	43.2	48.1	bdl	bdl	bdl	2.1	bdl	93.8
SB021	bdl	47.1	50.0	bdl	bdl	bdl	2.1	bdl	99.3

Sample	V_2O_5 (%)	FeO (%)	TiO_2 (%)	Al_2O_3 (%)	SiO_2 (%)	CaO (%)	MnO (%)	MgO (%)	Total
SB021	bdl	48.3	50.1	bdl	bdl	bdl	1.8	bdl	100.2
SB021	bdl	46.9	51.3	bdl	bdl	bdl	2.3	bdl	100.5
SB021	bdl	46.3	53.0	bdl	0.3	bdl	2.2	bdl	101.7
SB021	bdl	47.0	52.3	bdl	bdl	bdl	2.2	bdl	101.4
SB021	0.6	46.8	51.4	bdl	bdl	bdl	2.1	bdl	101.0
SB021	bdl	49.7	48.8	bdl	bdl	bdl	2.0	bdl	100.5
SB024	0.3	33.4	25.0	6.1	1.0	0.5	2.2	0.7	109.5
SB024	bdl	37.3	29.8	bdl	bdl	bdl	2.0	bdl	100.2
SB024	bdl	36.5	30.5	bdl	bdl	bdl	2.1	bdl	100.6
SB024	bdl	37.8	31.3	bdl	bdl	bdl	2.2	bdl	103.6
SB024	bdl	37.8	29.2	bdl	bdl	bdl	1.9	bdl	99.8
SB024	0.3	38.6	30.9	bdl	bdl	bdl	2.2	bdl	104.5
SB033	bdl	46.5	51.9	bdl	bdl	bdl	1.4	bdl	99.8
SB033	0.8	61.1	37.3	1.6	bdl	bdl	bdl	bdl	108.0
SB033	bdl	48.4	52.2	bdl	bdl	bdl	1.5	bdl	102.1
SB033	bdl	47.2	52.9	bdl	bdl	bdl	1.6	bdl	101.6
SB033	bdl	49.4	53.3	bdl	bdl	bdl	1.5	bdl	104.2
SB033	bdl	48.6	52.7	bdl	bdl	bdl	1.4	bdl	102.7
SB033	bdl	48.7	52.4	bdl	bdl	bdl	1.3	bdl	102.5
SB033	bdl	48.5	52.9	bdl	bdl	bdl	1.5	bdl	102.9
SB033	bdl	49.3	53.6	bdl	bdl	bdl	1.6	bdl	104.5
SB033	bdl	45.7	49.2	bdl	bdl	bdl	1.4	bdl	96.3
SB033	bdl	49.7	53.4	bdl	bdl	bdl	1.6	bdl	104.6
SB034	bdl	46.9	53.6	bdl	bdl	bdl	1.5	1.3	103.2
SB034	1.3	72.6	19.6	4.6	bdl	bdl	bdl	0.7	98.9
SB034	bdl	47.4	52.2	bdl	bdl	bdl	1.3	0.6	101.6
SB034	bdl	45.7	52.6	0.3	bdl	bdl	1.4	0.8	100.8
SB034	bdl	46.8	53.6	0.5	bdl	bdl	1.6	1.1	103.7
SB034	bdl	41.3	46.1	bdl	bdl	bdl	1.2	0.7	89.1
SB034	bdl	47.0	53.1	bdl	bdl	bdl	1.4	bdl	101.5
SB034	bdl	46.9	52.8	bdl	bdl	bdl	1.4	0.9	102.0
SB034	bdl	46.9	52.8	bdl	bdl	bdl	1.2	1.0	101.9

* bdl (below detection limit)

Appendix F. LA-ICP-MS

* Oxide mode (Ox mode): Semi-massive oxide (SMO) - Heavily disseminated oxide (HDO) - Weakly disseminated oxide (WDO) - Massive oxide (MO).

Drill hole	14-902	14-902	14-902	14-902	14-902	14-902	14-902
Thin section	SB004	SB004	SB004	SB004	SB006	SB006	SB006
Ox mode	SMO	SMO	SMO	SMO	HDO	HDO	HDO
Line	SB004 ilm006	SB004 ilm007	SB004 ilm009	SB004 mag010	SB006 ilm011	SB006 ilm012	SB006 ilm013
Mineral	magnetite	magnetite	magnetite	magnetite	magnetite	magnetite	magnetite
Mg24 (ppm)	583.72	918.63	430.59	1389.44	270.20	401.13	540.67
Al27 (ppm)	1651.63	2438.68	2203.09	3060.36	6795.82	2187.52	3736.42
Si29 (ppm)	1630.56	2501.40	2239.38	3061.44	1031.83	670.59	2805.81
P31 (ppm)	0.01	0.01	0.01	0.01	1.04	0.01	2.20
Ca44 (ppm)	331.92	263.94	275.48	481.57	111.89	437.44	756.38
Sc45 (ppm)	7.96	4.31	2.15	6.44	1.27	1.19	2.80
Ti49 (ppm)	25535.86	33007.09	16762.13	13790.28	5974.94	3001.08	39077.23
V51 (ppm)	8577.98	8440.54	8610.88	9138.54	7989.25	7147.40	7899.69
Cr52 (ppm)	662.02	602.46	538.17	368.01	150.55	153.86	72.52
Mn55 (ppm)	1267.60	1723.98	926.20	767.80	486.49	237.15	1904.71
Fe57 (ppm)	685692.70	673560.20	695414.40	693817.60	702396.00	714958.90	663772.30
Co59 (ppm)	59.85	44.54	42.45	65.05	99.70	87.94	134.32
Ni60 (ppm)	93.55	85.78	88.97	111.38	89.10	82.21	92.08
Cu63 (ppm)	0.07	0.09	0.06	0.48	0.16	0.91	3.57
Zn66 (ppm)	162.79	218.09	310.99	208.54	1383.31	130.73	9975.71
Ga71 (ppm)	41.46	37.99	44.20	47.10	56.96	57.36	51.28
Ge74 (ppm)	0.80	0.84	0.83	0.87	0.73	0.67	0.84
As75 (ppm)	0.03	0.06	0.06	0.03	0.01	0.05	0.09
Y89 (ppm)	0.01	0.01	0.01	0.01	0.00	0.00	0.01
Zr90 (ppm)	0.01	0.08	0.02	0.03	0.12	0.11	0.24
Nb93 (ppm)	0.11	0.09	0.07	0.01	0.00	0.02	0.02
Mo95 (ppm)	0.02	0.01	0.02	0.02	0.02	0.06	0.04
Sn118 (ppm)	0.12	0.15	0.08	0.13	0.15	0.12	0.20
La139 (ppm)			0.01	0.01	0.00	0.01	0.01
Yb172 (ppm)	0.01			0.00			0.01
Hf178 (ppm)	0.01	0.01		0.00	0.02	0.00	0.01
Ta181 (ppm)	0.00	0.00	0.00	0.01		0.00	0.01
W182 (ppm)	0.34	0.38	0.11	0.27	0.02	0.00	

Ir193 (ppm)	0.01	0.01		0.01		0.01	
Pb208 (ppm)	0.02	0.15	0.02	0.06	0.01	0.06	0.07

Drill hole	14-902	14-902	14-902	14-902	14-902	14-902	14-902
Thin section	SB006	SB008	SB008	SB008	SB008	SB013	SB013
Ox mode	HDO	HDO	HDO	HDO	HDO	HDO	HDO
Line	SB006 mag014	SB008 mag1	SB008 mag3	SB008 mag4	SB008 mag5	SB013 mag1	SB013 mag2
Mineral	magnetite	magnetite	magnetite	magnetite	magnetite	magnetite	magnetite
Mg24 (ppm)	215.48	64.30	230.46	7.59	98.76	3530.39	2768.56
Al27 (ppm)	1724.19	868.40	2032.66	733.95	1156.55	11320.10	10194.23
Si29 (ppm)	1242.23	136.19	2212.91	0.01	739.25	332.31	753.72
P31 (ppm)	1.68	0.01	0.01	0.01	0.01	0.01	3.26
Ca44 (ppm)	843.96	4.87	209.44	1.38	38.51	124.16	34.35
Sc45 (ppm)	1.18	0.09	0.09	0.07	0.06	6.88	6.58
Ti49 (ppm)	14061.83	589.61	620.04	524.24	481.43	15889.50	16889.65
V51 (ppm)	6495.83	6379.52	5642.89	6560.19	5898.85	7968.16	8019.74
Cr52 (ppm)	89.66	4.35	3.52	3.84	2.46	995.35	966.39
Mn55 (ppm)	792.59	191.79	169.20	168.74	195.06	634.68	650.59
Fe57 (ppm)	700203.60	721215.20	715996.50	721909.30	719871.00	683438.20	684228.90
Co59 (ppm)	68.14	83.29	56.46	46.69	76.69	147.54	108.17
Ni60 (ppm)	66.71	8.77	6.63	18.50	6.37	731.63	662.42
Cu63 (ppm)	0.04	0.01	0.03	0.01	0.02	2.20	0.35
Zn66 (ppm)	203.30	109.83	87.40	122.36	86.97	80.80	61.44
Ga71 (ppm)	48.30	30.65	31.96	34.65	26.66	40.83	38.64
Ge74 (ppm)	0.76	0.65	0.45	0.63	0.55	0.61	0.64
As75 (ppm)	0.05	0.15	0.13	0.11	0.12	0.14	0.13
Y89 (ppm)	0.01	0.01	0.00	0.01	0.00	0.00	0.00
Zr90 (ppm)	0.04	0.00	0.00	0.00	0.00	0.86	1.30
Nb93 (ppm)	0.01	0.01				0.00	0.00
Mo95 (ppm)	2.68	0.01	0.00	0.10	0.01	0.05	0.05
Sn118 (ppm)	0.06	0.02	0.01	0.02	0.01	0.68	0.63
La139 (ppm)	0.00	0.01				0.01	0.00
Yb172 (ppm)	0.01			0.01		0.01	0.01
Hf178 (ppm)	0.01	0.01		0.01		0.04	0.04
Ta181 (ppm)	0.01	0.01	0.01	0.01			0.01
W182 (ppm)	0.03	0.01	0.06		0.00	0.01	0.01
Ir193 (ppm)	0.01	0.01	0.01	0.01		0.01	
Pb208 (ppm)	0.01	0.00	0.00	0.00	0.01	0.04	0.06

Drill hole	14-902	14-902	14-902	14-902	14-902	14-902	14-902
Thin section	SB013	SB013	SB013	SB016	SB016	SB016	SB016
Ox mode	HDO	HDO	HDO	WDP	WDO	WDO	WDO
Line	SB013 mag3	SB013 mag4	SB013 mag5	SB016 mag1	SB016 mag2	SB016 mag4	SB016 mag5
Mineral	magnetite	magnetite	magnetite	magnetite	magnetite	magnetite	magnetite
Mg24 (ppm)	2515.33	3773.19	2771.95	488.45	2558.64	568.19	863.37
Al27 (ppm)	9570.61	12604.54	10874.86	2184.30	3654.23	1987.93	2084.53
Si29 (ppm)	1223.31	509.76	1626.95	1272.89	4015.28	2152.01	1567.93
P31 (ppm)	0.89	1.90	1.44	0.01	0.01	3.79	0.01
Ca44 (ppm)	20.54	21.85	26.81	404.54	445.83	384.39	266.33
Sc45 (ppm)	7.96	8.68	7.76	0.63	1.76	0.65	0.42
Ti49 (ppm)	16267.72	20957.33	21504.70	1640.28	21075.44	1622.22	973.80
V51 (ppm)	7752.83	7808.35	7342.01	7555.93	6478.43	7583.00	8506.90
Cr52 (ppm)	811.10	889.20	898.79	4250.39	3332.92	2888.50	3408.99
Mn55 (ppm)	631.57	787.91	791.12	134.86	844.50	157.78	111.83
Fe57 (ppm)	684936.80	676028.60	675629.10	715436.80	679392.20	713741.60	715519.40
Co59 (ppm)	90.48	134.75	113.67	70.72	93.81	91.79	77.92
Ni60 (ppm)	581.13	669.88	571.64	305.46	186.25	395.58	272.04
Cu63 (ppm)	1.60	1.01	828.11	1.67	1.48	0.89	1.49
Zn66 (ppm)	69.00	84.42	132.95	102.40	180.67	63.93	77.53
Ga71 (ppm)	37.61	41.30	38.16	30.57	24.60	35.27	33.95
Ge74 (ppm)	0.62	0.63	0.58	0.41	0.41	0.47	0.43
As75 (ppm)	0.14	0.11	0.14	0.19	0.29	0.29	0.15
Y89 (ppm)	0.00	0.00	0.01	0.00	0.01	0.00	0.00
Zr90 (ppm)	0.95	1.13	1.38	0.04	0.08	0.04	0.02
Nb93 (ppm)	0.00	0.00	0.00	0.02	0.36	0.01	0.00
Mo95 (ppm)	0.05	0.06	0.07	0.04	0.01	0.18	0.02
Sn118 (ppm)	0.65	0.76	0.95	0.04	0.15	0.06	0.03
La139 (ppm)	0.00	0.00	0.00	0.01	0.04	0.01	0.01
Yb172 (ppm)		0.01	0.01			0.01	0.01
Hf178 (ppm)	0.03	0.05	0.06	0.01	0.00	0.01	0.01
Ta181 (ppm)	0.00	0.00	0.01	0.00	0.02	0.00	0.01
W182 (ppm)	0.01	0.01	0.01	0.17	0.33	0.31	0.05
Ir193 (ppm)	0.00	0.01	0.01	0.01	0.01	0.01	
Pb208 (ppm)	0.25	0.06	0.28	0.08	0.18	0.13	0.05

Drill hole	14-902	14-902	14-902	14-902	14-902	14-902	14-902
Thin section	SB021	SB021	SB021	SB021	SB021	SB021	SB024
Ox mode	HDO	HDO	HDO	HDO	HDO	HDO	WDO
Line	SB021 ilm021	SB021 ilm022	SB021 ilm023	SB021 ilm024	SB021 mag024	SB021 mag025	SB024 mag1
Mineral	magnetite	magnetite	magnetite	magnetite	magnetite	magnetite	magnetite
Mg24 (ppm)	1508.49	2861.76	1712.96	1025.91	2817.64	1478.17	369.29
Al27 (ppm)	1936.95	3460.95	1914.67	1935.89	3486.84	2346.94	3831.35
Si29 (ppm)	2650.31	3795.62	3280.52	2093.88	3050.12	2467.83	920.94
P31 (ppm)	0.85	3.00	0.78	0.01	0.01	0.01	1.02
Ca44 (ppm)	440.98	280.50	270.63	279.70	213.49	273.49	125.27
Sc45 (ppm)	1.29	4.57	1.28	1.54	1.03	2.13	2.71
Ti49 (ppm)	12025.34	9693.66	4929.04	4208.02	1225.03	3752.22	2711.11
V51 (ppm)	11023.25	9834.79	10478.07	9860.28	10100.95	11098.52	9455.66
Cr52 (ppm)	1935.00	2680.91	2129.01	2352.63	2109.33	1395.08	3705.46
Mn55 (ppm)	727.77	744.24	394.90	340.63	175.29	321.95	282.68
Fe57 (ppm)	699534.10	689673.00	705527.20	708090.80	705825.50	708256.80	712363.20
Co59 (ppm)	75.33	67.19	88.80	45.85	49.53	38.25	106.53
Ni60 (ppm)	329.58	371.33	328.26	351.68	314.60	401.55	1351.90
Cu63 (ppm)	0.35	0.12	0.01	0.18	0.06	0.34	0.10
Zn66 (ppm)	335.14	505.74	347.55	642.37	276.84	299.38	114.53
Ga71 (ppm)	21.91	25.94	22.37	23.26	28.54	24.63	35.95
Ge74 (ppm)	0.53	0.57	0.65	0.56	0.58	0.63	0.65
As75 (ppm)	0.09	0.02	2.57	0.06	0.00	0.06	0.17
Y89 (ppm)	0.01	0.01	0.01	0.00	0.00	0.01	0.00
Zr90 (ppm)	0.07	0.19	0.42	0.06	0.02	0.04	0.30
Nb93 (ppm)	0.04	0.08	0.04	0.03	0.01	0.01	0.01
Mo95 (ppm)	0.01	0.00	0.02	0.00	0.01	0.02	0.15
Sn118 (ppm)	0.06	0.03	0.04	0.04	0.02	0.09	0.27
La139 (ppm)	0.02	0.01	0.02	0.01	0.00	0.01	0.00

Yb172 (ppm)	0.01	0.01	0.01			0.00	
Hf178 (ppm)	0.01	0.01	0.03	0.01		0.01	0.01
Ta181 (ppm)	0.01	0.00	0.00	0.01		0.00	0.01
W182 (ppm)	0.02	0.03	0.00	0.01	0.01	0.01	0.00
Ir193 (ppm)	0.01	0.01	0.01	0.01	0.01		
Pb208 (ppm)	0.07	0.05	0.06	0.02	0.01	0.06	0.03

Drill hole	14-902	14-902	14-902	14-902	14-902	14-902	14-902
Thin section	SB024	SB024	SB024	SB024	SB027	SB027	SB027
Ox mode	WDO	WDO	WDO	WDO	HDO	HDO	HDO
Line	SB024 mag2	SB024 mag3	SB024 mag4	SB024 mag5	SB027 mag1	SB027 mag2	SB027 mag3
Mineral	magnetite	magnetite	magnetite	magnetite	magnetite	magnetite	magnetite
Mg24 (ppm)	1681.05	793.94	741.28	1435.07	667.32	393.07	536.29
Al27 (ppm)	3194.42	7386.83	4082.29	3432.56	4987.26	3114.63	5182.14
Si29 (ppm)	2444.65	1510.77	1593.84	3723.78	508.68	823.11	295.88
P31 (ppm)	0.01	0.01	0.68	0.81	0.80	5.54	0.01
Ca44 (ppm)	49.43	137.62	237.25	2151.83	19.07	37.15	8.91
Sc45 (ppm)	1.99	2.12	2.54	7.67	3.43	3.63	3.55
Ti49 (ppm)	7753.68	1416.71	2889.96	9170.18	6154.03	8197.92	5304.36
V51 (ppm)	8820.24	9102.06	9183.83	8836.09	9323.35	8737.23	9266.22
Cr52 (ppm)	2763.16	3137.66	3145.37	3060.75	2437.17	3953.06	2388.78
Mn55 (ppm)	645.21	183.02	318.03	634.15	336.68	421.10	321.26
Fe57 (ppm)	703231.20	708162.20	710445.90	693388.20	706364.40	707115.30	708031.00
Co59 (ppm)	70.74	86.71	162.89	60.67	124.65	153.23	161.16
Ni60 (ppm)	1183.37	1109.35	1387.73	1058.57	1027.00	1066.93	1039.39
Cu63 (ppm)	0.09	0.73	0.36	0.22	0.37	7.85	0.27
Zn66 (ppm)	163.04	87.53	45.35	74.54	56.26	30.90	32.35
Ga71 (ppm)	16.17	37.14	34.89	25.14	37.49	38.03	37.53
Ge74 (ppm)	0.53	0.61	0.64	0.60	0.67	0.84	0.65
As75 (ppm)	0.14	0.21	0.15	0.20	0.14	0.20	0.17
Y89 (ppm)	0.01	0.00	0.01	0.26	0.00	0.00	0.00
Zr90 (ppm)	0.44	0.44	0.28	3.02	0.45	1.11	0.54
Nb93 (ppm)	0.01	0.00	0.06	0.12	0.00	0.02	0.00
Mo95 (ppm)	0.14	0.15	0.18	0.18	0.08	0.07	0.10

Sn118 (ppm)	0.23	0.18	0.31	0.29	0.24	0.23	0.20
La139 (ppm)	0.02	0.00	0.01	0.03	0.00	0.00	0.00
Yb172 (ppm)	0.00	0.01	0.01	0.02	0.01	0.01	0.01
Hf178 (ppm)	0.02	0.02	0.02	0.19	0.01	0.04	0.01
Ta181 (ppm)	0.00	0.01	0.00	0.01	0.01	0.00	0.01
W182 (ppm)	0.01	0.00	0.01	0.02	0.00	0.00	0.01
Ir193 (ppm)	0.01	0.01	0.01	0.01	0.01	0.01	0.01
Pb208 (ppm)	0.02	0.20	0.06	0.07	0.05	0.29	0.05

Drill hole	14-902	14-902	14-902	14-902	14-902	14-902	14-902	14-902
Thin section	SB027	SB027	SB029	SB029	SB029	SB029	SB029	SB034
Ox mode	HDO	HDO	HDO	HDO	HDO	HDO	HDO	MO
Line	SB027 mag4	SB027 mag5	SB029 mag1	SB029 mag2	SB029 mag3	SB029 mag4	SB029 mag5	SB034 ilm031
Mineral	magnetite	magnetite	magnetite	magnetite	magnetite	magnetite	magnetite	magnetite
Mg24 (ppm)	425.67	874.69	308.77	236.07	679.96	788.62	1242.53	906.17
Al27 (ppm)	3634.57	5675.48	4436.55	1971.35	3174.03	4045.29	4861.42	2909.00
Si29 (ppm)	853.23	671.81	648.26	1115.61	3422.94	4070.94	4430.36	548.03
P31 (ppm)	2.37	0.80	2.44	0.01	0.01	0.16	0.88	0.01
Ca44 (ppm)	31.48	27.90	29.40	403.45	659.13	385.98	27.56	22.59
Sc45 (ppm)	1.87	3.25	1.61	0.28	0.53	0.54	0.83	26.68
Ti49 (ppm)	3609.87	3469.18	9400.41	1355.01	1403.99	1277.49	2019.04	46022.70
V51 (ppm)	7828.84	9272.81	8079.94	9085.86	9200.01	8860.58	7495.84	10382.73
Cr52 (ppm)	2255.94	2394.55	123.13	116.98	138.16	111.86	143.81	252.94
Mn55 (ppm)	208.07	243.52	450.63	144.50	149.77	157.54	192.84	1775.49
Fe57 (ppm)	712030.40	709130.40	704296.60	715014.50	707427.40	708708.20	705793.80	660438.40
Co59 (ppm)	158.04	185.43	111.56	57.43	33.41	45.04	42.80	36.49
Ni60 (ppm)	713.52	1150.61	72.41	61.76	56.17	60.30	61.70	476.73
Cu63 (ppm)	0.67	0.07	0.22	0.09	0.48	0.58	0.08	0.30
Zn66 (ppm)	29.79	75.81	1515.06	133.17	128.11	156.90	231.87	150.54
Ga71 (ppm)	38.04	38.59	49.75	42.79	40.83	46.18	39.21	36.77
Ge74 (ppm)	0.56	0.67	0.68	0.71	0.62	0.63	0.63	0.55
As75 (ppm)	0.15	0.15	0.16	0.10	0.13	0.11	0.09	0.05
Y89 (ppm)	0.00	0.00	0.00	0.00	0.01	0.00	0.00	0.01

Zr90 (ppm)	0.21	0.27	0.20	0.01	0.06	0.03	0.04	0.95
Nb93 (ppm)	0.00	0.01	0.00	0.00	0.00	0.00	0.00	0.38
Mo95 (ppm)	0.12	0.07	0.08	0.09	0.06	0.04	0.26	0.03
Sn118 (ppm)	0.11	0.27	0.12	0.03	0.06	0.08	0.03	0.27
La139 (ppm)	0.00	0.01	0.01	0.00	0.01	0.00	0.00	0.05
Yb172 (ppm)	0.01	0.01	0.01		0.01	0.01	0.01	0.01
Hf178 (ppm)	0.00	0.00	0.01	0.01	0.01	0.01	0.01	0.11
Ta181 (ppm)	0.01	0.01	0.01	0.01	0.01	0.01	0.01	0.01
W182 (ppm)	0.01		0.00	0.01	0.02	0.01	0.00	0.05
Ir193 (ppm)	0.01	0.01	0.01	0.01		0.01	0.01	0.01
Pb208 (ppm)	0.08	0.02	0.06	0.03	0.14	0.08	0.01	0.07

Drill hole	14-902	14-902	14-902	14-902	14-902	14-902	14-902	14-902
Thin section	SB034	SB034	SB034	SB034	SB036	SB036	SB036	SB036
Ox mode	MO	MO	MO	MO	HDO	HDO	HDO	HDO
Line	SB034 ilm033	SB034 ilm034	SB034 mag034	SB034 mag035	SB036 ilm037	SB036 ilm038	SB036 mag039	SB036 mag040
Mineral	magnetite	magnetite	magnetite	magnetite	magnetite	magnetite	magnetite	magnetite
Mg24 (ppm)	1183.40	2281.98	913.19	894.00	705.62	2449.77	112.04	826.58
Al27 (ppm)	2465.38	8259.94	3090.85	4108.15	1132.73	3177.39	759.78	1640.45
Si29 (ppm)	127.21	443.39	276.62	503.79	1375.44	3265.60	321.91	2469.34
P31 (ppm)	0.74	1.48	1.39	0.39	0.31	0.02	0.72	0.83
Ca44 (ppm)	4.91	20.00	4.85	9.34	376.74	146.15	16.21	418.19
Sc45 (ppm)	3.32	11.51	3.27	3.81	0.83	1.75	0.21	0.38
Ti49 (ppm)	5656.91	17862.98	4724.29	2235.60	7018.01	22859.53	599.22	1503.87
V51 (ppm)	10721.62	9814.01	10962.29	12813.90	10158.61	8916.14	10013.06	9551.86
Cr52 (ppm)	229.18	177.27	197.29	278.48	1488.50	1574.94	1362.28	1640.51
Mn55 (ppm)	264.00	725.00	217.72	154.09	289.39	1010.16	79.73	122.38
Fe57 (ppm)	711998.10	685069.40	711417.00	711471.20	707560.60	679599.20	721105.60	713786.50
Co59 (ppm)	55.15	86.99	41.24	40.55	32.20	90.00	78.34	77.16
Ni60 (ppm)	556.56	657.92	619.71	560.35	653.06	455.97	539.09	445.78
Cu63 (ppm)	0.21	1.27	0.35	1.01	0.18	0.17	0.02	0.61
Zn66 (ppm)	272.06	411.89	85.73	125.77	135.66	54.25	354.73	111.12
Ga71 (ppm)	39.79	50.20	35.01	51.12	20.63	17.47	20.52	14.22
Ge74 (ppm)	0.68	0.61	0.69	0.67	0.43	0.41	0.45	0.56

As75 (ppm)	0.02	0.05	0.07	0.09	0.02	0.08	0.01	0.03
Y89 (ppm)	0.01	0.01	0.00	0.03	0.00	0.00	0.00	0.01
Zr90 (ppm)	0.16	3.36	0.27	2.49	0.03	0.07	0.00	0.04
Nb93 (ppm)	0.02	0.03	0.02	0.05	0.03	0.07	0.01	0.01
Mo95 (ppm)	0.05	0.02	0.03	0.02	0.01	0.01	0.02	0.02
Sn118 (ppm)	0.02	0.67	0.06	0.40	0.06	0.05	0.02	0.06
La139 (ppm)	0.00	0.01	0.01	0.03	0.00	0.01	0.00	0.00
Yb172 (ppm)			0.01	0.01	0.01	0.01		0.01
Hf178 (ppm)	0.01	0.17	0.01	0.12		0.00	0.01	
Ta181 (ppm)		0.01	0.01	0.00	0.00	0.00	0.01	0.01
W182 (ppm)		0.01	0.00	0.02	0.06	0.06	0.01	0.01
Ir193 (ppm)	0.01			0.01	0.01	0.01		0.01
Pb208 (ppm)	0.04	0.12	0.04	0.28	0.03	0.08	0.02	0.05

Drill hole	14-902	14-902	14-902	14-902	14-902	14-902	14-902	14-902
Thin section	SB004	SB004	SB004	SB004	SB004	SB004	SB006	SB006
Ox mode	SMO	SMO	SMO	SMO	SMO	SMO	HDO	HDO
Line	SB004 ilm006	SB004 ilm007	SB004 ilm008	SB004 ilm010	SB004 mag009	SB004 mag010	SB006 ilm011	SB006 ilm012
Mineral	ilmenite	ilmenite	ilmenite	ilmenite	ilmenite	ilmenite	ilmenite	ilmenite
Mg24 (ppm)	468.28	445.27	630.89	496.59	489.93	507.60	608.14	1051.54
Al27 (ppm)	209.20	476.48	431.04	210.52	463.92	363.24	450.96	239.02
Si29 (ppm)	256.83	670.03	760.30	494.48	1379.08	451.34	369.81	233.33
P31 (ppm)	0.01	0.01	0.34	2.02	0.01	0.01	1.77	0.01
Ca44 (ppm)	59.14	71.73	213.88	0.01	1211.41	68.25	173.56	2363.01
Sc45 (ppm)	117.51	49.43	53.02	68.82	44.05	86.73	59.06	74.27
Ti49 (ppm)	297210.90	295532.70	297667.50	297809.40	298170.90	291772.50	297896.50	296387.30
V51 (ppm)	1429.72	1477.34	1342.65	1336.18	1440.36	1979.80	1523.91	1338.22
Cr52 (ppm)	39.45	62.40	28.41	50.78	54.89	59.19	19.73	10.57
Mn55 (ppm)	13624.57	13621.13	14285.45	13640.04	13854.45	13572.31	11788.37	11112.36
Fe57 (ppm)	350767.20	351031.20	346980.80	348393.20	345221.90	356791.50	350522.10	350040.30
Co59 (ppm)	61.83	56.62	48.46	34.86	37.23	34.15	103.71	83.23
Ni60 (ppm)	7.52	9.71	21.04	28.67	5.69	46.91	12.36	10.46
Cu63 (ppm)	0.43	0.42	0.69	0.32	0.85	0.38	0.33	0.39
Zn66 (ppm)	41.81	51.65	42.53	35.94	46.91	37.86	61.83	78.96

Ga71 (ppm)	0.57	0.84	0.48	0.56	0.69	1.73	1.02	1.39
Ge74 (ppm)	0.06	0.06	0.08	0.07	0.06	0.08	0.06	0.05
As75 (ppm)	0.03	0.07	0.09	0.03	0.12	0.01	0.03	0.07
Y89 (ppm)	0.01	0.01	0.04	0.01	0.03	0.02	0.01	0.01
Zr90 (ppm)	0.21	0.40	0.45	0.38	0.83	0.31	1.84	4.57
Nb93 (ppm)	5.27	3.71	7.83	4.33	4.13	1.84	2.33	3.28
Mo95 (ppm)	0.15	0.12	0.13	0.14	0.11	0.12	0.11	0.13
Sn118 (ppm)	0.99	0.88	0.81	0.91	0.85	0.95	0.57	0.64
La139 (ppm)			0.01	0.01	0.00	0.01	0.00	0.00
Yb172 (ppm)	0.01	0.01			0.02	0.01	0.00	
Hf178 (ppm)	0.06	0.03	0.06	0.04	0.04	0.04	0.45	0.62
Ta181 (ppm)	0.41	0.26	0.83	0.29	0.45	0.09	0.10	0.31
W182 (ppm)	0.01	0.18	0.28	0.07	0.61	0.35	0.07	0.16
Ir193 (ppm)	0.01	0.01		0.01	0.01	0.01		0.01
Pb208 (ppm)	0.01	0.02	0.03	0.01	0.06	0.02	0.01	0.01

Drill hole	14-902	14-902	14-902	14-902	14-902	14-902	14-902	14-902
Thin section	SB006	SB006	SB006	SB008	SB008	SB013	SB013	SB013
Ox mode	HDO	HDO	HDO	HDO	HDO	HDO	HDO	HDO
Line	SB006 ilm013	SB006 ilm015	SB006 mag014	SB008 ilm4	SB008 mag1	SB013 mag1	SB013 mag2	SB013 mag4
Mineral	ilmenite	ilmenite	ilmenite	ilmenite	ilmenite	ilmenite	ilmenite	ilmenite
Mg24 (ppm)	676.31	1280.45	616.61	122.32	300.87	8223.60	5056.93	8777.17
Al27 (ppm)	799.73	1311.94	1209.31	20.58	186.10	838.76	770.12	2400.27
Si29 (ppm)	776.38	1917.65	1983.67	8.14	285.60	147.00	1620.02	1466.52
P31 (ppm)	0.51	0.61	0.74	0.01	0.35	0.01	2.63	2.89
Ca44 (ppm)	174.47	83.33	876.84	14.57	159.54	36.01	242.04	24.86
Sc45 (ppm)	37.17	23.99	20.65	5.64	7.23	103.76	86.18	87.51
Ti49 (ppm)	298535.10	293645.60	290804.30	277324.60	275685.60	290773.40	289971.30	292207.90
V51 (ppm)	1492.22	1434.00	1085.99	1566.54	1804.62	547.35	544.56	515.65
Cr52 (ppm)	9.89	7.55	16.58	0.57	0.85	114.27	116.38	362.29
Mn55 (ppm)	12815.52	13314.33	13421.13	15286.03	14022.01	8247.74	9070.00	8840.83
Fe57 (ppm)	346114.70	349699.80	352614.30	374453.90	376316.00	355110.30	354802.80	349508.90
Co59 (ppm)	55.31	38.53	69.58	48.23	72.14	79.87	48.58	62.21

Ni60 (ppm)	23.10	5.01	9.77	2.03	1.18	94.89	47.65	66.50
Cu63 (ppm)	0.43	0.33	0.32	0.33	0.38	0.46	0.36	0.93
Zn66 (ppm)	77.26	48.81	44.64	29.22	44.57	34.17	24.65	98.15
Ga71 (ppm)	1.36	1.56	1.83	0.38	0.47	1.54	1.16	6.15
Ge74 (ppm)	0.06	0.07	0.08	0.07	0.07	0.01	0.03	0.10
As75 (ppm)	0.06	0.03	0.02	0.05	0.11	0.10	0.07	0.16
Y89 (ppm)	0.01	0.02	0.02	0.01	0.01	0.01	0.01	0.00
Zr90 (ppm)	1.38	0.98	0.93	4.04	4.38	38.43	34.62	32.32
Nb93 (ppm)	1.25	2.58	1.92	1.48	0.47	3.58	2.64	2.02
Mo95 (ppm)	0.10	0.11	0.99	0.63	0.10	0.08	0.04	0.09
Sn118 (ppm)	0.34	0.15	0.36	0.35	0.65	0.48	0.64	0.63
La139 (ppm)	0.00	0.00	0.01	0.00	0.01	0.00	0.00	0.00
Yb172 (ppm)	0.00	0.01	0.01	0.01		0.01	0.01	0.01
Hf178 (ppm)	0.18	0.06	0.10	0.27	0.45	1.30	1.24	1.31
Ta181 (ppm)	0.04	0.11	0.13	0.09	0.06	0.27	0.37	0.24
W182 (ppm)	0.01	0.06	9.36	2.61	0.05	0.01	0.03	0.01
Ir193 (ppm)		0.01	0.01	0.01	0.01	0.01		0.01
Pb208 (ppm)	0.02	0.00	0.02	0.01	0.01	0.01	0.02	0.09

Drill hole	14-902	14-902	14-902	14-902	14-902	14-902	14-902	14-902
Thin section	SB013	SB016	SB016	SB016	SB016	SB021	SB021	SB021
Ox mode	HDO	WDO	WDO	WDO	WDO	HDO	HDO	HDO
Line	SB013 mag5	SB016 ilm1	SB016 mag2	SB016 mag3	SB016 mag4	SB021 ilm021	SB021 ilm022	SB021 ilm023
Mineral	ilmenite	ilmenite	ilmenite	ilmenite	ilmenite	ilmenite	ilmenite	ilmenite
Mg24 (ppm)	3950.94	501.81	836.43	485.91	3861.71	594.95	594.95	388.94
Al27 (ppm)	1360.43	248.04	141.49	411.72	2879.07	211.25	211.25	153.49
Si29 (ppm)	1348.79	243.48	184.50	158.07	5567.49	428.74	428.74	467.16
P31 (ppm)	1.83	0.01	0.01	0.01	3.78	1.33	1.33	0.24
Ca44 (ppm)	594.52	126.51	31.94	175.05	1957.29	241.53	241.53	479.49
Sc45 (ppm)	98.33	30.61	22.33	12.46	24.33	25.43	25.43	59.78
Ti49 (ppm)	291867.60	272205.80	270194.40	276316.00	273163.30	291906.40	291906.40	290294.70
V51 (ppm)	509.63	2441.76	2158.86	2349.16	2047.96	2826.11	2826.11	2805.34
Cr52 (ppm)	137.72	419.45	265.26	773.66	483.44	298.46	298.46	260.41

Mn55 (ppm)	8678.22	8465.55	8810.60	10801.05	8749.06	17185.19	17185.19	16292.52
Fe57 (ppm)	353434.20	384954.40	387580.80	406681.10	366460.60	351933.10	351933.10	355782.40
Co59 (ppm)	64.41	148.94	109.15	87.27	104.65	86.63	86.63	101.85
Ni60 (ppm)	76.81	55.14	25.83	50.79	72.23	42.76	42.76	30.80
Cu63 (ppm)	0.70	1.17	0.82	0.99	0.85	0.31	0.31	0.01
Zn66 (ppm)	41.39	64.88	67.50	59.60	74.66	98.19	98.19	128.62
Ga71 (ppm)	2.12	0.49	0.77	2.01	1.46	0.59	0.59	0.43
Ge74 (ppm)	0.05	0.05	0.07	0.05	0.09	0.07	0.07	0.08
As75 (ppm)	0.08	0.27	0.17	0.21	0.40	0.07	0.07	0.04
Y89 (ppm)	0.01	0.01	0.01	0.01	0.01	0.01	0.01	0.01
Zr90 (ppm)	45.07	5.85	3.20	4.18	4.38	0.43	0.43	3.10
Nb93 (ppm)	6.69	5.57	6.12	7.43	6.02	2.29	2.29	4.36
Mo95 (ppm)	0.08	0.81	0.77	0.39	2.60	0.19	0.19	0.19
Sn118 (ppm)	0.70	0.23	0.52	0.20	0.35	0.44	0.44	0.62
La139 (ppm)	0.01	0.02	0.01	0.05	0.07	0.05	0.05	0.05
Yb172 (ppm)	0.01	0.01			0.01			0.01
Hf178 (ppm)	1.48	0.20	0.11	0.09	0.20	0.48	0.48	0.70
Ta181 (ppm)	0.60	0.73	0.56	0.50	0.41	0.11	0.11	0.38
W182 (ppm)	0.05	21.37	12.03	15.52	15.89	0.07	0.07	0.15
Ir193 (ppm)	0.01		0.01	0.01	0.01	0.01	0.01	0.01
Pb208 (ppm)	0.15	0.03	0.11	0.09	0.07	0.02	0.02	0.04

Drill hole	14-902	14-902	14-902	14-902	14-902	14-902	14-902	14-902
Thin section	SB021	SB021	SB021	SB021	SB024	SB024	SB024	SB024
Ox mode	HDO	HDO	HDO	HDO	WDO	WDO	WDO	WDO
Line	SB021 ilm024	SB021 ilm025	SB021 mag024	SB021 mag025	SB024 ilm1	SB024 ilm4	SB024 mag3	SB024 mag5
Mineral	ilmenite	ilmenite	ilmenite	ilmenite	ilmenite	ilmenite	ilmenite	ilmenite
Mg24 (ppm)	496.33	396.16	908.23	1575.71	539.92	1187.68	713.40	3817.95
Al27 (ppm)	225.48	92.81	662.26	1240.84	377.95	1496.78	1775.07	4714.27
Si29 (ppm)	1060.65	176.50	1626.55	2066.60	309.80	1460.75	406.04	4600.03
P31 (ppm)	0.45	0.01	0.01	0.01	1.56	0.01	0.01	0.01
Ca44 (ppm)	1245.06	130.78	895.65	923.06	44.10	326.81	58.85	166.67
Sc45 (ppm)	53.37	89.67	55.45	86.02	117.42	131.37	118.10	88.48
Ti49 (ppm)	299597.00	290176.80	299251.30	284489.70	289004.60	301556.60	292242.60	294482.20

V51 (ppm)	2528.34	2980.21	2384.61	2747.75	1870.50	1460.88	1552.72	1134.44
Cr52 (ppm)	195.68	190.12	234.34	252.25	314.74	217.45	417.23	347.48
Mn55 (ppm)	16371.08	15047.07	14452.51	16171.28	17813.15	16479.69	19171.36	19094.14
Fe57 (ppm)	342641.00	358027.10	344563.70	357307.50	356502.30	337178.20	348835.40	333181.90
Co59 (ppm)	50.48	44.89	48.47	45.33	107.34	119.09	114.03	89.15
Ni60 (ppm)	50.11	68.94	71.01	93.37	160.63	151.18	94.07	187.39
Cu63 (ppm)	0.34	0.29	1.07	0.31	0.28	0.66	0.75	0.37
Zn66 (ppm)	75.90	90.12	81.25	77.65	119.70	61.31	308.14	706.30
Ga71 (ppm)	0.52	0.52	1.26	2.01	1.44	1.47	3.53	5.42
Ge74 (ppm)	0.10	0.09	0.12	0.15	0.06	0.06	0.07	0.05
As75 (ppm)	0.08	0.03	0.05	0.01	0.13	0.19	0.10	0.19
Y89 (ppm)	0.03	0.01	0.01	0.01	0.01	0.03	0.02	0.02
Zr90 (ppm)	1.09	1.55	1.09	0.62	76.98	23.59	28.21	239.63
Nb93 (ppm)	2.51	3.02	2.94	1.49	11.50	9.85	10.64	9.69
Mo95 (ppm)	0.15	0.16	0.13	0.15	0.26	0.19	0.25	0.19
Sn118 (ppm)	0.28	0.67	0.26	0.45	1.32	2.06	1.50	1.36
La139 (ppm)	0.13	0.01	0.08	0.04	0.00	0.03	0.05	0.06
Yb172 (ppm)				0.01	0.03	0.00	0.01	0.01
Hf178 (ppm)	0.36	0.98	0.32	0.62	3.55	2.47	2.95	5.54
Ta181 (ppm)	0.18	0.21	0.22	0.07	0.77	0.79	0.84	0.82
W182 (ppm)	0.08	0.11	0.07	0.08	0.42	0.13	0.30	0.17
Ir193 (ppm)	0.01	0.01	0.01		0.01		0.01	0.01
Pb208 (ppm)	0.05	0.02	0.06	0.06	0.01	0.08	0.02	0.02

Drill hole	14-902	14-902	14-902	14-902	14-902	14-902	14-902	14-902
Thin section	SB027	SB027	SB027	SB029	SB029	SB029	SB029	SB029
Ox mode	HDO	HDO	HDO	HDO	HDO	HDO	HDO	HDO
Line	SB027 mag1	SB027 mag2	SB027 mag4	SB029 ilm4	SB029 ilm5	SB029 mag1	SB029 mag2	SB029 mag3
Mineral	ilmenite	ilmenite	ilmenite	ilmenite	ilmenite	ilmenite	ilmenite	ilmenite
Mg24 (ppm)	3218.39	1889.02	1475.03	197.59	511.37	3218.39	216.08	598.65
Al27 (ppm)	2947.22	260.84	1871.04	524.22	810.99	2947.22	237.32	1057.98
Si29 (ppm)	176.80	636.54	1688.91	1303.84	1270.95	176.80	485.77	1287.89
P31 (ppm)	1.97	5.02	2.72	0.20	1.11	1.97	0.57	0.01
Ca44 (ppm)	92.35	12.18	692.73	992.97	222.15	92.35	689.67	202.69

Sc45 (ppm)	98.98	104.82	63.77	31.02	29.86	98.98	13.42	26.33
Ti49 (ppm)	293124.20	293395.30	284591.10	296644.70	294815.40	293124.20	290011.60	301228.90
V51 (ppm)	1611.19	1872.34	1526.78	1632.92	1363.18	1611.19	1727.57	1600.52
Cr52 (ppm)	572.02	406.90	310.36	16.13	13.34	572.02	29.34	21.45
Mn55 (ppm)	9193.97	9787.15	8155.61	10611.81	10426.20	9193.97	10477.04	10809.34
Fe57 (ppm)	353108.50	356561.20	363535.50	350852.10	352824.90	353108.50	361417.70	345852.40
Co59 (ppm)	129.56	165.49	194.02	40.58	40.88	129.56	56.20	33.18
Ni60 (ppm)	168.28	141.48	112.70	4.28	5.33	168.28	5.47	13.88
Cu63 (ppm)	0.30	1.30	0.61	0.25	0.23	0.30	1.71	1.50
Zn66 (ppm)	118.54	42.31	87.99	95.88	66.55	118.54	87.63	77.83
Ga71 (ppm)	6.74	0.88	2.99	0.56	0.93	6.74	1.69	0.70
Ge74 (ppm)	0.07	0.08	0.08	0.04	0.04	0.07	0.08	0.04
As75 (ppm)	0.12	0.14	0.17	0.13	0.10	0.12	0.36	0.18
Y89 (ppm)	0.01	0.02	0.02	0.02	0.01	0.01	0.01	0.02
Zr90 (ppm)	23.68	31.82	15.22	2.30	7.42	23.68	0.66	4.43
Nb93 (ppm)	0.99	0.65	1.03	1.26	3.84	0.99	0.93	1.48
Mo95 (ppm)	0.09	0.10	0.16	0.10	0.59	0.09	0.13	0.15
Sn118 (ppm)	1.10	1.39	0.80	0.21	0.26	1.10	0.10	0.18
La139 (ppm)	0.00	0.01	0.06	0.01	0.01	0.00	0.00	0.02
Yb172 (ppm)	0.01	0.00	0.00	0.00	0.01	0.01		0.01
Hf178 (ppm)	0.95	1.13	0.59	0.31	0.31	0.95	0.09	0.34
Ta181 (ppm)	0.02	0.02	0.05	0.09	0.52	0.02	0.12	0.12
W182 (ppm)	0.01	0.05	0.64	0.18	3.91	0.01	0.37	0.36
Ir193 (ppm)	0.01	0.01	0.01	0.01	0.01	0.01	0.01	
Pb208 (ppm)	0.01	0.20	0.04	0.03	0.02	0.01	0.04	0.11

Drill hole	14-902	14-902	14-902	14-902	14-902	14-902	14-902	14-902
Thin section	SB034	SB034	SB034	SB034	SB034	SB034	SB036	SB036
Ox mode	MO	MO	MO	MO	MO	MO	HDO	HDO
Line	SB034 ilm031	SB034 ilm032	SB034 ilm033	SB034 ilm034	SB034 ilm035	SB034 mag034	SB036 ilm036	SB036 ilm037
Mineral	ilmenite	ilmenite	ilmenite	ilmenite	ilmenite	ilmenite	ilmenite	ilmenite
Mg24 (ppm)	1509.53	2854.30	7098.16	9072.52	2943.24	8642.15	445.92	556.42
Al27 (ppm)	380.73	354.85	634.77	861.27	369.26	1714.77	114.67	256.06
Si29 (ppm)	216.90	201.71	204.85	566.11	361.73	215.83	415.76	534.72

P31 (ppm)	0.57	0.01	1.20	0.43	1.01	1.14	0.01	0.24
Ca44 (ppm)	16.45	3.52	233.15	150.29	3.97	5.97	432.54	81.26
Sc45 (ppm)	165.62	161.56	122.13	124.95	142.80	120.16	16.33	19.58
Ti49 (ppm)	298857.00	302473.80	296293.60	303481.90	298516.40	301004.90	299351.50	296655.80
V51 (ppm)	2353.36	2232.82	1914.34	2325.52	2443.51	2440.36	2195.78	2356.94
Cr52 (ppm)	34.01	34.31	18.55	22.80	30.05	26.43	137.04	197.20
Mn55 (ppm)	10527.52	10133.47	9958.08	9594.52	9895.45	9647.21	12945.68	12208.02
Fe57 (ppm)	350175.60	344427.50	346496.00	334278.30	348292.80	338123.10	347764.00	350547.90
Co59 (ppm)	30.55	19.67	19.58	49.40	23.84	32.35	100.28	35.47
Ni60 (ppm)	94.81	146.15	167.33	144.29	95.87	166.71	78.88	150.85
Cu63 (ppm)	0.59	0.29	0.47	1.40	0.24	0.65	0.22	0.21
Zn66 (ppm)	171.86	176.06	162.12	214.04	187.87	253.41	123.77	142.27
Ga71 (ppm)	0.76	0.35	2.69	1.59	0.63	4.84	0.33	0.48
Ge74 (ppm)	0.04	0.04	0.05	0.07	0.07	0.08	0.07	0.05
As75 (ppm)	0.10	0.04	0.02	0.12	0.06	0.12	0.03	0.06
Y89 (ppm)	0.04	0.03	0.03	0.02	0.01	0.02	0.01	0.01
Zr90 (ppm)	3.41	3.98	9.57	7.40	7.42	7.27	0.47	0.53
Nb93 (ppm)	5.48	2.84	6.72	2.23	13.59	2.05	3.71	3.15
Mo95 (ppm)	0.12	0.12	0.09	0.09	0.11	0.11	0.16	0.16
Sn118 (ppm)	0.68	0.52	0.23	0.07	0.69	0.23	0.36	0.39
La139 (ppm)	0.04	0.04	0.02	0.01	0.03	0.01	0.01	0.02
Yb172 (ppm)	0.01	0.01	0.01		0.00	0.00	0.00	0.01
Hf178 (ppm)	0.22	0.27	0.54	0.25	0.55	0.25	0.06	0.05
Ta181 (ppm)	0.65	0.32	0.74	0.10	1.31	0.13	0.31	0.33
W182 (ppm)	0.16	0.20	0.07	0.02	0.12	0.04	1.11	0.78
Ir193 (ppm)	0.01	0.01	0.01		0.01			0.01
Pb208 (ppm)	0.03	0.01	0.18	0.02	0.01	0.02	0.04	0.06

14-902	14-902	14-902
SB036	SB036	SB036
HDO	HDO	HDO
SB036 ilm038	SB036 ilm039	SB036 ilm040
ilmenite	ilmenite	ilmenite
328.95	354.41	1172.55

73.14	127.40	1107.08
226.57	1854.04	2895.95
0.01	0.81	0.00
28.33	2262.35	2081.07
17.32	20.58	11.55
297979.90	295761.00	296432.20
2230.12	2187.19	2225.89
173.55	154.36	181.76
12653.01	11181.24	11876.42
350579.10	350771.00	345932.70
103.06	99.38	91.76
47.30	98.84	59.96
1.10	0.30	1.71
124.70	114.40	106.82
0.21	0.71	0.91
0.06	0.08	0.09
0.03	0.03	0.07
0.01	0.01	0.02
0.60	0.58	0.47
2.68	3.87	2.25
0.17	0.16	0.11
0.43	0.39	0.30
0.01	0.01	0.11
0.01	0.01	
0.10	0.04	0.04
0.35	0.33	0.21
0.45	0.58	0.75
0.01	0.01	
0.02	0.08	0.06